DISTRIBUTION MAPPING AND HOST PLANT PREFERENCES OF THE BAGWORM *EUMETA CRAMERI* WESTWOOD 1854 FROM KERALA, INDIA[1]

Usha, A.U.[2,4,*], Joyce Jose[2,5] and T.J. Roby[3]

[1]Accepted January 27, 2021
First published: September 30, 2021 | doi: 10.17087/jbnhs/2021/v118/150537
[2]Research and Post-Graduate Department of Zoology, St Thomas' College (Autonomous), Thrissur 680 001, Kerala, India.
[3]Department of Botany, Carmel College, Mala Thrissur, 680 732, Kerala, India.
Email: robyjosethekkudan@gmail.com
[4]Email: ushaunni77@gmail.com
[5]Email: joyceofthejungle@gmail.com
*Corresponding author

Bagworms (Lepidoptera: Psychidae) are sexually dimorphic polyphagous insects with a unique life cycle. *Eumeta crameri* is a common species of bagworm in Kerala, India. This paper documents the distribution mapping of *Eumeta crameri* in Kerala by QGIS method, and also includes an account of its host plant selection and utilization. Morphology and life cycle of the species is also discussed. We observed more than 100 individuals of *Eumeta crameri* from 19 localities in randomly selected human habitations of Kerala. The plant family most preferred by *Eumeta crameri* was found to be Fabaceae, and bag attachment was mainly seen on the middle portion of the preferred plant or tree.

Key words: Lepidoptera, Psychidae, distribution mapping

INTRODUCTION

Bagworms (Lepidoptera: Psychidae) are characterized by the bag-making habit of the larvae, and extreme sexual dimorphism in adults. Family Psychidae constitutes 1,350 species in 241 genera (van Nieukerken *et al*. 2011), reported worldwide except from Antarctica. Hampson (1892) listed 36 species from "British India", including Sri Lanka and Myanmar, which is the oldest record of bagworms from India. A recent study indicates 106 species belonging to 34 genera in India (Sobczyk 2011). In most species, only the male emerges as a winged moth from the bag, while the females are apterous and persist as an egg sac inside the bag (Rhainds *et al*. 2009).

Bagworms were recorded as occasional pests from forested areas in Kerala but their polyphagous nature, as well as deficient documentation in human-altered habitats, suggests that they can become serious pests, in light of climate change and land use change (Mathew and Nair 1983, 1986; Nair and Mathew 1992; Varma *et al*. 1989). Many species are defoliators of cultivated crops and cause moderate to severe economic damage (Basri 1993), so the documentation of these insects is significant.

Eumeta crameri Westwood is a common bagworm species in Kerala. It is found in different habitats and on various kinds of vegetation, including herbs, shrubs, and trees (Usha and Jose 2017). Up to four generations per year, with the male population much higher than the female (Ameen and Sultana1977) were recorded from Bangladesh. Thangavelu and Ravindranath (1985) did extensive work on the morphology and larval chaetotaxy of the species collected from Karnataka.

The present study documents the spatial distribution of *Eumeta crameri* Westwood by QGIS mapping and detailed study of host plant selection and utilization. Description of morphological characters like wing venation and genitalia, and observations on the life cycle are also presented in this paper.

MATERIAL AND METHODS

Study area and collection: Collections were made from randomly selected sites in seven districts of Kerala, namely Thrissur, Palakkad, Wayanad, Malappuram, Ernakulam, Thiruvananthapuram, and Kannur. The bags of *Eumeta crameri* were handpicked from the host plants. Position coordinates, host plants, bag attachment, were recorded at the time of collection. Once a bag was noticed on a plant, observations were made around that plant in all directions wherever possible till no more bags were seen.

Distribution mapping: The position coordinates recorded were tabulated according to the presence of species in each site, and maps were created in QGIS technology, based on the occurrence of species. Concentric buffer zones of 2 km each were created to predict the range of dispersal from a mother bag.

Host plant selection and utilization: Data collected during field work was classified as follows: i. Bag position

was noted as top, middle, and lower, by roughly dividing the plant into three equal parts. ii. Bag attachment was classified as "on stem" and "on leaf". On stem, the attachments were classified as on node or on internode regions. On leaves, bag attachment was noted "on leaflet" or "on midrib". iii. The bags were also classified as small, medium, and large, based on the length of the sticks used in the bag, or the size of the bag.

Damage to the leaves near the bags, and all over the host plant, due to feeding by the larvae was calculated as follows: Damaged leaves were randomly selected for measurement. Based on the damage observed in the plant parts, i.e. mainly in the leaf area, we gave different scores. For no damage observed, score zero; less than ¼ of the leaf area damaged, score 1; ¼ to ½ of the leaf area damaged, score 2; and ½ to ¾ of the leaf area damaged, score 3; more than ¾ of the leaf area damaged, score 4. The utilization of host plants by the bag moths based on the bag size (instars), bag position, number of bags, plant type, and feeding, was visualized using Principal Component Analysis (PCA).

Morphological study: The larvae were transferred into rearing bottles and kept until the emergence of adults. A few emerged male moths were sacrificed, spread, and pinned using standard protocol. The wing venation and genitalia were microscopically studied by preparing slides.

Lifecycle and dispersal: The study was conducted in an artificially created experimental set up with conditions similar to those in the wild. The larvae used in this study emerged from female bags of *Eumeta crameri* collected from Palakkad. The transfer of the hatched larvae to the plant top was done artificially and the distribution of larvae was observed. The larvae were released on a potted *Phyllanthus emblica* tree (hitherto referred as mother plant), placed near the wall of a building. The plant was kept on a plinth of height 53 cm, which raised the height to a total of 153 cm from ground level. Observations on the number of larvae dispersed, direction of dispersion, and number of larvae remaining on the plant, were noted. The number of larvae in each instar was noted and a survivorship curve was plotted.

RESULTS AND DISCUSSION

Distribution maps

Bags of *Eumeta crameri* Westwood, which are renovated by each instar and consist of silk and extraneous material like leaves, twigs, and thorns (Agrawal and Pati 2003), were collected from 19 sites in human altered areas of 7 districts in Kerala (Fig. 1). Distribution of *Eumeta crameri* was plotted using QGIS technology, according to the geographical coordinates of each collection site (Table 1). The larvae were seen to disperse and establish new bags up to 2 km away

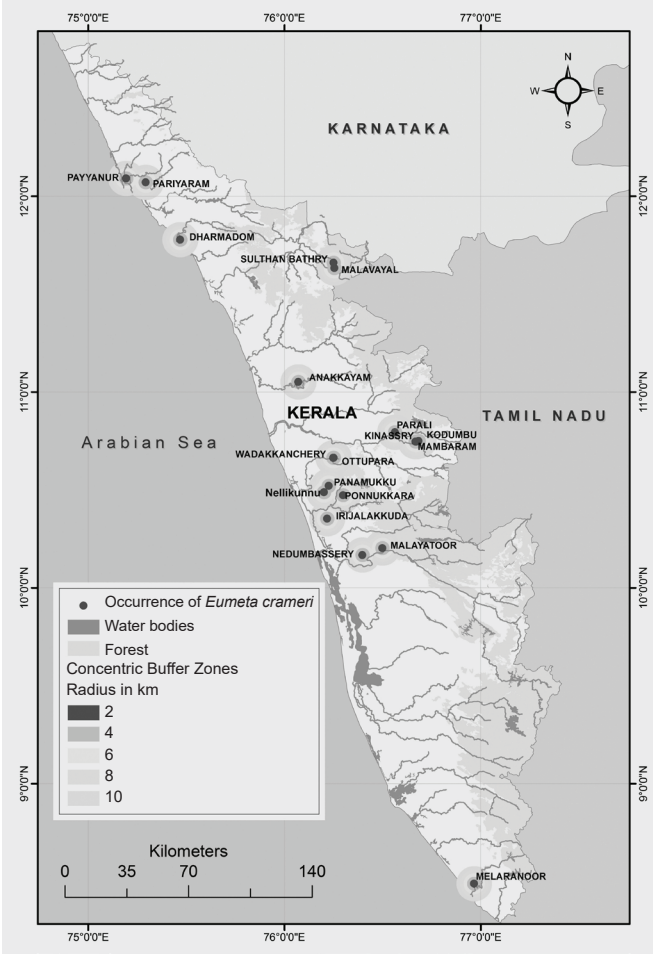

Fig. 1: Map of occurrence zones of *Eumeta crameri*

from the mother plant; the dispersal range of these insects was plotted upto five generations. Ameen and Sultana (1977) observed four generations in a year, while our own observations (71 days) indicate that 5.1 generations/year are theoretically possible. Based on the observed dispersal along a radius of up to two km per generation from the mother plant, dispersal up to 10 km radius from the mother plant was predicted per year (provided that all factors such as climatic conditions, availability of suitable host plants, and lack of predators were favourable) (Fig. 2).

Host plant selection and utilization: Bagworms in the study area show polyphagy, as 24 species of plants belonging to 14 known and 3 unknown families were seen to be infested by bagworms. Out of 24 species, 8 were trees, 6 were herbs and 10 were shrubs. *Phyllanthus emblica*, *Terminalia catappa*, *Psidium guajava*, *Tamarindus indica*, *Lawsonia inermis*, and *Hibiscus rosa-sinensis* were frequently found infested by *Eumeta crameri*, and Fabaceae was the most affected plant family (Fig. 3). The bags were mostly positioned in the middle of the host plant, irrespective of the species being a tree, herb,

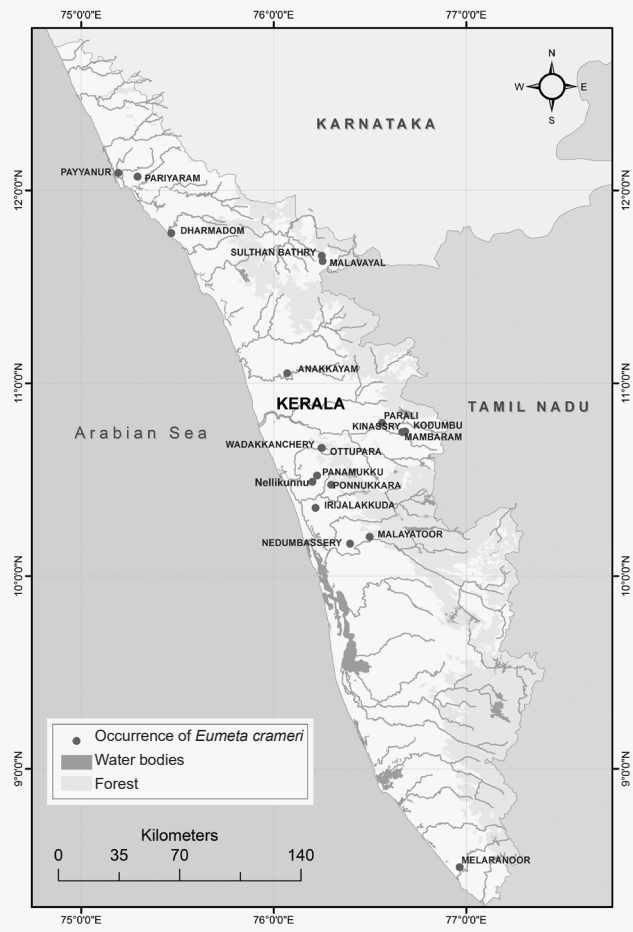

Fig. 2: Concentric zones showing hypothetical range of dispersal from the mother bag

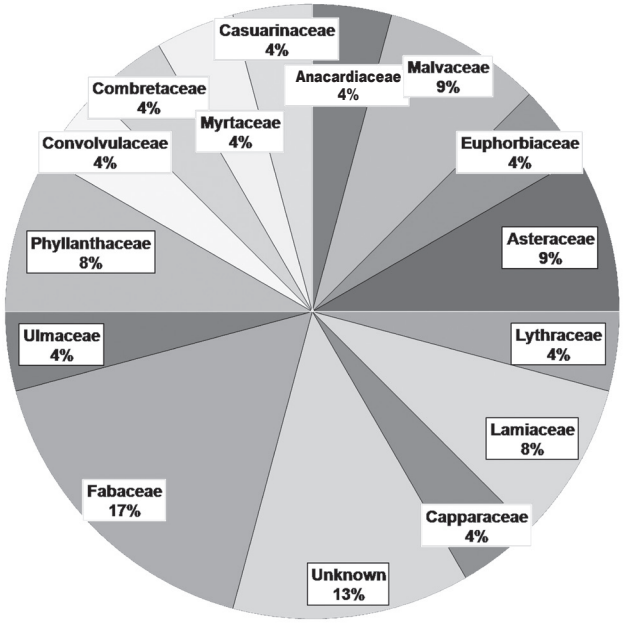

Fig. 3: Distribution of host plant families infested by *Eumeta crameri*

or shrub (Fig. 4). The maximum number of bag attachments was seen at the internodes (Fig. 5).

Bags on the leaves were fewer in number than those attached to the stem. Though more bags were found in the middle third of the host plant in general, there was a significant increase in the bags attached to the upper third in trees, compared to shrubs and herbs. Less feeding was observed in trees than in shrubs and herbs.

Results of previous studies (Usha and Jose 2017) indicate that the mature larval instars migrate to trees after feeding on herbs and shrubs in the early instars. Relative size of the bags collected from the trees and reduced feeding (less damage observed) shows that mature larvae move to trees before pupation. This could indirectly help in better dispersal of the larvae, as air currents assist the ballooning technique used by larvae for dispersal.

While small and medium sized bags did not show any special preference for the top, middle, or lower parts of the host plant, and kept moving about, larger bags remained in the top region and were not observed to move much. As larger bags contain the final instars which feed less, as well as the pupal stage and egg sac-like adult females, they are less mobile, whereas the smaller bags move about actively and their larvae feed voraciously, dragging the bag from one host plant to another. The maximum feeding was seen on herbs and shrubs. The size of the host plant was negatively correlated to feeding damage, but not significantly so. More feeding damage was observed in the top third of the host plants, as there are tender and succulent twigs and leaves on the upper part of the stem which the bagworms prefer.

Principal Component Analysis: The PCA biplot (Fig. 6) based on the moth bag size (instars), bag positioning, and number of bags, plant type, and feeding indicate that *Mangifera indica* was unique among the host species, as the number of bags found on *Mangifera indica* was much higher other than plants and also because the majority of the bags were final instars. *Phyllanthus emblica*, *Trema orientalis*, *Tamarindus indica*, *Lawsonia inermis*, *Mangifera indica*, *Hyptis suaveolens*, and *Psidium guajava* form a cluster in which most of the trees were included. Other plants cluster together towards the centre of the biplot, indicating that more data is needed to delineate host plant preferences.

Plant species code: *Acacia auriculiformis* = AA, *Casuarina* sp. = C1, *Chromolaena odorata* = CO, *Cleome viscosa* = CV, *Crotalaria pallida* = CP, *Hyptis suaveolens* = HV, *Ipomoea marginata* = IM, *Lawsonia inermis* = LI,

Table 1: Occurrence data of *Eumeta crameri* Westwood

Sl no	District	Locality	Latitude	Longitude
1.	Ernakulam	Malayatoor	10° 12′ 11.16″	76° 29′ 56.4″
2.	Ernakulam	Nedumbassery	10° 10′ 4.44″	76° 23′ 52.08″
3.	Kannur	Pariyaram	12° 4′ 16.68″	75° 17′ 35.88″
4.	Kannur	Payyanur	12° 5′ 27.708″	75° 11′ 37.14″
5.	Kannur	Dharmadom	11° 46′ 41.52″	75° 28′ 8.4″
6.	Malappuram	Anakkayam	11° 3′ 6.48″	76° 4′ 17.04″
7.	Palakkad	Kinassery	10° 44′ 49.344″	76° 40′ 6.924″
8.	Palakkad	Mambaram	10° 44′ 47.69″	76° 40′ 14.376″
9.	Palakkad	Kodumbu	10° 45′ 0″	76° 41′ 2.4″
10.	Palakkad	Parali	10° 47′ 41.21″	76° 33′ 47.81″
11.	Thiruvananthapuram	Melaranoor	8° 29′ 19.33″	76° 57′ 59.8″
12.	Thrissur	Panamukku	10° 29′ 18.204″	76° 12′ 7.02″
13.	Thrissur	Nellikunnu	10° 31′ 14.88″	76° 13′ 33.96″
14.	Thrissur	Ponnukkara	10° 28′ 24.0″	76° 17′ 57″
15.	Thrissur	Irinjalakkuda	10° 21′ 12.096″	76° 13′ 4.73″
16.	Thrissur	Wadakkanchery	10° 39′ 51.84″	76° 14′ 57.48″
17.	Thrissur	Ottuppara	10° 39′ 52.2″	76° 15′ 5.4″
18.	Wayanad	Sulthanbathery	11° 39′ 38.84″	76° 15′ 2.27″
19.	Wayanad	Malavayal	11° 38′ 0.456″	76° 15′ 16.56″

Mangifera indica = MI, *Mikania micrantha* = MM, *Mimosa pudica* = MP, *Phyllanthus emblica* = PE, *Phyllanthus myrtifolium* = PM, *Phyllanthus reticulatus* = PR, *Psidium guajava* = PG, *Sida acuta* = SA, *Tamarindus indica* = TI, *Tectona grandis* = TG, *Terminalia catappa* = TC, *Trema orientalis* = TO, Unknown sp. 1 = U1, Unknown sp. 2 = U2, Unknown sp. 3 = U3, *Urena sinuata* = US.

MORPHOLOGY

The identification of species was done with the help of Hampson (1892), referring to experts, and also from the sequenced molecular data by BLAST. The Cytochrome oxidase subunit1 of *Eumeta crameri* was sequenced and uploaded in GenBank with the accession number MN717271.

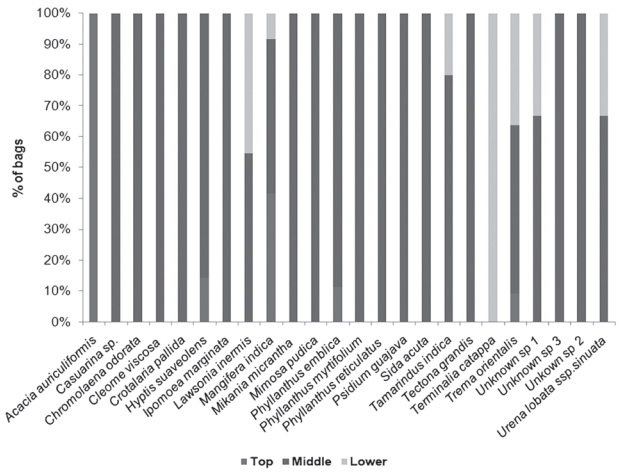

Fig. 4: Graphical representation of bag positioning on plants in each plant species

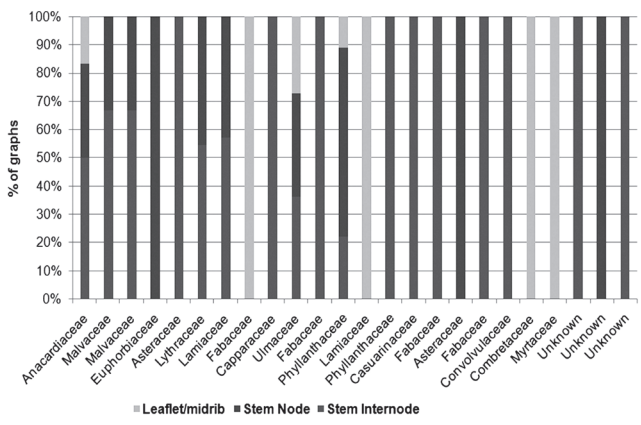

Fig. 5: Graphical representation of bag attachment on plants in each plant make it family

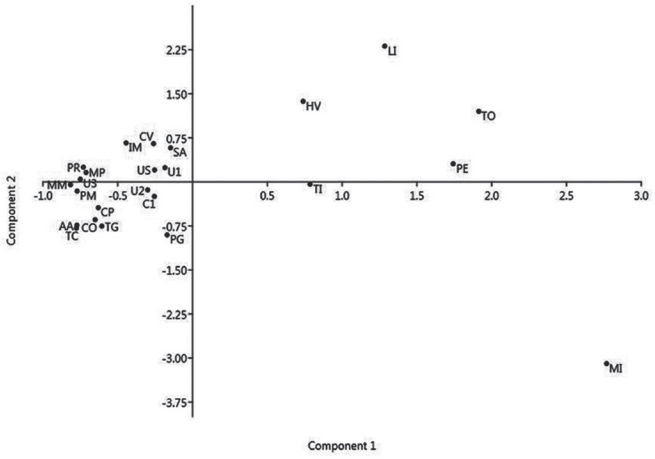

Fig. 6: PCA map showing three plant clusters based on utilization by bagworm moth larvae and bag attachment

The bag of this species (Fig. 7) is cylindrical, mainly made by attaching dry twigs from the host plants in a circular pattern, as described by Agrawal and Pati (1995, 2003). Before attaching the twigs, the larva makes a tough leathery silk bag around its body, on to which cut twigs are attached using silk threads. The silk bag is whitish cream and open at the anterior and posterior ends. Most of the bags have one especially long stick. Mean measurements of mature larval bags were 38 mm length, 30 mm circumference, and 9 mm outer diameter. Our observations concurred with earlier studies in northern India (Agrawal and Pati 1995, 2003). Similar data was not available in the studies conducted in Bangladesh (Ameen and Sultana 1977) and Karnataka (Thangavelu and Ravindranath 1985). The larvae stay inside the bag throughout their lifetime, with only the head and thoracic legs protruding outside while feeding and moving about. Newly hatched larvae are pale buff, becoming dark brown or black as they grow.

Mean length of the newly hatched larvae was 1 mm. As described earlier by Agrawal and Pati (1995, 2003), the larvae reconstructed and increased the bag size by using longer sticks at each progressive instar. Thangavelu and Ravindranath (1985) have provided detailed descriptions of the larval stages of *Eumeta crameri* population from Karnataka.

Adult males (Fig. 8) are medium-sized (mean body length 11 mm), dark brown, with almost transparent wings; head,

Fig. 7: Larval bag

Fig. 8: Adult male

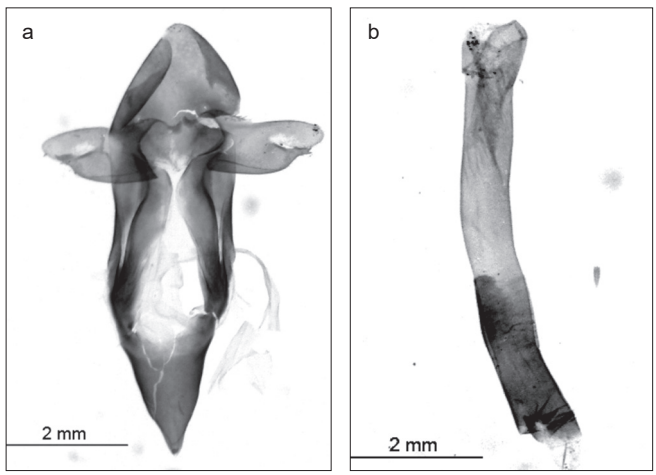

Fig. 9: a. Male genitalia, b. Aedeagus

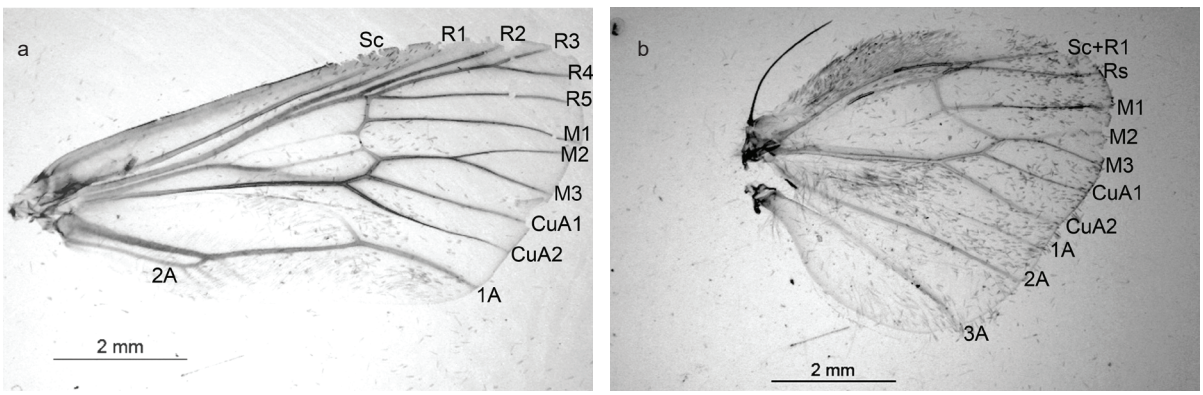

Fig. 10: a. Forewing. b. Hindwing

thorax, and abdomen are covered with light brown hairs. The upper parts of forewings and hind wings are covered with tiny brown scales. Head small, capsule-like with one pair of compound eyes, mean length 1.5 mm, antennae bipectinate. Legs pale brown with dark brown hairs covering the coxa to femur region. Fore and mid legs with thick brown hairs, mean length 8.5 mm and 6.6 mm respectively. Forelegs with elongated hair-like process parallel with the length of tibia, originating from tibia-tarsal segment or junction. Hind legs comparatively shorter mean length 4.5 mm.

Adult females are distinct from males, cylindrical (vermiform) in shape with the appearance of an egg sac. Body filled with pale yellow eggs inside a sac, and with partially sclerotized head. Appendages are lacking.

Wing venation: Wingspan 26 mm. (Fig. 10a, b) Wings almost triangular in shape, transparent in spite of the presence of scales; major veins clearly visible. All 12 veins in forewing and 8 veins in hind wing as reported by Hampson (1892) were seen in the specimens collected from the study area. Forewing with vein R3 and R4, M2 and M3 stalked, as described by Hampson (1892). Hind wing in some individuals showed an interconnected cell-like structure between the middle of veins 7 and 8. Veins M2 and M3 in hind wing were stalked.

Genitalia: (Fig. 9a) Male genitalia a long tube-like structure measuring 3 mm. External genitalia consist of the tip of aedeagus and valve, which protrude out of the last abdominal segment. Aedeagus (Fig. 9b) long tube-like, with cup-shaped anterior end measuring 2 mm.

Lifecycle and larval dispersal: Male and female bagworms do not possess any distinguishable external characteristics, so it is difficult to differentiate their bags in the early instars. In the final IXth instar, males are smaller and lack pigmentation (Thangavelu and Ravindranath 1985). The newly hatched (first instar) larvae were active and dispersed from the mother plant to the nearest plants by ballooning with the wind current. They build their bag by using silk and plant materials within 2 or 3 hrs after hatching. The wind was the primary medium of their dispersal. There was no feeding observed before ballooning. All the larvae were seen spinning silky threads for ballooning. The dispersal was carried mainly to the north-east direction following to the direction of wind (Usha and Jose 2018).The larvae form a single line while ballooning and move forward with the wind current. Dispersed larval bags were rediscovered after a few days from various plants around the mother plant, with the larvae actively feeding and building bags. Bags were not marked due to its minute size but the experiment was carried out in a wall compound and all plants were regularly checked before and after dispersal of bags, initial number of bags on the mother plant and final number of bags on other plants were compared and the latter was much less.

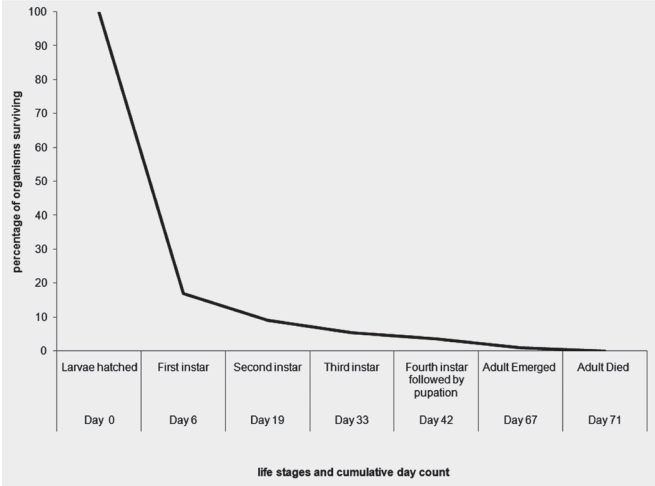

Fig. 11: *Eumeta crameri* Survivorship curve

According to Usha and Jose (2018), out of 200 larvae hatched in natural conditions, only 34 relocated, to 12 individual plants of 5 species. The total lifecycle was of 71 days duration, larval and pupal duration was 42 and 25 days respectively. Adult lifespan is 3–4 days. A previous study (Agrawal and Pati 2003) stated that *Eumeta crameri* has three bag renovations, i.e. four instars per generation. But Thangavelu and Ravindranath (1985) delineated nine larval instars, based on the morphometric analysis of larvae. In this study, the life stages of *Eumeta crameri* were delineated based on bag renovations and a survivorship curve was plotted using the number of larvae at the time of each bag renovation.

Survivorship curve: The survivorship curve of *Eumeta crameri* was Type III or concave type. (Fig.11). This species produced large numbers of offspring and the mortality of larvae increased in each progressive bag renovation. Only two adult moths emerged in a generation from a brood of more than 200. There are various reasons for a species to exhibit a particular survivorship curve; environmental factors could be the reason for decrease in survival. "An outside element that preferentially reduces the survival of young individuals is likely to yield a Type III curve" (Demetrius 1978).

CONCLUSION

The Bagworm Moth *Eumeta crameri* Westwood is one of the commonest bagworm species found in the study area. The distribution mapping and host plant preferences of this species enable an understanding of the ecology of

this common moth. Four different studies conducted in four different environments and time periods, with differing results, reveal that variations in the duration of its lifecycle could be influenced by environmental parameters. Further studies on the effect of specific climatic and other abiotic factors on the life cycle and dispersal of *Eumeta crameri* are essential, as climate change and other anthropogenic factors may transform this polyphagous low-profile feeder into a major agro-economic destructor.

ACKNOWLEDGEMENTS

We are indebted to UGC-NFSC for financial assistance. We thank our Principal and Head of the Department of Zoology, St Thomas College (Autonomous), Thrissur, for the facilities provided for our research work. We are grateful to Dr Anto P.V., Department of Botany, St Thomas College (Autonomous), Thrissur, for confirming the identification of host plants.

REFERENCES

Agrawal, A. & A.K. Pati (1995): Nest architecture of a bagworm species: Rhythmic pattern in the arrangement of sticks. *Journal of Bioscience 20(3)*: 409–416.

Agrawal, A. & A.K. Pati (2003): Larval case renovation – a unique behaviour in bagworm moth *Eumeta crameri* Westwood. *Current Science 85(12)*: 1674–1679.

Ameen, M.U. & P. Sultana (1977): Biology of the bagworm moth *Eumeta crameri* (Lepidoptera: Psychidae) from Dacca, Bangladesh. *Journal of Natural History 11(1)*: 17–24.

Basri, M.W. (1993): Life history, ecology and economic impact of the bagworm, *Metisa plana* Walker (Lepidoptera: Psychidae) on the oil palm, *Elaeis guineensis* Jacquin (Palmae) in Malaysia. PhD thesis, University of Guelph, Canada.

Demetrius, L. (1978): Adaptive value, entropy and survivorship curves. *Nature 275 (5677)*: 213–214.

Hampson, G.F. (Eds) (1892): The Fauna of British India including Ceylon and Burma. Moths, Vol. 1 Taylor and Francis, London, pp. 289–304.

Mathew, G. & K.S.S. Nair (1983): The bagworm, *Pteroma plagiophleps* Hampson (Lepidoptera: Psychidae) spreads to the ornamental tree, *Delonix regia* (Boj.) Rafin. in Kerala, India. *Indian Journal of Forestry 6*: 240–241.

Mathew, G. & K.S.S. Nair (1986): Bagworms (Lepidoptera: Psychidae) of Kerala – Their potential as pests of tree crops. *Proc. Ill. Oriental Entomology Symposium 2*: 163–167.

Nair, K.S.S. & G. Mathew (1992): Biology, infestation characteristic and impact of the bagworm, *Pteroma plagiophleps* Hampson in forest plantations of *Paraserianthes falcataria*. *Entomon 11*: 1–13.

Rhainds, M., D.R. Davis & W.P. Peter (2009): Bionomics of bagworms (Lepidoptera: Psychidae). *Annual Review of Entomology 54*: 209–226.

Sobczyk, T. (2011): Psychidae (Lepidoptera) – *World Catalogue of Insects 10*. Apollo Books, Stenstrup, Denmark. 467 pp.

Thangavelu, S. & M.H. Ravindranath (1985): Morphology and life-history of the bag-worm moth *Clania cramerii* (Westwood). *Journal of Natural History 19(1)*: 1–19.

Usha, A.U. & J. Jose (2017): Host plant selection and utilization by *Eumeta crameri* (Lepidoptera: Psychidae) from non-cultivated human habitations of northern Kerala. Publishing Inc., Proceedings of 29th Kerala Science Congress. pp. 685–688.

Usha, A.U. & J. Jose (2018): First quantified report of first instar dispersal behaviour of the bagworm moth *Eumeta crameri* Westwood (Lepidoptera: Psychidae). *Proceedings of 42nd ESI Annual Conference and National Symposium*: pp. 32–33.

van Nieukerken, E.J., L. Kaila, I.J. Kitching, N.P. Kristensen, D.C. Lees, J. Minet, C. Mitter, M. Mutanen, J.C. Regier, T.J. Simonsen, N. Wahlberg, S.H. Yen, R. Zahiri, D. Adamski, J. Baixeras, D. Bartsch, B.A. Bengtsson, J.W. Brown, S.R. Bucheli, D.R. Davis, J. De Prins, W. De Prins, M.E. Epstein, P. Gentili-Poole, C. Gielis, P. Hättenschwiler, A. Hausmann, J.D. Holloway, A. Kallies, O. Karsholt, A.Y. Kawahara, S.J.C. Koster, M.V. Kozlov, J.D. Lafontaine, G. Lamas, J.F. Landry, S. Lee, M. Nuss, K.T. Park, C. Penz, J. Rota, A. Schintlmeister, B.C. Schmidt, J.C. Sohn, M.A. Solis, G.M. Tarmann, A.D. Warren, S. Weller, R.V. Yakovlev, V.M. Zolotuhin & A. Zwick (2011): Order Lepidoptera Linnaeus, 1758. *In*: Zhang, Z.Q. (Ed.): Animal Biodiversity: an outline of higher classification and survey of taxonomic richness. *Zootaxa (3148)*: 212–221.

Varma, R.V., K. Mohandas, G. Mathew & K.S.S. Nair (1989): Laboratory evaluation of some insecticides against *Pteroma plagiophleps* Hampson, a bagworm pest of *Albizia falcataria*. *Indian Journal of Plant Protection 18*: 89–90.

Recommended Citation

Usha, A.U., Joyce Jose, & T.J. Roby (2021): Distribution mapping and Host plant preferences of the Bagworm *Eumeta crameri* Westwood 1854 from Kerala, India. *J. Bombay Nat. Hist. Soc. 118*. doi: 10.17087/jbnhs/2021/v118/150537

■ ■ ■

PLANT SCIENCE TODAY
ISSN 2348-1900 (online)
Vol 9(sp1): 12–18
https://doi.org/10.14719/pst.1552

HORIZON
e-Publishing Group
HePG

RESEARCH ARTICLE

A comprehensive account on the genus *Hedychium* J. Koenig (Zingiberaceae) in south India

Sinjumol Thomas[1], S. John Britto[2] & Bince Mani[3*]

[1]Department of Botany, Carmel College, Mala, Thrissur 680 732, India
[2]The Rapinat Herbarium and Centre for Molecular Systematics, St. Joseph's College (Autonomous), Tiruchirappalli 620 002, India
[3]Department of Botany, St. Thomas College, Palai, Kottayam 686 574, India

*Email: binsnm@gmail.com

OPEN ACCESS

ARTICLE HISTORY

Received: 20 October 2021
Accepted: 29 December 2021

Available online
Version 1.0: 24 February 2022

Check for updates

Additional information

Peer review: Publisher thanks Sectional Editor and the other anonymous reviewers for their contribution to the peer review of this work.

Reprints & permissions information is available at https://horizonepublishing.com/journals/index.php/PST/open_access_policy

Publisher's Note: Horizon e-Publishing Group remains neutral with regard to jurisdictional claims in published maps and institutional affiliations.

Indexing: Plant Science Today, published by Horizon e-Publishing Group, is covered by Scopus, Web of Science, BIOSIS Previews, Clarivate Analytics, etc. See https://horizonepublishing.com/journals/index.php/PST/indexing_abstracting

CITE THIS ARTICLE

Thomas S, John Britto S, Mani B. A comprehensive account on the genus *Hedychium* J. Koenig (Zingiberaceae) in south India. Plant Science Today. 2022;9(sp1):12-18. https://doi.org/10.14719/pst.1552

Abstract

The genus *Hedychium* J. Koenig in south India is revised based on field investigations and herbarium analysis. Seven species and one variety are recognised, along with *H. flavum* J. Koenig found to be new distributional record. A brief history of the taxonomy of south Indian *Hedychium* along with diagnostic morphological characters are discussed. Photographs and details of distribution and conservation status are also presented. A comprehensive identification key to the species and variety is provided. The name *H. flavum* is lectotypified.

Keywords

Karnataka, Kerala, Western Ghats, Tamil Nadu, Taxonomy

Introduction

Hedychium J. Koenig, an economically, medicinally and horticulturally important genus, comprises about 80 species chiefly distributed in India, south China and Southeast Asia with some species extending to Australia (1–4). The genus was established on the basis of a single species, *H. coronarium* J. Koenig (5). This is considered to be the largest genus of Zingiberaceae in India with about 45 taxa, with the centre of distribution in the northeast states of India, whilst a few species are occurring in south India (3, 6).

An account on floristic wealth of south Indian region with description of *Hedychium* was published in 1839 by Graham (7). He reported five species such as *H. coronarium*, *H. flavum* Roxb., *H. angustifolium* Roxb., *H. sulphureum* Wall. and a novelty, *H. scaposum* Nimmo. Subsequently, Dalzell (8) treated the latter as *Monolophus scaposus* (Nimmo) Dalzell, followed by Bentham and Hooker (9) as *Kaempferia scaposa* (Nimmo) Benth. & Hook.f. and recently to *Curcuma scaposa* (Nimmo) Škorničk. & M.Sabu (10). Wight (11) described two new species of *Hedychium* from the Western Ghats, namely *H. cernuum* Wight and *H. venustum* Wight.

A remarkable floristic work in south India was published in early 20th century as "Flora of Presidency of Madras", wherein Fischer (12) treated three species of *Hedychium* from South India such as *H. coronarium*, *H. flavescens* Carey ex Roscoe and *H. venustum.*

Hedychium griffithianum Wall. had been merged with *H. venustum* based on the relative length of the stamen and the lip (13). Later, these two were (14) reinstated as distinct species and later it was confirmed by further studies (15).

Recently, reports (16–17) are on 5 species of *Hedychium*, including a

cultivated one (*H. coccineum* Buch.-Ham. ex Sm.), from south India. Further field explorations have resulted in the discovery of 2 new taxa and 2 new distributional records of *Hedychium* (3, 4, 18) from south India.

The present studies, based on study of herbarium specimens and literature and supplemented by extensive field observations, recognizes 6 species and 1 variety of *Hedychium* in peninsular India, namely *H. coronarium*, *H. flavescens*, *H. venustum*, *H. forrestii* Diels, *H. forrestii* var. *palaniense* Sanoj & M. Sabu, *H. matthewii* Sinj. Thomas, B. Mani & Britto and *H. spicatum* Sm. (3, 4, 18). The present investigation also attempts to solve the problems in the identification of some south Indian taxa. Moreover, we recognised *H. flavum* Roxb. as a new distributional record to this area.

Taxonomic treatment

Hedychium J. Koenig in Retz., Observ. Bot. 3: 73. 1783.

Type: *Hedychium coronarium* J. Koenig.

Key to the south Indian taxa

1. Bracts imbricate ……..……..……..…….... 2

   Bracts lax……..……..……..……..……4

2. Flowers yellow, stamen equal to or exceeding the labellum……..……..……..……..……..3

   Flowers white, stamen shorter than labellum ……..... ……..……..…..…..... *H. coronarium*

3. Flowers creamy yellow, stamens exceeding lip . ……....*H. flavescens*

   Flowers sulphur yellow, stamen equalling lip…..…….. ……..……..……..……*H. flavum*

4. Stamen white…..……..…….. 5

   Stamen red…….....……..…….. 6

5. Calyx shorter than bract, cincinnus 2–5-flowered……..…. ……..... *H. forrestii*

   Calyx equal/longer than bract, cincinnus strictly 3-flowered.....*H. forrestii* var. *palaniense*

6. Stamen shorter than labellum…..……7

   Stamen longer than labellum ……..…..….. *H. matthewii*

7. Stamen 'L'shaped, cincinnus strictly 1-flowered ……..... ……..……..……..……..…. *H. spicatum*

Stamen straight/arching, cincinnus 1–3-flowered…..……. ……..……. *H. venustum*

Enumeration of taxa

1. *Hedychium venustum* Wight, Icon. Pl. Ind. Orient. t. 2012. 1853.

= *Hedychium cernuum* Wight, Icon. Pl. Ind. Orient. t. 2011. 1853.

Perennial rhizomatous herb. Rhizome 3.0–6 cm wide, aromatic. Leaves 10–14 in number, sessile or slightly petiolate; lamina 37.0–50.0 × 12.5–15.5 cm, elliptic. Inflorescence 23.0–46.0 cm, upright or cernuous, dense; bracts 3.3–4.3 × 1.7–2.6 cm, ovate, lax, convolute, cincinnus 1–3 flowered; bracteoles 2.6–3.2 × 1.5–1.8 cm, tubular, entire or 2-toothed. Flower 11.2–14.0 cm, white or creamy white with red tinge at centre; calyx 4.3–5.8 cm, longer than bract, 3-toothed; corolla tube 6.3–9.1 cm, hairy internally, lobes yellow, drooping, dorsal lobe 4.4–5.2 × 0.7–0.8 cm, lateral lobe4.0–5.0 × 0.5–0.7 cm; lateral staminodes 4.4–5.9 × 0.3–0.8 cm, linear, white, red towards base; labellum 4.6–5.8 × 2.3–3.3 cm, obovate, white, clawed, apex split about 1.6–2.5 cm; stamen 3.8–4.6 cm, red, shorter than labellum, straight or slightly arching; filament red; anther red; ovary 3–5 × ca. 3 mm, barrel-shaped; epigynous glands oblong, orange, bifid at apex. Fruits globose; seeds red; aril red.

Phenology

Flowering: June - September; Fruiting: August - October.

Distribution

Hedychium venustum is an endemic species distributed in various parts of Kerala and Tamil Nadu at an elevations of 800–1500 m a.s.l. It grows as small populations on thin layer of soil over wet rocks in evergreen forest, wet and dripping rocks in grasslands and on banks of streams.

Notes

Hedychium venustum shows wide variations in morphology especially on the habit and floral characters. Plants growing in the lower altitudes (800–1200 m) often have slender leafy shoots, attaining a height only up to 1 m, whereas those in the higher altitudes (1200–1450 m) are robust forms and the leafy shoots attain a height up to 2 m. Similarly, the inflorescence of former is slender (Fig. 1A) whereas the latter is massive (Fig. 1B). Additionally, the length of the inflorescence, number of bracts per inflorescence, size of the bract and the size of the flowers are also different. The number of flowers per bract is often three in the robust form whereas it may range from one to three in slender low altitude forms. Additionally, fruiting is common in the former and often three fruits per bract are seen.

Specimens examined

India. Kerala: Idukki district, Peermedu, 09 Aug 2015, Thomas *et al*. 67229 (RHT); Idukki, 21 Oct 2014, *S.* Thomas *et al.* 66462 (RHT); Munnar, Thomas 67233 (RHT); Vazhikadavu, 23 Sept 2012, Thomas *et al.* 65149 (RHT); Trichur district, Sholayar, 15 Aug 2013, Thomas 65148 (RHT); Thiruvananthapuram district, Ponmudi, 26 Jul 2012, Thomas 65127 (RHT). Tamil Nadu: Valparai, 15 Aug 2013, Thomas 65187 (RHT).

2. *Hedychium coronarium* J. Koenig, Observ. Bot. (Retzius) 3: 73. 1783.

Perennial rhizomatous herb. Rhizome slightly aromatic, fleshy or fibrous. Leafy shoot 86–370 cm long, upright. Leaves sessile; lamina 26.0–60.0 × 7.5–14.3 cm, elliptic or narrowly oblong–lanceolate, pubescent below. Inflorescence 6.4–17.0 cm long, upright, compact; bracts 4.2–7.0 × 1.6–6.6 cm, ovate-elliptic or widely elliptic-orbicular, imbricate, cincinnus 1–4 flowered. Flowers 12.0–15.5 cm long, white; calyx 3.1–4.5 cm long, tubular, shorter

Fig. 1. Inflorescence of *Hedychium venustum* (**A–B**), *H. coronarium* (**C–D**), *H. flavescens* (**E**), *H. flavum* (**F**), *H. forrestii* (**G**), *H. forrestii* var. *palaniense* (**H**), *H. matthewii* (**I**) and *H. spicatum* (**J–K**)

than bract; corolla tube 8.2–9.6 cm long, lobes oblanceolate or narrowly oblong, white, dorsal lobe 4.2–5.5 × 1.0–1.5 cm, lateral lobes 4.0–4.8 × 0.8–1.5 cm; lateral staminodes 4.7–5.8 × 2.4–3.4 cm, elliptic or obovate, clawed, white; labellum 5.0–6.2 × 5.2–6.2 cm, orbicular, emarginated, white, clawed; stamen 4.2–5.4 cm long, shorter than labellum; filament white; anthers creamy white; ovary barrel shaped; epigynous glands 2, oblong, yellow. Fruits ovoid; seeds red, aril red.

Phenology

Flowering: July - January; however, some populations flower throughout the year. Fruiting: rare in wild populations.

Distribution

Native to Myanmar and widely distributed all over India. It is cultivated as ornamental throughout the tropics (19).

Notes

It is the most common species of *Hedychium* in the area and widely cultivated as an ornamental plant (Fig.1C). The wild plants are larger in size than garden varieties and are slightly fragrant. While sampling the specimens of *H. coronarium* from various parts of south India, the authors came across with a specimen having strobili-form spikes (Fig.1D). Detailed analysis shows that it differs from rest of the collections of *H. coronarium* by characters such as robust habit,

fibrous rhizome, pubescent and larger bracts and bracteoles, 3–4-flowered cincinnii, pubescent calyx and large flowers. Additionally, fruit development has so far not been observed in this population. In 2004, the Board of trustees of the Royal Botanic Gardens, Kew (20) treated a number of names under *H. coronarium*. Following their norms, even if those populations have the above mentioned variations, we treated it as *H. coronarium*.

Specimens examined

India. Kerala: Idukki district, Munnar, 13 Oct 2012, Thomas 65120 (RHT); Anayirankal, 13 Oct 2012, Thomas *et al*. 65129 (RHT); Tamil Nadu: Dindigul district, Kodaikanal, 12 Dec 2013, Britto & Thomas 65199 (RHT); Coimbatore district, Sholayar submergible area, Ramamoorthy 18120 (MH!); Valparai, 20 Oct 2013, Thomas 65186 (RHT). Karnataka: Kodagu district, Coorg, Sivarajan *s.n.* (CALI!).

3. *Hedychium flavescens* Carey ex Roscoe, Monandr. Pl. Scitam. t. 50. 1825.

Perennial rhizomatous herb. Rhizome slightly aromatic. Leafy shoot robust. Leaves sessile; lamina elliptic–oblanceolate, pubescent on abaxial surface. Inflorescence 10–18 cm long, moderately lax; bracts 6.2–6.5 × 3.0–3.8 cm, ovate, often imbricate, cincinnus 3–5 flowered; Flowers 14.0–15.5 cm long, lemon yellow; calyx 3.9–4.3 cm, yellow; corolla tube 8.2–8.9 cm long, yellow, lobes oblanceolate, yellow; lateral staminodes 5.0–5.2 × 1.7–1.9 cm, elliptic, yellow, reflexed back; labellum 5.0–5.2 × 4.0–4.6 cm, obovate, yellow, reflexed back on upper half, deeply emarginated, clawed; stamen yellow, longer than labellum, filament yellow, straight, anther elliptic; ovary barrel shaped,; epigynous glands 2, oblong, orange.

Phenology

Flowering: August–November; Fruiting: Not observed.

Distribution

Hedychium flavescens (Fig.1E) is found in all south Indian states of Kerala, Karnataka, Andhra Pradesh, Telangana and Tamil Nadu. This species shows a narrow range of distribution in Karnataka, Andhra Pradesh and Telangana.

Notes

It may be reproductively isolated from other species of *Hedychium* because of the absence of fruit set.

Specimens examined

India. Kerala: Idukki district, Munnar, 13 Oct 2012, Thomas 65130 (RHT); Gavi, 25 Sept 2013, Thomas 65133 (RHT); Tamil Nadu: Dindigul district, Kodaikanal, near Silver Cascade, 12 Dec 2013, Britto & Thomas 65198 (RHT); Maharashtra: Kohlapur, Tillari, 5 Oct 2006, Malpure 7 (SUK); Andhra Pradesh: East Godavari district: Dummakonda R.F., 28 Sep 1980, Subba Rao 68626 (MH); Visakapatnam district, Cherukanda, 29 Aug 1966, Subba Rao 28192 (MH); Karnataka: Kodagu district, Mercara, 25 May 1976, Sivadasan 17533 (CALI!).

4. *Hedychium flavum* Roxb., Fl. Ind. 1: 81. 1820.

Type (lectotype, designated here): India orientalis (possibly Calcutta Botanic Garden), *Roxburgh s.n.* (BM000958140, digital image!). Additional original material: [unpubl. icon] *Icones Roxburghianae*, No. 2153 (CAL, digital image!, copy at K, digital image!).

Table 1. Comparison of diagnostic characters of *H. flavescens* and *H. flavum*

Characters	*H. flavescens*	*H. flavum*
Inflorescence	Compact to lax flowered, cylindrical	Compact, cone-like
Bracts	Imbricate to non-imbricate, hairs golden-yellow	Imbricate, hairs hyaline
Cincinnus	3–5 flowered	3–4 flowered
Flowers	Creamy yellow	Sulphur yellow
Length of the corolla tube	8.2–8.9 cm	6.0–6.8 cm
Cleft of the labellum	ca. 1.5 cm deep	<5 mm deep
Length of the stamen	5.2–5.8 cm, exceeding the labellum	4.0–4.2 cm, equal to the labellum
Anther attachment	At 45˚ angle	Parallel to filament
Ovary	Densely pubescent, hairs golden-yellow	Moderately pubescent, hairs hyaline

Perennial rhizomatous herb. Rhizome slightly aromatic. Leafy shoot robust. Leaves sessile; lamina elliptic-oblanceolate, pubescent below. Inflorescence 12–22 cm, compact; bracts imbricate, orbicular–ovate, cincinnus 3–4 flowered. Flowers 11.2–12.5 cm, sulphur yellow; calyx 3.8–4.1 cm, yellow; corolla tube 6.0–6.8 cm, yellow; lobes oblanceolate, yellow; lateral staminodes 3.3–3.5 × 1.0–1.2 cm, elliptic, sulphur yellow, reflexed back; labellum 3.5–3.8 × 2.7–3.0 cm, obovate, sulphur yellow, clawed at base, apex rounded, 4–5 mm emarginated; stamen equal to the labellum, sulphur yellow; filament yellow, straight; anther elliptic; ovary barrel shaped; epigynous glands 2, oblong, orange.

Phenology

Flowering: profusely in September–December and it lasts up to February. Fruiting: So far not observed.

Distribution

India, Thailand, China, Bangladesh and Myanmar. In India it is common in North-East region. Presently, this taxon is reported from south India (Tamil Nadu).

Notes

Roxburgh (21) described *H. flavum* along with admirable illustrations. However, this species has been wrongly treated by various authors (22, 23). *Hedychium flavum* was described on the basis of plants cultivated in the Calcutta Botanic Garden grown from seeds obtained from Sylhet in Bangladesh received from Mr. M. R. Smith in 1810 (24). It was illustrated by him in his unpublished *Flora Indica* drawings (available at CAL and K). In addition, a specimen col-

lected by Roxburgh could be traced out at BM. These drawings and specimen represent the uncited original material of the name. Although, an uncited drawing as well as specimen have equal priority in lectotype designation as per Art. 9.2 of *ICN* (25), we are selecting herewith the well preserved flowering specimens at BM as the lectotype of the name.

Graham (7) reported *H. flavum* in Parell garden, Bombay. However, it was introduced from Bengal, as noted by him it in the publication. During the expedition in Western Ghats, it was by accident that a few populations of *Hedychium* growing in Nilgiris possessing characteristics similar to *H. flavum* were seen (Fig. 1F). Upon careful scrutiny, it is authenticated as *H. flavum* (Table 1). Consequently, it forms the first valid report of this species from south India.

Specimens examined

India. Tamil Nadu: Nilgiri district, Nilgiris, 22 Dec 2012, Thomas 65139 (RHT).

5. *Hedychium forrestii* Diels, Notes Roy. Bot. Gard. Edinburgh 5: 304. 1912.

Rhizomatous perennial herb; rhizome aromatic. Leafy shoot robust; lamina sessile, narrowly elliptic, sparsely hairy below. Inflorescence 16–24 cm long, lax, erect; bracts lance-ovate, lax, cincinnus 2–4 flowered; Flowers 12.4–13.2 cm long, white; calyx 3.7–4.1 cm long, shorter than bract; floral tube 6.5–6.8 cm long, white; corolla lobes linear, white; lateral staminodes, oblanceolate to obovate, white, reflexed back; labellum orbicular, clawed, shallowly emarginated; stamen white, exceeding the labellum; ovary puberulous; epigynous glands two, oblong, yellow. Fruits terete; seeds red, aril red.

Phenology

Flowering: August–October; Fruiting: October–December.

Distribution

It grows on thin soil over exposed wet rocks in evergreen montane forests and marshes in grasslands at an elevation of 950–1200 m. In south India, it is reported from Idukki and Thrissur districts of Kerala and Nilgiris in Tamil Nadu.

Notes

When compared with *H. coronarium, H. forrestii* could be distinguished by its lax spikes (Fig.1G), closely convolute bracts, stamen exceeding the lip and oblong–cylindric capsules.

Specimens examined

China. 1908, Cavalerie 00211021 (E); 1912 Forrest 00211015 (E). NEPAL. 1821, Wallich 000574704 (BM). India. Kerala: Thrissur, Sholayar, 15 Aug 2013, Thomas *et al*. 65146 (RHT); Idukki, Nellippara slopes, 07 Feb 1981, Nair 70106 (MH); 28 July 2013 Thomas *et al*. 65490 (RHT!); Tamil Nadu: Nilgiri district, Kailas Pillai Estate to Sirur (near Ebanad), Subba Rao 36524 (MH).

6. *Hedychium forrestii* Diels var. ***palaniense*** Sanoj & M. Sabu, J. Bot. Res. Inst. Texas 4: 633–639. 2010.

Perennial rhizomatous herb. Rhizome slightly aromatic. Leaves sessile; lamina elliptic, puberulent below. Inflorescence 16.5–29.2 cm, lax, upright; bracts lanceolate, convolute, cincinnus ca. 3 flowered. Flowers 15.0–15.2 cm, white; calyx 3-toothed at apex; corolla tube 9.2–9.4 cm long, white; lobes oblong, white; lateral staminodes 4.1–4.4 × 1.9–2.0 cm, elliptic, white, reflexed back; labellum 4.3–4.6 × 4.0–4.2 cm, ovate, white, clawed at base, 1.9–2.1 cm emarginated at apex; stamen longer than labellum, white; ovary barrel-shaped; epigynous glands two, oblong, yellow. Fruits three-angled; seeds red, aril red.

Phenology

Flowers: June–November; Fruiting: starts September onwards.

Distribution

Hedychium forrestii var. *palaniense* is a narrow endemic reported only from Palni Hills, Tamil Nadu at an altitudinal range of 1300–1600 m.

Notes

Matthew, Charles and Rajendran (RHT*46992*) collected this specimen from the Palni hills in 1986 and were able to distinguish it from other south Indian species of *Hedychium*, but not to identify it as *H*. *forrestii*. Subsequently, this plant had been collected from the same locality and described it as *H. forrestii* var*. palaniense* (18) (Fig.1 H). It differs from *H. forrestii* var. *forrestii* in having longer flowers and corolla tube (9.2–9.4 cm) and calyx equal or slightly longer than bracts (18).

Specimens examined

India. Tamil Nadu: Dindigul district, Vadakavungi, Palar Dam view, 12 Dec 2013, Thomas & Britto 65200 (RHT); Kodaikanal, Palani Ghat Road between Perumal Malai and Vadakavunchi, 23 Sept 1986, Matthew, Charles and Rajendran 46992 (RHT, E).

7. *Hedychium matthewii* Sinj. Thomas, B. Mani & Britto, Webbia 70: 221. 2015.

Rhizomatous perennial herb. Leafy shoot robust; lamina sessile, narrowly oblong to narrowly elliptic, abaxial side pubescent. Inflorescence lax, upright; bracts narrowly elliptic, involute, cincinnus 1–3 flowered. Flowers 13–15.3 cm long, spreading; calyx 4.5–6.1 cm long, tubular; floral tube 6 –8 cm long, pale yellow; corolla lobes linear, pale yellow; lateral staminodes linear, white, pale yellow–red tinged towards base; labellum spathulate, clawed, apex rhombic, white; stamen 7.1–7.8 cm long, bright red, exceeding labellum; ovary barrel-shaped; epigynous glands two, narrowly cylindrical, orange. Fruits terete; seeds red, aril red.

Phenology

Flowering: August - September; Fruiting: September - November.

Distribution

Hedychium matthewii shows a narrow range of distribution and reported only from Kerala (Idukki and Thrissur). It occurs as small populations in thin soil over rocky slopes of moist evergreen forests at elevations of 1150–1230 m. This species is assessed as Critically Endangered (3, 26).

Notes

This is the only species with very long stamen among the different species reported from the peninsular India (Fig. 1I).

8. *Hedychium spicatum* Sm., Cycl. 17: 8. 1811.

Perennial rhizomatous herbs; rhizome aromatic. Leafy shoot slender; lamina sessile, narrowly elliptic to lanceolate. Inflorescence 12–32 cm, lax; bracts 2.6–4.7 × 0.9–1.5 cm, subulate, lax, cincinnus strictly 1–flowered. Flowers 10.6–12 cm long, spreading; calyx 3.4–3.6 cm long, tubular; floral tube 5.3–5.6 cm long, pale yellow; corolla lobes linear, yellow; lateral staminodes 4.6–5.1 × ca. 0.3 cm, linear, creamy white, red tinged towards base; labellum obovate, pale red, clawed, apex obovate, creamy white, deeply clefted with incision 2–3.7 cm; stamen red, shorter than labellum, bent at middle; ovary glabrous; epigynous glands two, oblong, yellow, bifid. Fruits sub-globose; seeds red, aril red.

Phenology

Flowering: Starts on end of June - August. Fruiting: July–September.

Distribution

It is reported from south India from moist and shady places under shola forests at an altitude of 1500–1600 m in Idukki, Kerala. These populations are under extreme decline due to habitat loss.

Notes

Hedychium spicatum shows ample distribution in the North-eastern parts of India, but shows only a narrow range of distribution in the southern parts of India. *Hedychium venustum* has been occasionally misidentified as *H. spicatum*. However, *H. spicatum* (Fig. 1J) could easily be distinguished from *H. venustum* by its slender habit, strictly 1–flowered cincinnii, sessile leaves, narrow labellum, shorter and bent stamen and spurred thecae (4). During the present investigation the authors met with an interesting specimen from Old Devikulam, Idukki characterised by flowers with tripartite and non-clawed labellum, subulate and short bracts, non-tubular and short bracteoles and apically hairy calyx tube. At the same time, it is related to *H. spicatum* in all other features. Therefore, we treating it as a variant form of *H. spicatum* (Fig. 1K).

Specimens examined

Nepal. 1819, Wallich 000574705 (BM); 1819, Wallich 000574708 (BM). INDIA. Sikkim: 1887, Hooker 72407 (MH); Khasia, 1887, Hooker 72408 (MH); Kerala: Munnar 16 July 2012 Thomas *et al*. 65121 (RHT); Old Devikulam, 04 Aug2013, Thomas *et al*. 65488 (RHT).

Acknowledgements

We are grateful to Principal Chief Conservator of Forests (Wildlife) & Chief Wildlife Warden, Kerala Forest Department for granting research permission. The authors are indebted to curators of CAL, MH, CALI, K, E, BM, and P for their kind approval of consultation of their herbaria.

Authors contributions

All authors contributed equally to the work.

Compliance with ethical standards

Conflict of interest: No potential conflict of interest was reported by the authors.

Ethical issues: None.

References

1. Sirirugsa P, Larsen K. The genus *Hedychium* (Zingiberaceae) in Thailand. Nordic J Bot. 1995;15:301–04.https://doi.org/10.1111/j.1756-1051.1995.tb00156.x
2. Wu TL. Zingiberaceae. In: Wu ZY, Raven PH, Hong DY editors. Flora of China. Vol.24. Beijing: Science Press & St. Louis: Missouri Botanical Garden Press; 2000. p. 322–77.
3. Thomas S, Mani B, Britto SJ. A new species of *Hedychium* (Zingiberaceae) from the southern Western Ghats, India. Webbia. 2015; 70: 221–25. https://doi.org/10.1080/00837792.2015.1082270
4. Thomas S, Britto SJ, Mani B. First records of two ginger Lilys *Hedychium* (Zingiberaceae) species from the Western Ghats, India. J Threat Taxa. 2017;9:10914–19. https://doi.org/10.11609/jott.3117.9.11.10914-10919
5. Koenig JG. Descriptiones monandrarum et epidendrorum in India Orientali factae. In: Retzius AJ, editor. Observationes Botanicae, Vol. 3. Lipsiae; 1783. p. 73–74.
6. Thomas S. Classical and Molecular Taxonomy and Systematics in *Hedychium* from the Western Ghats [Ph. D thesis]. Tamilnadu: Bharathidasan University, Tiruchirappalli; 2015.
7. Graham JA. Catalogue of the plants growing in Bombay and its vicinity. Bombay: Government Press; 1839.
8. Dalzell NA. Contributions to the Botany of Western India. Hooker's J Bot Kew Gard Misc.1850; 2:143. https://www.biodiversitylibrary.org/page/776587#page/149/mode/1up
9. Bentham G, Hooker J D. Genera plantarum. Vol. 3(2). Londini: A. Black; 1883. https://www.biodiversitylibrary.org/page/656183#page/203/mode/1up
10. Leong-Škorničková J, Šída O, Jarolímová V, Sabu M, Fér T, Trávníček P, Suda J. Chromosome Numbers and Genome Size Variation in Indian Species of *Curcuma* (Zingiberaceae). Ann Bot. 2007;100:505–26. https://doi.org/10.1093/aob/mcm144
11. Wight R. Icones plantarum Indiae Orientalis. Vol. 6. Madras: J.B. Pharoah; 1853.
12. Fischer CEC. Zingiberaceae. In: Gamble JS (editor). Flora of the Presidency of Madras. Vol. 3. London: Bishen Singh Mahendra Pal Singh; 1928. p. 1478–93.
13. Naik VN, Panigrahi G. Genus *Hedychium* in eastern India. Bull Bot Surv India. 1961; 3: 67–73.
14. Rao AS, Verma DM. Notes on *Hedychium* Koenig, including four new species from Khasi and Jaintia Hills, Assam. Bull Bot Surv India. 1971;11:120–28.
15. Sanoj E. Taxonomic revision of the genus *Hedychium* J. Koenig (Zingiberaceae) in India [Ph. D thesis]. Kerala: University of Calicut; 2011.
16. Sabu M. *Hedychium spicatum* Ham. ex Smith var. *acuminatum* (Roscoe) Wall. A new record for Peninsular India. Rheedea. 2000;10:73–76. http://www.iaat.org.in/images/journalprev/2000/1/73-76.pdf
17. Sabu M. Zingiberaceae and Costaceae of South India. Indian

Association for Angiosperm Taxonomy; 2006.

18. Sanoj E, Sabu M, Rajeshkumar T. *Hedychium forrestii* (Zingiberaceae) with a new synonymy and a variety from India. J Bot Res Inst Texas. 2010;4:633–39. https://www.jstor.org/stable/41972085

19. Larsen K, Lock JM, Mass H, Maas PJM. Zingiberaceae. In: Kubitzki K, editor. The families and genera of vascular plants. Vol. 4. Berlin: Springer; 1998.p.474–95. https://doi.org/10.1007/978-3-662-03531-3_49

20. Govaerts R. World Checklist of Monocotyledons Database in ACCESS: 1–54382.London: The Board of Trustees of the Royal Botanic Gardens, Kew; 2004. Available from: http://apps.kew.org/wcsp/nonacceptedRef.do?name_id=248176.

21. Roxburgh W. Flora Indica or Descriptions of Indian plants. Serampore: Mission Press; 1820.

22. Loddiges C. *Hedychium urophyllum*. The Botanical Cabinet. Vol. 18. London: John & Amp; 1832.

23. Baker JG. Scitamineae. In: Hooker JD. (editor). Flora of British India. Vol. 6. London: L. Reeve & Co.;1890–1892. p.198–264.

24. Roxburgh W. Hortus bengalensis, or a catalogue of the plants growing in the honourable East India Company's Botanic Garden at Calcutta. Serampore: Mission Press; 1814.

25. Turland NJ, Wiersema JH, Barrie FR, Greuter W, Hawksworth DL, Herendeen PS, Knapp S, Kusber W-H, Li D-Z, Marhold K, May TW, McNeill J, Monro AM, Prado J, Price MJ, Smith GF (editors). International Code of Nomenclature for algae, fungi, and plants (Shenzhen Code) adopted by the Nineteenth International Botanical Congress Shenzhen, China, July 2017. Regnum Vegetabile 159. Glashütten: Koeltz Botanical Books; 2018. https://doi.org/10.12705/Code.2018

26. IUCN Standards and Petitions Subcommittee. Guidelines for using the IUCN red list categories and criteria, ver. 12. – IUCN Species Survival Commission; 2016. Available from: http://www.iucnredlist.org/documents/RedListGuidelines.pdf

§§§

Journal for Studies in Management and Planning
(*Peer Reviewed Journal*)

ISSN: 2395-0463
Volume 07 Issue 06
June 2021

Role of Extraversion Personality on Mutual Investment Decision

Celin K A[1], Revathy A R[2], Nayana P[3]

[1,2] Assistant Professor, Department of Commerce, Carmel College Mala
[3] Assistant professor, Department of Business Adminstration, Carmel College Mala

Abstract:

Behavioural finance assumes that characteristics of market participants and information structure systematically have an influence on individuals' investment decisions. This research paper aims at identifying the factors that influences the individual investor behaviour. Data collection is made with the help of structured questionnaires. Investment decisions have gained importance due to the general increase in employment opportunities and economic development of a nation. Mutual Funds provide a platform for a common investor to participate in the Indian capital market with professional fund management irrespective of the amount invested. The Indian mutual fund industry is growing rapidly and this is reflected in the increase in Assets under management of various fund houses. Mutual fund investment is less risky than directly investing in stocks and is therefore a safer option for risk averse investors. The main purpose of the study is to identify the role of extraversion personality affects the relationship between personality traits and investment management. However, in case of Long run Risk behaviour partially mediates the relationship of "Extraversion", "Agreeableness", "Openness to Experience", and "Conscientious".

Keywords: Mutual Fund, Investors, awareness, knowledge, Returns & Risk, Big Five Personality Traits, Extraversion

Introduction:

Investment is one of the foremost concerns of every individual investor as their small savings of today are to meet the expenses of tomorrow. Every individual investor possesses different mindset when they decide about investing in a particular investment avenue such as stocks, bonds, mutual funds, fixed deposit, real estate, bullion etc. In each life cycle stage, every individual desire his hard-earned money to be invested in most secure and liquid avenue. However, the decision varies for every individual depending on their risk-taking ability and the purpose for which such investment is to be done. Purpose of investment can be related with

ISSN: 2395-0463
Volume 07 Issue 06
June 2021

saving objective. Each individual investor selects the investment option for certain time period looking at their personal financial goals. Investment behaviour of an individual investor reveals how he/she wants to allocate the surplus financial resources to various instruments for investment available. The investment behaviour consists of why they want to invest, how much of their disposable income they want to invest, for how many years/months they want to invest and most importantly the timing of such investment. In various empirical studies, it has been found that information being an important factor on taking decision to invest, which influences them on choice of investment and later on how they act after investment (Kasilingam & Jayabal, 2008). The study was conducted mainly to know about the individual investor's perception towards the deciding on the objective for which they save money for future. In every life cycle stage, saving objective by an individual always changes. Such a change occurs not only due to the age of the investors, but also due to the occupation and income level category, where they fall.

Savings and investments play a major role in economic development of any country and the primary objective of all government's policy has been to promote savings and capital formation in the economy which is a primary instrument of economic growth. Personal Savings in India is attributed to growth in income of individuals and the rising rate of inflation. The role and importance of individual investors and their trading behaviour in Indian financial market is also imperative. Expected utility theory views, individual investment decision as a trade-off between immediate consumption and deferred consumption. But individuals do not always prefer according to classical theory of economics. Recent studies on individual investor behaviour have shown that they do not act in a rational manner, rather than several factors influences their investment decision. The purpose of this study is to analyse the determinants of individual investor's behaviour in Indian financial market.

The Indian Mutual fund industry has witnessed considerable growth since its inception in 1963. The impressive growth in the Indian Mutual fund industry in recent years can largely be attributed to various factors such as rising household savings, comprehensive regulatory framework, favourable tax policies, and introduction of several new products, investor education campaign and role of distributors.

The concept of Mutual funds has been on the financial landscape for long in a primitive form. The story of mutual fund industry in India started in 1963 with the formation of Unit Trust of India at the initiative of the Government of India and Reserve Bank. The launching

ISSN: 2395-0463
Volume 07 Issue 06
June 2021

of innovative schemes in India has been rather slow due to prevailing investment psychology and infrastructural inadequacies. Risk averse investors are interested in schemes with tolerable capital risk and return over bank deposit, which has restricted the launching of more risky products in the Indian Capital market. But this objective of the Mutual Fund industry has changed over the decades. For many years funds were more of a service than a product, the service being professional money management. In the last 15 years Mutual funds have evolved to be a product. A competent fund manager should analyse investor behaviour and understand their needs and expectations, to gear up the performance to meet investor requirements. It is the time for mutual fund companies to understand the fund selection/ switching behaviour of the investors' and to design the fund schemes according to the changing needs of consumer, otherwise survival of funds will be difficult in future. The present study made efforts in this regard to suggest ways to penetrate this mode of investment deep in Indian society it also provides the information that what present investor expects.

Mutual Funds have become a widely popular and effective way for investors to participate in financial markets in an easy, low-cost fashion, while muting risk characteristics by spreading the investment across different types of securities, also known as diversification. It can play a central role in an individual's investment strategy. They offer the potential for capital growth and income through investment performance, dividends and distributions under the guidance of a portfolio manager who makes investment decisions on behalf of mutual fund unit holders. Over the past decade, mutual funds have increasingly become the investor's vehicle of choice for long-term investment. It becomes pertinent to study the performance of the mutual fund. The relation between risk-return determines the performance of a mutual fund scheme. As risk is commensurate with return, therefore, providing maximum return on the investment made within the acceptable associated risk level helps in segregating the better performers from the laggards. Many asset management companies are working in India, so it is necessary to study the performance of it which may be useful for the investors to select the right mutual fund.

In the big 5 theory of personality, extroversion (often known as extraversion) is one of the five core traits believed to make up human personality. Extroversion is characterized by sociability, talkativeness, assertiveness, and excitability.

People who are high in extroversion tend to seek out social stimulation and opportunities to engage with others. These individuals are often described as being full of life, energy, and

ISSN: 2395-0463
Volume 07 Issue 06
June 2021

positivity. In group situations, extroverts (extraverts) are likely to talk often and assert themselves.

Extraversion and Investment Intention

An Extraversion is "active, optimistic, excitement seeking and tend to socialize in large crowd" (Leary, Reilly, & Brown, 2009; McCrae & Costa J, 1997). Pan and Statman (2013) revealed "extraversion deliberate only positive information, which influences their assessment of the probability of success and instigated overconfidence in financial decision making". Mayfield et al. (2008) directed a study among business school undergraduates and revealed that extraversion trade frequently and tend to invest their more money in stock market. Furthermore, he finds negative association between extraversion and risk aversion. Another study who examine the association between personality traits and financial decision making of household, finds that "extroversion is associated with unsecured debts and financial assets" (Brown & Taylor, 2014). R. B. Durand et al. (2008) in his study divulged that" individuals with higher degrees of extraversion appear to take more risk to achieve higher returns".

Literature Review:

Lenard et. al. (2003) empirically investigated investor"s attitudes toward mutual funds. The results indicate that the decision to switch funds within a fund family is affected by investor"s attitude towards risk, current asset allocation, investment losses, investment mix, capital base of the fund age, initial fund performance, investment mix, fund and portfolio diversification. The study reported that these factors are crucial to be considered before switching funds regardless of whether they invest in non-employer plans or in both employer and non-employer plans. Ronald T. Wilcox (2003) examined how investors choose a mutual fund and found that investors pay a great attention to past performance and also indicated that the educated investors demonstrated greater knowledge of basic finance made poorer, not better, decisions than their less financially savvy. Paula A. Tkac (2004) found that investors are irrational or in some other sense cannot look out for their own best interests. Mutual fund industry provides a variety of products and price structures to heterogeneous consumer preferences and budgets. Consumer who prefer more style, features or power willingly pay higher prices and the investor rely on and pay to the financial advisors or brokers for processing and formulating guidance regarding fund allocation. They are facing risk because of misconduct by advisory firms. They are not demanding any disclosures of their fund. The risks reduced to zero if investors are

ISSN: 2395-0463
Volume 07 Issue 06
June 2021

willing to pay with their own time and energy to monitor their fund position. J.Lilly and DrAnasuya (2014) published a research paper "An empirical study of performance evaluation of selected ELSS mutual fund schemes" which examined the performance of 49 selected tax saving elss schemes by applying Sharpe ratio, Treynor ratio, Sortino ratio and Jensen's alpha measure and found out LIC NOMURA MF GROWTH and dividend schemes has the highest return and are risk borne when compared to other schemes. Sadiq and Ishaq (2014) conducted a study to examine the effect of demographic factors on investors level of risk tolerance on the choice of investment with 100 investors from two cities of Pakistan. Results of their study indicated that demographic factors of investors: academic education, income level, investment knowledge and investment experience effect the investors level of risk tolerance. Further, study revealed that gender, marital status, occupation and family size did not show any effect on investment level of risk tolerance. There is another study carried out to examine the impact of demographical factors on investment decision on Vietnam Stock Market by Ton and Nguyen in 2014. Results of their study made known that the demographic factors (gender, age and marital status) influenced on the decision making of investors on Vietnam Stock Market. Rosemary and Bitrus (2016) conducted a study with the aim to identify the fundamental factors influencing individual investors in the shares of Nigerian capital market. Primary data was collected from 130 individuals using structured questionnaires. Study identified the followings influencing factors on individual investors decision making: past performance, expected bonus issue, growth potential, future dividend and the profitability of the company. Chavali and Mohanraj (2016) studied to examine the impact of demographic variables and risk tolerance on investment decisions in India. 110 investors participated in the survey and data was collected using questionnaires. The study found that gender had an impact on the investment pattern and decision making of respondents. Perera (2016) examined the influence of investor's gender attitudes on investor behaviour in Colombo Stock Exchange. The Outcome of the study revealed that individual's gender differences significantly influenced on cognitive factors, emotional factors and herding factors. Also study found that there was a strong correlation among the investor's demographic factors, market factors, risk bearing capacity, lifestyle characteristics and behaviour. The accurate measurement of risk tolerance in an investment portfolio proves to be a difficult task (Kannadhasan, Aramvalarthan, Mitra, Goyal, 2016). However, the various factors, influencing risk tolerance, aid in overcoming said difficulties. Risk tolerance is influenced by a variety of factors, including, but not limited to demographic variables, financial well-being, life satisfaction as well as personality traits. Other factors

ISSN: 2395-0463
Volume 07 Issue 06
June 2021

include environmental and economic factors (Kannadhasan et al., 2016). Caspi, Roberts, Shiner (2005) suggest that an individual's level of risk tolerance is more stable over time than their personality traits. Furthermore, Kannadhasan et al. (2016) argue that an investor's personality traits heavily influence his decision-making processes. The five main personality traits according to the five-factor model are (i) neuroticism, (ii) extraversion, (iii) openness to experience, (iv) agreeableness, and (v) conscientiousness (Cooper, 2003; Rothmann & Coetzer, 2003; Vazifehdoost et al., 2012). Mayfield, Perdue, & Wooten (2008) found in their study that personality traits have a strong association with investment management. They found that neuroticism has no impact on investment management while people with extraversion and openness to experience traits are involved in both short term and long term investment intentions. They argued that anxious individuals feel more insecure, so it is possible that they would be less preferred to engage in shortterm investing. Conversely, optimistic and outgoing people can involve in both short term and long term investment intentions. Personality traits are determinants of investors' behavior (Baik, Kang, & Kim 2010; Akhtar & Batool 2012; and M. Moradi et al. 2013). They studied that some personality traits have strong association with both short-term and long-term investment and some have are associated with either short-term or long-term investment intentions.

Objectives:

1. To analyze the demographic variables of the mutual fund investors.
2. To find out the relationship between the risk acceptance and occupation level of extraversion personality investors.
3. To evaluate the awareness level about the mutual fund among investors
4. To know the relationship between occupation of investors and the time holding of investment in mutual fund

Research Methodology:

The basic design of survey instrument consists of structured questionnaires. It is so designed to collect all required information from investors of mutual funds. Based on their knowledge, information source and investment decision factors related to their selection of a particular scheme fund. Descriptive type of research was used for this study. Data used for the research has been collected from primary and secondary sources. Percentage analysis, Graphical Representation and Hypothetical test were used for data analysis.

ISSN: 2395-0463
Volume 07 Issue 06
June 2021

Data Analysis and Interpretation:

Table 1

Demographic Variable		**Frequency**	**Percentage**
Gender	Male	100	100
	Female	0	0
Occupation	Private job	32	32.0
	Government job	50	50.0
	Retired	18	18.0
Educational Qualification	ITI	39	39.0
	SSLC	30	30.0
	Degree	7	7.0
	Post Graduate	24	24.0
Marital Status	Married	92	92.0
	Unmarried	8	8.0

Source: Primary Data

Interpretation:

a) Gender

From table 1 it is clear that, all the respondents (100%) are males.

b) Occupation

From the above table 1, it depicts that most of the respondents are government employees i.e., 50%. 32% of the employees fall under the private job. Only 18% of them are retired.

c) Educational Qualification

From the above table 1, educational qualification of the employees reveals that 7% of the respondents have only taken degree. Most of the employees (39%) are qualified with ITI. 30% of employees just have the basic qualification. 24% of the employees have post graduation qualification.

d) Marital Status

ISSN: 2395-0463
Volume 07 Issue 06
June 2021

From the above table 1, it is clear that 92% of the employees are married and only 8% employees are unmarried.

- **Relation between risk acceptance and investor's occupation**

To know whether there is significant difference in the risk acceptance with different occupation the following hypothesis are framed:

H_0 : There is no significant difference in the risk acceptance with different occupation

H_1 : There is significant difference in the risk acceptance with different occupation

These hypotheses are tested using one way ANOVA and the result is exhibited in the table below.

Mean, F value and P value of different occupation

Table 2

Experience	**N**	**Mean**	**F value**	**P value**
Private job	32	88.8167	1.301	0.277
Government job	50	88.8307		
Retired	18	90.0296		
Total	100	89.0420		

P value is greater than 0.05 thus there exist no significant difference in the mean of risk acceptance with different occupation and thus accepted the null hypothesis.

- *Awareness level about mutual funds*

Hypothesis 1:-

Ho – There is no significant difference between the investors' age and the awareness about mutual fund.

ISSN: 2395-0463
Volume 07 Issue 06
June 2021

H1 – There is significant difference between the investors' age and the awareness about mutual fund.

Table No 3

The Investors' Age And Awareness About Mutual Fund.

ONE WAY ANOVA TEST				
	Sum of squares	Degree of freedom	Mean square	F
Between Groups	0.985	3.00	0.328	1.316
Within Groups	73.895	296.00	0.250	
Total	74.880	299		
SIGNIFICANT VALUE: 0.541				

Inference:-

The above table communicates the result with regarding to the calculated value of "F" test. The calculated "F" value is less than the tabulated value at 5% level of significance for v1 = 3, and V2 = 296 degrees of freedom. Hence, the null hypothesis is rejected and alternative hypothesis is accepted. It is proven from the analysis that there is a significant difference between the age of the respondents and awareness about mutual fund

Hypothesis 2:-

Ho – There is no significant difference between the investors' income group and the knowledge level about mutual fund.

H1 – There is significant difference between the investors' income group and the knowledge level about mutual fund.

Table No 4:

Income group and the knowledge level about mutual fund.

ISSN: 2395-0463
Volume 07 Issue 06
June 2021

ONE WAY ANOVA TEST				
	Sum of squares	Degree of freedom	Mean square	F
Between Groups	0.54	3.00	0.181	0.72
Within Groups	74.34	296.00	0.251	
Total	74.880	299		
SIGNIFICANT VALUE: 0.269				

The above table communicates the result with regarding to the calculated value of "F" test. The calculated "F" value is less than the tabulated value at 5% level of significance for v1 = 3, and V2 = 296 degrees of freedom. Hence, the null hypothesis is accepted and alternative hypothesis is rejected. There is a least significant difference between the means of the income group of investors and the awareness level.

- *Relationship between occupation of investors and the time holding of investment in mutual fund*

Table 5

Time of holding investments

Particulars	**Frequency**	**Percentage**	**Cumulative percentage**
Less than 1 year	50	13.8	13.8
1 – 3 Years	201	55.4	69.1
4 – 6 years	76	20.9	90.1
7 – 9 years	28	7.7	97.8
More than 10 Years	8	2.2	100.0
Total	363	100	

ISSN: 2395-0463
Volume 07 Issue 06
June 2021

As the tests revels that 69.1% investor prefer to hold the investment in mutual fund for one – three year period, 20.9% for four – six year period. So it can be concluded that about 90% investor hold their investment for not less than six years.

Table 6

Correlation between Time of holding Investment and Occupation of Investors

		Time of holding Investment	Occupation
Time of holding Investment	Pearson Correlation	1.000	0.313
	Sig. (2-tailed)	-	0.000
	N	363	363
Occupation	Pearson Correlation	.313	1.000
	Sig. (2-tailed)	0.000	-
	N	363	363

Table 4, shows that there is significant relationship in time of fund holding pattern of investor and occupation, $r(363) = 0.147$, $p < 0.05$.

Finding:

92% of the employees are married and only 8% employees are unmarried. Educational qualification of the employees reveals that 7% of the respondents have only taken degree. Most of the employees (39%) are qualified with ITI. 30% of employees just have the basic qualification. 24% of the employees have post graduation qualification. Most of the respondents are government employees i.e., 50%. 32% of the employees fall under the private job. Only 18% of them are retired. Extraversion type of personality has a great impact or role in the mutual funding investment. There is no significant difference in the risk acceptance with different occupation. The respondents' awareness level shows that many people have knowledge about Growth and Income Schemes rather than Balanced and Dividend Schemes. There is a least significant difference between the means of the income group of investors and the awareness level. There is a significant difference between the age of the respondents and awareness about mutual fund. There is significant relationship in time of fund holding pattern of investor and occupation.

ISSN: 2395-0463
Volume 07 Issue 06
June 2021

Conclusion:

Mutual fund companies should come forward with full support for the investors in terms of advisory services, participation of investor in portfolio design, ensure full disclosure of related information to investor, proper consultancy should be given by mutual fund companies to the investors in understanding terms and conditions of different mutual fund schemes, such type of fund designing should be promoted that will ensure to satisfy needs of investors, mutual fund information should be published in investor friendly language and style, proper system to educate investors should be developed by mutual fund companies to analyse risk in investments made by them, etc. Financial risk tolerance refers to the degree of uncertainty an investor is willing to accept, and can often be influenced by individual characteristics. However, personal psychological preferences play a prominent role in an investor's judgement and relationship with their finances. Extraversion type of personality has a great impact or role in the mutual funding investment. Mutual funding investment is risk associated. So that it suitable for extraversion type of investors.

Reference:

Allport, G. W., & Odbert, H. S. (1936). Trait-names: A psycho-lexical study. Psychological Monographs, 47(1). doi: 10.1037/h0093360

Tversky, A. & Kahneman, D. (1981). The framing of decisions and the psychology of choice. Science, 211:453-458.

Durand, R. B., Newby, R., & Sanghani, J. (2008). An intimate portrait of the individual investor. The Journal of Behavioral Finance, 9(4), 193–208.

Dolan, P., Elliott, A., Metcalfe, R., & Vlaev, I. (2012). Influencing financial behavior: From changing minds to changing contexts. Journal of Behavioral Finance, 13(2), 126–142.

J.Lilly and DrAnasuya."An empirical study of performance evaluation of selected ELSS mutual fund schemes". International journal of scientific research .2014

Vipinkumar, PreetiBansal (2014), "A study on Investors Behavior towards mutual funds in Rohtak, Haryana, International Journal of Engineering and Management Research, February 2014, Vol. 4, Issue 1, ISSN 2250-0758.

Mukesh. H. V. (2015), "Investors perception towards mutual funds : An Indian perspective, Global Journal for Research Analysis, April 2015, volume – 4, Issue 4, ISSN 2277-8160.

ISSN: 2395-0463
Volume 07 Issue 06
June 2021

Subramanya PR (2015), "Investors perception towards mutual fund (with special consideration of socio – Economic variables), Research hub – International Multidisciplinary Research Journal, January 2015, Vol. 2, Issue 1, ISSN 23497637.

D. Rajasekhar (2013), "A study on investor's preference towards mutual funds with reference to Reliance private limited, Chennai – An empirical Analysis, International Research Journal of Business and Management, September 2013, Vol. III, ISSN 2322-083X.

Kannadhasan, M., Aramvalarthan, S., Mitra, S.K. & Goyal, V. (2016). Relationship between biopsychosocial factors and financial risk tolerance: an empirical study. The Journal for Decision Makers, 41(2):117-131

Chavali, K. and Mohanraj, M.P. 2016. Impact of demographic variables and risk tolerance on investment decision: An empirical analysis. International Journal of Economics and Financial Issues, vol. 6, no. 1, pp. 169-175.

Customer Preferences for Branded Apparels in Bangalore

Blesson Babu

Assistant Professor, Department of Business Administration,

Carmel College Mala

Abstract

The aim of this research is to identify the customer preference level and buying behavior of customers towards the branded apparels in Bangalore. Data collection is made with help of structured questionnaire. Many consumers are becoming brand conscious each and every day. Peoples taste and preference are changing each and every day. So it is essential to know the brand preferences of the customer, the buying behavior of the consumers and the factors affecting the purchase decision. Also to understand the effect of branding on sales. Entire study based on the consumer preference for branded apparels in Bangalore. Many developments and changes are taking place around us with all the industries and firms within each industry including garment industry with an intention to keep pace with the changes and diverse needs of the people. Not only competition has become intense but over and above with the market being flooded with many products. Challenge before the marketers is to understand the diversity of consumer behavior and offer goods and services accordingly. So the study

will help the apparel industry to identify the buying behavior of its customers and to produce according to the needs.

Key Words: Branded apparels, Customer preference, Buying behavior

Introduction

Consumer shop for various reasons and occasion. apparel industry is one of the fastest growing industry in India, so to remain in this competitive market place and to increase the revenue the industry should understand the needs and of its customer and they should continuously try to satisfy these needs and wants at a profitable margin. The word customer preferences mean what type of product an individual customer likes or dislikes. As a part of understanding the customer we should understand the buying behavior of the customer. Why customer makes a purchase, what are the factors affecting the buying decision. The central focusing of marketing is, the consumer. To devise good marketing plans, it is necessary to examine consumer behavioral attributes and needs, lifestyle purchase processes and then make a proper marketing mix decision.

"Consumers are evolving entities. Their aspirations & expectations are continuously changing. Today shopper is more intelligent, discerning& tuned to their Individual labels which

ISSN: 2349-0217

define who they are or who they want to be. The biggest challenge for all the brands is to create loyal consumer who love them"- (Shopper' Stop Ltd)

"Indian textile and apparel have a history of fine craftsmanship and global appeal. Cotton, silk and denim from India are highly popular abroad and with the upsurge in Indian design talent, Indian apparel too has found success in the fashion Centre of the world. The fashion and apparel industry encompasses a wide variety of garments and uses almost every type of textiles manufactured. It generally subdivided into two categories. Clothing for man and boys and clothing for women and girls. Apparel industry is the makers and seller of the fashionable. Fashion business, fashion industry, garment industry, rag trade comes under this head. The manufacturing side of the industry includes workers who produces apparels such as those who use patterns to cut a variety of textiles into apparels individual pieces, and assemblers, sewers, presser, and inspectors to create the apparels from the textile pattern pieces. Clothing production also requires the support of workers that include fashion designers to design the article of clothing. Patternmakers to draw and construct a pattern for the garments based on the designer's specification. Merchandisers and retail buyers who places the apparel in stores and retail salespeople who sells the finished garments to the consumers."

There are various factors which affect the apparels industry. Macro environmental factors affecting the clothing industry are those which lie outside small companies and their competitors. Business owners have less control of these external factors and their impact should be minimized. The way that each company deals with these external factors will determine the success rate of the company and will differentiate them from their competitors. Some of these the external factors are consumer factors, economical factors, technological, legal and political factors. Consumer factors include the culture, norms, and lifestyle and population changes. For example, a sales person needs to create a style which is appealing to that particular city than only the people will be attracted to that particular item. Technological factors are related to the demand availability of raw material etc. if in a certain place a certain type of material is very cheap the production will be based on that item. If price of raw material has been increased, it will affect the selling price of product. Legal and political factors are based on the rules and regulations. There are certain rules and regulations prevail in each places these rules will affect the sales strategy of each places. Economic factors are the factors which are based on the economic conditions of the industry. If there is boom people will have a lot of money it will leads to purchase of more cloths. If the industry is having a recession it may leads to opposite effect.

ISSN: 2349-0217

Nowadays Apparel brands are spending huge amount of money to acquire and maintain their customers. More amount of budget is allocated for this purpose so it is essential to study how particular person will take decision of a particular apparel. There is a huge financial risk related to the switching of one customer from a particular brand to another. So its essential part of a marketer to learn the effect of the marketing activities which are taken place.it helps him to know why customer choose that particular item and how he gets to know about that particular item.

Today's branded apparel industry is harder than ever. There are so many challenges they have to face every day, they are consumerism is one of the example where consumer has the power these days so the sellers are forced to sell products as per the consumer needs and wants it will put pressure on the retailer's same time it leads to law profit. Which adversely affect the business another challenge is brand sensitivity that if a band is not available in a shop customer will switch if the quality of the item is bad than they switch the shop and they will criticize the seller through social media thy will also tell this to their friends also. These days the bands image is very important if they have associated to a negative issue they will lose their customers. Everyone is observing the seller's activities, so they have to keep a good image in the society then only they can

retain their customers. Inventory intelligence is an important thing fashion are changing to quickly these days so if you kept a huge amount of stock it will be obsolete. The fashion these days are very quick changing and apparel industry is based on the current trends so if the industry is not up to the trend they cannot maintain their customer. There are other things will also big challenge these days, like amazon effect. Walmart effect is a situation where the customers are expecting goods at a lower price. Now there is a new effect which is called black Friday effect. It is considered as the official start of the holyday shopping. It's a situation where the retailers will offer huge offers and discounts to attract huge number of customers in the beginning of the sales. These ways they can increase the sales.

The history of textile in India dates back to the year of 3000 BC. The diversity of fiber found in India and has been attracted by all over the world. The British has been left India in a worst form when they left the country but the independent India saw a huge possibility in the textile industry and done a diversification of its product base. Now India employees more than 35 million people in the apparel industry and India is the second largest country in the textile industry. And this industry alone contributes $1/5^{th}$ of the total export and 4%of the GDP and thereby making it the largest industry of the country. It is

ISSN: 2349-0217

expected that the firms with robust capabilities will gain in the global trade of textile and apparel.

Literature Review

Pandian, Varathani, Keerthivasan (2012) according to him lifestyle of people changing each day. Main challenge of a business is to know the wants of the customer's brand loyalty of customers may help the brands to manage the competition and maintain market share. As a result of globalization we are more attracted to the foreign brands. Nowadays people are more likely to where branded product. So the should understand this and create strategies to proper branding. The study is based on Trichy it shows that people are more attracted to branded shirt.

Rajput, N., Kesharwani, S. & Khanna, A. (2012) as per the article Indian customers are highly developed. Years before Indian customer don't have enough money to buy his necessities. Now with increased income purchase rate also has been increased standard of living also increased. Shops has been filled with variety of products new mall and supermarkets introduced. To survive in the market a business should understand the customer needs and maintain a proper database. By evaluating these Database Company can prepare its strategies and also can reduce unnecessary expenses related to it. This is a study conducted to know the buying behavior of youngsters to the apparels and also to know the personal

character of youngster related to the buying behavior. Population in our country is very young. Through the effect of media most of us are trying to live as per abroad style. And most youngsters are making their own income they spend this on apparels and mobiles mostly. It increases the possibility of our study.

Vikkraman and Sumathi (2012) the article suggest that the growth rate of apparel industry is 4.70 percent. Value of goods is also growing. Retail market in India in the revolutionary stage. It is due the urbanization, coming up of new shopping malls, people are becoming brand conscious, emerging breed brands, adaptation of western culture etc. India has more outlets than the whole world. India has 15 million outlets. Indian market is controlled by 12 million 'dad and mom' shops which provide job opportunity for 21 million people. Each and every year the volume of sales in the apparel industry is growing rapidly. This study is to identify the consumer preference of foreign brands instead of Indian brands. In order to fulfil the objective of the study we need to add the details like purchase intention, emotional value, clothing interest etc. Indian consumers are changing their habits these days. They are willing to pay more amount for pleasure, education of their children. They are looking for both foreign and Indian brand. Their global brand awareness has been increased. From the article we can

ISSN: 2349-0217

understand that uniqueness is something that Indian customers are looking these days.

Dr. Anand Thakur, Mr. BhuvanLamba (2013) as per the article Indian textile industry has been a pillar for our country's development. Our country ranks 6th in clothing and also 7th in the case of textile. Readymade garments are also part of textile industry readymade alone contributes to half of the total export of Indian textile industry. Textile industry is the largest employment provider after agriculture. It is the largest foreign exchange earner in India. This industry is growing constantly. So to know our customer well will boost this growth. This study will try to know the satisfaction level of its customers and factors affecting the purchase of apparel also to know the most popular brands that the customers are more likely to buy at different situation. Clothing is considered to be part of body. Today we live in a society where the customer is considered to be the king. Customer preferences will be changed as per the market condition, fashion, society etc.

Statement of Problem

We are trying to assess the present level of satisfaction to the readymade apparels. To find the factors affecting the readymade apparels to know the most popular brand apparels. The need for understanding the consumer mind and the companies should proceed accordingly. It understood that many

employees and management. More over selection of sample collection of data methods of collecting data analysis of data interception of data is also included in this study so that descriptive research design is more suitable for the study.

Data collection

Determining the source of data is one of the most important step in conducting a research. The source of data can be classified into two:-

- Primary data
- Secondary data

Primary data

A primary source is also known as first-hand information. It is collected by the researcher himself directly from original source. The important source of primary data is: -

- Questionnaire

Secondary data

The data which have been collected and compiled for some other purpose by someone else and is used by researcher for the interest of his research study is known as secondary data. The important sources of secondary data are: -

- Journal
- Magazines / article
- Web page

company fails to do that. Marketing strategy of those companies should be changed. Marketers should observe its customers before jumping into the findings.

Objective of Study

- To study consumers preference towards the branded apparels in Bangalore.
- To study the socio-economic characteristics of selected consumer in Bangalore
- To study impact of advertisement, marketing, communication, and other factors influences on customer preference.

Research Sethodology

The basic design of survey instrument consists of structured questionnaires. It is so designed to collect all required information from users of apparels. Based on their knowledge, information source and purchase decision factors related to their selection of a different apparels. Descriptive type of research was used for this study. Data used for the research has been collected from primary and secondary sources. Percentage analysis, Graphical Representation and Hypothetical test were used for data analysis.

Research Design

The researcher used descriptive research design because here the study deals with describing the characteristics of each

ISSN: 2349-0217

Data analysis

Table 1 showing the age of the respondents

Particulars	Response	Percentage
15-25	32	64%
25-35	8	16%
35-45	7	14%
Above 45	3	6%

Analysis

From the above Table we can understand that more people are between the age categories of 15 to 25. Second highest group is between 25 to 35.So it can analyzed that age group between 15 to 35 are more conscious about branded apparels.

Table 2 showing the prestige issue of respondents linked with brand apparel: -

Particulars	Response	Percentage
Yes	38	76%
No	12	24%

Analysis

From the figure 4.2 we can understand that 76% people thinks that brand represent prestige 24% people thinks it's not. Most of the respondent thinks that brand represent prestige.

ISSN: 2349-0217

Table 3 Showing rating of brand apparels

Analysis

Particulars	Response	Percentage
Highly agree	31	62%
Agree	10	20%
Moderately agree	7	14%
Disagree	2	4%

From the figure 3 we can understand that 64% are highly agree branded products are over rated. 21% are agree with it. 14% are moderately agree with it. 4% is dis agree with it. Most of the respondents highly agrees that branded products are over rated.

Table 4 showing availability of branded product

Analysis

Particulars	Response	Percentage
Yes	28	56%
No	22	44%

From the figure 56% suggest that branded products are available like non branded product. 44% people thinks they are

not. Respondents are neutral about the availability of branded apparels

Table 5 showing respondent willingness recommend brand to friends or family

Analysis

Particulars	Response	Percentage
Once	37	74
Several times	9	18
Never	4	8

From the figure 79% will suggest at least once to their friends or family. 19% will suggest several time. 2% won't suggest. Most of the respondent are ready to suggest brand apparels to their family and friends.

Table 6 showing the reach of branded apparels among customer

Particulars	Response	Percentage
Advertisement	29	58
Friends	7	14
Family	3	6
Other	9	18

Among the total respondent 60% comes to know through advertisement. 15% through friends. 6% through family. 19%

ISSN: 2349-0217

through other sources. Most people suggest advertising is the main way they get to know about the branded apparels

Table 7 showing impact of advertisement, marketing, communication, and other factors influences on customer preference

Analysis

Particulars	Response	Percentage
Yes	48	96
No	2	4

From the figure, 96% of the people bought branded apparels because of the advertisement, marketing, communication techniques used by the companies

Findings

- Most people are using branded apparels are aged between 15 to 25.
- Majority of respondent thinks that branded apparels represents prestige.
- Except a few people, everyone thinks the branded apparels are over rated.
- Respondents are neutral about the availability of the branded apparels.
- Majority of respondents are like to recommend their brand to others.

- Most respondents are coming to know about apparels through advertisement.
- Majority respondent believes that branded apparels are of high quality.
- People are satisfied with the services provide in the brand showrooms.
- Many people regularly buy branded apparels
- Almost every customer believes in the products promoted by their favourite celebrities.

Conclusion

From the study we figured that the availability is one of the major problem of the branded apparels. Most people recommend brand to others because of their high quality. It's the best feature so they have to stick on to it. Yet they should try to reduce cost so they can gain more customers. The number of people visiting the showroom with a brand in mind, is same as the number of people visiting the showroom with no brand in mind. Most of the time buyer's visit the showroom of branded wears with the purpose of shopping however compared to women, male consumer visits the showroom for passing time, even though pop, advertisement, promotional schemes and other factors influence the consumer purchase decision and consumer stimulated to buy. With the effective marketing mix and strategies can extend the sustainable growth of this industry.

ISSN: 2349-0217

Austrian Journal of Statistics
January 2022, Volume 51, 124–143.
http://www.ajs.or.at/
doi:10.17713/ajs.v51i2.1253

Applications of HLMOL-X Family of Distributions to Time Series, Acceptance Sampling and Stress-strength Parameter

Lishamol Tomy
Department of Statistics,
Deva Matha College

Meenu Jose
Department of Statistics,
Carmel College, Mala

Abstract

In this paper, the applications of the half logistic-Marshall Olkin X family of distributions are investigated with special emphasis to the half logistic-Marshall Olkin Lomax distribution. The specific areas we concentrated are time series modeling, acceptance sampling plan and stress- strength analysis. Different autoregressive minification structures of order one are introduced. The acceptance sampling plan is detailed by considering life time of products following the half logistic-Marshall Olkin Lomax distribution. The stress-strength reliability of the half logistic-Marshall Olkin Lomax distribution is derived and estimated. A simulation study is carried out to examine the bias, mean square error, average confidence length and coverage probability of the maximum likelihood estimator of the stress-strength reliability. Finally a real-life data analysis has also been presented.

Keywords: half logistic-Marshall Olkin X family of distribution, half logistic-Marshall Olkin Lomax distribution, autoregressive minification process, acceptance sampling plan, stress-strength analysis.

1. Introduction

Many real life phenomena are well described by statistical distributions. Although in case where existing distributions are found inadequate for a phenomenon, new generated classes of distributions are defined to meet the requirements. Such extended distributions are proved to be extremely useful for modeling real life situations by many authors. Several generators are existing in statistical literature. Two well known generators are, the Marshall-Olkin generator (MO-G) by Marshall and Olkin (1997) and the transformer (T-X) by Alzaatreh, Lee, and Famoye (2013).

For the last decades, there has been increasing interest in developing time series models for real valued observations using non-Gaussian distributions and the reason behind this is that many naturally occurring time series are non-Gaussian with Markovian structure. The pioneering work of autoregressive models with minification structure were proposed by Tavares (1980), and it followed by Sim (1986), Yeh, Arnold, and Robertson (1988), Arnold and Robertson (1989), Pillai (1991), Jose, Naik, and Ristić (2010) and others .

The acceptance sampling plan is an important tool in statistical quality control because it helps manufactures to minimize variability and protect the outgoing quality of their products. It is a sampling inspection procedure for determining the acceptability of the product. The acceptance sampling plans have been investigated in the past few decades by many authors, for instance Rosaiah, Gadde, Kalyani, and Kumar (2018), Rosaiah and Kantam (2005), Gillariose and Tomy (2018), Jose and Joseph (2018), Jose and Sebastian (2011) and Jose, Tomy, and Thomas (2018).

When assessing system reliability, a satisfactory performance is done when the strength applied to the component exceeds stress. Suppose that X represents the strength of a component with a stress Y, then R=$P(X > Y)$ can be considered as a measure of reliability of system. The system becomes out of control if the system stress exceeds its strength. Since R represents a relation between the stress and strength of a system. The estimation of the stress-strength reliability R has received considerable attention in the statistical literature. The pioneering work is given by Birnbaum *et al.* (1956) and Birnbaum, McCarty *et al.* (1958) .

Tomy and Jose (2020) introduced a new family of distributions called T-Marshall Olkin X family of distributions, it having the properties contained in both Marshall-Olkin and T-X family of distributions. They showed that several families of distributions can be derived from T-Marshall Olkin X family for different choices of variable T. In this article as a special case, the half logistic-Marshall Olkin X (HLMO-X) family of distributions is investigated. The cumulative density function (CDF) of the HLMO-X family of distributions by Tomy and Jose (2020) is given by

$$R(x) = \frac{1 - \left\{\frac{c(1-F(x))}{c+(1-c)F(x)}\right\}^{\lambda}}{1 + \left\{\frac{c(1-F(x))}{c+(1-c)F(x)}\right\}^{\lambda}} \tag{1}$$

where F(x) is the CDF of a random variable X. For convenience one special model of this family, the half logistic-Marshall Olkin Lomax (HLMOL) distribution, is studied in detail.

The Lomax distribution is one of the most commonly used distributions to model lifetime data and it has applications in several fields such as lifetime and reliability modeling, biological sciences and actuarial sciences. The CDF of the Lomax distribution is given by.

$$F(x) = 1 - [1 + \frac{x}{\theta}]^{-\alpha};\ x > 0,\ \alpha, \theta > 0$$

The HLMOL distribution has CDF given by

$$R(x) = \frac{\left[(1 + \frac{x}{\theta})^{\alpha} + c - 1\right]^{\lambda} - c^{\lambda}}{\left[(1 + \frac{x}{\theta})^{\alpha} + c - 1\right]^{\lambda} + c^{\lambda}} \tag{2}$$

The corresponding probability density function (PDF) is

$$r(x; c, \lambda, \alpha, \theta) = \frac{2\lambda\alpha c^{\lambda}}{\theta} \frac{\left[(1 + \frac{x}{\theta})^{\alpha} + c - 1\right]^{\lambda-1} [1 + \frac{x}{\theta}]^{\alpha-1}}{\left[\left[(1 + \frac{x}{\theta})^{\alpha} + c - 1\right]^{\lambda} + c^{\lambda}\right]^{2}};\ x > 0,\ c, \lambda, \alpha, \theta > 0 \tag{3}$$

With this context the main motivation behind this study is to investigate the diverse applications of the HLMO-X family of distributions in various fields like time series, quality control and reliability.

The paper unfolds as follows: In Section 2, we consider some applications of the HLMOL distribution in time series modeling. Section 3 presents the acceptance sampling plan of HLMOL distribution. In Section 4, The derivation and estimation of stress-strength reliability parameter R are given. The conclusion of the paper appears in Section 5.

2. Autoregressive time series modeling

Here, we develop different autoregressive minification processes of order one with HLMOL distribution as marginal distribution. We call the processes as HLMOL AR(1) Processes. Now we have the following theorem.

Theorem 2.1. *Consider an AR(1) structure given below*

$$X_n = \begin{cases} \varepsilon_n & \text{with probability } c \\ min(X_{n-1}, \varepsilon_n) & \text{with probability 1-c, } 0 \leq c \leq 1, \ n \geq 1 \end{cases} \tag{4}$$

where $\{\varepsilon_n\}$ *is a sequence of independent and identically distributed (iid) random variables and is independent of* $\{X_n\}$*. Then the process is stationary AR(1) minification process with HLMOL(1,*α*,*θ*,c) as marginals if and only if* ε_n *is distributed as half logistic Lomax(*α, θ*) and* $X_0 \stackrel{d}{=}$ *HLMOL(1,*α*,*θ*,c).*

Proof. From (4) it follows that

$$P(X_n > x) = cP(\varepsilon_n > x) + (1-c)P(X_{n-1} > x)P(\varepsilon_n > x)$$

That is,

$$\bar{R}_{X_n}(x) = \bar{R}_{\varepsilon_n}(x)[c + (1-c)\bar{R}_{X_{n-1}}(x)] \tag{5}$$

If the process is stationary with HLMOL(1,α,θ,c) marginals, then

$$\begin{aligned} \bar{R}_{\varepsilon_n}(x) &= \frac{\bar{R}_X(x)}{c + (1-c)\bar{R}_X(x)} \\ &= \frac{\frac{2c}{(1+\frac{x}{\theta})^{\alpha}+2c-1}}{c + (1-c)\frac{2c}{(1+\frac{x}{\theta})^{\alpha}+2c-1}} \\ &= \frac{2}{(1+\frac{x}{\theta})^{\alpha}+1} \end{aligned} \tag{6}$$

Which is the survival function of half logistic Lomax(α, θ) distribution.

Coversely, If $\varepsilon_n(x)'s$ are iid random variables follows half logistic Lomax(α, θ) distribution with $X_0 \stackrel{\text{d}}{=}$ HLMOL(1,α,θ,c), then from (5), we have

$$\begin{aligned} \bar{R}_{X_1}(x) &= \bar{R}_{\varepsilon_1}(x)[c + (1-c)\bar{R}_{X_0}(x)] \\ &= \frac{2}{(1+\frac{x}{\theta})^{\alpha}+1}\left\{c + (1-c)\frac{2c}{(1+\frac{x}{\theta})^{\alpha}+2c-1}\right\} \\ &= \frac{2}{(1+\frac{x}{\theta})^{\alpha}+1}\left\{\frac{c(1+\frac{x}{\theta})^{\alpha}-c+2c}{(1+\frac{x}{\theta})^{\alpha}+2c-1}\right\} \\ &= \frac{2c}{(1+\frac{x}{\theta})^{\alpha}+2c-1} \end{aligned} \tag{7}$$

That is X_1 has HLMOL(1,α,θ,c) distribution.
Similarly if X_{n-1} has HLMOL(1,α,θ,c) distribution, we get X_n also has HLMOL(1,α,θ,c) distribution. Hence the process $\{X_n\}$ is stationary with HLMOL marginals. □

The corresponding sample paths are given in Figure 1. The sample path behaviour of the process seems to be distinct and is adjustable through the parameters c,α and θ.

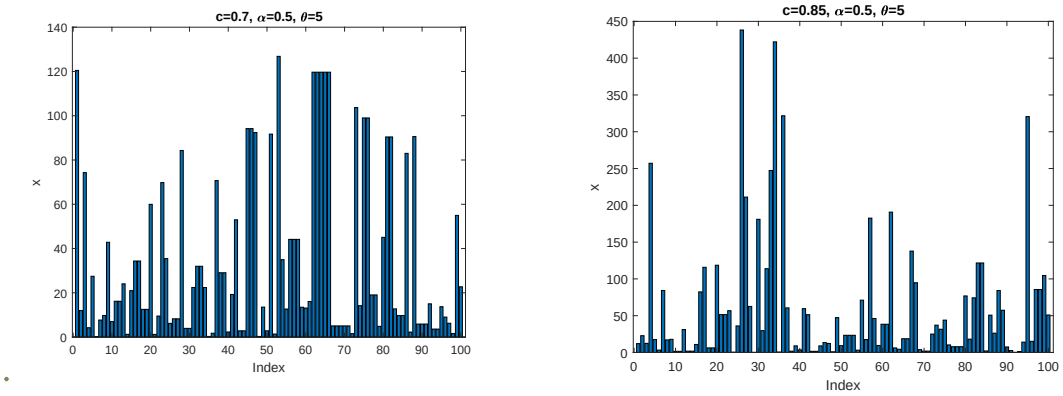

Figure 1: Sample path behaviour of HLMOL minification process given in Theorem 2.1

The following theorem gives a first order autoregressive minification process with marginals following HLMOL(λ, α, θ, β) distribution.

Theorem 2.2. *Consider an AR(1) structure given below*

$$X_n = \begin{cases} \varepsilon_n & \text{with probability } c \\ min(X_{n-1}, \varepsilon_n) & \text{with probability 1-c, } 0 \leq c \leq 1, \ n \geq 1 \end{cases} \tag{8}$$

where $\{\varepsilon_n\}$ is a sequence of iid distributed random variables and is independent of $\{X_n\}$. Then the process is stationary AR(1) minification process with HLMOL(λ, α, θ, β) as marginals if and only if $\varepsilon_n(x)'s$ having the survival function,

$$\bar{R}_{\varepsilon_n}(x) = \frac{2\beta^\lambda}{c[(1+\frac{x}{\theta})^\alpha + \beta - 1]^\lambda + (2-c)\beta^\lambda} \tag{9}$$

and $X_0 \underline{d}$ HLMOL (λ, α, θ, β).

Proof. From (8) it follows that

$$P(X_n > x) = cP(\varepsilon_n > x) + (1-c)P(X_{n-1} > x)P(\varepsilon_n > x)$$

That is,

$$\bar{R}_{X_n}(x) = \bar{R}_{\varepsilon_n}(x)[c + (1-c)\bar{R}_{X_{n-1}}(x)] \tag{10}$$

If the process is stationary with HLMOL(λ, α, θ, β) marginals, then

$$\begin{aligned} \bar{R}_{\varepsilon_n}(x) &= \frac{\bar{R}_X(x)}{c + (1-c)\bar{R}_X(x)} \\ &= \frac{\frac{2\beta^\lambda}{[(1+\frac{x}{\theta})^\alpha+\beta-1]^\lambda+\beta^\lambda}}{c + (1-c)\frac{2\beta^\lambda}{[(1+\frac{x}{\theta})^\alpha+\beta-1]^\lambda+\beta^\lambda}} \\ &= \frac{2\beta^\lambda}{c[(1+\frac{x}{\theta})^\alpha + \beta - 1]^\lambda + (2-c)\beta^\lambda} \end{aligned} \tag{11}$$

That is, $\varepsilon_n(x)$'s are iid random variables having survival function given in (11).

Coversely, If $\varepsilon_n(x)'s$ are iid random variables having survival functions given in (11) with X_0 $\underline{d}$ HLMOL(λ, α, θ, β), then from (10), we have

$$\bar{R}_{X_1}(x) = \bar{R}_{\varepsilon_1}(x)[c + (1-c)\bar{R}_{X_0}(x)] \tag{12}$$

$$= \frac{2\beta^\lambda}{c[(1+\frac{x}{\theta})^\alpha + \beta - 1]^\lambda + (2-c)\beta^\lambda}\left\{c + (1-c)\frac{2\beta^\lambda}{[(1+\frac{x}{\theta})^\alpha + \beta - 1]^\lambda + \beta^\lambda}\right\} \tag{13}$$

$$= \frac{2\beta^\lambda}{[(1+\frac{x}{\theta})^\alpha + \beta - 1]^\lambda + \beta^\lambda} \tag{14}$$

That is X_1 has HLMOL$(\lambda, \alpha, \theta, \beta)$ distribution.
Similarly if X_{n-1} has HLMOL$(\lambda, \alpha, \theta, \beta)$ distribution, we get X_n also has HLMOL(λ, α, θ, β) distribution. Hence the process $\{X_n\}$ is stationary with HLMOL marginals. □

The corresponding sample paths are given in Figure 2. The sample path behaviour of the process seems to be distinct and is adjustable through the parameters c, λ, α, θ and β.

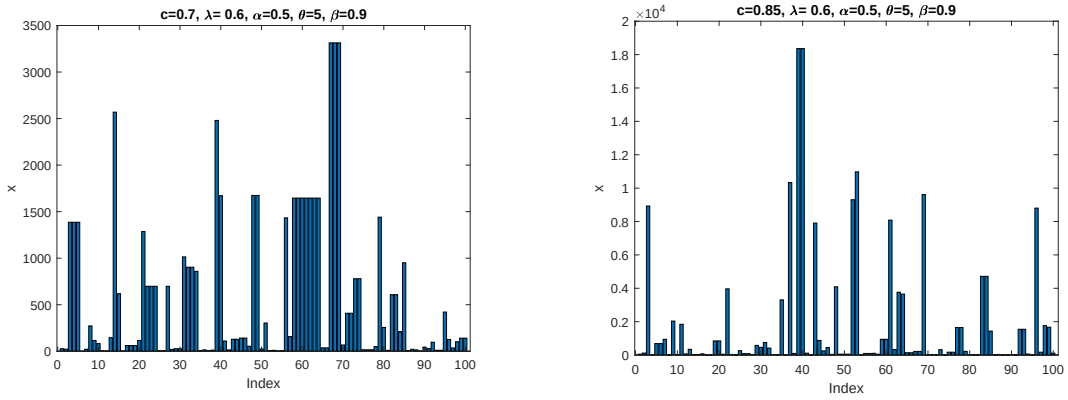

Figure 2: Sample path behaviour of HLMOL minification process given in Theorem 2.2

Krishnarani and Jayakumar (2008) gives a general class of autoregressive process with the following monotone transformation $\phi(x) = log\frac{R(x)}{\bar{R}(x)}$ where R(x) is a nondegenerate CDF, $\phi(-\infty) = -\infty$, $\phi(\infty) = \infty$ and $\bar{R}(x) = 1 - R(x)$. The corresponding markov process is

$$X_n = \begin{cases} \phi^{-1}[\phi(X_{n-1}) - log(c)] & \text{with probability c} \\ min[\phi^{-1}(\phi(X_{n-1}) - log(c)), \varepsilon_n] & \text{with probability 1-c, } 0 < c < 1, \end{cases} \tag{15}$$

where $\{\varepsilon_n\}$ is a sequences of iid random variables with CDF R , ε_n independent of X_i's, i=0, 1, 2,...n-1 with X_0 having distribution function R.
We use this concept in HLMOL(λ, α, θ, c) distribution. Then we get Theorem 2.3.

Theorem 2.3. *Consider an AR(1) structure given below*

$$X_n = \begin{cases} \theta\left\{\left[\left[\frac{[(1+\frac{X_{n-1}}{\theta})^\alpha + c - 1]^\lambda + c^\lambda(c-1)}{c}\right]^{1/\lambda} + 1 - c\right]^{1/\alpha} - 1\right\} & \textit{with probability } c \\ min\left\{\theta\left\{\left[\left[\frac{[(1+\frac{X_{n-1}}{\theta})^\alpha + c - 1]^\lambda + c^\lambda(c-1)}{c}\right]^{1/\lambda} + 1 - c\right]^{1/\alpha} - 1\right\}, \varepsilon_n\right\} & \textit{with probability 1-c} \end{cases} \tag{16}$$

where $0 < c < 1$, $\{\varepsilon_n\}$ is a sequence of iid distributed random variables and $\varepsilon_n$is independent of X_i, i=0, 1, 2,..n-1. Then the process is stationary AR(1) minification process with HLMOL(λ,α,θ,c) as marginals if and only if $\{\varepsilon_n\}$ is distributed as HLMOL(λ,α,θ,c) and $X_0 \underline{d} \varepsilon_1$.

Proof. From (16) it follows that

$$\begin{aligned} P(X_n > x) = {} & cP\left\{X_{n-1} > \theta\left\{\left[[c((1+\frac{x_{n-1}}{\theta})^\alpha + c - 1)^\lambda - c^\lambda(c-1)]^{1/\lambda} + 1 - c\right]^{1/\alpha} - 1\right\}\right\} \\ & + (1-c)P\left\{X_{n-1} > \theta\left\{\left[[c((1+\frac{x_{n-1}}{\theta})^\alpha + c - 1)^\lambda - c^\lambda(c-1)]^{1/\lambda} + 1 - c\right]^{1/\alpha} - 1\right\}\right\} \\ & P(\varepsilon_n > x) \end{aligned} \tag{17}$$

That is,

$$\bar{R}_{X_n}(x) = \bar{R}_{X_{n-1}}\left\{\theta\left\{\left[[c((1+\frac{x_{n-1}}{\theta})^\alpha + c - 1)^\lambda - c^\lambda(c-1)]^{1/\lambda} + 1 - c\right]^{1/\alpha} - 1\right\}\right\}\left[c + (1-c)\bar{R}_{\varepsilon_n}(x)\right] \tag{18}$$

If the process is stationary with HLMOL(λ,α,θ,c) marginals, then

$$\begin{aligned}\left[c+(1-c)\bar{R}_{\varepsilon}(x)\right] &= \frac{\bar{R}_X(x)}{\bar{R}_X\left\{\theta\left\{\left[c((1+\frac{x}{\theta})^{\alpha}+c-1)^{\lambda}-c^{\lambda}(c-1)\right]^{1/\lambda}+1-c\right]^{1/\alpha}-1\right\}\right\}} \\ &= \frac{\frac{2c^{\lambda}}{[(1+\frac{x}{\theta})^{\alpha}+c-1]^{\lambda}+c^{\lambda}}}{\frac{2c^{\lambda}}{c[(1+\frac{x}{\theta})^{\alpha}+c-1]^{\lambda}-c^{\lambda}(c-2)}} \\ &= \frac{c[(1+\frac{x}{\theta})^{\alpha}+c-1]^{\lambda}-c^{\lambda}(c-2)}{[(1+\frac{x}{\theta})^{\alpha}+c-1]^{\lambda}+c^{\lambda}} \end{aligned} \tag{19}$$

That is, $\bar{R}_{\varepsilon}(x) = \frac{2c^{\lambda}}{[(1+\frac{x}{\theta})^{\alpha}+c-1]^{\lambda}+c^{\lambda}}$, which is the survival function of HLMOL$(\lambda,\alpha,\theta,c)$ distribution.

Conversely, If $\varepsilon_n(x)'s$ are iid random variables following HLMOL$(\lambda,\alpha,\theta,c)$ distribution with $X_0 \stackrel{\mathrm{d}}{=}$ HLMOL$(\lambda,\alpha,\theta,c)$, then from (18), we have

$$\begin{aligned}\bar{R}_{X_1}(x) &= \bar{R}_{X_0}\left\{\theta\left\{\left[c((1+\frac{x_{n-1}}{\theta})^{\alpha}+c-1)^{\lambda}-c^{\lambda}(c-1)\right]^{1/\lambda}+1-c\right]^{1/\alpha}-1\right\}\right\}\left[c+(1-c)\bar{R}_{\varepsilon_n}(x)\right] \\ &= \frac{2c^{\lambda}}{c[(1+\frac{x}{\theta})^{\alpha}+c-1]^{\lambda}-c^{\lambda}(c-2)}\left\{c+(1-c)\frac{2c^{\lambda}}{[(1+\frac{x}{\theta})^{\alpha}+c-1]^{\lambda}+c^{\lambda}}\right\} \\ &= \frac{2c^{\lambda}}{c[(1+\frac{x}{\theta})^{\alpha}+c-1]^{\lambda}-c^{\lambda}(c-2)}\left\{\frac{c[(1+\frac{x}{\theta})^{\alpha}+c-1]^{\lambda}+c^{\lambda+1}+2c^{\lambda}-2c^{\lambda+1}}{[(1+\frac{x}{\theta})^{\alpha}+c-1]^{\lambda}+c^{\lambda}}\right\} \\ &= \frac{2c^{\lambda}}{[(1+\frac{x}{\theta})^{\alpha}+c-1]^{\lambda}+c^{\lambda}} \end{aligned} \tag{20}$$

That is X_1 has HLMOL$(\lambda,\alpha,\theta,c)$ distribution.
Similarly if X_{n-1} has HLMOL$(\lambda,\alpha,\theta,c)$ distribution, we get X_n also has HLMOL$(\lambda,\alpha,\theta,c)$ distribution. Hence the process $\{X_n\}$ is stationary with HLMOL marginals. □

The corresponding sample paths are given in Figure 3. The sample path behaviour of the process seems to be distinct and is adjustable through the parameters c, λ, α and θ.

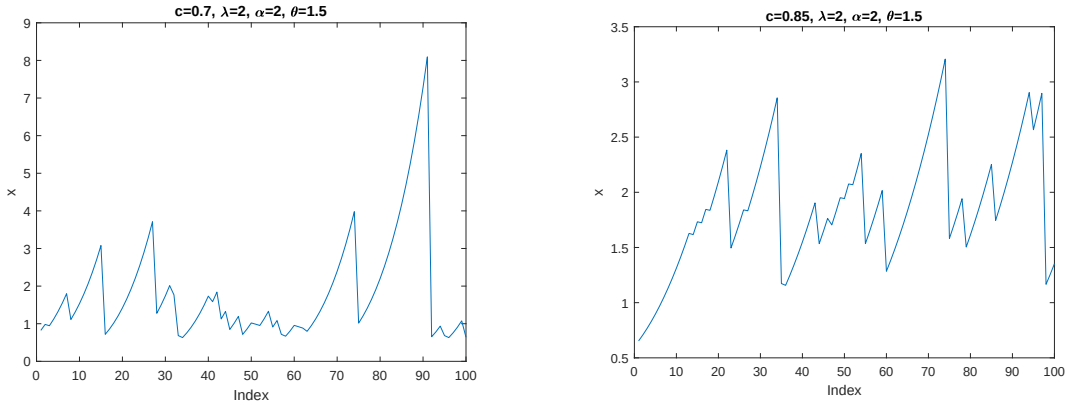

Figure 3: Sample path behaviour of HLMOL minification process given in Theorem 2.3

Theorem 2.4 stated below is a particaular case of Theorem 2.3, that is it gives a first order autoregressive minification process with marginals following HLMOL(1, α, θ, β) distribution.

Theorem 2.4. *Consider an AR(1) structure given below*

$$X_n = \begin{cases} \theta\left\{\frac{\left[(1+\frac{X_{n-1}}{\theta})^{\alpha}+c-1\right]^{1/\alpha}-c^{1/\alpha}}{c^{1/\alpha}}\right\} & \textit{with probability } c \\ min\left\{\theta\left\{\frac{\left[(1+\frac{X_{n-1}}{\theta})^{\alpha}+c-1\right]^{1/\alpha}-c^{1/\alpha}}{c^{1/\alpha}}\right\}, \varepsilon_n\right\} & \textit{with probability 1-c} \end{cases} \tag{21}$$

where $0 < c < 1$, $\{\varepsilon_n\}$ is a sequence of iid distributed random variables and $\varepsilon_n$is independent of X_i, i=0, 1, 2,..n-1. Then the process is stationary AR(1) minification process with HLMOL(1,α,θ,c) as marginalas if and only if $\{\varepsilon_n\}$ is distributed as HLMOL(1,α,θ,c) and $X_0 \underline{d} \varepsilon_1$.

Proof. The proof is similar to that of Theorem 2.3. □

The corresponding sample paths are given in Figure 4. The sample path behaviour of the process seems to be distinct and is adjustable through the parameters c, α and θ.

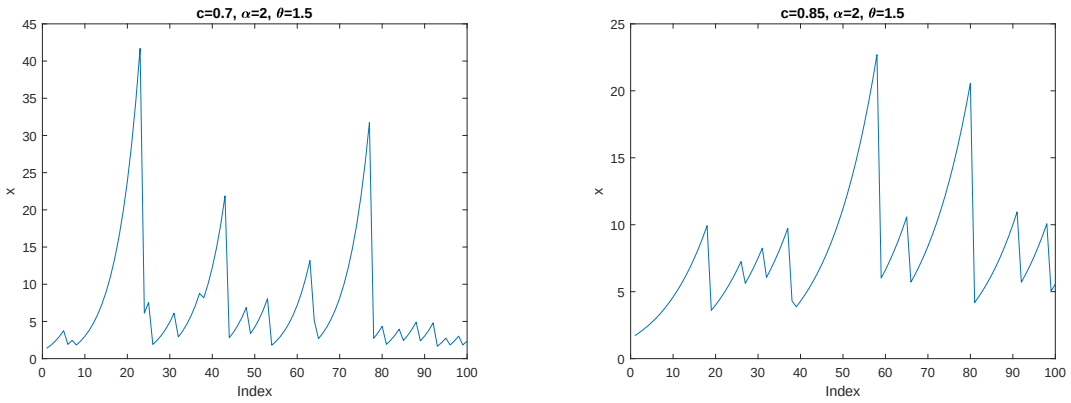

Figure 4: Sample path behaviour of HLMOL minification process given in Theorem 2.4

3. Acceptance sampling plan

In this section, we provide the acceptance sampling plan (ASP) under the assumption that lifetime of items follows a four parameter HLMOL$(\lambda, \alpha, \theta, c)$ distribution. The ASP involves determining the number of items to be inspected (n) and the maximum allowable number of defective items among the inspected items for acceptance of the item, that is the acceptance number (C). The test is terminated at a pre-specified time t and note the number of defective items(D). The decision procedure is to accept the lot if and only if at the end of the fixed time t, D does not exceed C, with a given probability $p^\star$. The test may get terminated before the time t is reached when D exceed C in which case we reject the lot. Here we are interested in obtaining the minimum sample size required to reach at the decision. It is assumed that the distribution parameters λ, α, c are known, while θ is unknown. In this case the average lifetime depends only on θ. Let θ_0 be the required minimum average lifetime, then the following holds:

$$R(t, \lambda, \alpha, \theta, c) \leq R(t, \lambda, \alpha, \theta_0, c) \Longleftrightarrow \theta \geq \theta_0$$

An ASP consists of the following quantities

- The number of units 'n' on test
- The acceptance number ' C'
- The ratio $\frac{t}{\theta_0}$, where θ_0 is the specified average life and t is the maximum test duration

The probability of accepting a bad lot, that is consumers risk is not to exceed $1 - p^\star$, so that $p^\star$ is a minimum confidence level with which a lot of true average life θ below θ_0 is rejected, by the sampling plan. Therefore, for fixed $p^\star$, the ASP can be characterized by the triplet $(n, C, \frac{t}{\theta_0})$. Here we consider sufficiently large lots so that the binomial distribution can be applied. Then our aim is to find the minimum positive integer n for given values of $p^\star$ $(0 < p^\star < 1)$, θ_0 and C such that.

$$\sum_{i=0}^{C} \binom{n}{i} p_0^i (1 - p_0)^{n-i} \leq 1 - p^\star \tag{22}$$

where $p_0 = R(t, \lambda, \alpha, \theta_0, c)$, indicates the failure probabilities before time 't' which depends only on the ratio $\frac{t}{\theta_0}$. The minimum values of n satisfying the inequality (22) are obtained and displayed in Table 1 for $p^\star$=0.75, 0.90, 0.95, 0.99 and $\frac{t}{\theta_0}$ =0.4, 0.6, 0.8, 1.0, 1.2, 1.4, 1.6, 1.8, 2.0, C=0, 1, 2,...,10, $\lambda = 2, \alpha = 2$ and c=2.

If $p_0 = R(t, \lambda, \alpha, \theta_0, c)$ is small and n is large, the binomial probability may be approximated by Poisson probability with parameter $\beta = np$ so that (22) can be written as

$$\sum_{i=0}^{C} \frac{e^{-\beta}\beta^i}{i!} \leq 1 - p^\star \tag{23}$$

where $\beta = nR(t; \theta_0)$. The minimum values of 'n' satisfying (23) are obtained for the same combination of $p^\star$, $\frac{t}{\theta_0}$, C, λ, α and c values as those used for (22). The results are given in Table 2.

The operating characteristic (OC) function is the probability of accepting the lot with:

$$L(p) = \sum_{i=0}^{C} \binom{n}{i} p^i (1-p)^{n-i}$$

where $p = R(t, \lambda, \alpha, \theta, c)$, is considered as a function of θ, that is, the true average life of the lot. For given $p^\star$, $\frac{t}{\theta_0}$, the choice of C and n will be made on the basis of OC. Values of OC as a function of $d = \frac{\theta}{\theta_0}$ for the sampling plan $(n, 2, \frac{t}{\theta_0})$ with $\lambda = 2, \alpha = 2$ and c=2 are given in Table 3. Figure 5 shows the OC curves for the sampling plan $(n, C, 0.6)$ with $p^\star = 0.75$ for $\lambda = 2, \alpha = 2$ and c=2.

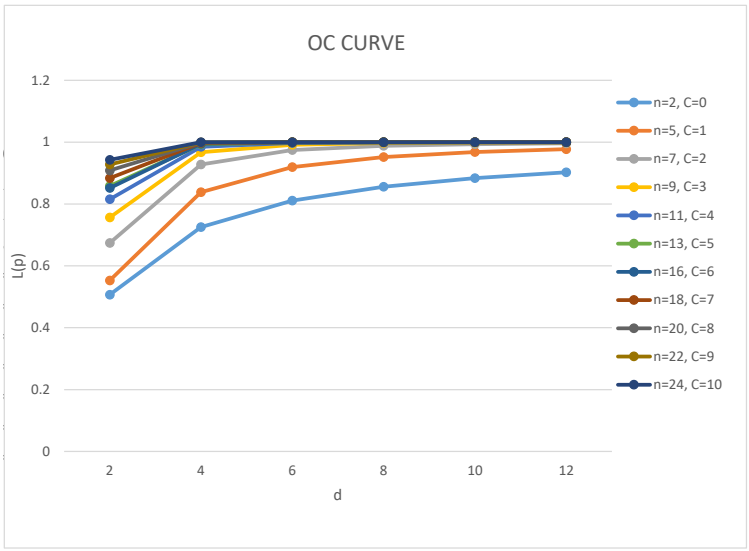

Figure 5: OC curves for C = 0, 1, 2, 3, 4, 5, 6, 7, 8, 9, 10, respectively under $p^\star = 0.75$, $\frac{t}{\theta_0}$ = 0.6, $\lambda = 2$, $\alpha = 2$ and c = 2, of ASP for HLMOL distribution

The producer's risk is the probability of rejecting a good lot. For a specified value of the producer's risk, say 0.05, one may be interested in knowing what value of the ratio d will ensure a producer's risk less than or equal to 0.05 for a given sampling plan. Hence, the value of d, is the smallest positive number for which $p = R\left(\frac{t}{\theta_0}\frac{\theta_0}{\theta}\right)$ holds the following inequality

$$\sum_{i=C+1}^{n} \binom{n}{i} p^i (1-p)^{n-i} \leq 0.05$$

Table 1: Minimum sample size for the specified ratio $\frac{t}{\theta_0}$, confidence level $p^\star$, acceptance number C, $\lambda = 2$, $\alpha = 2$ c $= 2$ using the binomial approximation

$p^\star$	C	$\frac{t}{\theta_0}$								
		0.4	0.6	0.8	1	1.2	1.4	1.6	1.8	2
0.75	0	3	2	2	2	1	1	1	1	1
	1	7	5	4	3	3	3	2	2	2
	2	10	7	6	5	4	4	4	4	3
	3	13	9	7	6	6	5	5	5	5
	4	16	11	9	8	7	6	6	6	6
	5	19	13	11	9	8	8	7	7	7
	6	22	16	12	11	10	9	9	8	8
	7	25	18	14	12	11	10	10	9	9
	8	28	20	16	14	12	12	11	11	10
	9	31	22	18	15	14	13	12	12	11
	10	34	24	19	17	15	14	13	13	12
0.9	0	5	4	3	2	2	2	2	1	1
	1	9	6	5	4	4	3	3	3	3
	2	13	9	7	6	5	5	4	4	4
	3	16	11	9	7	7	6	6	5	5
	4	20	14	11	9	8	7	7	7	6
	5	23	16	13	11	9	9	8	8	7
	6	26	18	14	12	11	10	9	9	9
	7	29	20	16	14	12	11	11	10	10
	8	33	23	18	15	14	13	12	11	11
	9	36	25	20	17	15	14	13	13	12
	10	39	27	21	18	16	15	14	14	13
0.95	0	7	5	3	3	2	2	2	2	2
	1	11	8	6	5	4	4	3	3	3
	2	15	10	8	7	6	5	5	4	4
	3	19	13	10	8	7	7	6	6	6
	4	22	15	12	10	9	8	7	7	7
	5	26	18	14	12	10	9	9	8	8
	6	29	20	16	13	12	11	10	9	9
	7	32	22	17	15	13	12	11	11	10
	8	36	25	19	16	15	13	13	12	11
	9	39	27	21	18	16	15	14	13	13
	10	42	29	23	20	17	16	15	14	14
0.99	0	10	7	5	4	3	3	3	2	2
	1	15	10	8	6	5	5	4	4	4
	2	20	13	10	8	7	6	6	5	5
	3	24	16	12	10	9	8	7	7	6
	4	27	18	14	12	10	9	9	8	8
	5	31	21	16	14	12	11	10	9	9
	6	35	24	18	15	13	12	11	11	10
	7	38	26	20	17	15	14	13	12	11
	8	42	29	22	19	16	15	14	13	13
	9	45	31	24	20	18	16	15	14	14
	10	49	33	26	22	19	18	16	16	15

Table 2: Minimum sample size for the specified ratio $\frac{t}{\theta_0}$, confidence level $p^\star$, acceptance number C, $\lambda = 2$, $\alpha = 2$ c $= 2$ using the Poisson approximation

$p^\star$	C	$\frac{t}{\theta_0}$								
		0.4	0.6	0.8	1	1.2	1.4	1.6	1.8	2
0.75	0	4	3	3	2	2	2	2	2	2
	1	8	6	5	4	4	4	4	3	3
	2	11	8	7	6	5	5	5	5	5
	3	14	10	9	8	7	7	6	6	6
	4	17	13	10	9	8	8	8	7	7
	5	20	15	12	11	10	9	9	9	9
	6	23	17	14	12	11v	11	10	10	10
	7	26	19	16	14	13	12	12	11	11
	8	29	21	17	15	14	13	13	12	12
	9	32	23	19	17	16	15	14	14	13
	10	35	26	21	18	17	16	15	15	15
0.9	0	7	5	4	4	3	3	3	3	3
	1	11	8	7	6	5	5	5	5	5
	2	15	11	9	8	7	7	7	6	6
	3	18	13	11	10	9	8	8	8	8
	4	22	13	13	12	11	10	10	9	9
	5	25	18	15	13	12	12	11	11	11
	6	29	21	17	15	14	13	13	12	12
	7	32	23	19	17	15	15	14	14	13
	8	35	25	21	18	17	16	15	15	15
	9	39	28	23	20	18	17	17	16	16
	10	42	30	25	22	20	19	18	18	17
0.95	0	9	6	5	5	4	4	4	4	3
	1	13	10	8	7	7	6	6	6	6
	2	17	13	10	9	8	8	8	7	7
	3	21	15	13	11	10	10	9	9	9
	4	25	18	15	13	12	11	11	11	10
	5	29	21	17	15	14	13	13	12	12
	6	32	23	19	17	15	15	14	14	13
	7	37	26	21	19	17	16	16	15	15
	8	39	28	23	20	19	18	17	16	16
	9	43	31	25	22	20	19	18	18	18
	10	46	33	27	24	22	21	20	19	19
0.99	0	13	9	8	7	6	6	6	6	5
	1	18	13	11	10	9	8	8	8	8
	2	23	17	14	12	11	11	10	10	10
	3	27	20	16	14	13	12	12	12	11
	4	32	23	19	17	15	14	14	13	13
	5	36	26	21	19	17	16	15	15	15
	6	40	29	23	21	19	18	17	17	16
	7	43	31	26	23	21	20	19	18	18
	8	47	34	28	25	23	21	20	20	19
	9	51	37	30	26	24	23	22	21	21
	10	54	39	32	28	26	25	24	23	22

Table 3: OC values for the ASP $(n, C, \frac{t}{\theta_0})$ for given confidence level $p^\star$, acceptance number C=2, $\lambda = 2$, $\alpha = 2$ c = 2

$p^\star$	n	$\frac{t}{\theta_0}$	d					
			2	4	6	8	10	12
0.75	10	0.4	0.6890	0.9306	0.9752	0.9885	0.9938	0.9963
	7	0.6	0.6741	0.9282	0.9746	0.9883	0.9937	0.9963
	6	0.8	0.5999	0.9056	0.9661	0.9844	0.9916	0.9949
	5	1	0.5919	0.9038	0.9657	0.9843	0.9915	0.9950
	4	1.2	0.6566	0.9251	0.9742	0.9884	0.9938	0.9964
	4	1.4	0.5559	0.8905	0.96093	0.9821	0.9904	0.9943
	4	1.6	0.4618	0.8504	0.9445	0.9742	0.9861	0.9917
	4	1.8	0.3780	0.8057	0.92518	0.9645	0.9807	0.9884
	3	2	0.6203	0.9085	0.9681	0.9857	0.9924	0.9956
0.9	13	0.4	0.5155	0.8676	0.9491	0.9756	0.9865	0.9918
	9	0.6	0.4952	0.8626	0.9477	0.9751	0.9863	0.9917
	7	0.8	0.4796	0.8583	0.9465	0.9746	0.9861	0.9916
	6	1	0.4402	0.8417	0.9398	0.9714	0.9844	0.9905
	5	1.2	0.4622	0.8524	0.9449	0.9742	0.9859	0.9916
	5	1.4	0.3492	0.7929	0.9188	0.9611	0.9786	0.9870
	4	1.6	0.4618	0.8504	0.9445	0.9742	0.9861	0.9917
	4	1.8	0.3780	0.8057	0.9251	0.9645	0.9807	0.9884
	4	2	0.3060	0.7577	0.9027	0.9531	0.9742	0.9844
0.95	15	0.4	0.4121	0.8178	0.9266	0.9639	0.9797	0.9875
	10	0.6	0.4154	0.8244	0.9306	0.9663	0.9813	0.9885
	8	0.8	0.3740	0.8051	0.9226	0.9624	0.9791	0.9872
	7	1	0.3152	0.7710	0.9073	0.9546	0.9746	0.9845
	6	1.2	0.3067	0.7662	0.9056	0.9540	0.9744	0.9844
	5	1.4	0.3492	0.7929	0.9188	0.9611	0.9786	0.9870
	5	1.6	0.2573	0.7279	0.8878	0.9449	0.9693	0.9812
	4	1.8	0.3780	0.8057	0.9251	0.9645	0.9807	0.9884
	4	2	0.3061	0.7577	0.9027	0.9531	0.9742	0.9844
0.99	20	0.4	0.2178	0.6797	0.8556	0.9247	0.9562	0.9724
	13	0.6	0.2298	0.6981	0.8676	0.9321	0.9610	0.9756
	10	0.8	0.2146	0.6890	0.8641	0.9306	0.9602	0.9752
	8	1	0.2190	0.6962	0.8692	0.9339	0.9624	0.9767
	7	1.2	0.1948	0.6741	0.8583	0.9282	0.9591	0.9746
	6	1.4	0.2052	0.6841	0.8645	0.9320	0.9615	0.9762
	6	1.6	0.1332	0.5999	0.8175	0.9056	0.9457	0.9661
	5	1.8	0.1860	0.6601	0.8524	0.9258	0.9581	0.9742
	5	2	0.1326	0.5919	0.8135	0.9038	0.9449	0.9657

that is,

$$\sum_{i=0}^{C} \binom{n}{i} p^i (1-p)^{n-i} \geq 0.95 \tag{24}$$

For some sampling plan (n, C, $\frac{t}{\theta_0}$) and values of $p^\star$, minimum values of$\frac{\theta}{\theta_0}$ satisfying (24) are given in Table 4.

3.1. Description of the tables and example

Assume that the lifetime distribution is HLMOL distribution with $\lambda = 2$, $\alpha = 2$ c = 2. Suppose that the experimenter is wants to establishing that the true unknown average life is at least 1000 hours with confidence $p^\star = 0.75$. It is desired to stop the experiment at t = 600 hours. Then, for an acceptance number c = 2, the required n in Table 1 corresponding to the values of $p^\star = 0.75$, $\frac{t}{\theta_0}$=0.6 and C=2 is 7. If, during 600 hours, no more than 2 failures out of 7 are observed, then the experimenter can assert, with a confidence level of 0.75 that the average life is at least 1000 hours. If the Poisson approximation to binomial probability is used, the value of n = 8 is obtained from Table 2 for the same situation.
Figure 6 shows that all the values of n tabulated by us corresponding to the sampling plan (n,C,1) with the confidence $p^\star = 0.75$ are found to be less than the corresponding values of n tabulated in Rosaiah *et al.* (2018) for Odds Exponential Log-Logistic (OELL) Distribution, Rosaiah and Kantam (2005)) for Inverse Rayleigh (IR) distribution, Jose and Sebastian (2011) for Marshall–Olkin Gumbel-maximum (MOGM) distribution, and Jose *et al.* (2018) for Harris extended Weibull (HEW) distribution. This improvement makes the new ASP more advantageous and helps in making optimal decisions.

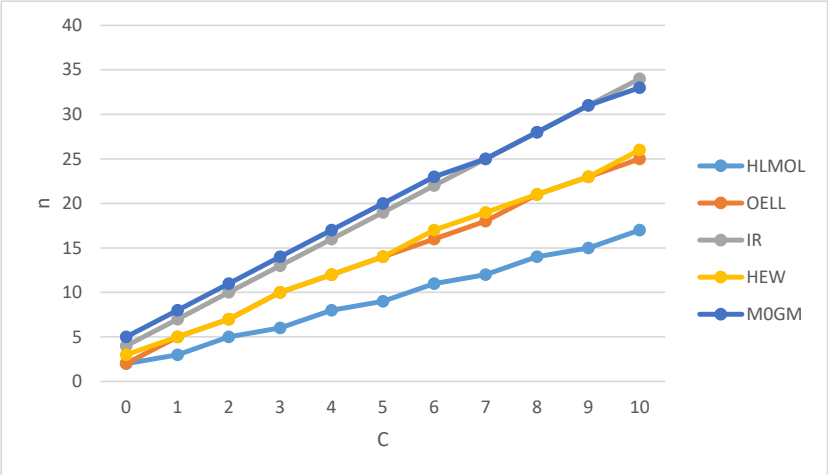

Figure 6: Comparisons between the sample sizes obtained by ASP for different distributions

For the sampling plan (n = 7, C = 2, $\frac{t}{\theta_0}$= 0.6) and confidence level $p^\star = 0.75$ under HLMOL distribution with $\lambda = 2$, $\alpha = 2$, c = 2, the values of the OC function from Table 3 are as given in Table 5.

Table 4: Minimum ratio of true average life to specified average life for the acceptability of a lot with producer's risk of 0.05

$p^\star$	C	$\frac{t}{\theta_0}$								
		0.4	0.6	0.8	1	1.2	1.4	1.6	1.8	2
0.75	0	28.569	28.565	38.087	47.609	27.247	31.788	36.329	40.870	45.411
	1	7.990	8.430	8.755	7.812	9.374	10.937	7.457	8.389	9.321
	2	4.689	4.965	5.461	5.629	5.084	5.931	6.779	7.626	5.555
	3	3.685	3.657	3.638	3.706	4.447	4.020	4.594	5.168	5.742
	4	3.125	3.108	3.171	3.436	3.445	3.182	3.637	4.092	4.546
	5	2.789	2.715	2.940	2.824	2.851	3.326	3.079	3.463	3.848
	6	2.550	2.663	2.505	2.777	2.920	2.883	3.295	3.001	3.335
	7	2.392	2.452	2.418	2.448	2.591	2.568	2.935	2.749	3.054
	8	2.265	2.328	2.336	2.448	2.309	2.694	2.668	3.001	2.766
	9	2.187	2.187	2.297	2.241	2.404	2.489	2.474	2.783	2.601
	10	2.080	2.102	2.090	2.241	2.231	2.305	2.296	2.583	2.415
0.9	0	45.453	54.542	55.167	45.444	54.532	63.621	72.710	40.870	45.411
	1	10.519	10.328	11.401	11.067	13.280	10.937	12.499	14.062	15.624
	2	6.545	6.640	6.620	6.923	6.755	7.881	6.779	7.626	8.473
	3	4.581	4.577	4.875	4.525	5.430	5.188	5.929	5.168	5.742
	4	3.980	4.039	4.137	3.963	4.124	4.020	4.594	5.168	4.546
	5	3.456	3.480	3.620	3.675	3.388	3.953	3.801	4.276	3.848
	6	3.051	3.020	3.039	3.132	3.333	3.407	3.295	3.706	4.118
	7	2.830	2.796	2.859	3.023	2.938	3.023	3.454	3.302	3.670
	8	2.730	2.728	2.697	2.688	2.938	3.048	3.078	3.001	3.335
	9	2.550	2.542	2.598	2.646	2.689	2.805	2.849	3.200	3.092
	10	2.422	2.430	2.377	2.433	2.437	2.602	2.634	2.964	2.870
0.95	0	63.491	68.179	55.167	68.020	54.532	63.621	72.710	81.798	90.887
	1	12.897	13.941	13.770	14.251	13.280	15.494	12.499	14.062	15.624
	2	7.537	7.293	7.727	8.275	8.368	7.881	9.007	7.626	8.473
	3	5.541	5.524	5.461	5.316	5.457	6.366	5.929	6.670	7.411
	4	4.427	4.339	4.503	4.547	4.756	4.811	4.594	5.168	5.742
	5	3.901	3.956	3.922	4.142	3.970	3.953	4.518	4.276	4.751
	6	3.456	3.418	3.551	3.436	3.758	3.888	3.893	3.706	4.118
	7	3.051	3.103	3.103	3.308	3.2787	3.427	3.454	3.886	3.669
	8	2.981	3.020	2.882	2.920	3.226	3.048	3.484	3.463	3.335
	9	2.789	2.796	2.739	2.871	2.920	3.137	3.206	3.200	3.556
	10	2.637	2.601	2.647	2.77	2.650	2.843	2.974	2.964	3.293
0.99	0	90.908	92.306	88.885	90.904	79.991	93.323	106.655	81.798	90.887
	1	18.177	17.637	18.588	17.213	16.859	19.395	17.707	19.920	22.134
	2	10.249	9.818	9.968	9.754	9.930	9.7624	11.157	10.133	11.259
	3	7.006	6.951	6.733	6.826	7.407	7.442	7.275	8.185	7.411
	4	5.465	5.324	5.423	5.629	5.457	2 5.549	6.341	6.186	6.873
	5	4.689	4.650	4.640	4.903	4.970	5.166	5.196	5.082	5.647
	6	4.192	4.244	4.092	4.142	4.124	4.384	4.445	4.999	4.867
	7	3.789	3.703	3.728	3.798	3.970	4.159	4.371	4.406	4.318
	8	3.518	3.544	3.421	3.602	3.504	3.764	3.917	3.919	4.355
	9	3.255	3.244	3.212	3.248	3.445	3.407	3.585	3.606	4.007
	10	3.125	3.020	3.103	3.132	3.125	3.376	3.250	3.656	3.718

Table 5: OC values for the ASP ($n = 7, C = 2, \frac{t}{\theta_0} = 0.6$) for given confidence level $p^\star = 0.75$, acceptance number C=2, $\lambda = 2$, $\alpha = 2$ c = 2

$\frac{\theta}{\theta_0}$	2	4	6	8	10	12
OC	0.6741	0.9282	0.9746	0.9883	0.9937	0.9963

Table 5 shows that if the true average life is twice the required mean lifetime ($\frac{\theta}{\theta_0} = 2$) the producer's risk is approximately 0.3259. The producer's risk is almost equal to 0.0063 when the true true average life is greater than or equal to 10 times the specified average life.

From Table 4, we can get the values of the ratio $\frac{\theta}{\theta_0}$ for different choices of C and $\frac{t}{\theta_0}$ in order to assert that the producer's risk was less than 0.05. For example if $p^\star = 0.75$, $\frac{t}{\theta_0} = 0.8$, C=2, Table 4 gives a reading of 5.461. This means the product can have an average life of 5.461 times the specified average lifetime in order that under the above acceptance sampling plan the product is accepted with probability of at least 0.95.

Practical example: Consider the following ordered failure times of the release of a software given in terms of hours(T) from the starting of the execution of the software denoting the times at which the failure of the software is experienced, it was presented by Wood (1996). This data can be regarded as an ordered sample of size 10 with observations ($t_i; i = 1, 2, ..., 10$): 519, 968, 1430, 1893, 2490, 3058, 3625, 4422, 5218, 5823. Let the specified average life be 1000 hours and the testing time be 600 hrs, this leads to ratio of $\frac{t}{\theta_0}$= 0.6 with corresponding n and C as 10, 2 from Table 1 for $p^\star = 0.95$. Therefore, the sampling plan for the above sample data is (n=10,C=2,$\frac{t}{\theta_0}$=0.6). Based on the 10 observations, we have to decide whether to accept the product or reject it. We accept the product only, if the number of failures before 600 hrs is less than or equal to 2. However, the confidence level is assured by the sampling plan only if the given life times follow HLMOL distribution. In order to confirm that the given sample is generated by lifetimes following at least approximately the HLMOL distribution, we have compared the sample quantiles and the corresponding population quantiles and found a satisfactory agreement. Thus, the adoption of the decision rule of the sampling plan seems to be justified. In the sample of 10 units, there is a 1 failure at 519 hours before t = 600 hours. Therefore we accept the product.

In the above example there is only one failure at 519 corresponding to the ASP for HLMOL (n=10,C=2,$\frac{t}{\theta_0}$=0.6) with confidence $p^\star$=0.95. If we compare it to the sampling plans suggested by Kantam, Rosaiah, and Rao (2001), Jose and Joseph (2018), Jose and Sebastian (2011), Rosaiah and Kantam (2005), Ravikumar, Kantam, and Durgamamba (2016) and Al-Nasser, Al-Omari, Bani-Mustafa, and Jaber (2018) correspnding to n=10, C=3, and $p^\star$=0.95. We can see that the termination time t in HLMOL sampling plan is smaller than the others.

4. Stress-strength reliability and its estimation

In this section, we derive and estimate the stress-strength reliability $R = P(X > Y)$. Let X and Y be two independent random variables with HLMO-X distribution with parameters c_1 and $\lambda = 1$, and HLMO-Y distribution parameters c_2 and $\lambda = 1$, that is, $X \sim$ HLMO-$X(1, C_1)$

and $Y \sim$ HLMO-$Y(1, C_2)$. Then, the stress strength reliability R is given by

$$\begin{aligned} R = P(X > Y) &= \int_0^\infty P(X > Y|Y = y) \;\; r(y)\; dy \\ &= \int_0^\infty \frac{2c_1\bar{F}(y)}{1+(2c_1-1)\bar{F}(y)} \;\; \frac{2c_2 f(y)}{[1+(2c_2-1)\bar{F}(y)]^2}\; dy \\ &= \int_0^1 \frac{4c_1c_2v}{[1+(2c_1-1)v][1+(2c_2-1)v]^2}\; dv \\ &= \frac{c_1c_2}{(c_2-c_1)^2}\int_0^1 \frac{1-2c_1}{1-(1-2c_1)v} - \frac{1-2c_2}{1-(1-2c_2)v} - \frac{2c_2-2c_1}{[1-(1-2c_2)v]^2}\; dv \\ &= \frac{c_1c_2}{(c_2-c_1)^2}\left[-ln(2c_1) + ln(2c_2) - (2c_2-2c_1)\frac{1-2c_2}{2c_2[1-2c_2]}\right] \\ &= \frac{c_1/c_2}{(1-c_1/c_2)^2}\left[-ln\left(\frac{c_1}{c_2}\right) + \frac{c_1}{c_2} - 1\right] \end{aligned} \tag{25}$$

4.1. Maximum likelihood estimation of R

The stress strength reliability R is the function of the parameters c_1 and c_2, respectively. Therefore, for maximum likelihood estimate (MLE) of R, we need to obtain the MLE of the parameters c_1 and c_2.

Suppose $x_1, x_2, ..., x_m$ is a random sample of size m from the HLMOL distribution with parameters $\lambda = 1$, α, θ and c_1, and $y_1, y_2, ..., y_n$ is a random sample of size n from the HLMOL distribution with parameters $\lambda = 1$, α, θ and c_2, and let α and θ be known.

Therefore, the log-likelihood function of the observed samples is given by

$$\begin{aligned} \ell(c_1, c_2) \propto\; & m\; ln\left(\frac{2\alpha}{\theta}\right) + m\; ln(c_1) + (\alpha-1)\sum_{i=1}^{m} ln\left(1+\frac{x_i}{\theta}\right) - 2\sum_{i=1}^{m} ln\left[\left(1+\frac{x_i}{\theta}\right)^{\alpha} + 2c_1 - 1\right] \\ & + n\; ln\left(\frac{2\alpha}{\theta}\right) + n\; ln(c_2) + (\alpha-1)\sum_{j=1}^{n} ln\left(1+\frac{y_j}{\theta}\right) - 2\sum_{j=1}^{n} ln\left[\left(1+\frac{y_i}{\theta}\right)^{\alpha} + 2c_2 - 1\right] \end{aligned} \tag{26}$$

So, the MLEs of c_1 and c_2, say $\hat{c_1}$ and $\hat{c_2}$, respectively, can be obtained as the solutions of the nonlinear equations

$$\frac{\partial \ell}{\partial c_1} = \frac{m}{c_1} - \sum_{i=1}^{m} \frac{4}{\left(1+\frac{x_i}{\theta}\right)^{\alpha} + 2c_1 - 1} = 0 \tag{27}$$

$$\frac{\partial \ell}{\partial c_2} = \frac{n}{c_2} - \sum_{j=1}^{n} \frac{4}{\left(1+\frac{y_j}{\theta}\right)^{\alpha} + 2c_2 - 1} = 0 \tag{28}$$

Then the MLE of R is

$$R = \frac{\hat{c_1}/\hat{c_2}}{(1-\hat{c_1}/\hat{c_2})^2}\left[-ln\left(\frac{\hat{c_1}}{\hat{c_2}}\right) + \frac{\hat{c_1}}{\hat{c_2}} - 1\right]$$

The elements of Fishers information matrix are

$$I_{11} = -E\left(\frac{\partial^2 \ell}{\partial c_1^2}\right) = \frac{m}{c_1^2} - 8mE\left(\frac{1}{\left(1+\frac{X}{\theta}\right)^{\alpha} + 2c_1 - 1}\right)$$
$$= m\left(\frac{1}{c_1^2} - 16c_1 \int_{2c_1}^{\infty} \frac{1}{u^4} du\right)$$
$$= m\left(\frac{1}{c_1^2} - \frac{2}{3c_1^2}\right)$$
$$= \frac{m}{3c_1^2} \tag{29}$$

$$I_{12} = I_{21} = -E\left(\frac{\partial^2 \ell}{\partial C_1 c_2}\right) = 0 \tag{30}$$

$$I_{22} = -E\left(\frac{\partial^2 \ell}{\partial c_2^2}\right) = \frac{n}{c_2^2} - 8mE\left(\frac{1}{\left(1+\frac{Y}{\theta}\right)^{\alpha} + 2c_2 - 1}\right)$$
$$= \frac{n}{3c_2^2} \tag{31}$$

Theorem 4.1. *As $m \to \infty$ and $n \to \infty$, then $[\sqrt{m}(\hat{c_1} - c_1), \sqrt{n}(\hat{c_2} - c_2)] \xrightarrow{d} N_2\big(0, A^{-1}(c_1, c_2)\big)$ where,*

$$A = \begin{pmatrix} a_{11} & 0 \\ 0 & a_{22} \end{pmatrix}$$

and

$$a_{11} = \lim_{m,n\to\infty} \frac{I_{11}}{m} = \frac{1}{3c_1^2}, \quad a_{22} = \lim_{m,n\to\infty} \frac{I_{22}}{m} = \frac{1}{3c_2^2}$$

Proof. We can use the asymptotics properties of MLEs to prove it. □

To obtain the asymptotic 100(1-α) % confidence interval for R, we proceed as follows

$$b_1(c_1, c_2) = \frac{\partial R}{\partial c_1} = \frac{c_2}{(c_2 - c_1)^3}\big[-2(c_2 - c_1) - (c_1 + c_2)\ ln\ \big(\frac{c_1}{c_2}\big)\big]$$

,

$$b_2(c_1, c_2) = \frac{\partial R}{\partial c_2} = \frac{c_1}{(c_2 - c_1)^3}\big[2(c_2 - c_1) + (c_1 + c_2)\ ln\ \big(\frac{c_1}{c_2}\big)\big] = -\frac{c_1}{c_2}\ b_1(c_1, c_2)$$

.

Then,

$$V(\hat{R}) = V(\hat{c_1})\ b_1^2(c_1, c_2) + V(\hat{c_2})\ b_2^2(c_1, c_2)$$
$$= c_1^2\ b_1^2(c_1, c_2)\ \left(\frac{3}{m} + \frac{3}{n}\right).$$

Thus we have the following result.
As $m \to \infty$, $n \to \infty$, $\frac{\hat{R} - R}{c_1\ b_1(c_1, c_2)\ \sqrt{\frac{3}{m} + \frac{3}{n}}} \xrightarrow{d} N(0, 1)$ and the asymptotic 100(1-α) % confidence interval for R is given by

$$\hat{R} \pm Z_{(\alpha/2)}\ \hat{c_1}\ b_1(\hat{c_1}, \hat{c_2})\ \sqrt{\frac{3}{m} + \frac{3}{n}}$$

where $Z_{(\alpha/2)}$ is the $(1 - \alpha/2)^{th}$ percentiles of the standard normal distribution.
Hence, the asymptotic 95% confidence interval for R is given by

$$\hat{R} \pm 1.96\ \hat{c_1}\ b_1(\hat{c_1}, \hat{c_2})\ \sqrt{\frac{3}{m} + \frac{3}{n}}$$

4.2. Simulation study for R

Here, we mainly present some simulation experimentes to study the performance of the MLE estimator and confidence interval for R. The simulation experiment was repeated N=10000 times each with different sample sizes, (m,n)=(15,15), (20,20), (25,20), (25,25), (25,30), (30,20),(30,25), (30,30). The values of c_1 and c_2 were combinations of c_1=0.2, 0.5, 0.6 and c_2=0.4, 0.8, 0.5. We fixed the values of α and θ as, $\alpha = 4$ and $\theta = 1$. In this simulation study, we computed four measures: the average bias (Bias), average mean square error(MSE), average length of the asymptotic 95% confidence intervals and coverage probability of R.

Table 6: Bias and MSE of the simulated estimates of R for $\alpha = 4$ and $\theta = 1$

	(c_1, c_2)					
	Bias			MSE		
(m,n)	(0.2, 0.4)	(0.5, 0.8)	(0.6, 0.5)	(0.2, 0.4)	(0.5, 0.8)	(0.6, 0.5)
(15,15)	0.0394	0.0356	-0.0141	0.0085	0.0077	0.0068
(20,20)	0.0383	0.0355	-0.0140	0.0067	0.0066	0.0055
(25,20)	0.0398	0.0379	-0.0103	0.0062	0.0063	0.0052
(25,25)	0.0370	0.0353	-0.0129	0.0055	0.0059	0.0049
(25,30)	0.0354	0.0348	-0.0160	0.0051	0.0058	0.0047
(30,20)	0.0416	0.0411	-0.0075	0.0059	0.0064	0.0049
(30,25)	0.0386	0.0381	-0.0109	0.0053	0.0059	0.0046
(30,30)	0.0346	0.0345	-0.0125	0.0048	0.0056	0.0044

Table 7: Average confidence length and coverage probability of the simulated estimates of R for $\alpha = 4$ and $\theta = 1$

	(c_1, c_2)					
	Average confidence length			Coverage probability		
(m,n)	(0.2, 0.4)	(0.5, 0.8)	(0.6, 0.5)	(0.2, 0.4)	(0.5, 0.8)	(0.6, 0.5)
(15,15)	0.3945	0.4010	0.4029	0.9593	0.9773	0.9791
(20,20)	0.3437	0.3487	0.3506	0.9624	0.9688	0.9795
(25,20)	0.3272	0.3315	0.3327	0.9622	0.9635	0.9747
(25,25)	0.3085	0.3125	0.3142	0.9621	0.9591	0.9715
(25,30)	0.2954	0.2994	0.3013	0.9605	0.9571	0.9701
(30,20)	0.3156	0.3195	0.3204	0.9612	0.9556	0.9741
(30,25)	0.2960	0.2998	0.3011	0.9590	0.9526	0.9717
(30,30)	0.2818	0.2855	0.2862	0.9576	0.9485	0.9666

The Bias and MSE of are presented in Table 6. The average confidence lengths and coverage probabilities are reported for 95% confidence intervals using exact MLE and asymptotic distribution of R in Table 7. When $c_1 < c_2$, the bias is positive and when $c_1 > c_2$, the bias is negative. The equal (m=n) and unequal (m$\neq$ n) choices of sample sizes are taken to evaluate the estimates of R. From this extensive study, it has been observed that the Bias decreases with increasing sample size n and fixed sample size m, also Bias increases with increase sample size m and fixed n. In general, Bias, MSE and length of the confidence interval decreases as the sample size increases. It verifies the consistency property of the MLE of R. For small sample sizes (m,n), the coverage probabilities for the MLE's are slight less than nominal value, with the increase of sample sizes (m,n), they more close to the nominal value. We also observe that there is no substantial difference in the Bias, MSE, average confidence lengths and coverage probabilities of R for different choices of the parameters.

4.3. Practical data example for R

In this subsection, We consider the real-life data sets of the waiting times (in minutes) before

service of the customers of two diffrent banks A and B, given by Ghitany, Atieh, and Nadarajah (2008). We are interested in estimating the stress-strength reliability $R = P(X > Y)$ where X (Y) denotes the customer service time in Bank A (B). The data sets are given below
Bank A: X(m=100)
0.8, 0.8, 1.3, 1.5, 1.8, 1.9, 1.9, 2.1, 2.6, 2.7, 2.9, 3.1, 3.2,3.3, 3.5, 3.6,4.0, 4.1, 4.2, 4.2, 4.3, 4.3, 4.4, 4.4, 4.6, 4.7, 4.7, 4.8, 4.9, 4.9, 5.0, 5.3, 5.5, 5.7, 5.7, 6.1, 6.2, 6.2, 6.2, 6.3, 6.7, 6.9, 7.1, 7.1, 7.1, 7.1, 7.4, 7.6, 7.7, 8.0, 8.2, 8.6, 8.6, 8.6, 8.8, 8.8, 8.9, 8.9, 9.5, 9.6, 9.7, 9.8, 10.7, 10.9, 11.0, 11.0, 11.1, 11.2, 11.2, 11.5, 11.9, 12.4, 12.5, 12.9, 13.0, 13.1, 13.3, 13.6, 13.7, 13.9, 14.1, 15.4, 15.4, 17.3, 17.3, 18.1, 18.2, 18.4, 18.9, 19.0, 19.9, 20.6, 21.3, 21.4, 21.9, 23.0, 27.0, 31.6, 33.1, 38.5.
Bank B: Y (n=60)
0.1, 0.2, 0.3, 0.7, 0.9, 1.1, 1.2, 1.8, 1.9, 2.0, 2.2, 2.3, 2.3, 2.3, 2.5, 2.6, 2.7, 2.7, 2.9, 3.1, 3.1, 3.2, 3.4, 3.4, 3.5, 3.9, 4.0, 4.2, 4.5, 4.7, 5.3, 5.6, 5.6, 6.2, 6.3, 6.6, 6.8, 7.3, 7.5, 7.7, 7.7, 8.0, 8.0, 8.5, 8.5, 8.7, 9.5, 10.7, 10.9, 11.0, 12.1, 12.3, 12.8, 12.9, 13.2, 13.7, 14.5, 16.0, 16.5, 28.0.

We fitted the HLMOL distribution for each dataset. Let us first assume that $X \sim \text{HLMOL}(\lambda = 1, \alpha = 4, \theta = 7, c_1)$ and $Y \sim \text{HLMOL}(\ \lambda = 1, \alpha = 4, \theta = 7, c_2)$. We used the Anderson-Darling (A-D), Cramer-von Mises and Kolmogorov-Smirnov (K-S) statistics to test the goodness-of-fit and found that the HLMOL distribution is good fitted. The values of A-D, Cramer-von Mises and K-S statistics along P-value are given in Table 8

Table 8: Statistic(P-value) of different goodness-of-fit tests for the data sets

	A-D	Cramer-von Mises	K-S
Bank A(X)	0.2466(0.9721)	0.0311(0.9729)	0.0451(0.987)
Bank B(Y)	0.3349(0.9095)	0.0542(0.852)	0.0748(0.89)

The MLEs of the unknown parameters are $\hat{c_1}$=10.5963, $\hat{c_2}$=3.9109. Replacing the parameters by the estimates we get the MLE of the stress-strength reliability R as 0.6608 and the 95% confidence interval of R is (0.5771, 0.7445).

5. Conclusion

The paper considers the applications of HLMOL distribution in the fields of time series modeling, ASP and stress-strength analysis. In time series modeling, different autoregressive minification processes of order one are developed. These can be used for modelling time series data from different contexts. We developed a ASP for HLMOL distribution by assuming the lifetime of products following HLMOL distribution. For fixed confidence level, the minimum sample size to assert the ratio of specified mean life and the maximum test duration are calculated. The OC values with OC curves and minimum ratio of mean life to the specified life are tabulated. The results are illustrated using a data set. It is shown that the suggested ASP is useful in minimizing the producer's risk. Also, the proposed ASP is more economical than some of the existing ASPs.

In stress-strength analysis, we derive and estimate the stress-strength reliability parameter R based on two independent samples from HLMOL distribution with different parameters. The results for estimation of R by MLE is reported. From the simulation results, it is observed that as the sample size (m,n) increases the Bias, MSE and average confidence length decreases and, the performance of the coverage probability is satisfactory. Also, a real-life data analysis is presented for illustrative purpose.

References

Al-Nasser AD, Al-Omari AI, Bani-Mustafa A, Jaber K (2018). "Developing Single-acceptance Sampling Plans Based on a Truncated Lifetime Test for an Ishita Distribution." *STATISTICS*, **19**(3), 393–406.

Alzaatreh A, Lee C, Famoye F (2013). "A New Method for Generating Families of Continuous Distributions." *Metron*, **71**(1), 63–79.

Arnold BC, Robertson CA (1989). "Autoregressive Logistic Processes." *Journal of Applied Probability*, pp. 524–531.

Birnbaum ZW, McCarty RC, *et al.* (1958). "A Distribution-Free Upper Confidence Bound for $Pr(Y < X)$, Based on Independent Samples of X and Y." *The Annals of Mathematical Statistics*, **29**(2), 558–562.

Birnbaum ZW, *et al.* (1956). "On a Use of the Mann-Whitney Statistic." In *Proceedings of the Third Berkeley Symposium on Mathematical Statistics and Probability, Volume 1: Contributions to the Theory of Statistics*. The Regents of the University of California.

Ghitany ME, Atieh B, Nadarajah S (2008). "Lindley Distribution and Its Application." *Mathematics and Computers in Simulation*, **78**(4), 493–506.

Gillariose J, Tomy L (2018). "A New Life Time Model: The Generalized Rayleigh-Truncated Negative Binomial Distribution." *International Journal of Scientific Research in Mathematical and Statistical Sciences*, **5**(6), 1–12.

Jose KK, Joseph J (2018). "Reliability Test Plan for the Gumbel-uniform Distribution." *Stochastics and Quality Control*, **33**(1), 71–81.

Jose KK, Naik SR, Ristić MM (2010). "Marshall–Olkin q-Weibull Distribution and Max–min Processes." *Statistical Papers*, **51**(4), 837–851.

Jose KK, Sebastian R (2011). "Marshall–Olkin Gumbel-maximum Distribution." Submitted.

Jose KK, Tomy L, Thomas SP (2018). "On a Generalization of the Weibull Distribution and Its Application in Quality Control." *Stochastics and Quality Control*, **33**(2), 113–124.

Kantam RRL, Rosaiah K, Rao GS (2001). "Acceptance Sampling Based on Life Tests: Log-logistic Model." *Journal of Applied Statistics*, **28**(1), 121–128.

Krishnarani SD, Jayakumar K (2008). "A Class of Autoregressive Processes." *Statistics & Probability Letters*, **78**(12), 1355–1361.

Marshall AW, Olkin I (1997). "A New Method for Adding a Parameter to a Family of Distributions with Application to the Exponential and Weibull Families." *Biometrika*, **84**(3), 641–652.

Pillai RN (1991). "Semi-pareto Processes." *Journal of Applied Probability*, pp. 461–465.

Ravikumar MS, Kantam RRL, Durgamamba AN (2016). "Acceptance Sampling Plans for Burr Type X Distribution." *International Journal of Advanced Technology in Engineering and Science*, **4**(8), 36–44.

Rosaiah K, Gadde SR, Kalyani K, Kumar DCU (2018). "Odds Exponential Log-logistic Distribution: An Economic Reliability Test Plan." *International Journal of Science and Research (IJSR)*, **7**, 1653–1660.

Rosaiah K, Kantam RRL (2005). "Acceptance Sampling Based on the Inverse Rayleigh Distribution." *Stochastics and Quality Control*, **20**(2), 277–286.

Sim CH (1986). "Simulation of Weibull and Gamma Autoregressive Stationary Process." *Communications in Statistics-Simulation and Computation*, **15**(4), 1141–1146.

Tavares LV (1980). "An Exponential Markovian Stationary Process." *Journal of Applied Probability*, **17**(4), 1117–1120.

Tomy L, Jose M (2020). "T-Marshall Olkin X Family of Distributions with Properties and Applications." *STATISTICA*. Submitted.

Wood A (1996). "Predicting Software Reliability." *Computer*, **29**(11), 69–77.

Yeh HC, Arnold BC, Robertson CA (1988). "Pareto Processes." *Journal of Applied Probability*, pp. 291–301.

Affiliation:

Lishamol Tomy
Department of Statistics, Deva Matha College
Kuravilangad, Kerala, 686633, India
E-mail: lishatomy@gmail.com

Meenu Jose
Department of Statistics, Carmel College Mala
Thrissur, Kerala, India
E-mail: meenusgc@gmail.com

International Journal of All Research Education and Scientific Methods (IJARESM), ISSN: 2455-6211
Volume 9, Issue 5, May -2021, Impact Factor: 7.429, Available online at: www.ijaresm.com

Calcium Content – A Comparative Study and Mineral analyses of Various Egg Shells

Roshini K. T

Department of Chemistry, Carmel College, Mala, India

----------**********----------

ABSTRACT

Egg shells are the rich source of mineral salts, mainly calcium carbonate, which was probably the best natural source of calcium and it was about 90% absorbable. Our study was designed to evaluate the percentage of calcium carbonate in various egg shell samples of our locality because of its potential applications that minimize their effect on environmental pollution. Mineral analyses were also done using common methods in literature. Six different samples of egg shells were taken under consideration which includes broiler chicken egg, duck egg, local hen egg, quail egg, black hen egg and turkey egg. The highest quantity of calcium carbonate observed was 84.40% and the least was72.68%. From the fore going analyses, it has been found out that, there was high amount of calcium carbonate ($CaCO_3$) in virtually all the samples analyzed, an average of 80 % was found to be present.Calcium, Magnesium, Iron and Aluminium were found in all the six samples

Keywords: Egg shells, Mineral Analysis, calcium carbonate

INTRODUCTION

Eggshell which forms the outer crust of an egg is a non edible product with very limited use & value and is largely disposed of as a waste.But actually, theywere a reserve of many bioactive compounds with high economic and monetary value, which can be extracted by the efficient separation of eggshell and membrane. The extraction of the many bioactive compounds present in the egg membrane would not only benefit the egg processing industry by giving them a new source of revenue but also the cosmetic and pharmaceutical industry by reducing the processing cost significantly; making the product cheaper and hence affordable for a wider section of society[1-8].

The eggshell which consists of various different layers can be described as a well-organized structure, the formation of which begins at different segments of the hen's oviduct. A number of different proteins (soluble and insoluble) and minerals are deposited during the process of eggshell formation which is later used up by the developing embryo. The insoluble proteins have been suggested to act as structural framework and the soluble proteins become embedded in the calcified layers. The deposited mobilized calcium is used for the development and formation of embryo's skeleton (Lammie et al. 2005; Stadelman and Cotterill 1996)[9].

Egg shells are the rich source of mineral salts, mainly calcium carbonate, which is probably the best natural source of calcium and it is about 90% absorbable. Our study was designed to evaluate the percentage of calcium carbonate in various Egg shell samples of our locality because of its potential applications that minimize their effect on environmental pollution.

MATERIALS AND METHODS

Fresh six egg sampleswere collected from locality.These include broiler chicken egg, duck egg, local hen egg, quail egg, black hen egg and turkey egg.All samples were washed with distilled water and all of the membranes were peeled off from the inside of the shell. Dry the shell with a paper towel and put into a beaker. Place the beaker with the shell in the oven, and dry the shell for about 30 minutes. It was important that the shell be dry in order to get best results. Remove the shell from the oven and grind it to a very fine powder using mortar and pestle. It was then then sieved and kept in an air tight container.

Estimation of Calcium Carbonate in Egg Shell

Calcium Carbonate is very insoluble in pure water but will readily dissolve in acid according to the equation below:

$2HCl(aq) + CaCO_3(s) \rightarrow CaCl_2(aq) + CO_2(g) + H_2O(l) + HCl(aq)$ (1)(in excess) (limiting reagent) (unreacted)

Estimation was achieved by adding on excess of acid to dissolve all of the $CaCO_3$ and then titrating the remaining HCl with NaOH solution to determine the amount of acid which has not reacted with the calcium carbonate. The reaction

used to determine the amount ofunreacted acid by titration was given below. This type of analysis was generally referred to as a back-titration.

$HCl(aq) + NaOH(aq) \rightarrow NaCl(aq) + H2O(l)$ (2)
(unreacted)

The difference between amount of the acid (HCl) initially added and the amount left over after the reaction was equal to the amount used by the $CaCO_3$.

Dissolution of the eggshell in excess HCl
Accurately weigh 0.35g of dried shell into 250ml beaker. Add 4 drops of ethanol to the beaker. This acts as a wetting agent and helps the hydrochloric acid dissolve the $CaCO_3$.Pour 10ml of the 0.1M HCl into the beaker. Swirl the flasks to wet all of the solids. Heat the solution in the beaker until they begin to boil and the solid egg shell dissolves. It is important that all of the eggshell solids dissolve because this contains the material to analyse. Eggshell was dense and will settle on the bottom of the beaker. A white proteinaceous substance may form, but it will be suspended in the solution. Maintain a consistent fluid level in the beaker by periodically washing down the walls of the flask with deionized water from bottle. Do not allow the liquid to completely evaporate. The process of dissolving the eggshell is complete when no more "the eggshell were visible in the flask. Allow the beaker to cool. Rinse the walls of the beaker one last time with water from wash bottle.

Titration of Unreacted HCl with 0.5N NaOH
Add 10 drops of phenolphthalein indicator to beaker. Fill the burette with standardized NaOH solution. Titrate the sample to the first persistent barely-pink colour. When close to the endpoint the colour will fade slowly. Add more NaOH dropwise until the colour remains for at least 30 seconds. Read and record the final volume.

Mineral Analysis
Test for Calcium
To a little of the sample solution ammonium hydroxide, ammonium chloride, and excess of ammonium carbonate solutions are added. A white precipitate is formed.

Test for Strontium
Reaction paper is impregnated with saturated solution of potassium chromate and dried.One drop of test solution is placed on the paper and after a minute drops of sodium rodisonate in water is placed on the moistened spot. A brownish red spot is observed.

Test for Magnesium
To little of the sample two drops of mageson reagent is added followed by two drops of NaOH. A blue precipitate is formed.

Test for Aluminum
To a little of the sample solution a drop of 2M NaOH and one drop of 1% aqueous solution of Alizarin reagent is added. Then acetic acid added in drops until violet colour disappear and one drop excess. A red precipitate is formed.

Test for Phosphorous
To a little of the sample solution concentrated HNO_3 is added and heated. Then ammonium molybdate is added to this solution. A scanty yellow colour is observed.

Test for Zinc
A little of mixture is heated with few drops of Con. HNO_3 and few drops of cobalt nitrate solution and a filter paper dipped in the solution is burnt to ashes, if it shows green colored ash; then presence of zinc.

Test for Iron
A drop of test solution is mixed with one small crystal of tartaric acid and a drop of dimethyl glyoxime followed by drops of ammonium hydroxide. A red colour is developed.

RESULTS AND DISCUSSION

Percentage of $CaCO_3$ in Egg Shell Samples
According to our experimental analysis of eggshell samples, the Broiler chicken egg and Local hen egg has the highest value of calcium content (0.2954g), percentage of $CaCO_3$ was 84.41%. The Turkey egg has the lowest value of calcium content (0.2544g), percentage of $CaCO_3$ was 72.69%.

Table 1: Percentage of Calcium Carbonate in egg samples

Sl.No.	Sample	Weight of $CaCO_3$ (g)	Percentage of $CaCO_3$ in the Sample (%)
1	Broiler chicken egg	0.2954	84.41
2	Duck egg	0.2911	83.17
3	Local hen egg	0.2954	84.41
4	Black hen egg	0.2846	81.32
5	Quail egg	0.2760	78.86
6	Turkey egg	0.2544	72.69

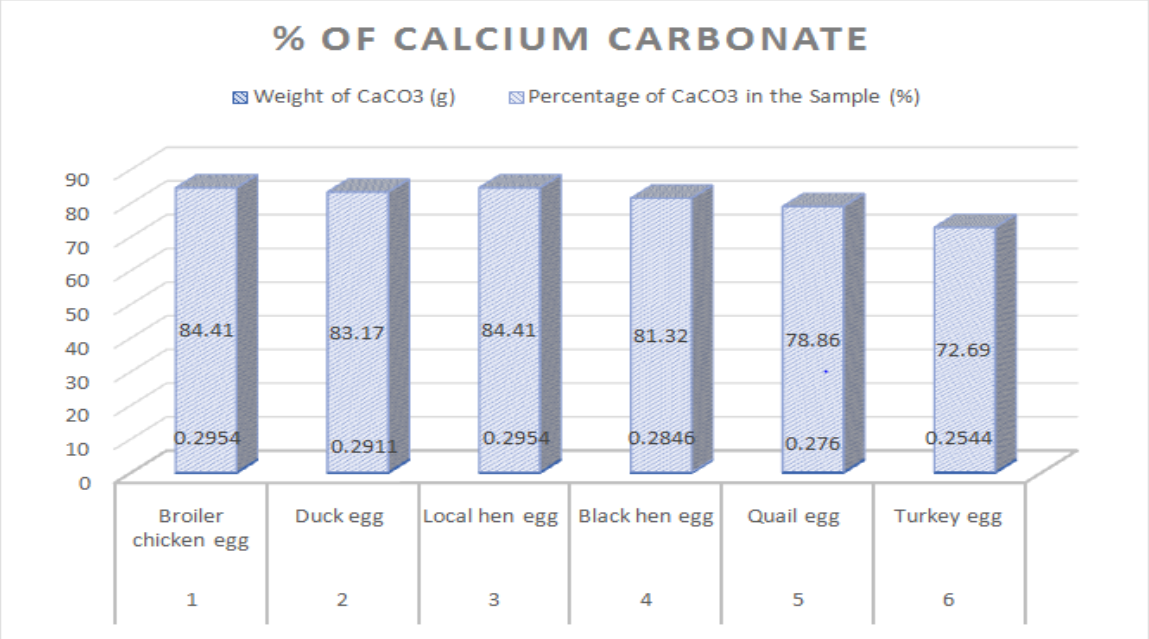

Fig 1: Percentage of Calcium Carbonate in egg samples

Increased or decreased calcium level in birds might be depending upon their habitat. In case of domestic hens, they are fed with supplementary feed. This may be one of the reason for the difference in the calcium content of some egg shell. This may increase the quality of egg shell.Numerous factors affect the functional quality of the egg shell mostly prior to the egg is laid. The thickness of the shell is determined by the amount of time it spends in the shell gland and the rate of calcium deposition during shell formation. If the egg spends a short period in the shell gland, the thickness will be less. Also, the time of the day when the egg is laid determines the thickness of the shell[11].

Mineral Analysis

Our mineral analysis results were shown in table below.It was found that the eggshells are rich in mineral elements. Calcium and magnesium which are often found together are present in all samples which can be used in bones development and so also the muscles. Phosphorus was present in all samples except Quail and Turkey which was required daily for proper physiological function such as bone formation, nucleotide for enzymes activities, ATP, ADP phosphate and energy transmitting forming system. Iron was present in all samples which can be used as a supplement in the body for oxygen transport by hemoglobin and enzymatic oxidation reactions. Strontium was found in Duck, Local Hen and Turkey whereas Aluminium was present in all.Zinc was present in Quail and Turkey egg shell only.

Table 2:Mineral Analysis in egg samples

Samples / Elements	Broiler Chicken	Duck	Local Hen	Black Hen	Quail	Turkey
Calcium	✓	✓	✓	✓	✓	✓
Strontium	X	✓	✓	X	X	✓
Magnesium	✓	✓	✓	✓	✓	✓
Aluminium	✓	✓	✓	✓	✓	✓
Phosphorus	✓	✓	✓	✓	**X**	**X**
Zinc	**X**	**X**	**X**	**X**	✓	✓
Iron	✓	✓	✓	✓	✓	✓

CONCLUSION

Present work was conducted with an overall view to determine the quantity of calcium carbonate in different types of egg shells, Six different samples of egg shells were taken under consideration. These include broiler chicken egg, duck egg, local hen egg, quail egg, black hen egg and turkey egg. The quantity of calcium carbonate was found to be more for local hen egg and broiler chicken egg and the turkey egg has the least amount of calcium carbonate. The highest quantity of calcium carbonate observed is 84.40% and the least is 72.68%. From the fore going analyses, it has been found out that, there is high amount of calcium carbonate ($CaCO_3$) in virtually all the samples analyzed, an average of 80 % was found to be present. It was also found that the eggshells are rich in mineral elements. Calcium, Magnesium, Iron and Aluminium were found in all the six samples. Phosphorus was detected in all the four samples except Quail and Turkey, instead Zinc was present in them, Strontium was the other element present in Duck, Local hen and Turkey.

Eggshells can be utilized for various purposes that minimize their effect on environmental pollution. Eggshells present healthy, balanced calcium due to its trace amounts of other minerals and is probably the best natural source of calcium[3].

ACKNOWLEDGEMENT

The author was thankful to Manager, Principal and Head of the Department of chemistry, Carmel College, Mala for the laboratory facility, constant support and encouragement.

REFERENCES

[1] Nakano T, Ikawa NI, Ozimek L. Chemical Composition of Chicken Eggshell and Shell Membranes. Journal of Poultry Science. 2003; 3:510-514.
[2] Aitken, R.N.C. The oviduct in D.J Bell and B.M. Freeman, Physiology and Biochemistry of Domestic fowl. Vol.3. Academic, London, 1971.
[3] E.I. Adeyeye**,**Comparative study on the characteristics of egg shells of some bird species, Bull. Chem. Soc. Ethiop. 2009, 23(2), 159-166.
[4] Amu OO, Fajobi AB, Oke BO. Effect of eggshell powder on the stabilizing potential of lime on an expansive clay soil. Res. J Agric. & Biol. Sci. 2005; 1:80-84.
[5] Ihekoronye, A.I.; Ngoddy, P.O. Intergraded Food Science and Technology for the Tropics, Macmillan Publishers: London and Basingstoke; 1985; pp 360-364.
[6] Bain M. A reinterpretation of eggshell strength. In: Solomon SE, editor. Egg and egg-shell quality, vol. 9. - London: Wolfe Publishing; 1991. p. 131–41.
[7] Baker JR, Balch DA. A study of the organic material of hen's egg-shell. Biochem J. 1962;82:352–61.
[8] Kingori AM. A Review of the uses of Poultry Eggshell and Shell Membranes. International Journal of Poultry Science. 2011; 10(11):908-912.
[9] John N. Maina , Structure and Function of the Shell and the Chorioallantoic Membrane of the Avian Egg: Embryonic Respiration, 2017; 219-247
[10] Hunton P. Research on eggshell structure and quality: an historical overview. Brazilian Journal of Poultry Science. 2005; 7:67-71.
[11] Shwetha A, Dhananjaya ,Ananda; Comparative study on calcium content in egg shells of different birds International Journal of Zoology Studies 2018,4 ,31-33
[12] Nys Y, Gautron J, Garcia-Ruiz JM, Hincke MT. Avian eggshell mineralization: biochemical and functional characterization of matrix proteins. ComptesRendusPalevol. 2004; 3:549-562.
[13] A.O.A.C. Official Methods of Analysis, 18th ed., Association of Analytical Chemists: Washington DC; 2005

[14] Pearson, D.; Chemical Analysis of Foods, 7th ed., Churchill Livingstone: London; 1976; pp 7-11.
[15] Adeyeye, E.I. *J. Chem. Soc. Nig*. **2005**, 30, 145.
[16] Adeyeye, E.I. *Int. J. Food Sci. Nutr*. **2008**, 59, 699.
[17] Adeyeye, E.I. *Orient. J. Chem*. **2004**, 20, 471.
[18] Alsmeyer, R.H.; Cunningham, A.E.; Happich, M.L. *Food Technol.* 1974, 28, 34.

IJCRT.ORG ISSN : 2320-2882

INTERNATIONAL JOURNAL OF CREATIVE RESEARCH THOUGHTS (IJCRT)

An International Open Access, Peer-reviewed, Refereed Journal

HYDROTHERMAL SYNTHESIS OF NANO-TIO_2 PHOTOCATALYST AND ITS CHARACTERIZATION

[1]Vidya Francis, [2]Ayswarya E P, [3]Ajalesh B Nair, [4]Eby Thomas Thachil
[1]Assistant Professor, [2]Assistant Professor, [3]Assistant Professor, [4]Professor
[1]Department of Chemistry, Carmel College, Mala, Thrissur, Kerala

Abstract: Nanoanatase having photocatalytic activity was successfully prepared by hydrothermal method under controlled conditions using Titanium-iso-propoxide. It is one of the most commonly used semiconductor oxide for environmental photocatalysis, being of low toxicity, insoluble in water and stable to photo and chemical corrosion over a wide range of pH. Their properties, which are determined by the preparation method, are very crucial in photocatalysis. The advantages of the hydrothermal method are that it is an easy method to obtain nanotube morphology, variation in the synthesis method can be implemented to enhance the properties of TiO_2 nanotubes, and it is a feasible method for different applications. A systematic characterization was done using XRD, BET, FTIR and SEM techniques. When compared to commercial form, nanostructures have several advantages like large surface area, controlled morphology, size, porosity to obtain desired surface chemistry.

Index Terms: TiO_2, Hydrothermal, anatase, photocatalyst

1.INTRODUCTION

Studies on the photochemical activity of pigments in commercial polyolefins have been mainly concerned with white pigments. Titanium dioxide (TiO_2) is the most widely studied of these, since it is technically outstanding in many respects (King, 1968). Anatase, brookite and rutile are the three crystalline forms of titania. Among these crytalline forms anatase-TiO_2 deserves more attention by virtue of its use as pigment (J.G. Balfour, 1994) and gas sensors (Y.C. Yeh et al,1989), catalysts (C.G. Bond et al, 1991; P.S.Awati et al, 2003) and photocatalysts (Hagfeldt et al, 1995; Y.H. Hsien et al, 2001; C. Lizama et al, 2002) in applications related to pollution control and in photovoltaics (N. Serpane et al, 2000). The catalytic and other properties of these materials strongly depend on the crystallinity, surface morphology, the particle sizes and preparation methods. TiO_2 nanoparticles have real advantages in relation to photocatalytic activity. Different preparation processes for them have been reported, such as sol–gel process (G. Colon et al, 2002), hydrolysis of inorganic salts (Y. Zhang et al, 2001), ultrasonic technique and hydrothermal process (X.M. Wu et al, 2001; E. Vigil et al, 2001; H. Zhang et al, 2001; X. Ju et al, 2002).

This study describes a rapid hydrothermal synthesis method to produce phase pure, monodisperse anatase particles with small grain size and high specific surface area at low temperature. Hydrothermal processing of either amorphous titania or a titanium containing precursor has been shown to be an ideal method for producing ultrafine (grain size< 10nm) anatase crystallites with high specific surface areas and high crystallinity, a property that is essential for photocatalytic reactions (J. Ovenstone et al, 2001).

II. MATERIALS AND METHODS

Materials

Titanium-iso-propoxide, $[Ti(OPr^i)_4]$ purchased from Alpha was used as titanium source for TiO_2 photocatalyst preparation. $Ti(OPr^i)_4$ was used without further purification. Glacial acetic acid ($C_2H_4O_2$, 99.5%) was used as a solvent. Distilled water was used for the hydrolysis of $Ti(OPr^i)_4$.

Preparation of nano-TiO_2 photocatalyst by hydrothermal method

The most popular technique to hydrolytically prepare nanocrystalline titania is hydrothermal processing, i.e., crystallization at elevated temperature and pressure in the presence of water (A.Rabenau et al, 1985). Hydrothermal crystallization is carried out in a sealed autoclave. A heating mantle or oven is used to raise the temperature above the standard boiling point of the solvent, at which point the evaporating solvent begins to generate a pressure inside the sealed vessel exclusively due to the refluxing solvent. Hydrothermal reaction times are often as short as 2 h and are rarely longer than 1-2 days. The following procedure was employed in this case.

10ml $Ti(OPr^i)_4$ was dissolved in 20ml acetic acid by stirring. After stirring for 10 minutes, 200ml distilled water was added dropwise from a burette at a rate of 1ml/min. The stirring without heating was continued till a clear solution was obtained. The clear solution was then transferred into a Teflon-lined autoclave. The autoclave was then maintained at 110^0C overnight without shaking or stirring. After the autoclave naturally cooled to room temperature, the sample soution (Fig.1) was transferred into a beaker and subjected to solvent evaporation at 110^0C for 2h. It was then dried in oven at 110^0C for a few minutes in a current of air. The sample was then calcined at 400^0C in the muffle furnace for different time intervals to ensure a crystalline product (Fig.2). During this processing titanium (IV) alkoxide reacts with water and forms Ti-O-Ti bridges to create solid TiO_2, according to the reaction;

$$Ti(OR)_4 + 2\,H_2O \rightarrow TiO_2 + 4\,ROH$$

Fig. 1 The solution obtained after hydrothermal treatment in an autoclave

Fig. 2 TiO_2 nano particles obtained after calcinations at 400^0C

Characterization of nanotitania

X-Ray diffraction

The crystalline phase of the hydrothermally synthesized TiO_2 nanoparticles was analyzed by X-ray powder diffraction (XRD) pattern obtained from Bruker D8 Advance Model Diffractometer with Cu Kα radiation in the region $2\theta = 10–80^0$ and Ni filter operating at 30kV and 20mA. The crystallite size of the anatase particles was calculated from the X-ray diffraction peak using Scherrer's equation (B. D. Cullity, 1978; L. E. Alexander, 1968);

$$d_{hkl} = k\lambda / (\beta \cos(2\theta))$$

where d_{hkl} is the average crystallite size (nm), λ is the wavelength of the Cu Kα radiation applied ($\lambda = 1.54A^0$), θ the Bragg's angle of diffraction, β the full-width at half maximum intensity of the peak observed at $2\theta = 25.3^0$ (converted to radians) (L.Q. Jing et al, 2001) and k the constant usually taken as 0.94.

Bulk density

The bulk density of the material was determined as per ASTM D 1895-96. The small end of the funnel is closed with hand or a suitable flat strip and 115±5 cm^3 of samples are poured into the funnel. Open the bottom of the funnel quickly and allow the material to flow freely into the cup. If caking occurs in the funnel, the material may be loosened with a glass rod. After the material has passed through the funnel immediately scrape off the excess on the top of the cup with a straight edge without shaking the cup. Weigh the material nearest to 0.1g and determine bulk density.

BET studies

Surface area of the titanium dioxide nano particles as well as commercial titania were measured using BET method. Measurements were carried out under nitrogen atmosphere using ASAP 2000 model, surface area and porosity analyzer. Surface area was determined using the equation,

$$S_{BET} = 4.353\ V_m$$

where S_{BET} is the surface area in m^2/g and V_m is the molar volume of adsorbate gas (N_2) at STP.

Fourier transform infrared spectroscopy

FTIR spectra of the commercial and synthesized TiO_2 in powder form was recorded in the range 400 to 4000 cm^{-1}.

Scanning electron microscopy

The surface morphology of TiO_2 was examined using a scanning electron microscope. The synthesized and commercial TiO_2 samples were sputter-coated with a thin layer of gold and examined under scanning electron microscope.

III.RESULTS AND DISCUSSION

X-Ray diffraction

The XRD pattern is shown in Figs. 3 to 7. All the sharp peaks observed belong to anatase-TiO_2. Rutile and brookite phases were absent as their characteristic d-spacing values were not observed. Apparently, a complete anatase TiO_2 crystalline phase was obtained.

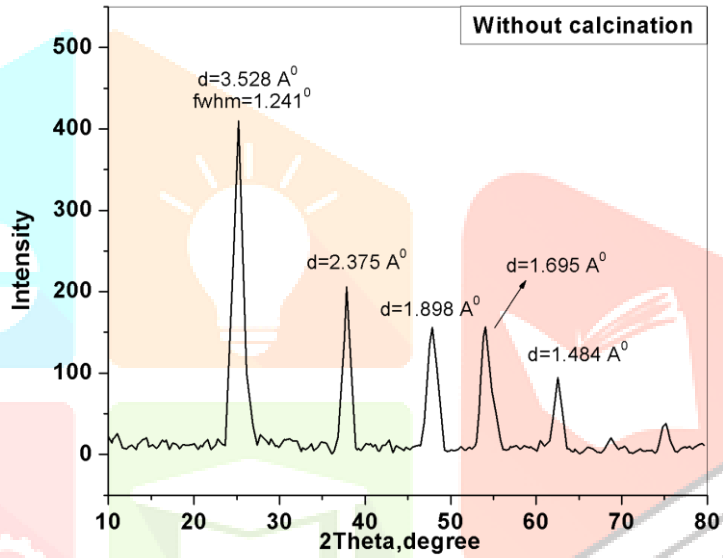

Fig.3 XRD pattern of hydrothermally synthesized nano-TiO_2 powder without calcination

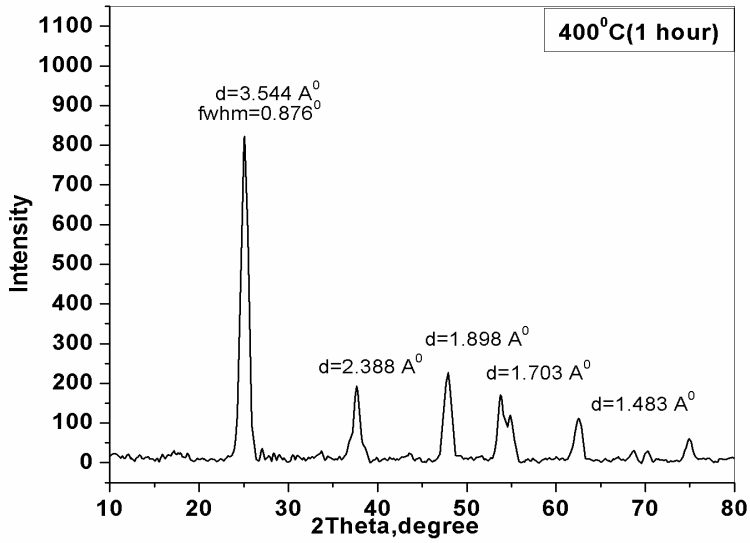

Fig.4 XRD pattern of hydrothermally synthesized nano-TiO_2 powder with calcination at 400^0C for 1 hour

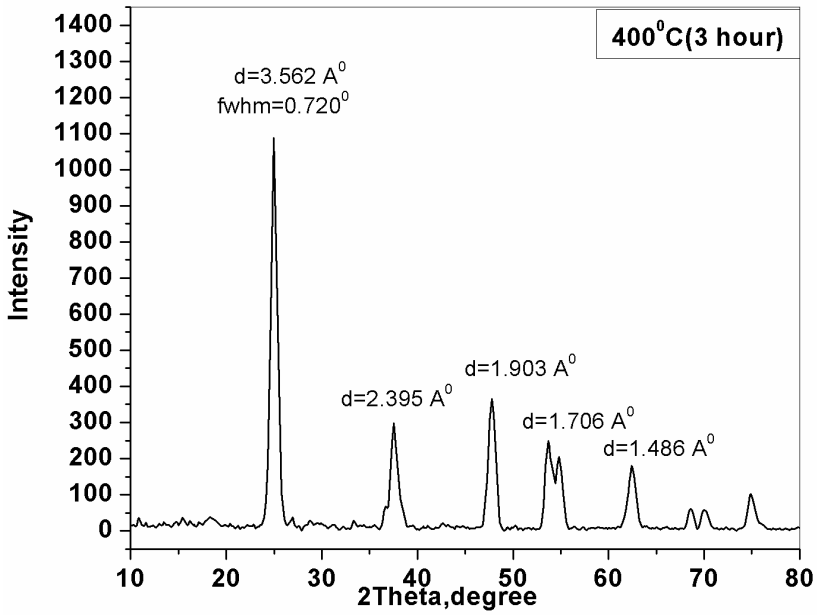

Fig.5 XRD pattern of hydrothermally synthesized nano-TiO_2 powder with calcination at 400^{0}C for 3 hours

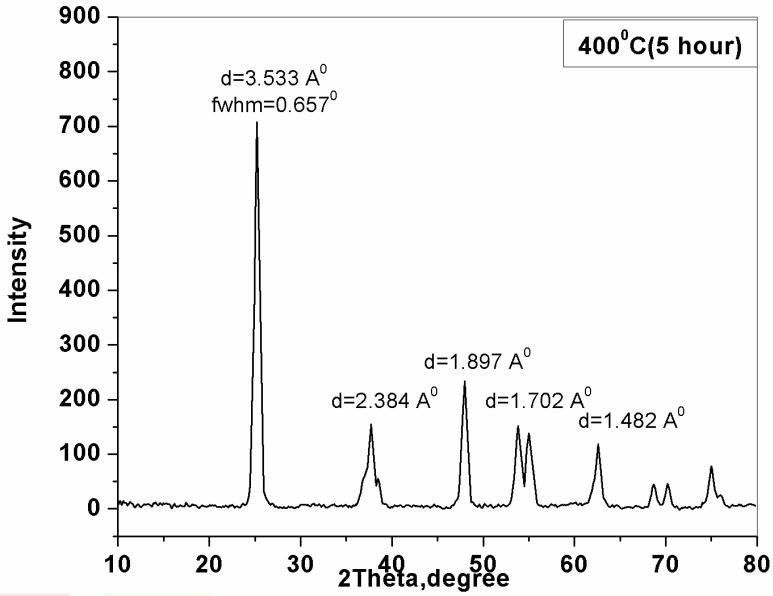

Fig.6 XRD pattern of hydrothermally synthesized nano-TiO_2 powder with calcination at 400^{0}C for 5 hours

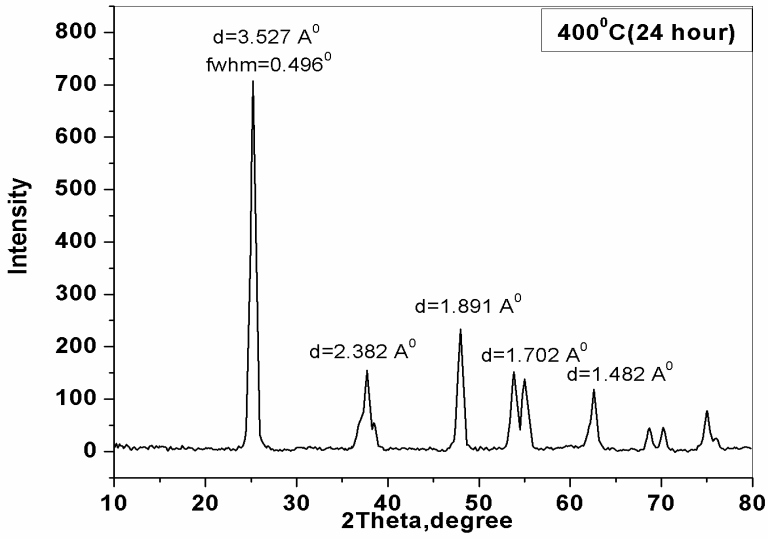

Fig.7 XRD pattern of hydrothermally synthesized nano-TiO_2 powder with calcination at 400^{0}C for 24 hours

Details of X-Ray diffraction studies are given in Table 1. Average crystallite size of TiO_2 was estimated by Scherrer's equation. The average crystallite size of the nano-TiO_2 (without calcinations) was estimated to be 6 nm and it is much lower than most other commercially available titania samples.

Table-1 Data of X-Ray diffraction studies

Catalyst	Calcination time (hour)	2θ (^{0})	Cos θ	β (^{0})	Crystallite size (nm)
A0	0	25.220	0.97	1.241	6.56
A1	1	25.108	0.97	0.876	9.29
A3	3	24.981	0.97	0.720	11.31
A5	5	25.188	0.97	0.657	12.39
A24	24	25.233	0.97	0.496	16.43

[A0 = Anatase sample without calcination, A1= Anatase sample after 1hour calcination, A3 = Anatase sample after 3hour calcination, A5 = Anatase sample after 5hour calcination, A24 = Anatase sample after 24hour calcination.]

The variation of β value and crystallite size with calcination time is shown in Figs. 8 and 9 respectively. The gradual narrowing of XRD lines with the increase in calcinations time (Fig. 8) reflects a corresponding increase in the average crystallite size (Fig. 9).

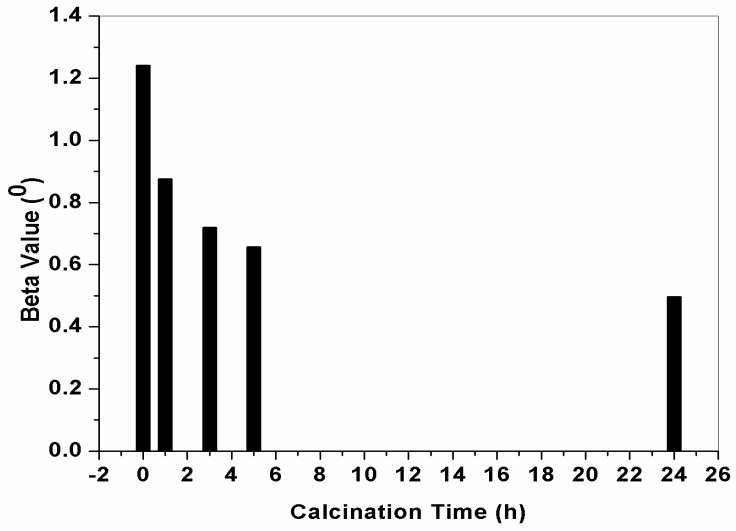

Fig. 8 Variation of β value with calcination time

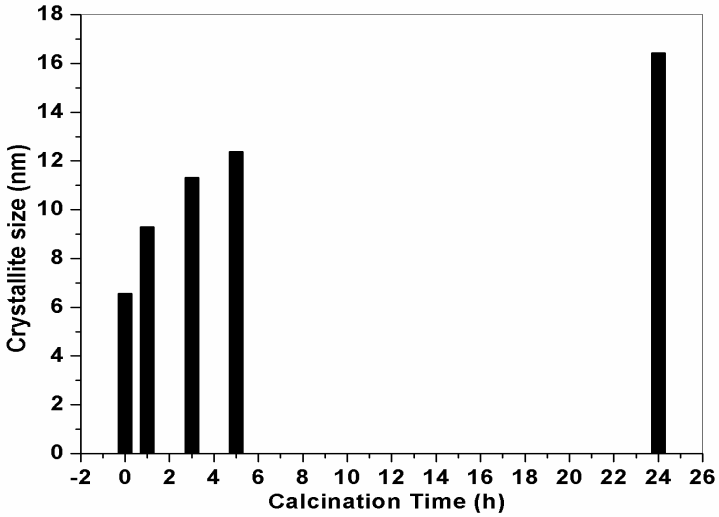

Fig. 9 Variation of crystallite size with calcination time

Bulk density

The bulk density of the commercial and synthesized samples is given in Table 2. It is found that the bulk density of the synthesized anatase (A0-A24) is higher than that of commercial anatase (A). This is due to the smaller particle size of synthesized anatase compared to that of commercial anatase.

Table-2 Bulk densities of the prepared anatase samples

Samples	Bulk density (g/cm^3)
A	0.979
A0	1.296
A1	1.282
A3	1.173
A5	1.136
A24	1.104

The variation of bulk density with calcination time is shown in Fig.10. Bulk density of the synthesized anatase samples decreases with increase in calcination time. This is due to the increase in particle size.

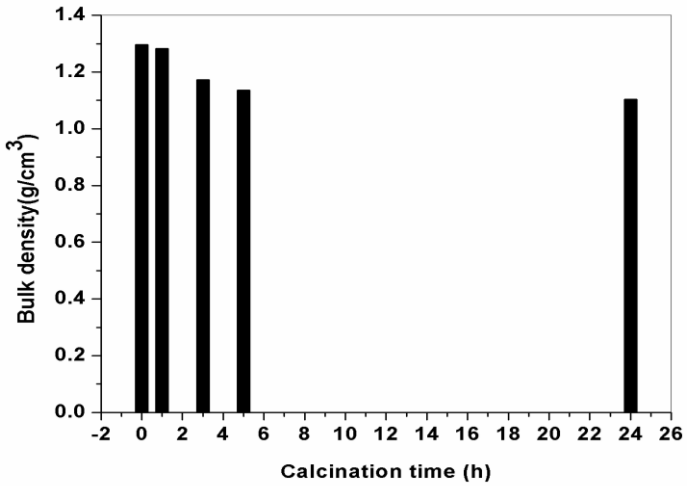

Fig.10. Variation of bulk density with calcination time

BET studies

Table 3 gives the BET adsorption results of nano and commercial anatase. From the table it is clear that nanoanatase has higher surface area than that of commercial anatase. Higher the surface area, lower the particle size. It is very well known that the photocatalytic effect of a catalyst is dependent on the crystallite size and surface area. The smaller the particles, the larger will be its specific surface area and the higher photocatalytic activity (M. Asilturk et al, 2005).

Table 3 Surface area of the TiO_2 samples

Samples	Surface area (m^2/g)
Commercial anatase	110
Nanoanatase	310

Infrared spectroscopy

The FTIR spectrum of nano and commercial forms of TiO_2 are shown in Figs. 11 and 12 respectivey. In the FTIR spectrum, the broad band at 3360 cm^{-1} is attributed to bound water. The peak at 1624 cm^{-1} is due to vibration frequency corresponding to the bending of water molecule (O-H bending vibration). Ti-(O-C) vibration is observed as a small band around 1053 cm^{-1}. The sharp band observed at 930 cm^{-1} is attributed to Ti-O stretching vibration.

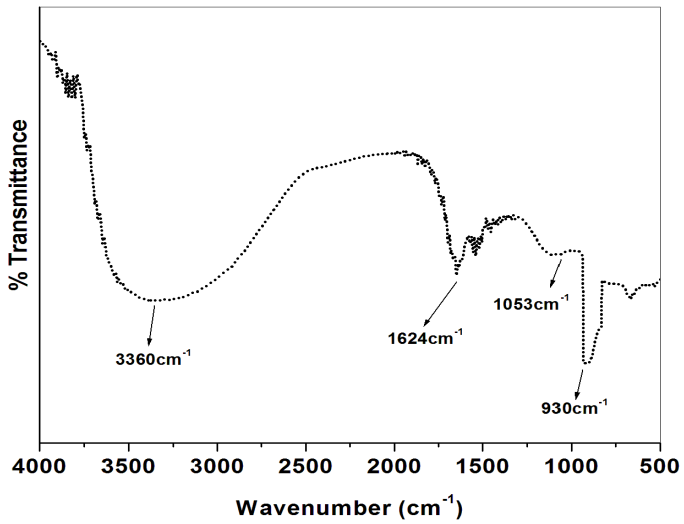

Fig. 11 FTIR spectrum of synthesized nano-TiO_2 particle dried at 110^{0}C

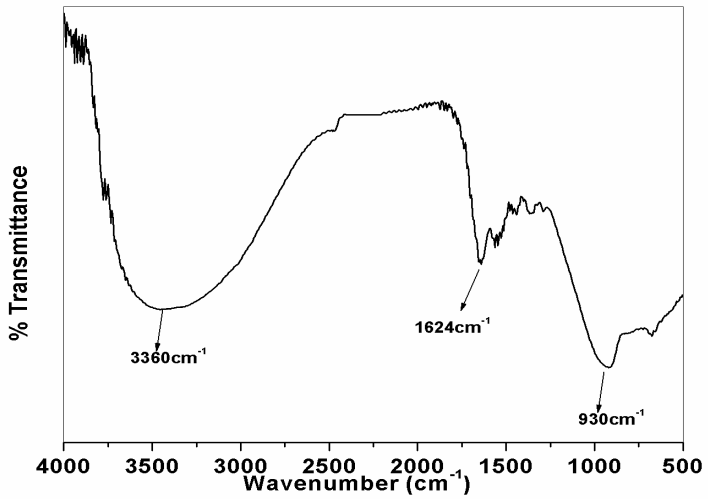

Fig. 12 FTIR spectrum of commercial-TiO_2

Scanning electron microscopy

The surface morphology of TiO_2 was examined by a JEOL JSM-6390LV Model scanning electron microscope. The scanning electron micrographs of the synthesized nano and commercial forms of TiO_2 are shown in Figs. 13 and 14. These micrographs show that the synthesized TiO_2 has lower particle size than the commercial TiO_2. From the micrographs it is clear that anatase particles are spherical in shape.

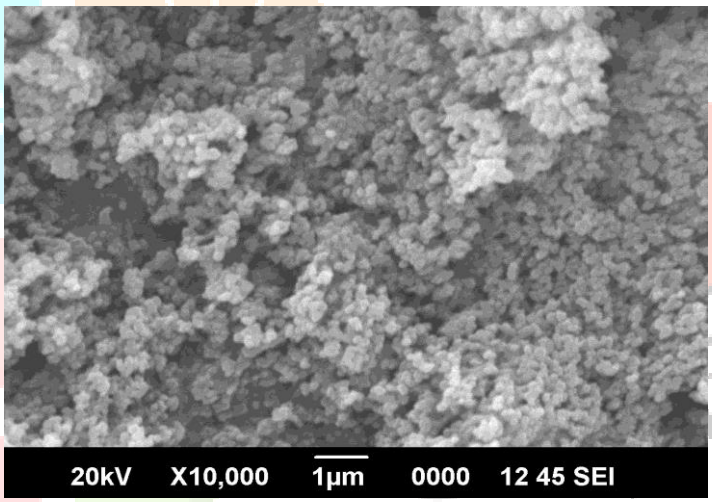

Fig.13 Typical SEM micrograph of hydrothermally synthesized nanoanatase particle

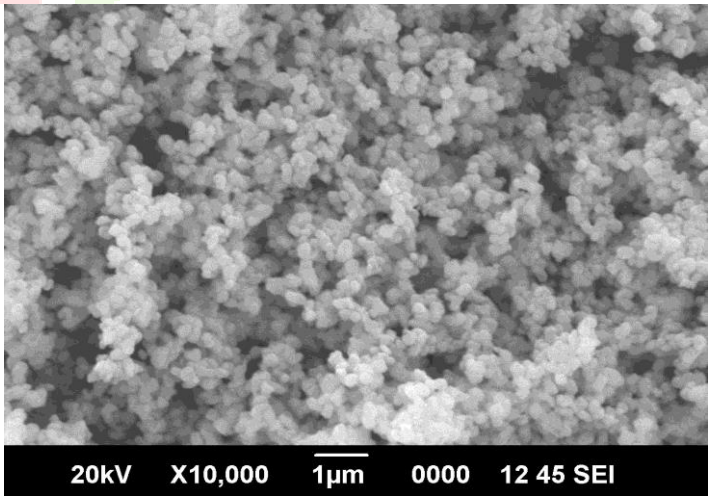

Fig. 14 Typical SEM micrograph of commercial anatase particle

IV.CONCLUSIONS

- Nanoanatase having photocatalytic activity was successfully prepared by hydrothermal method under controlled conditions.
- XRD studies showed that anatase was the only crystalline phase in the nano TiO_2 powder.
- The crystallite size of titania was calculated to be 6nm from the XRD results.
- Crystallite size increases as the calcination time of the synthesized anatase is increased.
- Anatase without any calcination showed the smallest crystallite size.
- From BET method the surface area was found to be $310m^2/g$ which is higher than that of commercial anatase ($110m^2/g$). Higher the surface area, lower the particle size.
- The smaller particle size and larger specific surface area indicates higher photocatalytic activity.
- SEM shows that nanoanatase prepared by this method is spherical in shape.

V. REFERENCES

[1] KING. 1968. Plastics and Polymers.
[2] J.G. Balfour. 1994. Technological Applications of Dispersions, Marcel Dekker, New York.
[3] Y.C. Yeh, T.T. Tseng, D.A. Chang. 1989. J. Am. Ceram. Soc.,72 ,1472.
[4] C.G. Bond, S. F. Tahir. 1991. Appl. Catal.,71, 1.
[5] P.S.Awati, S.V.Awate, P.P.Shah, V.Ramaswamy. 2003. Catal.Comm.,4, 393.
[6] Hagfeldt, M. Gratzel. 1995. Chem. Rev.,95,49.
[7] Y.H. Hsien, C.F. Chang, Y.H. Chen, S. Cheng. 2001. Appl. Catal., B Environ., 31, 241.
[8] C. Lizama, J. Freer, J. Baeza, H.D. Mansilla. 2002. Catal. Today, 76, 235.
[9] N. Serpane, J. Texier, A.V. Emeline, P. Pichat, H. Hidaka, J. Zhao; J. Photochem. Photobiol. 2000. A Chem.,136,145.
[10] G. Colon, M.C. Hidalgo, J.A. Navio. 2002. Catal. Today., 76, 91.
[11] Y. Zhang, G. Xion, N. Yao, W. Yang, X. Fu. 2001. Catal. Today., 68,220.
[12] X.M. Wu, L. Wang, Z.C. Tan, G.H. Li, S.S. Qu. 2001. J. Solid State Chem., 156, 220.
[13] E. Vigil, J.A. Ayllon, A.M. Peiro, R.R. Clemente. 2001. Langmuir,17,891.
[14] H. Zhang, M. Finnegan, J.F. Banfield. 2001. Nano Lett., 1, 81.
[15] X. Ju, P. Huang, N. Xu, J. Shi. 2002. J. Membr. Sci., 202, 63.
[16] J.Ovenstone. 2001. Journal of Materials Science., 36, 1325.
[17] A.Rabenau, C.Angewandte. 1985. International Edition English, 24, 1026.
[18] B. D. Cullity. 1978. Elements of X-Ray Diffraction, Addison Wesley.
[19] L. E. Alexander. 1968. X-ray diffraction methods in Polymer Science, John Wiley, New York.
[20] L.Q. Jing, Z. L. Xu, X. J. Sun, J. Shang, W. M. Cai. 2001. Appl. Surf. Sci. 180, 308.
[21] M. Asilturk, F. Sayilkan, S. Erdemoglu, M. Akarsu, H. Sayikan, M. Erdemoglu, E. Arpac. 2005 Journal of Hazardous Materials.

As per UGC guidelines an electronic bar code is provided to seure your paper

International Journal for Modern Trends in Science and Technology, 7(06): 14-17, 2021

ISSN: 2455-3778 online
DOI: https://doi.org/10.46501/IJMTST0706004
Available online at:http://www.ijmtst.com/vol7issue06.html

Temperature dependence study of Vitamin C invarious Citrus Fruits

Roshini K.T.

Assistant Professor, Department of Chemistry, Carmel College, Mala, Kerala, India.

To Cite this Article
Roshini K.T. Temperature dependence study of Vitamin C invarious Citrus Fruits. *International Journal for Modern Trends in Science and Technology* 7, 14-17 (2021).

Article Info
Received on 28-April-2021, Revised on 22-May-2021, Accepted on 28-May-2021, Published on 04-June-2021.

ABSTRACT

Temperature effects on Vitamin C content in citrus fruits were determined using iodometric titration method under three temperature regimes (room temperature, 60°C and 90°C), representing the range oftemperatures the fruits may be exposed to during processing and storage. It was observed that Vitamin C content was decreased as it was exposed to higher temperature. The decrease was observed high when the temperature of the juice was raised and kept at 60°C, which was further decreased when the temperature was raised to 90°C. This paper showed light on the effect of processing and storage on the ascorbic acid content of citrus fruits.

KEYWORDS: *Vitamin C, iodometric titration, ascorbic acid, citrus fruits.*

INTRODUCTION

Citrus species (Rutaceae) were the most popular fruits, originated in South-East Asia and then gradually spread to different parts of the world. These fruits contained a variety of sugars, citric acid, ascorbic acid, carotenoids, minerals, essential oils, etc and play an important role in human nutrition as excellent source of antioxidants (ascorbic acid, carotenoids and phenolic compounds). These constituents were considered to be essential components of functional foods. Many of these substances prevent damage to cell membrane and other structures by neutralizing free radicals.

Ascorbic acid was the most important antioxidant in citrus fruit juices and it protects the organism from oxidative stress. Vitamin C cannot be synthesized through body cells, nor does it store it. It was therefore important to include plenty of vitamin C containing foods in daily diet. More than 90% of the vitamin C in human diets is supplied by fruits and vegetables (including potatoes)1-6.

OBJECTIVES

One of the objectives of the present study was to relate the content of ascorbic acid of six citrus fruits namely Citrus sinensis (Orange), Citrus limon (Lemon), Citrus paradisi (Grape), Citrus maxima (Babloos naranga), Citrus limetta (Mosambi) and Punica granatum (Pomegranate) with the view of making recommendations for their intake.

A redox titration, involving an Iodometric method7-9, has been used to do the analysis. The redox reaction was better than an acid-base titration since there were additional acids in a juice, but few of them interfere with the oxidation of ascorbic acid by iodine. Vitamin C is a weak acid and a good reducing agent. Iodine is a weak oxidizing agent, so that it will not oxidize substances other than the ascorbic acid in the sample of fruit juice. As a strong reducing agent, vitamin C will reduce I_2 to I^- very easily. The excess of iodine reacts the starch as indicator in redox

reaction. In this reaction, the ascorbic acid molecule gains oxygen. Each iodine atom in the I_2molecule accepts an electron and become negatively charged to form iodide ion. Thus, the ascorbic acid molecule was oxidized and the iodine molecule was reduced. Excess iodine reacts with iodide ions (I^-) to form triiodide ion (I^{3-}) which forms a very intense blue color when it reacts with starch. To detect the end point, starch must be added at the beginning of the titration in the conical flask. When all ascorbic acids have finished, the excess of iodine solution will react the starch to form blue-black colour in the solution.

I^{3-} + starch → starch (I^{3-})

(Blackish-blue color)

Starch indicator is biodegradable and so fresh starch indicator must be prepared.

Various reports have shown fruits to be excellent sources of vitamin C. But it was lost from foods during preparation, cooking or storage10-12. To find out the effect of temperature on stability of Vitamin C, a temperature dependence study of vitamin C was carried out under three temperature regimes representing the ranges the fruits may be exposed to during processing and storage.

MATERIALS AND METHODS

Sample collection and preparation

Citrus fruits namely Citrus sinensis (Orange), Citrus limon (Lemon), Citrus paradisi (Grape), Citrus maxima (Babloos naranga), Citrus limetta (Mosambi) and Punica granatum (Pomegranate) were collected from local market. The selected fruits were then washed thoroughly with water. The 200g sample of citrus fruits were squeezed in a juicer together with 50ml of distilled water. After blending, strain the pulp and seed, washing it with a few 10ml portions of distilled water and make the extracted solution up to 250ml in volumetric flask.

Preparation of iodine solution

4.50 g Potassium iodide (KI) and 0.203 g potassium iodate (KIO3) were dissolved into 500 ml beaker with 200 mL of distilled water. 25 ml of 5 N sulfuric acid was added into the beaker and then diluted with distilled water until 500 ml solution.

Preparation of Vitamin C Standard Solution

0.250 g Ascorbic acid was dissolved in the beaker with 100 ml distilled water. The solution was transferred quantitatively into 250 ml volumetric flask and diluted to the mark with distilled water.

Standardization of Iodine Solution

25 mL of Vitamin C solution was pipetted into a 125 ml Erlenmeyer flask. 10 drops of 1% starch solution were added and then titrated against iodine solution until blue-black colour was observed. Titrations were repeated for concordency.

Estimation of Vitamin C in juice samples

40 mL of Juice samples were pipetted into a 125 mL Erlenmeyer flask. Following by 10 drops of 1% starch solution and titrated against iodine solution until blue-black colour was observed. Titrations were repeated.

Estimation of Vitamin C of juice samples at different temperatures

50 ml of selected Juice samples were pipetted out into labeled 250 ml beakers. They were heated to a temperature of 60°C and maintained at that temperature for 2hrs. The second group of juice sample (50 ml) selected in different beakers were heated to a temperature of 90°C and maintained at that temperature for 2hrs. All the 12 selected samples were then cooled. After that 40ml of juice samples were pipetted out into a 250 ml conical flask. 4 ml of 1% starch solution added and titrated against iodine solution until blue-black colour was observed. Titrations were repeated.

RESULTS AND DISCUSSION

The result of the average value of vitamin C in each fruit juice samples under the specified condition were tabulated in Table below. It showed the highest concentration of vitamin C found in Babloos juice, hitting 31.97 mg /100g, the lowest level was found in Grape juice, when it reached 2.34 mg /100 g of juice. The amount of Vitamin C in juices of six different citrus fruits : Orange, Mosambi, Pomegranate, Babloos, Grape and Lemon) were as follows.

Bambloos>Orange>Mosambi>Lemon>Pomegranate>Grape

Fruit Juice Samples	Temperature	Total Vitamin C (mg/100g)
Orange **Citrus sinensis**	32°C	31.24
Lemon **Citrus limon**	32°C	16.56
Grape **Citrus paradise**	32°C	2.3409
Babloos **Citrus maxima**	32°C	31.97
Mosambi **Citrus limetta**	32°C	30.506
Pomegranate **Punica granatum**	32°C	12.77

TABLE 1: TOTAL VITAMIN C CONTENT IN NATURAL FRUIT JUICE SAMPLES

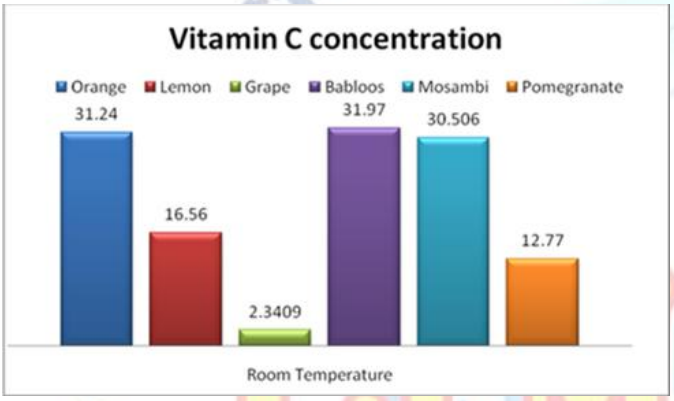

FIG 1: VITAMIN C CONCENTRATION (MG/100G)

The effect of temperature on the amount of Vitamin C in citrus fruits was also calculated by titrating the juices using iodine solution. It can be seen from analytical results in table 2 that the lower the temperature the better the concentration of Vitamin C in fruit juice.

Higher temperature does not favour Vitamin C. It is better to maintain or store Vitamin C in a place below the room temperature. This is consistent with reports that, climate, especially temperature affect vitamin C level. Areas with cool nights produce citrus fruits with higher vitamin C levels.Hot tropical areas produce fruit with lower levels of vitamin C. Vitamin C loss during storage depends on the type of storage methofor example, handling and storage; oxygen is the most destructive ingredient in juice, causing degradation of vitamin C.

Fruit Juice samples	Concentration		
	Roomtemp (mg/g)	60°C (mg/g)	90°C (mg/g)
Orange **Citrussinensis**	31.24	29.507	22.59
Lemon **Citrus limon**	16.56	14.035	3.196
Grape **Citrus paradise**	2.341	2.161	1.639
Babloos **Citrus maxima**	31.97	28.071	23.096
Mosambi **Citrus limetta**	30.506	28.229	24.35
Pomegranate **Punica granatum**	12.77	12.77	9.295

TABLE 2: TOTAL VITAMIN C CONTENT IN NATURAL FRUIT JUICE SAMPLES AT DIFFERENT TEMPERATURE

Juice should be discouraged from being display in the hot weather above room temperature in order to maintain production concentration.Our temperature dependence study on citrus fruits were found to follow a similar pattern of loss. This is because the vitamin C is more sensitive to temperature. Degradation was observed high in our selected samples as the temperature was raised to 90°C.

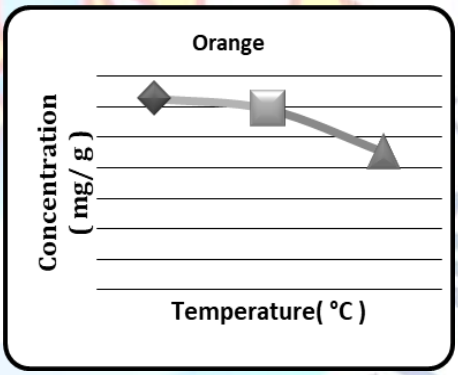

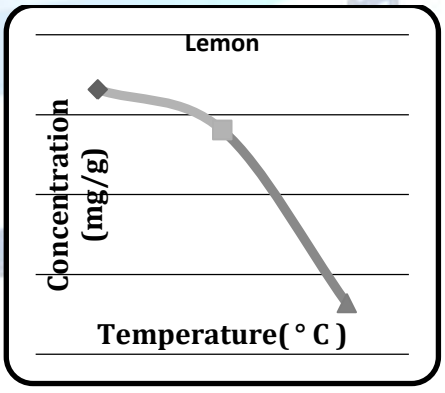

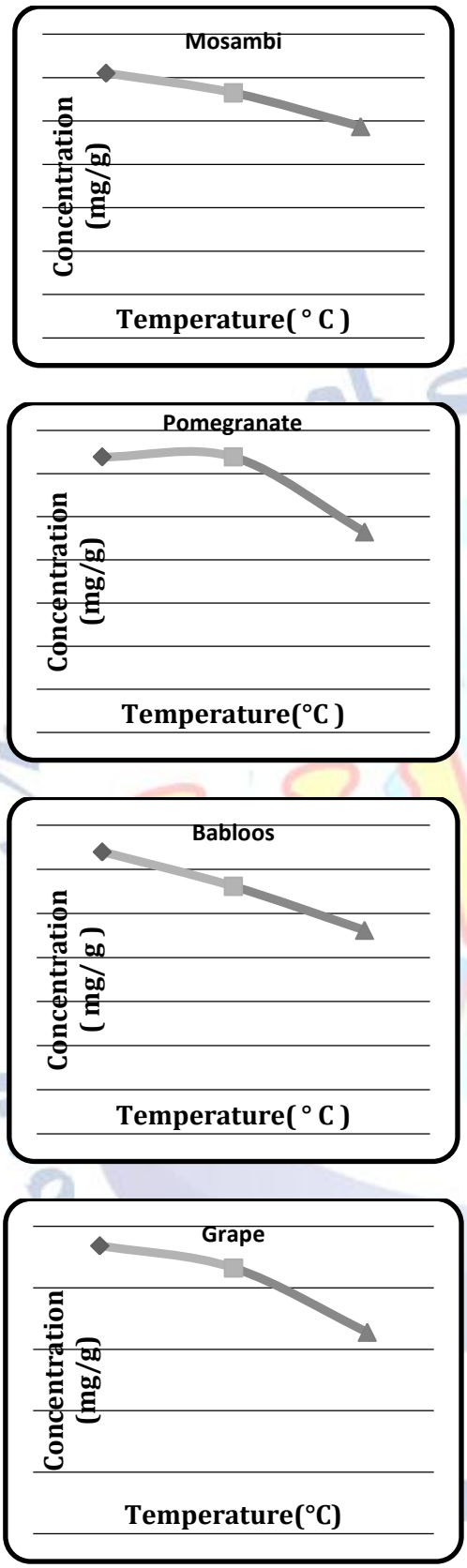

Fig 2: Temperature Dependence Of Vitamin C Concentration

CONCLUSION

Determination of ascorbic acid content by iodometric titration is an easy, safe, and fast method. The redox reaction is preferable to an acid-base titration because a number of other species in juice can act as acids. This would help in quickly determining an estimate of ascorbic acid content of fruits. Results showed that Bambloos had the highest value of ascorbic acid, 31.97mg/100g followed by Orange, 31.24 mg/100 g and then Mosambi, 30.50 mg/100 g. Grape had the least value, 2.34 mg/100g. It therefore follows that Bambloos would supply more ascorbic acid per 100 gm for body need compared to the other fruits. It was observed that Vitamin C content was decreased as it was exposed to higher temperature. The decrease was observed high when the temperature of the juice was raised and kept at 60oC. This was as a result of increase in oxidation of ascorbic acid with increase in temperature, as higher temperature favours redox reaction.

ACKNOWLEDGEMENTS

The author was thankful to UGC for financial support. Also remembered with gratitude, Principal and Head of the Department, Carmel College, Mala for the laboratory facility, constant support and encouragement.

REFERENCES

[1] Swaminathan, M., Handbook of Food and Nutrition, The Bangalore Printing and Publishing Co., Ltd, pp. 58–60.
[2] Akhilender N.K., Vitamin C in human health and disease is still a mystery? An overview, Nutr J, 2, 7 (2003)
[3] Vasanth K.G., Ajay K.K., Raghu Patel G.R. and Manjappa S., Determination of vitamin C in some fruits and vegetables in Davanagere city, (Karanataka) – India, Int j pharm life sci, 4(3), 2489 (2013)
[4] Rekha C., Poornima G., Manasa M., Abhipsa V., Pavithra Devi J., Vijay Kumar H.T. and Prashith Kekuda T. R., Ascorbic Acid, Total Phenol Content and Antioxidant Activity of Fresh Juices of Four Ripe and Unripe Citrus Fruits, Chem Sci Trans., 1(2), 303-310 (2012)
[5] Seung K.L. and Adel A.K., Pre harvest and post-harvest factors influencing vitamin C content of horticultural crops, Postharvest Biology and Technology, 20, 207–220 (2000)
[6] Marti, N., Mena, P., Canovas, J.A., Micol, V., Saura, D. 2009. Vitamin C and the role of citrus juices as functional food. Natural Product commun., 4(5): 677– 700.
[7] Gunjan K. and Mangla D.G., Analysis of Vitamin C in Commercial and Naturals substances by Iodometric Titration found in Nimar and Malwa regeion, J Sci Res Phar, 1(2), 8 (2012)
[8] Okiei W., Ogunlesi M., Azeez L., Obakachi V., Osunsanmi M. and Nkenchor G., The Voltammetric and Titrimetric Determination of Ascorbic Acid Levels in Tropical Fruit Samples, Int J Electrochem Sci, 4, 276- 287 (2009)
[9] Biswas S.K. and Mannan M.A. Determination of vitamin C (ascorbic acid) in some fruits and vegetables; B. J. Sci. & Ind. Res. 1996: 1; 31.
[10] N. V. Bhagavan, Medical Biochemistry, Elsevier, Amsterdam, The Netherlands, 4th edition, 2001.
[11] Nagamani k., Miracle Nutrient, IJPT, 3(2), 1140-1164 (2011)
[12] Davey, J.S., J.C. Rickman, D.M. Barret and C.M. Bruhn, 2000. Review: Nutritional comparison of fresh and frozen fruits. Sci. Food Agric., 87: 930-944.

Journal of Molecular Structure 1224 (2021) 129209

Contents lists available at ScienceDirect

Journal of Molecular Structure

journal homepage: www.elsevier.com/locate/molstr

Substituent effects in the formation of a few acenaphthenone-2-ylidene ketones and their molecular docking studies and in silico ADME profile

Daly Kuriakose[#], Roshini K. Thumpakara[#], Jesna A, Jomon P. Jacob[*]

Department of Applied Chemistry, Cochin University of Science and Technology, Kochi-682 022, Kerala, India

ARTICLE INFO

Article history:
Received 24 July 2020
Revised 3 September 2020
Accepted 4 September 2020
Available online 4 September 2020

Keywords:
Claisen-Schimdt reaction
Aldol condensation
acenaphthenequinone
Acetophenone
Acenaphthenone-2-ylidene ketones
Molecular docking

ABSTRACT

We observed intriguing substituent effects in the reaction between 4-substituted acetophenones and acenaphthenequinone in the presence of KOH in methanol. In all cases, expected Claisen-Schimdt condensation was the first step. However, depending on the nature of 4-substituent on acetophenone, the initially formed condensation product remain unchanged or underwent Domino sequence of reactions to give three different 2:2 adducts arising through three distinct pathways. The interactions of acenaphthenone-2-ylidene ketones with the target proteins were performed by molecular docking studies. The prediction of in silico ADME belongings of the synthesized compounds revealed substantial drug-likeness characters based on Lipinski's rules.

1. Introduction

Claisen-Schimdt reaction, also called crossed-aldol condensation, is the condensation between aldehydes/ketones and carbonyl compounds leading to the formation of β-hydroxycarbonyl compounds which undergo subsequent dehydration to form α,β- unsaturated carbonyl compounds. This reaction is generally catalysed by acids or bases under room temperature or conventional heating [1,2] or microwave irradiation [3]. To avoid by-products and increase the yield of the products several protocols are developed using different catalysts [4–8]. β-Hydroxycarbonyl compounds have played a major role in synthetic organic chemistry [9–11] and α,β-unsaturated carbonyl compounds are widely used in pharma industries [12–15].

Acetophenone undergoes base catalysed Aldol condensation with benzil to form α,β-unsaturated ketone as the stable end product [16]. Based in this observation, we examined the Claisen-Schimdt reaction between acetophenone (**2a**) and acenaphthenequinone (**1**) in methanol in the presence of KOH [17,18]. Interestingly, we obtained three complex molecules by Michael-aldol domino reaction sequence. These 2:2 domino products (**4a, 5a, 6a**) were formed from a common Claisen-Schmidt condensed product **3a** [17] and the detailed mechanism of the above reaction was established in our recent publication (Scheme 1) [18]. Even after repeated attempts we could neither isolate nor detect (GC-MS, LC-MS) the 1:1 adduct **3a**. However, we could successfully generate **3a** by alternative routes (*vide infra*).

Molecular docking studies were exploited to show the possible binding mode of the test molecule with its target protein aiming to explain its anticancer activity [19–21]. To study the drug like character of synthesised acenaphthenone-2-ylidene ketones (**3a-f**), we have explained with the help of Swiss ADME software.

2. Results and Discussion

We have repeated the Claisen-Schmidt reaction of acenaphthenequinone (**1**) with acetophenones having different substituents at the 4-position (**2b-f**) to study the generality of the reaction. We observed dramatic substituent dependence in these reactions. While 4-chloro and 4-methylacetophenone reacted with acenapthenequinone to give three 2:2 adducts (**4b, 4c** - **5b, 5c** - **6b, 6c**) as described earlier [18], other acetophenone derivatives behaved differently, 4-bromo, 4-methoxy and 4-phenyl substituted acetophenones gave the expected 1:1 adduct, **3d-f** as the only product (Scheme 1). The 2:2 adducts formed were separated

* Corresponding author.
E-mail address: jacobpjomon@yahoo.com (J.P. Jacob).
# These two authors contributed equally.

https://doi.org/10.1016/j.molstruc.2020.129209
0022-2860/

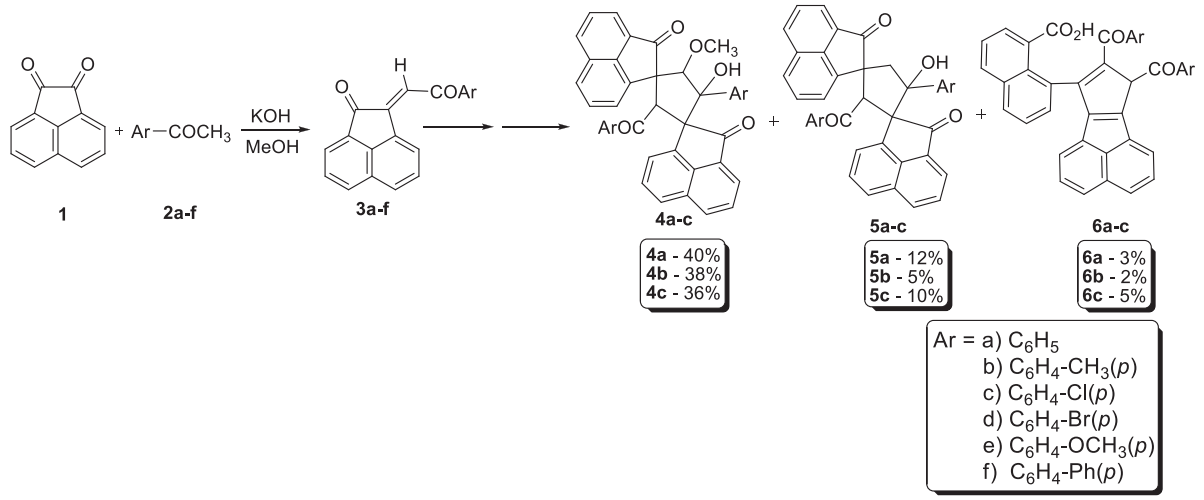

Scheme 1. Reaction between acenaphthenequinone (**1**) and acetophenones (**2a-f**).

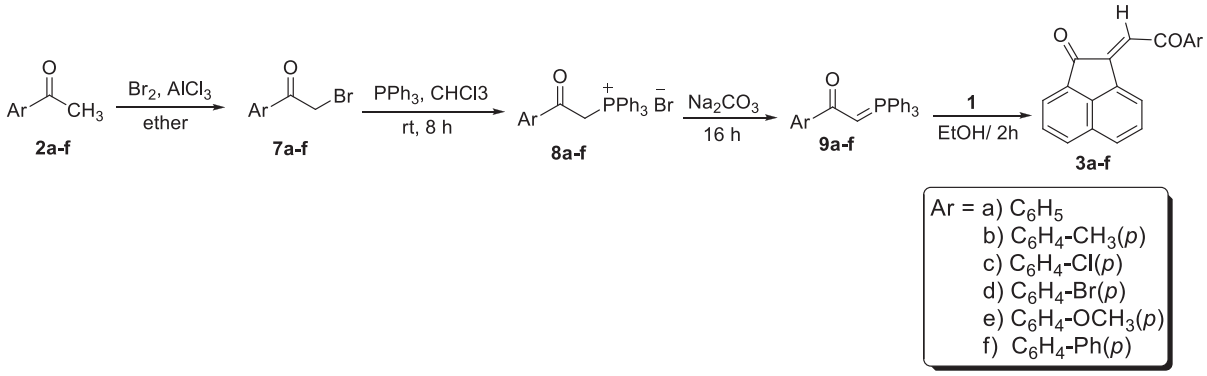

Scheme 2. Wittig route for the synthesis of acenaphthenone-2-ylidene ketones (**3a-f**).

by column chromatography and purified by recrystallization. The compounds were characterised by ^{1}H, ^{13}C NMR and SCXRD [18,22,23] analyses. Inductive, mesomeric and steric factors could not satisfactorily account for the dichotomous reaction sequence of acetophenone-acenaphthenequinone reaction.

Our further investigations to unravel the mechanism of the reaction pointed towards a remarkable substituent effect in controlling the reactivity of acenaphthenone-2-ylidene ketones (**3a-f**). We have independently synthesised the intermediate acenaphthenone-2-ylidene ketones **3a-f** by adopting the Wittig route (Scheme 2). ln this reaction sequence, phenacyl bromides **7a-f** were first synthesised by the bromination of various para-substituted acetophenones **2a-f** using diethyl ether as solvent in the presence of anhydrous aluminium chloride. Phenacyl bromide derivatives **7a-f** were converted to corresponding phenacyltriphenylphosphonium bromides **8a-f** by the reaction with triphenylphosphine. In the presence of sodium carbonate, corresponding ylides **9a-f** were formed and they reacted with acenaphthenequinone (**1**) to form required acenaphthenone-2-ylidene ketones **3a-f**.

Independently synthesised acenaphthenone-2-ylidene ketones **3a-c** were treated with KOH in methanol. While **3d-f** remained unchanged even after refluxing for 12 h, **3a-c** underwent further transformation to give the 2:2 adducts **4a-c** within 4 h. This observation supports the reaction sequence depicted in Scheme 1 indicating further transformations of **3** to give **4** and presumably, **5** and **6** attesting the role of remote substituents in the reactivity of acenaphthenone-2-ylidene ketones **3a-f**.

Diversity of the above reaction may depend on the geometry or electronic factors of acenaphthenone-2-ylidene ketones (**3a-f**) having different substituents. To study the effect of geometry, we have computationally optimized the geometry of acenaphthenone-2-ylidene ketones (**3a-f**) using the software Gaussian (Table 1).

Based on optimized structures collected in Table 1, it is clear that acenaphthenone-2-ylidene ketones **3a-f** have similar geometry and hence geometry is not a significant factor in controlling the reactivity of **3**. So the difference in reactivity of **3a-f** may be due to electromeric effects induced by substituents at the *para* position of the benzoyl group in the 1:1 adducts, **3a-f**. A clear correlation is elusive since both electron withdrawing (Cl) and electron releasing (CH_3) substituents assist 2:2 adduct formation while both Br and -OMe substituents rendered the initially formed 1:1 adducts unreactive towards further transformations under the conditions employed by us.

3. Molecular docking

The AutoDock is an automatic docking programme designed for the prediction of the binding among small molecules forexample drug candidates and the receptor having known 3D structure [24–30]. Molecular docking studies were performed using AutoDock 4.2 Vina software to confirm the anticancer activity of acenaphthenone-2-ylidene ketones (3a-f) against different proteins *viz* **4I4T, 4I55, 4YJ2** and **4YJ3**. Crystal structure of the target proteins were downloaded from the RSCB PDB website in the PDB

Table 1
Energy minimized structures of acenaphthenone-2-ylidene ketones (**3a-f**) using Gaussian.

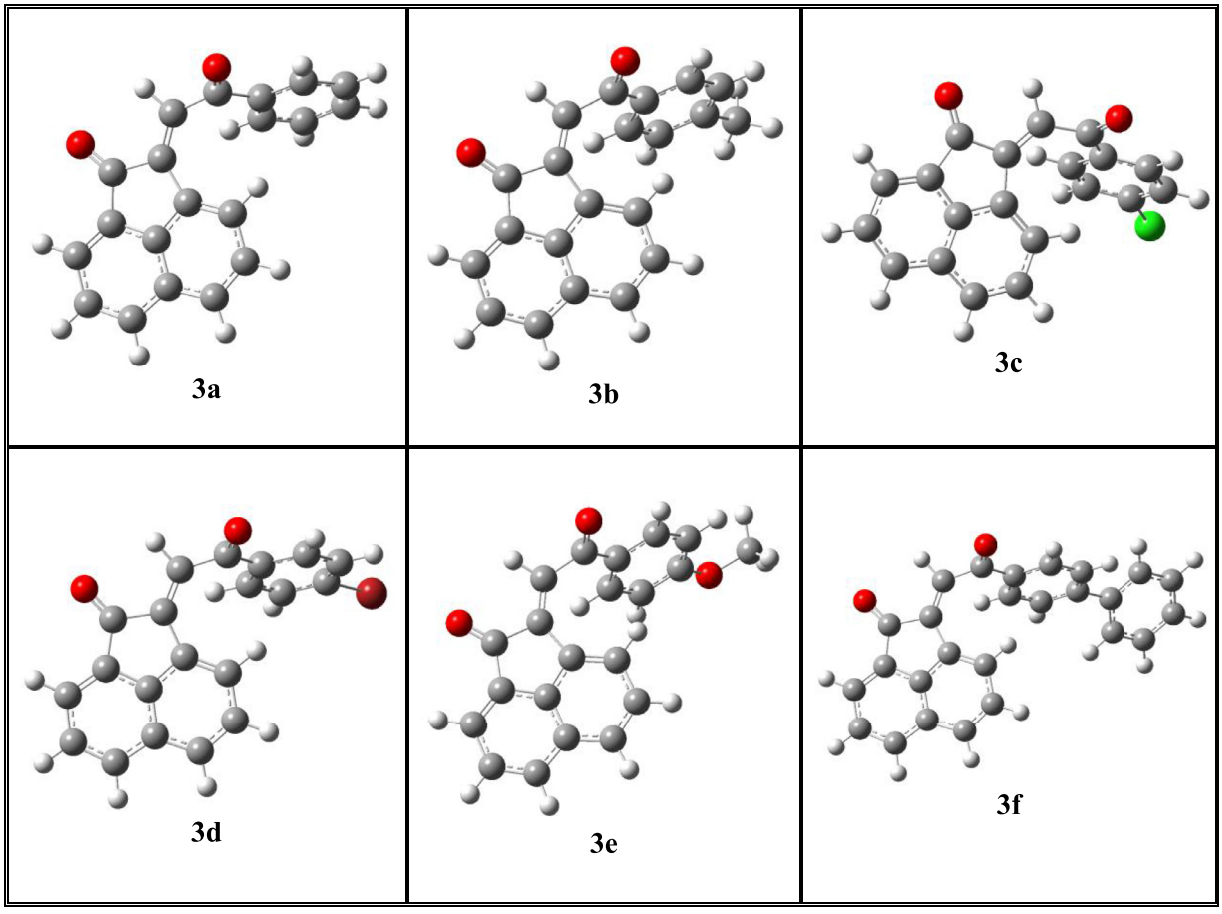

Table 2
All interacting residues between acenaphthenone-2-ylidene ketones and selected target proteins.

Proteins	Molecules	All interacting residues
4I4T	**3a**	ARG F: 44, PHE F: 49, ARG F: 66, ALA F: 68, ASP F: 69, ALA F: 335.
	3b	VAL F: 13, ALA F: 68, LEU F: 314, ALA F: 335, PRO F: 336.
	3c	PHE F: 49, ALA F: 68, ASP F: 69, ARG F: 73
	3d	ARG F: 44, ARG F: 46, PHE F: 49, ARG F: 66, ALA F:68, ASP F: 69, ALA F: 335.
	3e	ARG F: 44, LEU F: 47, PHE F: 49, ARG F: 66, ALA F: 68, ASP F: 69, ALA F: 335.
	3f	ARG F: 44, ARG F: 46, PHE F: 49, ARG F: 66, ALA F: 68, ASP F: 69, ALA F: 335.
4I55	**3a**	GLY B: 10, CYS B: 12, GLU B: 71, ALA B: 99, ASN B: 101, THR B: 145, GLY B: 146, ASP B: 179.
	3b	GLN B: 11, CYS B: 12, GLU B: 71, ASN B: 101, GLY B: 144, VAL B: 171, PRO B: 173.
	3c	VAL B: 177, ASP B: 179, TYR B: 224, LEU B: 227, VAL C: 250, VAL C: 353.
	3d	CYS B: 12, SER B: 140, VAL B: 171, MET B: 172, PRO B 173.
	3e	GLN B: 11, CYS B: 12, GLU B: 71, ALA B: 99, ASN B: 101, GLY B: 144, VAL B: 177, ASP B: 179.
	3f	TYR B: 224, LEU C: 248, PRO C: 325, VAL C: 353.
4YJ2	**3a**	VAL B: 177, SER B: 178, LEU C: 248, PRO C: 325, VAL C: 353, ILE C: 355.
	3b	VAL B: 177, SER B: 178, TYR B: 224, LEU B: 227, LEU C: 248, PRO C: 325, VAL C: 353, ILE C: 355.
	3c	VAL B:177, TYR B: 224, LEU C:248, PRO C: 325, VAL C: 353, ILE C: 355.
	3d	LYS B: 105, LYS C: 163.
	3e	CYS B: 12, GLN B: 15, GLU B: 71, ALA B: 99, GLY B: 144, THR B: 145, GLY B: 146, ASP B: 179.
	3f	SER B: 178, LEU C: 248, GLY C: 350, PHE C: 351, VAL C: 353.
4YJ3	**3a**	VAL B: 177, LEU C: 248, PRO C: 325, ILE C: 355, VAL C: 353.
	3b	CYS B:12, GLU B: 71, ALA B: 99, ASN B: 101, GLY B: 144, THR B: 145, GLY B: 146, ASP B: 179, TYR B: 224.
	3c	GLY B: 11, CYS B: 12, TYR B: 224
	3d	VAL B: 177, VAL C: 250.
	3e	GLN B: 11, CYS B: 12, GLY B: 142, GLY B:143, TYR B: 224.
	3f	VAL B: 177, TYR B: 224, LYS C: 352.

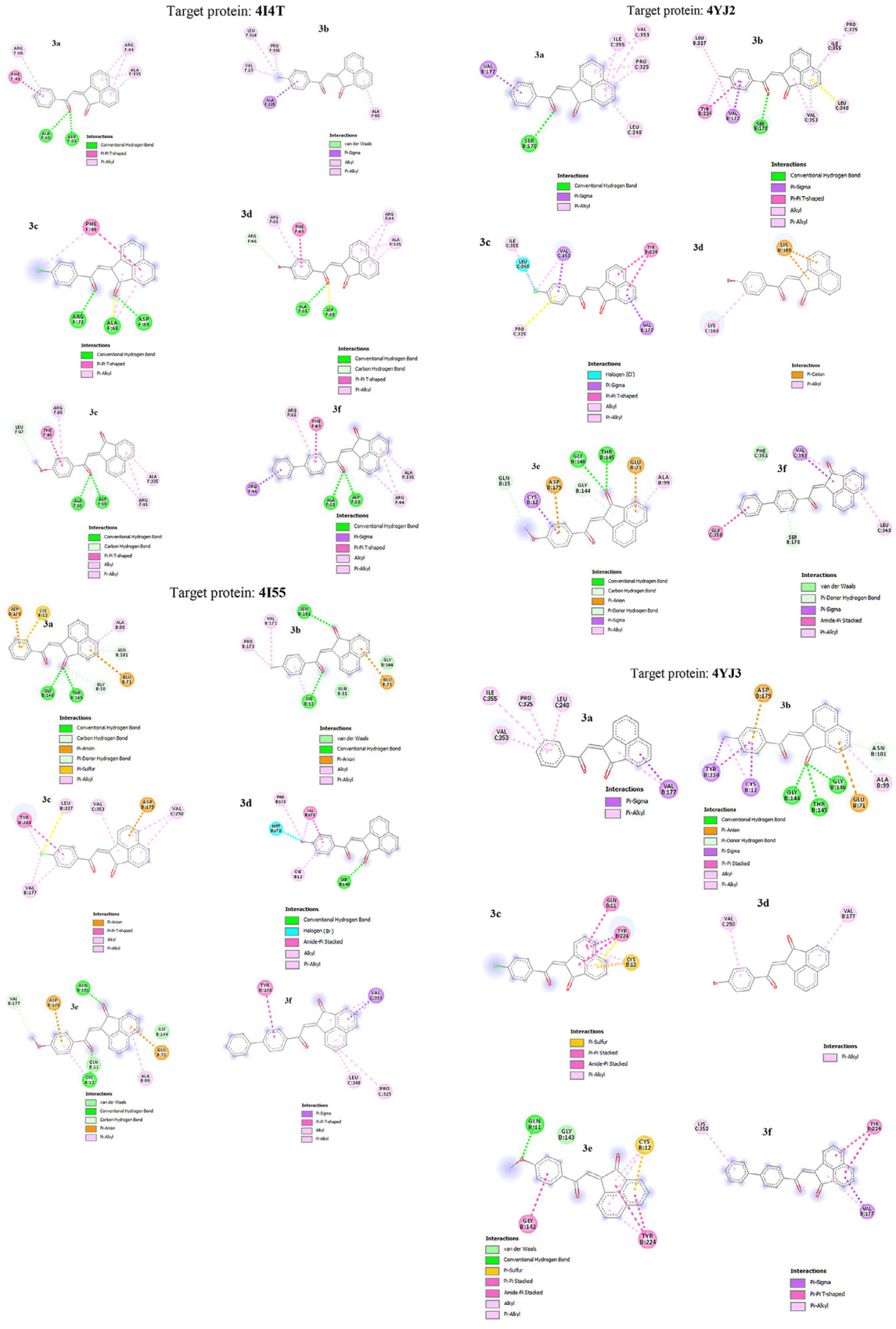

Fig 1. 2D diagram of acenaphthenone-2-ylidene ketones docked into the binding site of anti-cancer proteins.

Table 3
Prediction of in silico ADME properties of the acenaphthenone-2-ylidene ketones, **3a-f**.

Acenaphthenone-2-ylidene ketones	Molecular weight (g/mol)	Physicochemical parameters					Bioactivityscore
		Mi log P	TPSA (Å²)	No. of H-bond acceptor	No. of H-bond donor	No. of rotatable bonds	
3a	284.31	2.66	34.14	2	0	2	0.55
3b	298.33	2.59	34.14	2	0	2	0.55
3c	318.75	2.90	34.14	2	0	2	0.55
3d	363.20	3.01	34.14	2	0	2	0.55
3e	314.33	2.47	43.37	3	0	3	0.55
3f	360.40	3.31	34.14	2	0	3	0.55

format [31]. Before docking, the water molecules and other co-crystallized ligand molecules were removed from the target proteins and polar hydrogens were added using PyMoL software [32]. The active site of the protein was explained within the grid size 30Å × 30Å × 30Å in order to incorporate the residues of the active sites. The best fit conformation was analysed, which is based on the binding score, hydrogen bonding and other hydrophobic interactions. The binding interactions were visualized using Discovery studio visualizer. Affinity of best docked position of the molecule and protein target complex was determined by E-value (kcal/mol). It provides the prediction of binding free energy for docked molecule [21].

4I4T crystal structure of the tubulin-RB3-TTL-Zampanolide complex with binding energy (E) -9.20, -9.60, -8.80, -9.50, -9.30, -10.70 kcal/mol for **3a, 3b, 3c, 3d, 3e** and **3f** respectively. Organisms: Bos taurus, Rattus norvegicus, Gallus gallus. **4I55** Crystal structure of the tubulin-stathmin-TTL complex with binding energy (E) -9.00, -9.10, -7.80, -8.40, -8.40, -9.30 kcal/mol for **3a, 3b, 3c, 3d, 3e** and **3f** respectively. **4YJ2** Crystal structure of tubulin bound to MI-181 with binding energy (E) -8.60, -8.60, -8.80, -8.50, -8.70, -9.70 kcal/mol for **3a, 3b, 3c, 3d, 3e** and **3f** respectively. **4YJ3** crystal structure of tubulin bound with binding energy (E) -8.70, -8.80, -9.00, -8.10, -8.70, -9.40 kcal/mol for **3a, 3b, 3c, 3d, 3e** and **3f** respectively. From the above data, we can clear that 2-(2-(biphenyl-4-yl)-2-oxoethylidene)acenaphthylen-1(2H)-one (**3f**) shows good binding affinity to target proteins as shown in Fig 1. So, we can use **3f** as the best anticancer drugs in the acenaphthenone-2-ylidene ketones (**3a-f**) series. These acenaphthenone-2-ylidene ketones (**3a-f**) show good binding affinity to the target proteins than the binding affinity of the compounds to the same target proteins in a recently reported article [33].

By using Discovery studio visualizer, [34] we have to find the docking interaction of hydrogen bonds (classical and non-classical) and binding amino acid residues: alanine (ALA), asparagine (ASN), arginine (ARG), aspartic acid (ASP), cysteine (CYS), glutamine (GLN), glutamic acid (GLU), glycine (GLY), histidine (HIS), leucine (LEU), lysine (LYS), serine (SER), threonine (THR), tryptophan (TRP), tyrosine (TYR), valine (VAL) and phenylalanine (PHE) showed in the 2D interaction diagram (Fig 1).

4. In silico ADME property prediction

Computational simulation studies provide a quick and economic approach to determine the drug-like character of synthesized acenaphthenone-2-ylidene ketones, **3a-f**. SwissADME software was used to measure their bioactive score value of the prepared compounds. It was measured by estimating the different parameters Mi log P (partition coefficient), compound weight, heavy atoms, hydrogen donors, hydrogen acceptors and rotatable bonds Table 3.

Properties of absorption, distribution, metabolism, excretion and toxicity are included in In silico ADME and are exploited to predict the drug-likeness behaviour of the compounds based on Lipinski's rule of five [35–37]. According to Lipinski's rule, Mi log P values of compounds should be below 5, molecular weight is lower than 500, H-bond acceptors should be smaller than 10, H-bond donors should be lower than 5 and should have the bioactive score is smaller than one.

Mi Log P, is calculated by the methodology developed by Molinspiration [38] as a sum of fragment based contributions and correction factors. To determine the hydrophobic character of the synthesized compounds we are using the parameter Mi log P, which is necessary for analyzing the permeability skill of the compounds across the cell membrane. In the present study about the acenaphthenone-2-ylidene ketones **3a-f**, Mi log P values are found to be less than 5; it implies that the compounds should have appreciable penetrable talent across the central nervous system. The molecular weight of the synthesized compounds is less than 500. As per Lipinski regulation, these compounds have good drug-likeness criteria.

Here the number of H-acceptors is 2, 3 and the H-donor is zero for acenaphthenone-2-ylidene ketones, **3a-f**. Based on the Lipinski's rule of five, the compounds possess many H- acceptors and donors, they effectively interact with active sites. Topological molecular polar surface area (TPSA) is a commonly analyzed factor related to H-bonding (O and N atom counts) and is necessary to identify the cell permeability phenomena of **3a-f**. It is a significant parameter that was compared with the passive diffusion through the cell wall; hence, it agreed to pass the drug candidates inside the central nervous system. In the case of acenaphthenone-2-ylidene ketones **3a-f**, acquires TPSA values below 140 $Å^2$ and thereby possess good drug transport features and may be favoured for oral administration.

As per Lipinski's rule, molecule having higher number of rotatable bond, they become more stretchy and convenient for interface with the accurate active centre. Here the rotatable bonds are 2, 3 and have well-matched ability to interact with the living cells efficiently.

According to the Lipinski's rule, the compounds which possess bioactivity scores greater than 0 have excellent drug likeness proficiency [39]. In this case, acenaphthenone-2-ylidene ketones **3a-f**, have the bioactivity score is 0.55 and are scrutinized by measuring the activity score of GPCR (Human G-protein coupled receptors) ligand, ion channel modulator, nuclear receptor ligand, kinase inhibitor, protease inhibitor and enzyme inhibitor.

5. Conclusion

Acenaphthenone-2-ylidene ketones were independently synthesised and their propensity to undergo further transformations under conditions employed for Claisen-Schimidt reaction was examined. Geometry optimization using Gaussian, clearly revealed

that acenaphthenone-2-ylidene ketones have similar geometry, hence geometry has no role in controlling the Claisen-Schimidt reaction of acenaphthenone-2-ylidene ketones. Electromeric effects induced by substituents at the *para* position of the benzoyl group in the initially formed acenaphthenone-2-ylidene ketones may be responsible for the observed difference in their reactivity towards further transformations. Anticancer activity of the acenaphthenone-2-ylidene ketones were analysed (in silico) using AutoDock 4.2 Vina software. Drug likeness of the acenaphthenone-2-ylidene ketones were established using SwissADME software based on Lipinski's rule of five.

6. Experimental section

6.1. General methods

All reactions were conducted in oven-dried glassware. Reagents used were purchased from *Sigma Aldrich Chemical Co.* or *Spectrochem* and were used without further purification. Solvents used for experiments were distilled and dried according to procedures given in standard manuals. All reactions were monitored by thin layer chromatography (TLC). Analytical thin layer chromatography was performed on aluminium sheets coated with silica gel (*Spectrochem*); visualization was achieved by exposure to iodine vapours or UV radiation. Solvent removal was done on a *Heidolph* rotary evaporator. Gravity column chromatography was performed using 60-120 mesh silica gel (*Spectrochem*) and mixtures of hexane-ethyl acetate were used for elution. Melting points were recorded on a *Neolab* melting point apparatus. Infrared spectra were recorded using *JASCO FTIR 4100* spectrometer. NMR spectra were recorded a 400 MHz on a *Bruker* FT-NMR spectrometer. Chemical shifts are reported in δ (ppm) relative to TMS as the internal standard. Single Crystal XRD was done by *Bruker* XRD Instrument. Elemental analysis was performed using *Elementar Systeme (Vario EL III)*. Molecular mass was determined by fast atom bombardment (FAB) using *JMS 600 JEOL* mass spectrometer. Unless otherwise mentioned, all commercially available solvents and reagents were used as received and reactions were performed under normal conditions. Characterization data for **4a-c, 5a-c** and **6a-c** are available in earlier publications from our group [17,18].

6.2. Common procedure for the synthesis of acenaphthenone-2-ylidene ketones (3a-f) by Wittig's reaction

Para substituted acetophenones (**7a-f**, 25 mmol) was slowly added to a chloroform solution (6 mL) of triphenylphosphine (25 mmol) and the solution was filtered into anhydrous ether (1 Litre). The precipitate formed was filtered, collected and dried. The product formed was recrystallized from water in the form of white powder (**8a-f**, 60-68%).

A mixture of corresponding triphenylphosphonium bromide (**8a-f**, 7.0 g) and 10% aqueous sodium carbonate (250 mL) was well mixed for 15h. The mixture was filtered and insoluble portion was taken up in hot benzene (200 mL). Some unreacted bromide was removed by filtration; addition of petroleum ether to the benzene filtrate afforded the compound **9a-f** (58-65%) as white powder.

A solution of acenapthenequinone (**1**, 27 mmol) and triphenylphosphinebenzoylmethylene (**9a-f**, 27 mmol) in ethanol (30 mL) was stirred at room temperature for 2h. The product was separated, filtered and purified by recrystallization from ethanol-chloroform (1:3) mixture to give acenaphthenone-2-ylidene ketones **3a-f** (57-68%).

2-(2-oxo-2-phenylethylidene)acenaphthylen-1(2H)-one (3a) [17,18,40]**:** Yellow needles, Yield: 3.18 g (60%), mp: 108-110°C, IR ν_{max} (KBr): 1722, 1671 cm^{-1} (C=O), ^{1}H NMR ($CDCl_3$): δ 8.97-7.26 (12H, m, aromatic and vinylic protons), ^{13}C NMR ($CDCl_3$): δ 200.32, 199.21, 141.13, 140.84, 138.10, 134.86, 133.25, 131.02, 130.87, 130.38, 129.23, 128.40, 128.33, 127.62, 126.12, 123.19, 118.29,96.43. MS (FAB): m/z 284 (M^+), 105 Elemental analysis calculated for $C_{20}H_{12}O_2$: C 84.49, H 4.25. Found: C 84.43, H 4.39.

2-(2-oxo-2-p-tolylethylidene)acenaphthylen-1(2H)-one (3b) [17,18,40]**:** Yellow needles, Yield: 3.39 g (64%), mp: 143-145°C, IR ν_{max} (KBr): 1710, 1674 cm^{-1} (C=O), ^{1}H NMR ($CDCl_3$): δ 8.97-7.21 (11H, m, aromatic and vinylic protons), 2.40 (3H, singlet, methyl protons) ^{13}C NMR ($CDCl_3$): δ 200.16, 199.34, 153.81, 144.29, 134.93, 134.47, 132.01, 131.34, 131.34, 130.31, 129.80, 129.51, 129.51, 129.64, 127.50, 127.17, 126.81, 122.52, 25.80. MS (FAB): m/z 295 (M^+), 119. Elemental analysis calculated for $C_{21}H_{14}O_2$: C 84.54, H 4.74. Found: C 84.48, H 4.76.

2-(2-(4-chlorophenyl)-2-oxoethylidene)acenaphthylen-1(2H)-one (3c) [17,18,40]**:** Yellow needles, Yield: 3.60 g (68%), mp: 187-189°C, IR ν_{max} (KBr): 1716, 1668 cm^{-1} (C=O), ^{1}H NMR ($CDCl_3$): δ 8.81-7.14 (11H, m, aromatic and vinylic protons), ^{13}C NMR ($CDCl_3$): δ 200.4, 194.21, 140.93, 140.14, 139.10, 134.99, 132.05, 131.54, 130.77, 130.18, 129.08, 128.45, 128.39, 127.92, 126.85, 122.09, 117.99, 96.19. MS (FAB): m/z 318 (M^+), 139. Elemental analysis calculated for $C_{20}H_{11}ClO_2$: C 75.36, H 3.48. Found: C 75.39, H 3.41.

2-(2-(4-bromophenyl)-2-oxoethylidene)acenaphthylen-1(2H)-one (3d) [17,18,40]**:** Yellow needles, 2.62 g (57%), mp: 197-199°C, IR ν_{max} (KBr): 1710, 1663 cm^{-1} (C=O), ^{1}H NMR ($CDC1_3$): δ 8.80-7.12 (11H, m, aromatic and vinylic protons), MS (FAB): m/z 362 (M^+), 183. Elemental analysis calculated for $C_{20}H_{11}BrO_2$: C 66.14, H 3.05. Found: C 66.18, H 3.11.

2-(2-(4-methoxyphenyl)-2-oxoethylidene)acenaphthylen-1(2H)-one (3e) [17,18,40]**:** Yield: 2.90 g (63%), mp: 161-163°C, IR ν_{max} (KBr): 1722, 1670 cm^{-1} (C=O), ^{1}H NMR ($CDCl_3$): δ 8.84-6.91 (11H, m, aromatic and vinylic protons), 3.88 (3H, singlet, methoxy protons), ^{13}C NMR ($CDCl_3$): δ 193.66, 189.13, 164.04, 140.70, 138.22, 132.62, 131.31, 131.24, 130.80, 130.47, 129.84, 129.12, 128.37, 121.93, 117.69, 115.41, 114.62, 114.13, 113.98, 113.05, 110.99, 108.72, 107.71, 106.09, 104.37, 96.22, 55.40. MS (FAB): m/z 314 (M^+), 135. Elemental analysis calculated for $C_{21}H_{14}O_3$: C 84.54; H 4.73. Found: C 84.50, H 4.69.

2-(2-(biphenyl-4-yl)-2-oxoethylidene)acenaphthylen-1(2H)-one (3f) [17,18,40]**:** Yield: 2.76 g (60%), mp: 187-189°C, IR ν_{max} (KBr): 1715, 1650 cm^{-1} (C=O), ^{1}H NMR ($CDCl_3$) δ 8.78-7.25 (16H, m, aromatic and vinylic protons), ^{13}C NMR ($CDCl_3$) δ 201.89, 194.87, 146.41, 140.11, 135.31, 132.47, 132.37, 131.43, 130.81, 129.47, 128.94, 128.83, 128.39, 128.23, 127.79, 127.40, 127.14, 126.69, 126.48, 124.04, 122.04, 117.87, 112.89, 109.54, 108.14, 96.22. MS (FAB): m/z 360 (M^+), 181. Elemental analysis calculated for $C_{26}H_{16}O_2$: C 86.64, H 4.47. Found: C 86.68; H 4.42.

Declaration of Competing Interest

The authors declare that they have no known competing financial interests or personal relationships that could have appeared to influence the work reported in this paper.

Supplementary materials

Supplementary material associated with this article can be found, in the online version, at doi:10.1016/j.molstruc.2020.129209.

CRediT authorship contribution statement

Daly Kuriakose: Software, Formal analysis, Investigation, Data curation, Writing - original draft. **Roshini K. Thumpakara:** Investigation, Writing - original draft, Data curation, Formal analysis. **Jesna A:** Visualization, Investigation. **Jomon P. Jacob:** Conceptualization, Methodology, Supervision.

References

[1] M.R. Jayapal, K.S. Prasad, N.Y. Sreedhar, Synthesis and characterization of 2,6-dihydroxy substituted chalcones using PEG-400 as a recyclable solvent, J. Pharm. Sci. Res. 2 (2010) 450–458.

[2] A.F.M. Rahman, R. Ali, Y. Jahng, A.A Kadi, A facile solvent free claisen-schmidt reaction: synthesis of α,α'-bis-(Substituted-benzylidene)cycloalkanones and α,α'-bis-(Substituted-alkylidene)cycloalkanones, Molecules 17 (2012) 571–583.

[3] A. Rayar, M.S. Iyarreta Veitía, C. Ferroud, An efficient and selective microwave-assisted Claisen-Schmidt reaction for the synthesis of functionalized benzalacetones, SpringerPlus 4 (2015) 221.

[4] R. Pal, Ammonium chloride catalyzed microwave-assisted ClaisenSchmidt reaction between ketones and aldehydes under solvent free conditions, IOSR J. App. Chem. 3 (2013) 74–80.

[5] M.R. Mousavi, M.T. Maghsoodlou, H. Gharari, Sodium carbonate-catalyzed Claisen–Schmidt condensation: one-pot synthesis of highly functionalized cyclohexenones under environmental conditions, Res. Chem. Intermed. 42 (2016) 2233–2246.

[6] D. Ispán, E. Szánti-Pintér, M. Papp, J. Wouters, N. Tumanov, B. Zsirka, Á. Gömöry, L. Kollár, R. Skoda-Földes, The use of switchable polarity solvents for the synthesis of 16-Arylidene steroids via claisen–schmidt condensation, Eur. J. Org. Chem (2018) 3236–3244 2018.

[7] X. Qi, X. Yan, W. Peng, J. Zhang, Y. Tong, J. Li, D. Sun, G. Huid, J. Zhang, Graphene-induced hierarchical mesoporous MgO for the Claisen–Schmidt condensation reaction, New J. Chem. 43 (2019) 4698–4705.

[8] D. Kumar, J.S.Sandhu Suresh, An efficient green protocol for the synthesis of chalcones by a Claisen–Schmidt reaction using bismuth(III)chloride as a catalyst under solvent-free condition, Green Chem. Lett. Rev. 3 (2010) 283–286.

[9] R. L.Reeves, Wiley-Intersciences, New York, NY, USA, 1966, pp. 580–600.

[10] T. Mukaiyama, in: W.G. Dauben (Ed.), Organic Reactions, 28, J. Wiley & Sons, New York, NY, USA, 1982, pp. 203–331.

[11] A.T. NieIsen, W.J. Houlihan, in: R. Adams, A.H. Blatt, V. Boekelheide, T.L. Cairns, D.J. Cram, H.O. House (Eds.), Organic Reactions. In The Aldol Condensation, 16, J. Wiley & Sons, New York, NY, USA, 1968, pp. 1–438.

[12] Q.H. Fan, Y.M. Li, A.S.C. Chan, Recoverable catalysts for asymmetric organic synthesis, Chem. Rev. 102 (2002) 3385–3466.

[13] T. Narender, K.P. Reddy, A simple and highly efficient method for the synthesis of chalcones by using borontrifluoride-etherate, Tetrahedron Lett. 48 (2007) 3177–3180.

[14] S. Muthadi, B. Macha, P. Mamidi, S. Manchinella, A. Garlapati, R.R. Akkinepalli, Synthesis and evaluation of new brominated azaflavones and azaflavanone derivatives as cytotoxic agents against breast cancer cell line (MCF-7), Indian J. Pharm. Educ. 53 (2019) 117–126.

[15] T.P. Robinson, R.B. Hubbard, T.J. Ehlers, J.L. Arbiser, D.J. Goldsmith, J.P. Bowen, Synthesis and biological evaluation of aromatic enones related to curcumin, Bioorg. Med. Chem 13 (2005) 4007–4013.

[16] A.T. Nielsen, W.J. Houliban, The aldol condensation, Organ. React. 16 (1968) 1438.

[17] J.J. Vadakkan, V. Raman, N.B. Fernandez, S. Prathapan, B. Jose, A novel solvent-assisted domino Michael-aldol reaction of acenaphthenequinone with acetophenones, New J. Chem 27 (2003) 239–241.

[18] J.P. Jacob, C. Kunjachan, L.U. Sajitha, R.K. Thumpakara, K. Rakesh, V. Nidhisha, P.A. Unnikrishnan, S. Prathapan, Domino reaction sequences leading to the formation of 2:2 adducts between acenaphthenequinone and acetophenone, ARKIVOC (2014) 127–138 vi.

[19] O. Trott, A.J. Olson, Software news and update autodock vina: improving the speed and accuracy of docking with a new scoring function, efficient optimization, and multithreading, J. Comput. Chem. 31 (2010) 455–461.

[20] S. Dallakyan, A.J. Olson, in: Chemical Biology: Methods Protocols, Humana Press, New York, 2015, pp. 243–250.

[21] G.M. Morris, D.S. Goodsell, R.S. Halliday, R. Huey, W.E. Hart, R.K. Belew, A.J. Olson, Automated docking using a Lamarckian genetic algorithm and an empirical binding free energy function, J. Comput. Chem. 19 (1998) 1639–1662.

[22] L.U. Sajitha, M. Sithambaresan, J.P. Jacob, M.R.P. Kurup, Crystal structure of (4-chlorophenyl)[2-(10-hydroxyphenanthren-9-yl)phenanthro[9,10-b]furan-3-yl]methanone, Acta Cryst. E70 (2014) 355–358.

[23] J.P. Jacob, M. Sithambaresan, C. Kunjachan, M.R.P. Kurup, Crystal structure of 8-[7,8-bis(4-chlorobenzoyl)-7H-cyclopenta[a]acenaphthylen-9-yl]naphthalene-1-carboxylic acid, Acta Cryst. E71 (2015) 38–41.

[24] M. Hassan, Z. Ashraf, Q. Abbas, H. Raza, S.-Y. Seo, Exploration of novel human tyrosinase inhibitors by molecular modeling, docking and simulation studies, Interdiscip. Sci. 10 (2018) 68–80.

[25] A. Tan, S. Kizilkaya, U. Kelestemur, A. Akdemir, Y. Kara, The synthesis, anticancer activity, structure-activity relationships and molecular modelling studies of novel isoindole-1,3(2H)-dione compounds containing different functional groups, Anticancer Agents Med. Chem (2020), doi:10.2174/1871520620666200410080648.

[26] P. Bansode, P. Patil, P. Choudhari, M. Bhatia, A. Birajdar, I. Somasundaram, G. Rashinkar, Anticancer activity and molecular docking studies of ferrocene tethered ionic liquids, 290 (2019) 111182.

[27] S. Tahlan, S. Kumar, K. Ramasamy, S.M. Lim, S.A.A. Shah, V. Mani, B. Narasimhan, In-silico molecular design of heterocyclic benzimidazole scafolds as prospective anticancer agents, BMC Chemistry 13 (2019) 90.

[28] Z. Luo, A. Valeru, S. Penjarla, B. Liu, I. Khan, Synthesis, anticancer activity and molecular docking studies of novel pyrido[1,2-a]pyrimidin-4-one derivatives, Synth. Commun. 49 (2019) 2235–2243.

[29] Y.-L. Zhang, R. Yang, L.-Y. Xia, R.-J. Man, Y.-C. Chu, A.-Q. Jiang, Z.-C. Wang, H.-L. Zhu, Synthesis, anticancer activity and molecular docking studies on 1,2-diarylbenzimidazole analogues as anti-tubulin agents, Bioorg. Chem. 92 (2019) 103219.

[30] S.R. Shah, K.D. Katariya, D. Reddy, Quinoline-1,3-Oxazole hybrids: syntheses, anticancer activity and molecular docking studies, Chem. Select 5 (2020) 1097–1102.

[31] H.M. Berman, J. Westbrook, Z. Feng, G. Gilliland, T.N. Bhat, H. Weissig, I.N. Shindyalov, P.E. Bourne, The protein data bank, Nucl. Acids Res. 28 (2000) 235–242.

[32] The PyMOL Molecular Graphics System, Version 1.5.0.4 Schrodinger LLC.

[33] A. Viji, V. Balachandran, S. Babiyana, B. Narayana, V.V. Saliyan, Molecular docking and quantum chemical calculations of 4-methoxy-{2-[3-(4-chlorophenyl)-5-(4-(propane-2-yl) phenyl)-4, 5-dihydro-1H-pyrazol-1-yl]- 1, 3-thiazol-4-yl}phenol, J. Mol. Struct. 1203 (2020) 127452.

[34] Discovery Studio 4.5 Guide, Accelrys Inc., San Diego, 2009. http://www.accelrys.com.

[35] C.A. Lipinski, Lead- and drug-like compounds: the rule-of-five revolution, Drug Discov. Today Technol. 1 (2004) 337–341.

[36] S. Singh, A.K. Gupta, A. Verma, Molecular properties and bioactivity score of the aloe vera antioxidant compounds – in order to lead finding, RJPBCS 4 (2013) 876–881.

[37] S.S.A. Fathima, M.M.S. Meeran, E.R. Nagarajan, Synthesis of novel (E)-2-((anthracen-9-ylmethylene)amino)pyridin-3-ol and its transition metal complexes: multispectral characterization, biological evaluation and computational studies, J. Mol. Liq 279 (2019) 177–189.

[38] Molinspiration Cheminformatics [Homepage on the Internet], Nova Ulica, Slovensky Grob, Slovakia, (2012); http://www.molinspiration.com/.

[39] J. Lakshmipraba, S. Arunachalam, R.V. Solomon, P. Venuvanalingam, A. Riyasdeen, R. Dhivya, M.A. Akbarsha, Surfactant–copper(II) Schiff base complexes: synthesis, structural investigation, DNA interaction, docking studies, and cytotoxic activity, J. Biomol. Struct. Dyn. 33 (2015) 877–891.

[40] R.K. Thumpakara, Ph. D Thesis, CUSAT, 2007.

Quantitative Analysis of Oxalate content and Nutritive study of common Vegetables in Rural Market

Roshini K. Thumpakara
Department of Chemistry, Carmel College, Mala
roshinikt@gmail.com

Abstract

The oxalate content of different vegetables such Brassica oleracea (Cauliflower), Lycopersicon esculentum (tomato), Abelmoschus esculentus (Ladies Finger), Cucumis sativus (Cucumber), Brassica oleracea (Cabbage), Solanum melongena (Brinjal) Solanum tuberosum (potato) were determined permagnometrically in order to know which vegetable would supply more oxalate to our body. Oxalates are organic acids that occur naturally in plants, animals and humans. Determination of oxalate content by redox titration is an easy, safe and fast method. Potassium permanganate is a powerful oxidising agent in acid medium and can oxidise reducing agents like oxalate. This would help in determining the amount of oxalate content in various vegetables. The oxalate ion concentration were found to be 52.8mg/50g for Brassica oleracea var. botrytis *(Cauliflower), 61.6mg/50g for* Lycopersicon esculentum *(tomato), 93.72mg/50g for* Abelmoschus esculentus *(Ladies Finger), 105.6mg/50g for* Cucumis sativus *(Cucumber), 111.32mg/50g for* Brassica oleracea var. capitata *(Cabbage), 181.28mg/50g for* Solanum melongena *(Brinjal) and 216.9mg/50g for* Solanum tuberosum *(potato). Our analysis proved that selected samples were rich in carbohydrates, starch, iron, potassium and magnesium.*

Keywords: oxalate content, organic acids, redox titration

Introduction

Oxalate are organic acids that occur naturally in plants, animals, and humans, It is not an essential molecule and is excreted from our body, unchanged. Our body either produces oxalate ion on its own or converts other molecules to oxalate. Oxalate occurs in many plants, where it is synthesized by the incomplete oxidation of carbohydrates. Oxalic acid irritates the lining of the gut when consumed, and can prove fatal in large doses[1-5]. Healthy individuals can safely consume such vegetables in moderation, but those with kidney disorders, gout, rheumatoid arthritis or certain forms of chronic vulvar pain are typically advised to avoid foods high in oxalate.

Oxalate can become problematic, however, if they over accumulate inside our body. The key site for problems with over accumulation is our kidneys. It is being recommended to limit the intake of oxalate-rich foods, specifically for individuals at risk for kidney stone formation[6-9]. The oxalate content of food can vary considerably between plants of different vegetables due to difference in climate and soil quality. The content of oxalate ion present in a specific fruit or a vegetable can be determined by a carrying out experiment on the crushed pulp of that vegetable. The experiment gives the strength of oxalate ion content which can be directly related to the amount of oxalate ion present in that specific fruit or vegetable. For our present study we selected some common vegetables from our locality like Brassica oleracea var.botrytis (Cauliflower), Lycopersicon esculentum (tomato), Abelmoschus esculentus (Ladies Finger), Cucumis sativus (Cucumber), Brassica oleracea var. capitate (Cabbage), Solanum melongena (Brinjal) and Solanum tuberosum (potato) to

find out the most suitable variety (that contain low oxalate content) so that it could be referred to the people who were suffering from kidney stone.

Material and Methods

Sample collection and preparation

Vegetables such as Brassica oleracea (Cauliflower), Lycopersicon esculentum (tomato), Abelmoschus esculentus (Ladies Finger), Cucumis sativus (Cucumber), Brassica oleracea (Cabbage), Solanum melongena (Brinjal) and Solanum tuberosum (potato) were collected from a local market. The selected vegetables were then washed thoroughly with water. The vegetables are then weighed separately in an electronic balance and crushed to fine paste using pestle-mortar.

Weigh 50 g of fresh vegetable pulp and crush it to a fine pulp using pestle and mortar. Transfer the crushed pulp to a beaker and add about 50 ml dil. H_2SO_4 to it. Boil the content for 20 minutes. Cool and filter the contents in a 100 ml measuring flask. Make the volume up to 100 ml by adding distilled water.

Estimation of free oxalate ion present in vegetable samples

Take 20 ml of vegetable sample solution from the measuring flask into a titration flask and add 20 ml of dil. H_2SO_4 to it. Heat the mixture to about 60^oC and titrate it against standardized $KMnO_4$ solution taken in a burette. The end point is appearance of permanent pale pink colour. Repeat the above procedure for all samples.

Qualitative parameters of vegetables

Test for Starch

Take 2 ml of clear fruit juice and add a few drops of Iodine solution. Formation of blue complex indicates the presence of starch.

Test for Carbohydrate

Molisch's test: To the sample taken, 2 drops of 1% alcoholic 1-naphthol solution was added. Add about 1 ml of conc. H_2SO_4 carefully along the sides of the test tube. A violet ring at the junction of the two layer shows the presence of carbohydrate.

Benedict's test: To a little of the sample taken in a test tube, add a few drops of Benedict's reagent. The test tube was heated in a water bath for a few minutes. Appearance of rust brown colour indicates the presence of reducing sugar.

Fehling's Test: To a little of the sample taken in a test tube, add 1 ml of Fehling's solution and heat. Presence of red precipitate indicate the presence of reducing sugar.

Test for Protein

Ninhydrin Test: To a little of sample taken, add 2 ml of ninhydrin solution and heat. Presence of blue colour indicates the presence of protein

Xanthoprotic test: To a little of sample taken add a few drops of conc. HNO_3. Formation of yellow color indicates the presence of proteins**.**

Test for Flavanoids

Alkaline reagent test - Extracts were treated with few drops of NaOH solution. Formation of intense yellow color, which become colorless on addition of dilute acid indicates the presence of flavonoids.

Test for Iron

A drop of test solution is mixed with one small crystal of tartaric acid and a drop of dimethyl glyoxime followed by drops of ammonium hydroxide. Formation of red colour indicated presence of iron.

Test for Potassium

To a little of sample taken in a test tube, add picric acid. Presence of yellow precipitate indicated the presence of K^+ ions.

Test for Calcium

To a little of sample taken, Ammonium chloride and Ammonium hydroxide solutions were added. Filter the solution and to the filtrate 2 ml of Ammonium oxalate solution were added. White precipitate indicated presence of calcium.

Two drops of sample solution was acidified with acetic acid and three drops of saturated solution of Picrolinic acid in water were added. Presence of white crystals indicated presence of calcium.

Test for Magnesium

To about 2 ml of juice excess of Ammonium hydroxide solution and Ammonium chloride solutions were added followed by an excess of disodium hydrogen phosphate solution and shake well, scratch the sides of the test tube with a glass rod. Presence of white precipitate indicated the presence of Magnesium.

A little of sample was treated with few drops of Magneson reagent followed by excess of NaOH solution. Blue precipitate indicated the presences of magnesium.

Results and Discussion

From our investigations, we found that the amount of oxalate ion concentration was high in potato compared to others. Low concentration of oxalate ion was found in cauliflower which was a leafy vegetable. A moderate amount was found in ladies finger, cucumber, and cabbage.

No.	Name of vegetable	Amount of oxalate content/50g
1	Brassica oleracea var. botrytis Cauliflower)	52.8mg
2	Lycopersicon esculentum (Tomato)	61.6mg
3	Abelmoschus esculentus (Ladies Finger)	93.72mg
4	Cucumis sativus (Cucumber)	105.6mg
5	Brassica oleracea var.capitata (Cabbage)	111.32mg
6	Solanum melongena (Brinjal)	181.28mg
7	Solanum tuberosum (Potato)	216.9mg

Table 1: Total Oxalate content in vegetable sample

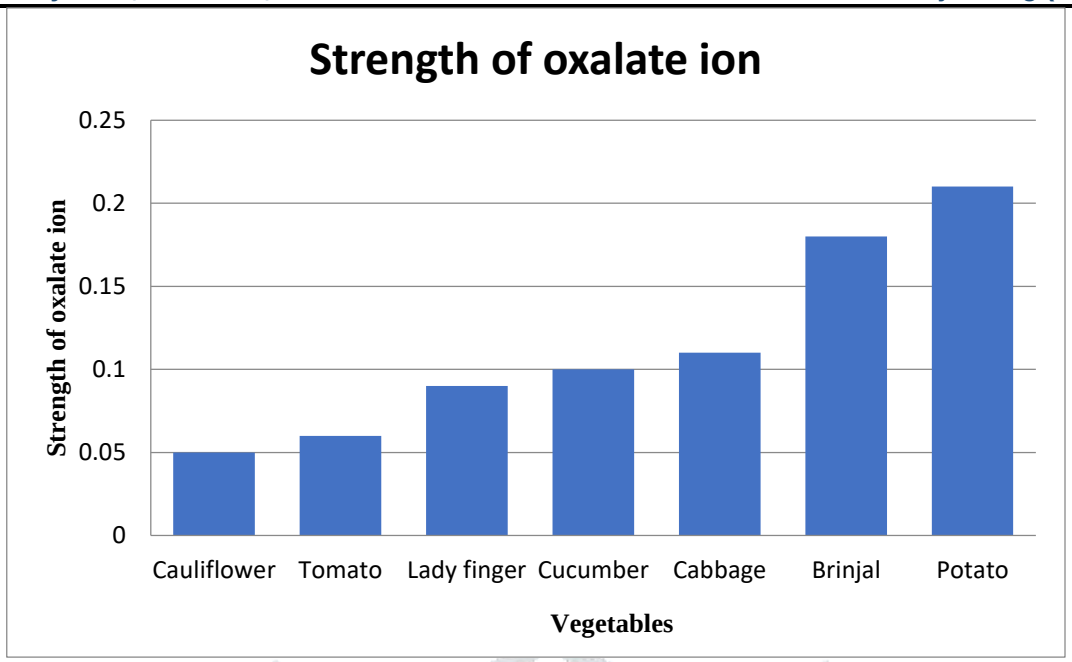

Fig 1: Oxalate ion concentration (mg/50g)

Table 2: Nutritive Analysis

Vegetables	Proteins	Flavanoids	Carbohydrates	Starch	Iron	Ca	K	Mg
Solanum melongena (Brinjal)	✓	✓	✓	✓	✓	×	✓	✓
Lycopersicon esculentum (Tomato)	×	×	✓	✓	✓	×	×	✓
Cucumis sativus (Cucumber)	×	×	✓	✓	✓	×	✓	✓
Abelmoschus esculentus (Ladies Finger)	✓	✓	✓	✓	✓	×	✓	✓
Solanum tuberosum (Potato)	✓	✓	✓	✓	✓	×	✓	✓
Brassica oleracea var. capitata (Cabbage)	×	×	✓	✓	✓	×	✓	✓
Brassica oleracea var. botrytis (Cauliflower)	✓	✓	✓	✓	✓	×	✓	✓

Our nutritive analysis on the selected vegetable samples showed the following results.Proteins and flavonoids were present in all our samples except tomato, cucumber and cabbage. Carbohydrates, starch, iron and magnesium were present in all our selected samples. Potasium was present in all samples except tomato. Calcium was present in none of our samples.

Conclusion

The oxalate content in vegetables vary considerably between plants due to difference in climate, soil quality state of ripeness or even which part of the plant is analyzed. Among our selected vegetable samples, amount of oxalate ion concentration was high in potato compared to others. Low concentration of oxalate ion was found in cauliflower which was a leafy vegetable. A moderate amount was found in ladies finger, cucumber, and cabbage. Nutritive analysis was also found to be fruitful.Healthy individuals can safely consume vegetables, high in oxalate content in moderation, but those with kidney disorders were typically advised to avoid foods high in oxalate. Oxalate can become problematic, however, if they over accumulate inside our body. It is being recommended to limit the intake of oxalate-rich foods, specifically for individuals at risk for kidney stone formation.

References

1. Trevaskis, M., & Trenerry, V. C. (1996). An investigation into the determination of oxalic acid in vegetables by capillary electrophoresis. Food Chemistry, 57(2), 323–330
2. Liu, E., Luo, W., Zhou, H. et al. Determination of oxalate in plant tissues with oxalate oxidase prepared from wheat. Biol Plant **53,** 129–132 (2009)
3. Noonan, S.C., Savage, G.P., 1999. Oxalic acid content of foods and its effect on humans. Asia Pacific Journal of Clinical Nutrition 8 (1), 64–74.
4. Gelot, H.A., Lover, G., Belleville, F., Nabet, P., 1980. Determination of oxalic acids in plasma and urine using gas chromatography. Clinica Chimica Acta 106 (3), 279–285.
5. Holloway, W.D., Argall, M.E., Jealous, W.T., Lee, J.A., Bradbury, J.H., 1989. Organic Acids and Calcium Oxalic acid in Tropical Root Crops. Journal of Agricultural and Food Chemistry 37, 337–341.
6. Eheart, J. F., & Massey, Jr. P. H. (1962). Factors affecting the oxalate content in spinach. Chemical Constituents of Plants, 10(4), 325.
7. Franceschi, V. R., & Horner, H. T. Jr. (1980). Calcium oxalate crystals in plants. The Botanical Review, 46, 361-427.
8. Arima H., Danno G., Isolation of antimicrobial compounds from guava (Psidium guajava L.) and their structural elucidation, Biosci Biotechnol Biochem, 66(8): 1727-1730, (2002)
9. Hönow, R., & Hesse, A. (2002). Comparison of extraction methods for the determination of soluble and total oxalate in foods by HPLC-enzyme-reactor. Food Chemistry, 78(4), 511-521.

ISSN 0971 - 2976

JOURNAL OF THE BOTANICAL SOCIETY OF BENGAL

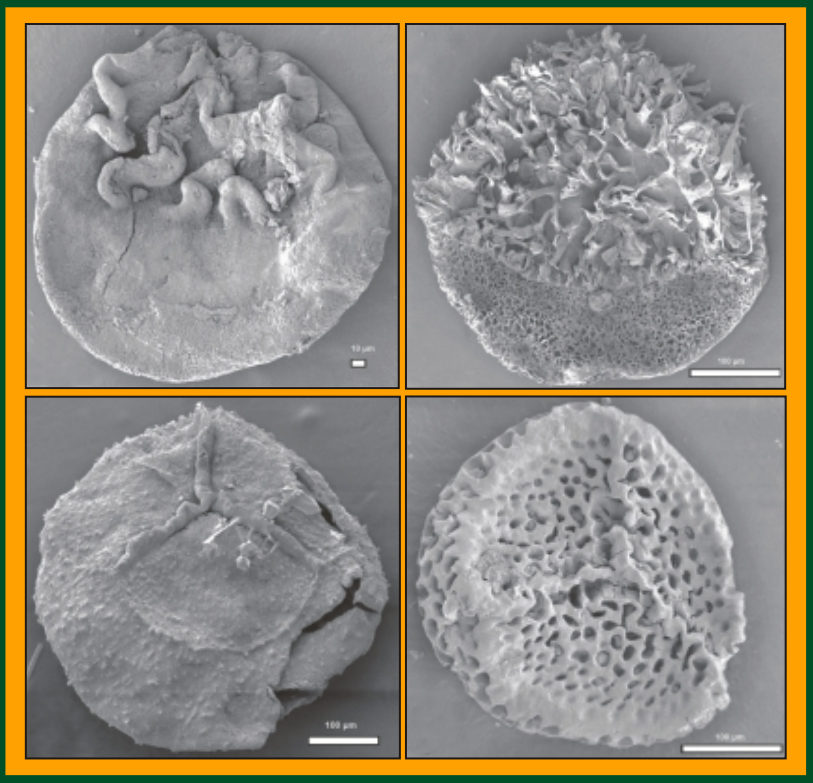

Volume 75
Number 2, December 2021

AN
OFFICIAL ORGAN
OF THE
BOTANICAL SOCIETY OF BENGAL

BOTANICAL SOCIETY OF BENGAL

(Established in 1935)

Website : www.botansocbengal.org

Aims and Scope

Journal of the Botanical Society of Bengal has a long history of publishing articles since its inception. It is a peer reviewed, biannual journal. The aim of this journal is to encourage publication of scientific knowledge on any branch of plant science, basic and applied. The topics range from cryptogams to phaneragams, morphology-anatomy, plant-microbe interaction, genomics and genetics, physiology and biochemistry, palaeobotany-palynology, plant molecular biology and biotechnology, embryology, systematics and other allied fields of plant sciences. Along with full articles, reviewed articles and short communications are also published.

Copyright and permission

Journal Website

www.botansocbengal.org

Publication Ethics

www.publicationethics.org
https://authorservices.willey.com/ethics-guidelines/index.html

Papers will be accepted only if they abide by the publication ethics and bioethics.

Subscription Information

All communications should be addressed to the Secretary, Botanical Society of Bengal, Department of Botany, University of Calcutta, 35 Ballygunge Circular Road, Kolkata 700019. The subscription price is Rs.2000.00 per volume (two numbers in a year) in India including ordinary Book Post charge. The subscription for foreign countries is US $ 500.00 per volume, including air mail charges.

Office of Publication

Department of Botany, University of Calcutta, 35, Ballygunge Circular Road, Kolkata 700019, West Bengal, India

The figure in the cover page showing : Megaspores of late permian lycopsids from Chhattisgarh, India, in the article by Subhankar Pramanik *et al., J. Botan. Soc. Bengal,* 75(2): 86-101, 2021

Executive Council : 2018-2021

President	Immediate Past President	Vice-Presidents
Balaram Majumder	Nandadulal Paria	Radhanath Mukhopadhyay Ruma Pal
Secretary	**Editor of Publication**	**Treasurer**
Ashalata D'Rozario	Subir Bera	Maumita Bandyopadhyay
Business Manager		**Librarian**
Sandip Mukhopadhyay		Rita Kundu

Members of the Council

Debabrata Maity
Pranab Kumar Bandyopadhyay
Santanu Paul
Prabir Kumar Saha
Bharati Nandi
Parimal Nag
Salil Kumar Basak
Shyamal Kumar Chakraborty
Sushovan Bera
Binod Kumar Pathak
Usha Chakraborty
Subrata Maiti
Pratima Nag (Co-opted)
Dipak Kumar Paruya (Co-opted)

Form IV

(See Rule 8)

1.	Place of Publication	:	Kolkata
2.	Periodicity of its Publication	:	Bi-annual (June and December)
3.	Printer Nationality Address	:	Mrs. Shyamali Das Indian 2, P. C. Das Lane, Serampore, Hooghly, Pin - 712204
4.	Publisher Nationality Address	:	Ashalata D'Rozario Indian Botanical Society of Bengal, Department of Botany, University of Calcutta, Kolkata 700019, India
5.	Editor-in-Chief Nationality Address	:	Subir Bera Indian Botanical Society of Bengal, Department of Botany, University of Calcutta, Kolkata 700019, India
6.	Names and address of individuals who own the newspapers and Partners or Shareholders holding more that one per cent of the total capital	:	Botanical Society of Bengal

I, Ashalata D'Rozario, hereby declare that the particulars given above are true to the best of my knowledge and belief.

December 27, 2021

Sd/ Ashalata D'Rozario
Signature of Publisher

J. Botan. Soc. Bengal 75 (2) December, 2021 Registration No. RN 16610/67

JOURNAL OF THE BOTANICAL SOCIETY OF BENGAL

(UGC-CARE enlisted; NAAS rated - 2021)
VOLUME 75 NUMBER 2 DECEMBER 2021

CONTENTS

Department of Botany, University of Calcutta,
Taraknath Palit Siksha Prangan,
35, Ballygunge Circular Road, Kolkata 700 019, India
Website: www.botansocbengal.org
E-mail: secbsbengal1935@gmail.com

Published bi-annualy by Ashalata D'Rozario, Secretary, Botanical Society of Bengal, Department of Botany, University of Calcutta, Taraknath Palit Siksha Prangan, 35, Ballygunge Circular Road, Kolkata 700 019, India and Printed by Mrs. Shyamali Das, Anima Printers, 2, P.C. Das Lane, Serampore, Hooghly, Pin 712204.

Journal of Nonlinear Modeling and Analysis
Volume 4, Number 1, March 2022, 1–19
http://jnma.ca; http://jnma.ijournal.cn
DOI:10.12150/jnma.2022.1

A Retrospective Study on Applications of the Lindley Distribution

Lishamol Tomy[1], Christophe Chesneau[2,†] and Meenu Jose[3]

Abstract The need for efficient statistical models has increased with the flow of new data, which makes distribution theory a particularly interesting and attractive field. Here, we provide a thorough study of the applications of the Lindley distribution and its diverse generalizations. More precisely, we review some special applications in various areas, such as time series analysis, stress strength analysis, acceptance sampling plans and data analysis. We also conduct a comparative study between the Lindley distribution and some of its generalizations by using four real-life data sets.

Keywords Lindley distribution, Stress-strength, Time series modeling, Quality control, Astrophysics.

MSC(2010) 60E05, 62H10.

1. Introduction

In recent years, there has been a growing interest in introducing new distributions and their generalizations because of the diversity of the data encountered in practice. Therefore, the statisticians aim to develop different distributions presenting flexible and original properties.

In this spirit, Lindley [45] coined the term "Lindley distribution" to refer to a one-parameter distribution used in fiducial and Bayesian inferences. Its properties and applications in reliability analysis were studied by Ghitany et al. [37], showing that it may provide a better fit than the exponential distribution. The Lindley distribution's simplicity and moderate flexibility paved the way for generalized versions, with the goal of building models and with better goodness of fit to data sets than the well-known basic distributions. Some of these generalizations are the size-biased Poisson-Lindley distribution by Ghitany and Al-Mutairi [33], discrete Poisson-Lindley distribution by Sankaran [56] and zero-truncated Poisson-Lindley distribution by Ghitany et al. [35], two-parameter Lindley distribution by Shanker and Mishra [61], power Lindley distribution by Ghitany et al. [34], inverse Lindley distribution by Sharma et al. [64], exponentiated power Lindley distribution by Ashour and Eltehiwy [13], generalized power Lindley distribution by Liyanage

[†]the corresponding author.
Email address: lishatomy@gmail.com (L. Tomy), christophe.chesneau@gmail.com (C. Chesneau), meenusgc@gmail.com (M. Jose)
[1]Department of Statistics, Deva Matha College Kuravilangad, Kottayam, India
[2,†]Department of Mathematics, LMNO, University of Caen- Normandie, Caen, France
[3]Department of Statistics, Carmel College Mala, Thrissur, India

and Parai [46], extended Lindley distribution by Bakouch et al. [14], Akash distribution by Shanker [58], quasi Akash distribution by Shanker [59], weighted Akash distribution Shanker and Shukla [63], quasi Lindley distribution by Shanker and Mishra [62], extended power Lindley distribution by Alkarni [4], discrete Lindley distribution by Deniz and Ojeda [29], weighted Lindley distribution by Ghitany et al. [36], discrete Poisson-Akash distribution by Shanker [60], new weighted Lindley distribution by Asgharzadeh [12], transmuted Lindley distribution by Merovci [49], new extended generalized Lindley distribution by Maya and Irshad [47], and transmuted two-parameter Lindley distribution by Kemaloglu and Yilmaz [40].

Some recent works based on the Lindley distribution are the Topp-Leone odd Lindley family of distributions by Reyad et al. [54], wrapped Lindley distribution by Joshi and Jose [39], Marshall-Olkin extended quasi Lindley distribution by Udoudo and Etuk [66], three-parameter generalized Lindley by Ekhosuehi and Opone [32], Lindley Weibull distribution by Cordeiro et al. [28], alpha power transformed power Lindley distribution by Hassan et al. [38], alpha power transformed Lindley distribution by Dey et al. [30], Weibull Marshall-Olkin Lindley distribution by Afify et al. [2], inverted modified Lindley distribution by Chesneau et al. [25], sum and difference of two Lindley distributions by Chesneau et al. [23], modified Lindley distribution by Chesneau et al. [24], wrapped modified Lindley distribution by Chesneau et al. [26], and Lindley-Lindley distribution by Chesneau et al. [27]. Tomy [65] contains a previous review of the Lindley distribution and its generalizations.

The main motivation behind this study is to expose the diverse applications of the Lindley distribution and its generalizations in various fields, like reliability, time series, quality control, astrophysics and the analysis of various kinds of data as well.

The paper unfolds as follows: In Section 2, we consider some applications of the Lindley distribution and some of its generalizations in time series modeling. Section 3 presents applications of stress-strength analysis. Section 4 contains applications for various acceptance sampling plans. Section 5 discusses applications in real data analysis. Finally, in Section 6, we conclude the paper.

2. Applications in time series modeling

Over the last decades, there has been increasing interest in developing time series models for real-valued observations by using Gaussian or non-Gaussian distributions. Among the existing time series models, let us evoke the autoregressive models, integer valued models for discrete distributions, stochastic volatility and autoregressive conditional duration models. In this section, we consider autoregressive minification processes, geometric processes and the first order non-negative integer valued autoregressive processes.

2.1. Autoregressive minification process

Udoudo and Etuk [66] proposed different minification processes with a generalized quasi Lindley distribution as a marginal distribution.
More precisely, let us consider the AR(1) structure given by

$$X_n = \begin{cases} \varepsilon_n & \text{with probability } p \\ \min(X_{n-1}, \varepsilon_n) & \text{with probability } 1-p \end{cases}$$

where $p \in (0,1)$ and $\{\varepsilon_n\}$ is a sequence of independent and identically (iid) distributed random variables with the quasi Lindley distribution, and also independent of $\{X_n\}$. Then, the process is a stationary AR(1) minification process with the Marshall-Olkin extended quasi Lindley distribution as a marginal distribution. The converse is also true. That is, if $\{X_n\}$ is a stationary Markovian process with the Marshall-Olkin extended quasi Lindley distribution as the marginal. Then, $\{\varepsilon_n\}$ follows the quasi Lindley distribution.
In addition, they gave a more general minification process, which is specified by

$$X_n = \begin{cases} X_{n-1} & \text{with probability } p_2 \\ \varepsilon_n & \text{with probability } p_1(1-p_2) \\ \min(X_{n-1}, \varepsilon_n) & \text{with probability } (1-p_1)(1-p_2) \end{cases}$$

where $p_1, p_2 \in (0,1)$ and $\{\varepsilon_n\}$ is a sequence of iid random variables independent of $\{X_n\}$. Then, the process $\{X_n\}$ is a stationary AR(1) minification process with Marshall-Olkin extended quasi Lindley distribution as marginal, if and only if $\{\varepsilon_n\}$ follows the quasi Lindley distribution.

In the literature, Bakouch et al. [15] considered the Lindley AR(1) model, and studied its applications.

2.2. Geometric process

Lam [43] introduced the Geometric process (GP) for modeling inter-arrival time data with a monotone trend. Bicer [17] has recently proposed a GP with power Lindley distribution as the first arrival time distribution. The GP was defined as follows. A stochastic process $\{X_n\}$ is said to be a GP, if there exists a real number $a > 0$ such that the random variables $Y_n = a^{n-1}X_n,\ n = 1, 2, \ldots$ are valid, where X_n is the inter-arrival time the $(n-1)^{th}$ and n^{th} events of a counting process $\{N(t), t \geq 0\}$, the number a is called the ratio parameter of the GP, and X_1 follows the power Lindley distribution.

Similarly, Demirci Bicer [18] proposed a GP with two-parameter Lindley distribution as the distribution of the first arrival time.

2.3. First order non-negative integer valued autoregressive process

The pioneering work of the first order non-negative integer valued autoregressive (INAR(1)) process was proposed by McKenzie [48], and Al-Osh and Alzaid [10]. It was used as a tool for modeling counting processes consist of dependent random variables. Mohammadpour [50] introduced a discrete stationary time series model based on INAR(1), called Poisson Lindley INAR(1) model by using the binomial thinning operator with a study on its properties. The model is given by

$$X_t = \alpha \circ X_{t-1} + \varepsilon_t, \quad t \geq 1,$$

where $\circ$ is the binomial thinning operator defined by $\alpha \circ X = \sum_{i=0}^{X} W_i$, $\alpha \in [0,1)$, $\{W_i\}$ is a sequence of iid random variables following the Bernoulli(α) distribution, and $\{\varepsilon_t\}$ is a sequence of iid random variables independent of the Bernoulli counting process $\{W_t\}$ and X_m for all $m \leq t$. If $\{X_t\}$ is a stationary process with the Poisson

Lindley distribution, then the innovation process $\{\varepsilon_t\}$ has the following probability generating function:

$$\Phi_\varepsilon(s) = \frac{2+\theta-s}{(1+\theta-s)^2}\frac{[\theta+\alpha(1-s)]^2}{1+\theta+\alpha(1-s)}, \quad s \in \mathbb{R}.$$

Similarly, Rostami [53] proposed a new stationary INAR(1) process based on the power series thinning operator under Poisson-Lindley innovations. Lvio et al. [44] introduced the INAR(1) model for modeling nonnegative integer valued time series with over dispersion using Poisson-Lindley innovations based on the binomial thinning operator.

3. Stress-strength analysis

When assessing system reliability, satisfactory performance is achieved when the strength applied to the component exceeds stress. It is a branch of reliability that aims to assess system performance. The pioneering work is given by Birnbaum [19] and Birnbaum and Mc Carty [20]. Al-Mutairi et al. [6] investigated stress-strength reliability inferences from the Lindley distribution. In this case, the reliability coefficient R is given by

$$\begin{aligned} R &= P(Y < X) \\ &= 1 - \frac{\theta_1^2[\theta_1(\theta_1+1)+\theta_2(\theta_1+1)(\theta_1+3)+\theta_2^2(2\theta_2+3)+\theta_2^3]}{(\theta_1+1)(\theta_2+1)(\theta_1+\theta_2)^3}, \end{aligned}$$

where $\theta_1, \theta_2 > 0$ and X and Y are two independent random variables following the Lindley distribution with parameters θ_1 and θ_2 respectively. They provide uniformly minimum variance unbiased estimator, maximum likelihood estimator and Bayesian inference of R, and study their effectiveness.

Furthermore, Khamnei [41] studied the reliability of the Lindley distribution when an outlier is present in the strength component, Krishna and Kumar [42] provided a reliability estimator by using the progressively type II censored sample, Al-Mutairi et al. [6] examined inferences on stress-strength reliability from the weighted Lindley distribution, Sadek et al. [55] discussed estimation of the stress-strength reliability for the quasi Lindley distribution, Pak et al. [52] studied the reliability of a multicomponent stress-strength model by assuming that the components follow the power Lindley distribution, and Akgul et al. [3] derived estimator of system reliability for the generalized inverse Lindley distribution by using several sampling designs.

4. Acceptance sampling plan

An acceptance sampling plan (ASP) is an important inspection and decision making tool, which has been often used by quality assurance managers to determine either to accept or to reject a product based on pre-specified quality standards. The objective of acceptance sampling is not to estimate the quality of the product, but to decide if the product is likely to be acceptable. There are different types of ASPs. Some of them are the single sampling plan, double sampling plan, multiple sampling plan, time truncated ASP, sequential sampling plan, skip lot sampling

plan and continuous sampling plan. If the quality characteristic is related to the product's lifetime, the acceptance sampling problem becomes a life's test.

Al-Omari and Al-Nasser [9] proposed an ASP based on a truncated life test, assuming the product's lifetime follows the two-parameter quasi Lindley distribution. By considering the minimum sample size, time and cost, it encourages practitioners to use this sampling plan. Al-Nasser et al. [8] developed a double ASP based on a truncated life test when the lifetime of the product follows the quasi Lindley distribution. Double sampling is used when the first sample does not give a decision and they recommend it to the researchers, Shahbaz et al. [57] introduced single and double ASP for the power Lindley distribution, and Dhanunjaya et al. [31] studied a continuous ASP for the truncated Lindley distribution.

5. Application in real data analysis

In this section, we perform a comparative study between Lindley, Akash, quasi Akash, two-parameter Lindley, inverse Lindley, quasi Lindley, power Lindley, exponentiated power Lindley, extended power Lindley, three-parameter generalized Lindley and new weighted Lindley distributions. The expressions of the probability density functions (pdfs) are given in the Appendix. These distributions were fitted to four different data sets. We estimate the unknown parameters of each model by the maximum likelihood method of estimation. Also, the statistics of the Akaike information criterion (AIC) and the Bayesian information criterion (BIC) are used to compare the eleven models. It is worth noting that $AIC = 2k - 2LogL$ and $BIC = k\log(n) - 2LogL$, where k is the number of parameters, n is the sample size, and $LogL$ is the maximized value of the log-likelihood function under the considered model.

5.1. The carbon fibers data set

This data set was given by Nichols and Padgett [51]. The carbon fibers data set consisting of 63 observations on breaking stress of carbon fibers (in Gba). The data are given below:
{0.81, 2.74, 2.73, 2.50, 3.60, 3.11, 3.27, 2.87, 1.47, 3.11, 3.56, 4.42, 2.41, 3.19, 3.22, 1.69, 3.28, 3.09, 1.87, 3.15, 4.90, 1.57, 2.67, 2.93, 3.22, 3.39, 2.81, 4.20, 3.33,2.55, 3.31, 3.31, 2.85, 1.25, 4.38, 1.84, 0.39, 3.68, 2.48, 0.85, 1.61, 2.79, 4.70, 2.03, 1.89, 2.88, 2.82, 2.05, 3.65, 3.75, 2.43, 2.95, 2.97, 3.39, 2.96, 2.35, 2.55, 2.59, 2.03,1.61, 2.12, 3.15, 1.08}
Table 1 gives the relevant numerical summaries for the fits of the considered distributions based on this data set.

Table 1. Estimated values, minus log-likelihood ($-LogL$), AIC and BIC for the carbon fibers data set

Distribution	Estimates	$-LogL$	AIC	BIC
Lindley	$\hat{\theta} = 0.5947$	116.568	235.1361	237.2792
Akash	$\hat{\theta} = 0.8894$	110.1611	222.3222	224.4654
Quasi Akash	$\hat{\alpha} = -0.1404$ $\hat{\theta} = 1.1615$	96.4044	196.8089	201.0952
Two-parameter Lindley	$\hat{\alpha} = -0.3721$ $\hat{\theta} = 0.9219$	97.9329	199.8658	204.1521
Inverse Lindley	$\hat{\theta} = 2.8076$	128.4222	258.8445	260.9876
Quasi Lindley	$\hat{\alpha} = -0.3431$ $\hat{\theta} = 0.9220$	97.9329	199.8658	204.1521
Power Lindley	$\hat{\beta} = 2.4048$ $\hat{\theta} = 0.1404$	84.61056	173.2211	177.5074
Exponentiated power Lindley	$\hat{\alpha} = 0.5380$ $\hat{\beta} = 3.2614$ $\hat{\theta} = 0.03651$	83.95305	173.9061	180.3355
Extended power Lindley	$\hat{\alpha} = 2.7625$ $\hat{\beta} = 0.1592$ $\hat{\theta} = 0.0812$	84.06479	174.1296	180.559
Three-parameter generalized Lindley	$\hat{\alpha} = 2.7620$ $\hat{\beta} = 6.2712$ $\hat{\lambda} = 0.0812$	84.06479	174.1296	180.559
New weighted Lindley	$\hat{\alpha} = 0.00017$ $\hat{\lambda} = 0.9767$	102.1854	208.3708	212.6571

Figures 1 and 2 give the graphs of the estimated pdfs and cumulative density functions (cdfs) respectively.

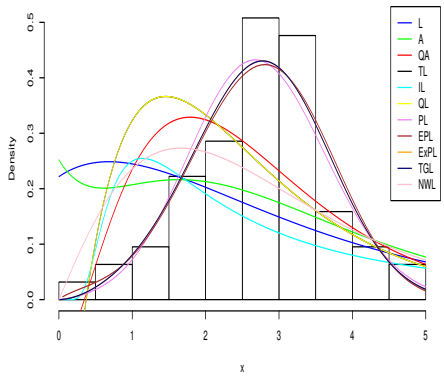

Figure 1. Estimated pdfs of the considered generalized Lindley distributions for the carbon fibers data set

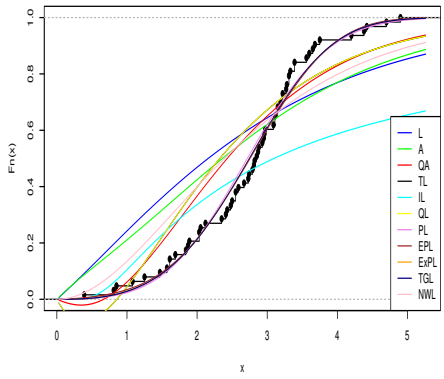

Figure 2. Estimated cdfs of the considered generalized Lindley distributions for the carbon fibers data set

At the end of the section, there will be comments on these results as well as those of the coming applications.

5.2. Guinea pigs data set

This data set was given by Bjerkedal [22]. It is the survival times (in days) of 72 guinea pigs infected with virulent tubercle bacilli. It is given below:
{12, 15, 22, 24, 24, 32, 32, 33, 34, 38, 38, 43, 44, 48, 52, 53, 54, 54, 55, 56, 57, 58, 58, 59, 60, 60, 60, 60, 61, 62, 63, 65, 65, 67, 68, 70, 70, 72, 73, 75, 76, 76, 81, 83, 84, 85, 87, 91, 95, 96, 98, 99, 109, 110, 121, 127, 129, 131, 143, 146, 146, 175, 175, 211, 233, 258, 258, 263, 297, 341, 341, 376}

Table 2 gives the relevant numerical values for the fits of the considered distributions based on long-axis orientations of guinea pigs data set.

Table 2. Estimated values, $-LogL$, AIC and BIC for the guinea pigs data set

Distribution	Estimates	$-LogL$	AIC	BIC
Lindley	$\hat{\theta} = 0.0198$	394.5197	791.0395	793.3161
Akash	$\hat{\theta} = 0.03004$	397.3508	796.7017	798.9783
Quasi Akash	$\hat{\alpha} = -0.2197$ $\hat{\theta} = 0.0301$	397.3555	798.7109	803.2643
Two-parameter Lindley	$\hat{\alpha} = -10.3902$ $\hat{\theta} = 0.0232$	391.5727	787.1454	791.6987
Inverse Lindley	$\hat{\theta} = 61.05642$	402.6685	807.3371	809.6137
Quasi Lindley	$\hat{\alpha} = -0.2413$ $\hat{\theta} = 0.0232$	391.5727	787.1454	791.6987
Power Lindley	$\hat{\beta} = 0.9951$ $\hat{\theta} = 0.0203$	394.5179	793.0358	797.5891
Exponentiated power Lindley	$\hat{\alpha} = 19.6531$ $\hat{\beta} = 0.4107$ $\hat{\theta} = 0.7839$	390.0966	786.1933	793.0233
Extended power Lindley	$\hat{\alpha} = 0.9863$ $\hat{\beta} = 1.9751$ $\hat{\theta} = 0.02131$	394.3916	794.7832	801.6132
Three-parameter generalized Lindley	$\hat{\alpha} = 0.9943$ $\hat{\beta} = 0.9228$ $\hat{\lambda} = 0.0204$	394.4989	794.9978	801.8278
New weighted Lindley	$\hat{\alpha} = 3.0381$ $\hat{\lambda} = 0.0209$	393.2794	790.5588	795.1121

Figures 3 and 4 give the graphs of the estimated pdfs and cdfs respectively.

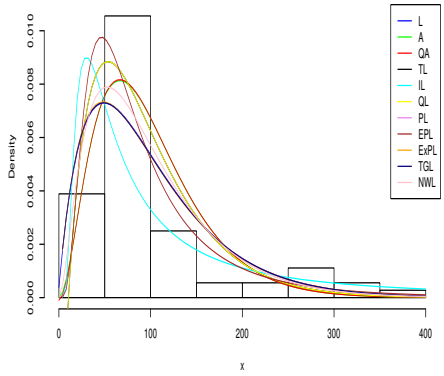

Figure 3. Estimated pdfs of the considered generalized Lindley distributions for the guinea pigs data set

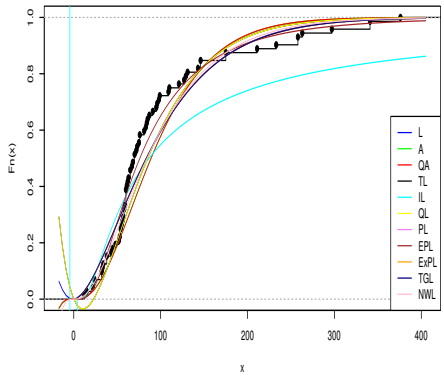

Figure 4. Estimated cdfs of the considered generalized Lindley distributions for the guinea pigs data set

5.3. The vinyl chloride data set

The real data represent 34 observations of the vinyl chloride data (in mg/L) that was obtained from cleaned-up gradient ground-water monitoring wells. The data are obtained from Bhaumik et al. [21] and are presented below.

{5.1, 1.2, 1.3, 0.6, 0.5, 2.4, 0.5, 1.1, 8, 0.8, 0.4, 0.6, 0.9, 0.4, 2, 0.5, 5.3, 3.2, 2.7, 2.9, 2.5, 2.3, 1, 0.2, 0.1, 0.1, 1.8, 0.9, 2, 4, 6.8, 1.2, 0.4, 0.2}

Table 3 gives the relevant numerical values for the fits of the considered distributions based on vinyl chloride data set.

Table 3. Estimated values, $-LogL$, AIC and BIC for vinyl chloride data set

Distribution	Estimates	$-LogL$	AIC	BIC
Lindley	$\hat{\theta} = 0.8238$	56.30364	114.6073	116.1336
Akash	$\hat{\theta} = 1.1657$	57.57463	117.1493	118.6756
Quasi Akash	$\hat{\alpha} = 15.9587$ $\hat{\theta} = 0.6946$	55.34411	114.6882	117.7409
Two-parameter Lindley	$\hat{\alpha} = 176.972$ $\hat{\theta} = 0.5376$	55.45269	114.9054	117.9581
Inverse Lindley	$\hat{\theta} = 0.8774$	61.81358	125.6272	127.1535
Quasi Lindley	$\hat{\alpha} = 538.4519$ $\hat{\theta} = 0.5329$	55.4526	114.9052	117.9579
Power Lindley	$\hat{\beta} = 0.8831$ $\hat{\theta} = 0.9139$	55.75992	115.5198	118.5726
Exponentiated power Lindley	$\hat{\alpha} = 3.7939$ $\hat{\beta} = 0.4988$ $\hat{\theta} = 2.1571$	54.9229	115.8458	120.4249
Extended power Lindley	$\hat{\alpha} = 1.0101$ $\hat{\beta} = 0.00015$ $\hat{\theta} = 0.5264$	55.44962	116.8992	121.4783
Three-parameter generalized Lindley	$\hat{\alpha} = 1.0099$ $\hat{\beta} = 507.164$ $\hat{\lambda} = 0.5283$	55.44963	116.8993	121.4783
New weighted Lindley	$\hat{\alpha} = 29.2320$ $\hat{\lambda} = 0.8348$	55.97061	115.9412	118.9939

Figures 5 and 6 give the graphs of the estimated pdfs and cdfs respectively.

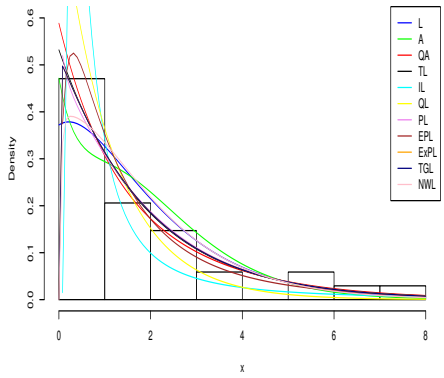

Figure 5. Estimated pdfs of the generalized Lindley distributions for the vinyl chloride data set

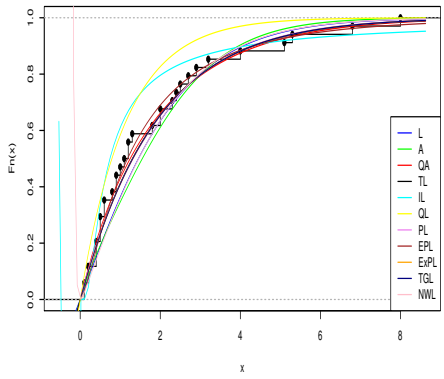

Figure 6. Estimated cdfs of the generalized Lindley distributions for the vinyl chloride data set

5.4. Fatigue fracture data set

The fatigue fracture data set is extracted from Abdul-Moniem and Seham [1], and it has previously been used by Andrews and Herzberg [11] and Barlow et al. [16]. It represents the life of fatigue fracture of Kevlar 373/epoxy subjected to constant pressure at 90% stress level until all had failed. The data are as follows:
{0.0251, 0.0886, 0.0891, 0.2501, 0.3113, 0.3451, 0.4763, 0.5650, 0.5671, 0.6566, 0.6748, 0.6751, 0.6753, 0.7696, 0.8375, 0.8391, 0.8425, 0.8645, 0.8851, 0.9113, 0.9120, 0.9836, 1.0483, 1.0596, 1.0773, 1.1733, 1.2570, 1.2766, 1.2985, 1.3211, 1.3503, 1.3551, 1.4595, 1.4880, 1.5728, 1.5733, 1.7083, 1.7263, 1.7460, 1.7630, 1.7746, 1.8275, 1.8375, 1.8503, 1.8808, 1.8878, 1.8881, 1.9316, 1.9558, 2.0048, 2.0408, 2.0903, 2.1093, 2.1330,

2.2100, 2.2460, 2.2878, 2.3203, 2.3470, 2.3513, 2.4951, 2.5260, 2.9911, 3.0256, 3.2678, 3.4045, 3.4846, 3.7433, 3.7455, 3.9143, 4.8073, 5.4005, 5.4435, 5.5295, 6.5541, 9.0960}
Table 4 gives the relevant numerical values for the fits of the distributions based on this data set.

Table 4. Estimated values, $-LogL$, AIC and BIC for the fatigue fracture data set

Distribution	Estimates	$-LogL$	AIC	BIC
Lindley	$\hat{\theta} = 0.7947$	123.6751	249.3503	251.681
Akash	$\hat{\theta} = 1.1324$	124.5755	251.151	253.4817
Quasi Akash	$\hat{\alpha} = 0.3095$ $\hat{\theta} = 1.3542$	122.4782	248.9563	253.6178
Two-parameter Lindley	$\hat{\alpha} = 0.1567$ $\hat{\theta} = 0.9544$	121.6503	247.3006	251.962
Inverse Lindley	$\hat{\theta} = 0.9459$	177.1091	356.2183	358.549
Quasi Lindley	$\hat{\alpha} = 0.1497$ $\hat{\theta} = 0.9543$	121.6503	247.3006	251.962
Power Lindley	$\hat{\beta} = 1.1423$ $\hat{\theta} = 0.7047$	122.4001	248.8001	253.4616
Exponentiated power Lindley	$\hat{\alpha} = 1.5372$ $\hat{\beta} = 0.9496$ $\hat{\theta} = 1.0213$	121.8663	249.7326	256.7248
Extended power Lindley	$\hat{\alpha} = 1.3256$ $\hat{\beta} = 0.00012$ $\hat{\theta} = 0.3666$	122.5247	251.0494	258.0416
Three-parameter generalized Lindley	$\hat{\alpha} = 0.9931$ $\hat{\beta} = 0.1478$ $\hat{\lambda} = 0.9634$	121.6487	249.2973	256.2895
New weighted Lindley	$\hat{\alpha} = 2.4729$ $\hat{\lambda} = 0.9090$	122.8925	249.7851	254.4465

Figures 7 and 8 give the graphs of the estimated pdfs and cdfs, respectively.

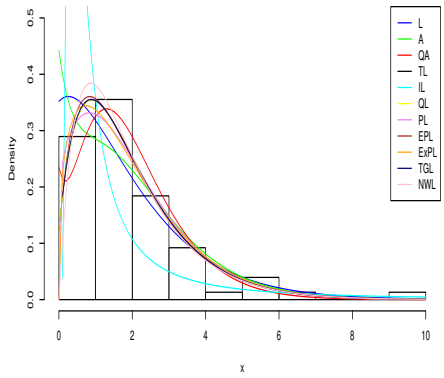

Figure 7. Estimated pdfs of the considered generalized Lindley distributions for the fatigue fracture data set

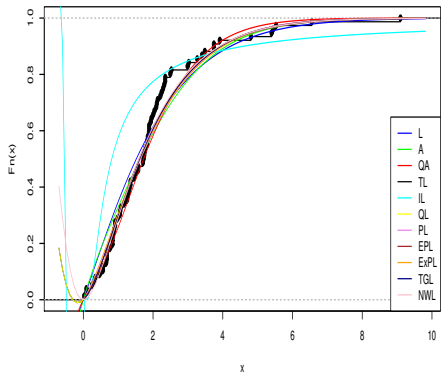

Figure 8. Estimated cdfs of the considered generalized Lindley distributions for the fatigue fracture data set

In Tables 1, 2, 3 and 4, the maximum likelihood estimates of the parameters for the fitted distributions along with the $-LogL$, AIC and BIC values are presented for the four different data sets. It is observed that the power Lindley distribution is appropriate for modeling carbon data, exponentiated power Lindley distribution is appropriate for modeling guinea pigs data, Lindley and quasi Akash distributions are appropriate for modeling vinyl chloride data, and quasi Lindley distribution is appropriate for modeling fatigue fracture data. These conclusions can also be drawn visually from Figures 1, 3, 5, and 7 for the estimated pdfs, and Figures 2, 4, 6 and 8 for the estimated cdfs.

In full generality, the Lindley distribution and its generalized versions are used for analyzing different types of data. In this regard, for circular type data, Joshi and

Jose [39] introduced the wrapped Lindley distribution, Chesneau et al. [26] studied the wrapped modified Lindley distribution, and Al-khazaleh and Alkhazaleh [5] suggested the wrapped quasi Lindley distribution. Zaninetti [67] applied Lindley and truncated Lindley distribution to model initial mass function in stars. This work also introduced the Lindley luminosity function and truncated Lindley luminosity function for galaxies. Similarly, Zaninetti [68] studied a three-parameter double truncated Lindley distribution and applied it to model initial mass function in stars. Therefore, we can say that the Lindley distribution and its generalizations have promising applications in Astrophysics.

6. Conclusion

In this article, we provide an overview on applications of the Lindley distribution and its generalizations. This review is based on applications in time series analysis, stress-strength analysis, ASP and various kinds of datas. Modeling of four real life data sets shows the suitability of the Lindley distribution and its generalizations for fitting real lifetime data. For researchers and practitioners, we hope that this review will give a summary of applications of the Lindley distribution and its generalizations as well as references for further study in the theory and applications of statistical distributions.

Appendix

Here, we provide the pdfs of the distributions, which are used in comparative study.

- Lindley distribution

$$f(x;\theta) = \frac{\theta^2}{1+\theta}(1+x)e^{-\theta x} \ ; \quad x > 0, \ \theta > 0$$

- Akash distribution

$$f(x,\theta) = \frac{\theta^3}{\theta^2+2}(1+x^2)e^{-\theta x} \ ; \ x > 0, \ \theta > 0$$

- Quasi Akash distribution

$$f(x;\alpha,\theta) = \frac{\theta^2}{\alpha\theta+2}(\alpha+\theta x^2)e^{-\theta x}; \ x > 0, \ \alpha > 0, \ \theta > 0$$

- Two-parameter Lindley distribution

$$f(x;\alpha,\theta) = \frac{\theta^2}{\alpha\theta+1}(\alpha+x)e^{-\theta x} \ ; \ x > 0, \ \theta > 0, \ \alpha\theta > -1$$

- Inverse Lindley distribution

$$f(x;\theta) = \frac{\theta^2}{1+\theta}\left(\frac{1+x}{x^3}\right)e^{-\frac{\theta}{x}} \ ; \ x > 0, \ \theta \ > 0$$

- Quasi Lindley distribution

$$f(x;\alpha,\theta) = \frac{\theta(\alpha+\theta x)}{\alpha+1}e^{-\theta x} \ ; \ x > 0, \alpha > -1, \ \theta > 0$$

- Power Lindley distribution

$$f(x;\alpha,\theta)=\frac{\alpha\theta^2}{\theta+1}(1+x^{\alpha})x^{\alpha-1}e^{-\theta x^{\alpha}}\ ;\ x>0,\ \alpha>0,\ \theta>0$$

- Exponentiated power Lindley distribution

$$f(x;\alpha,\beta,\theta)=\frac{\alpha\theta^2\beta x^{\beta-1}}{\theta+1}(1+x^{\beta})e^{-\theta x^{\beta}}\left[1-\left(1+\frac{\theta x^{\beta}}{\theta+1}\right)e^{-\theta x^{\beta}}\right]^{\alpha-1}$$
$$x>0,\ \alpha>0,\ \beta>0,\ \theta>0$$

- Extended power Lindley distribution

$$f(x;\alpha,\beta,\theta)=\frac{\alpha\theta^2}{\theta+\beta}(1+\beta x^{\alpha})x^{\alpha-1}e^{-\theta x^{\alpha}}\ ;\ x>0,\ \alpha>0,\ \beta>0,\ \theta>0$$

- Three-parameter generalized Lindley distribution

$$f(x;\alpha,\beta,\lambda)=\frac{\alpha\lambda^2(\beta+x^{\alpha})x^{\alpha-1}e^{-\lambda x^{\alpha}}}{1+\lambda\beta}\ ;\ x>0,\ \alpha>0,\ \beta>0,\ \lambda>0$$

- New weighted Lindley distribution

$$f(x;\alpha,\lambda)=\frac{\lambda^2(1+\alpha)^2}{\alpha\lambda(1+\alpha)+\alpha(2+\alpha)}(1+x)(1-e^{-\lambda\alpha x})e^{-\lambda x};\ x>0,\ \alpha>0,\ \lambda>0$$

Acknowledgements

The authors would like to express their gratitude to the reviewers for their detailed comments on our manuscript, which has helped to improve it in several ways.

References

[1] I. B. Abdul-Moniem and M. Seham, *Transmuted Gompertz distribution*, Computational and Applied Mathematics, 201), 1(3), 88–96.

[2] A. Z. Afify, M. Nassar, G. M. Cordeiro and D. Kumar , *The Weibull Marshall-Olkin Lindley distribution: properties and estimation*, Journal of Taibah University for Science, 2020, 14(1), 192–204.

[3] F. G. Akgul, K. Yu and B. Senoglu, *Estimation of the system reliability for generalized inverse Lindley distribution based on different sampling designs*, Communications in Statistics-Theory and Methods, 2020, 1–15.

[4] S. H. Alkarni, *Extended power Lindley distribution: a new statistical model or non-monotone survival data*, European Journal of statistics and probability, 2015, 3, 19–34.

[5] A. M. H. Al-khazaleh and S. Alkhazaleh, *On wrapping of quasi Lindley distribution*, Mathematics, 2019, 7(10), 930.

[6] D. K. Al-Mutairi, M. E. Ghitany and D. Kundu, *Inferences on stress-strength reliability from Lindley distributions*, Communications in Statistics-Theory and Methods, 2013, 42(8), 1443–1463.

[7] D. K. Al-Mutairi, M. E. Ghitany and D. Kundu, *Inferences on stress-strength reliability from weighted Lindley distributions*, Communications in Statistics-Theory and Methods, 2015, 44(19), 4096–4113.

[8] A. D. Al-Nasser, A. I. Al-Omari and F. S. Gogah, *A double acceptance sampling plan for quasi Lindley distribution*, Journal of the North for Basic and Applied Sciences, 2018, 3(2), 120–130.

[9] A. Al-Omari and A. D. Al-Nasser, *A two-parameter quasi Lindley distribution in acceptance sampling plans from truncated life tests*, Pakistan Journal of Statistics and Operation Research, 2019, 15, 39–47.

[10] M. A. Al-Osh and A. A. Alzaid, *First-order integer-valued autoregressive (INAR(1)) process*, Journal of Time Series Analysis, 1987, 8(3), 261–275.

[11] D. F. Andrews and A. M. Herzberg, *Data: a collection of problems from many fields for the student and research worker*, Springer Series in Statistics, New York, 1985.

[12] A. Asgharzadeh, H. S. Bakouch, S. Nadarajah and F. Sharafi, *A new weighted Lindley distribution with application*, Brazilian Journal of Probability and Statistics, 2016, 30(1), 1–27.

[13] S. K. Ashour and M. A. Eltehiwy, *Exponentiated power Lindley distribution*, Journal of Advanced Research, 2015, 6(6), 895–905.

[14] H. S. Bakouch, B. M. Al-Zahrani, A. A. Al-Shomrani, V. A. A. Marchi and F. Louzada, *An extended Lindley distribution*, Journal of the Korean Statistical Society, 2012, 41(1), 75–85.

[15] H. S. Bakouch and B. V. Popovic, *Lindley first-order autoregressive model with applications*, Communications in Statistics-Theory and Methods, 2016, 45(17), 4988–5006.

[16] R. E. Barlow, R. H. Toland and T. Freeman, *A Bayesian analysis of stress rupture life of Kevlar 49/epoxy sphere-cal pressure vessels*, in 'Proceeding Conference on Applications of Statistics', Marcel Dekker, New York, 1984.

[17] C. Bicer, *Statistical inference for geometric process with the power Lindley distribution*, Entropy, 2018, 20(10), 723.

[18] H. D. Bicer, *Statistical inference for geometric process with the two-parameter Lindley distribution*, Communications in Statistics-Simulation and Computation, 2019, 1–22.

[19] Z. W. Birnbaum, *On a use of the Mann-Whitney statistic. In: Proceedings of Third Berkeley Symposium on Mathematical Statistics and Probability*, University of California Press, Berkeley, 1956, 1, 13–17.

[20] Z. W. Birnbaum and R. C. Mc Carty, *A distribution-free upper confidence bound for* $\Pr\{Y < X\}$ *based on independent samples of* X *and* Y, The Annals of Mathematical Statistics, 1958, 29(2), 558–562.

[21] D. K. Bhaumik, K. Kapur and R. D. Gibbons, *Testing Parameters of a Gamma Distribution for Small Samples*, Technometrics, 2009, 51(3), 326–334.

[22] T. Bjerkedal, *Acquisition of resistance in guinea pigs infected with different doses of virulent tubercle bacilli*, American Journal of Epidemiology, 1960, 72(1), 130–148.

[23] C. Chesneau, L. Tomy and J. Gillariose, *On a sum and difference of two Lindley distributions: Theory and applications*, REVSTAT-Statistical journal, 2020, 18(5), 673–695.

[24] C. Chesneau, L. Tomy and J. Gillariose, *A new modified Lindley distribution with properties and applications*, Journal of Statistics and Management Systems, 2021, 1–21.

[25] C. Chesneau, L. Tomy, J. Gillariose and F. Jamal, *The inverted modified Lindley distribution*, Journal of Statistical Theory and Practice, 2020, 14(46), 1–17.

[26] C. Chesneau, L. Tomy and M. Jose, *Wrapped modified Lindley distribution*, Journal of Statistics and Management Systems, 2021, 1–16.

[27] C. Chesneau, H. M. Yousof, G. G. Hamedani and M. Ibrahim, *The Lindley-Lindley Distribution: Characterizations, Copula, Properties, Bayesian and Non-Bayesian Estimation*, International Journal of Mathematical Modelling & Computations, 2021 (to appear).

[28] G. M. Cordeiro, A. Z. Afify, H. M. Yousof, S. Cakmakyapan and G. Ozel, *The Lindley Weibull distribution: properties and applications*, Anais da Academia Brasileira de Ciencias, 2018, 90(3), 2579–2598.

[29] E. Deniz and E. Ojeda, *The discrete Lindley distribution: properties and application*, Journal of Statistical Computation and Simulation, 2011, 81(11), 1405–1416.

[30] S. Dey, I. Ghosh and D. Kumar, *Alpha-power transformed Lindley distribution: properties and associated inference with application to earthquake data*, Annals of Data Science, 2018, 6(4), 623–650.

[31] S. Dhanunjaya, P. A. Mohammed and G. Venkatesulu, *Continuous acceptance sampling plans for truncated Lindley distribution based on CUSUM schemes*, International Journal of Mathematics Trends and Technology, 2019, 65(7), 117–129.

[32] N. Ekhosuehi and F. Opone, *A three-parameter generalized Lindley distribution: properties and application*, Statistica, Department of Statistics, University of Bologna, 2018, 78(3), 233–249.

[33] M. E. Ghitany and D. K. Al-Mutairi, *Size-biased Poisson-Lindley distribution and its applications*, Metron-International Journal of Statistics, 2008, LXVI(3), 299–311.

[34] M. E. Ghitany, D. K. Al-Mutairi, N. Balakrishnan and L.J. Al-Enezi, *Power Lindley distribution and associated inference*, Computational Statistics and Data Analysis, 2013, 64, 20–33.

[35] M. E. Ghitany, D. K. Al-Mutairi and S. Nadarajah, *Zero-truncated Poisson-Lindley distribution and its applications*, Mathematics and Computers in Simulation, 2008b, 79(3), 279–287.

[36] M. E. Ghitany, F. Al-Qallaf, D. K. Al-Mutairi and H. A. Husain, *A two parameter weighted Lindley distribution and its applications to survival data*, Mathematics and Computers in Simulation], 2011, 81(6), 1190–1201.

[37] M. E. Ghitany, B. Atieh and S. Nadarajah, *Lindley distribution and its applications*, Mathematics and Computers in Simulation, 2008a, 78(4), 493–506.

[38] A. S. Hassan, M. Elgarhy, R. E. Mohamd and S. Alrajhi, *On the alpha power transformed power Lindley distribution*, Journal of Probability and Statistics, 2019, 1–13.

[39] S. Joshi and K. K. Jose, *Wrapped Lindley distribution*, Communications in Statistics-Theory and Methods, 2018, 47(5), 1013–1021.

[40] S. A. Kemaloglu and M. Yilmaz, *Transmuted two-parameter Lindley distribution*, Communications in Statistics-Theory and Methods, 2017, 46(23), 11866–11879.

[41] J. H. Khamnei, *Reliability for Lindley distribution with an outlier*, Bulletin of Mathematical Sciences and Applications, 2013, 2, 20–23.

[42] H. Krishna and K. Kumar, *Reliability estimation in Lindley distribution with progressively type II right censored sample*, Mathematics and Computers in Simulation, 2011, 82(2), 281–294.

[43] Y. Lam, *Geometric processes and replacement problem*, Acta Mathematicae Applicatae Sinica, 1988, 4, 366–377.

[44] T. Lvio, N. K. Mamode, M. Bourguignon and H. S. Bakouch, *An INAR(1) model with Poisson-Lindley innovations*, Economics Bulletin, AccessEcon, 2018, 38(3), 1505–1513.

[45] D. V. Lindley, *Fiducial distributions and Bayes theorem*, Journal of the Royal Statistical Society. Series B, 1958, 20, 102–107.

[46] G. Liyanage and M. Parai, *The generalized power Lindley distribution with its applications*, Asian Journal of Mathematics and Applications, 2014, 73, 331–359.

[47] R. Maya and M. R. Irshad, *New extended generalized Lindley distribution: Properties and applications*, Statistica, 2017, 77(1), 33–52.

[48] E. McKenzie, *Some simple models for discrete variate time series*, Water Resource Bulletin, 1985, 21(4), 645–650.

[49] F. Merovci, *Transmuted Lindley distribution*, International Journal of Open Problems in Computer Science and Mathematics, 2013, 238(1393), 1–20.

[50] M. Mohammadpour, H. S. Bakouch and M. Shirozhan, *Poisson-Lindley INAR(1) model with applications*, Brazilian Journal of Statistics, 2018, 32(2), 262–280.

[51] M. D. Nichols and W. J. Padgett, *A bootstrap control chart for Weibull percentiles*, Quality and Reliability Engineering International, 2006, 22(2), 141–151.

[52] A. Pak, A. K. Gupta and N. B. Khoolenjani, *On reliability in a multicomponent stress-strength model with power Lindley distribution*, Revista Colombiana de Estadistica, 2018, 41(2), 251–267.

[53] A. Rostami, E. Mahmoudi and R. Roozegar, *A new integer valued AR(1) process with Poisson-Lindley innovations*, 2018.
arXiv:1802.00994

[54] H. Reyad, M. Alizadeh, F. Jamal and S. Othman, *The Topp-Leone odd Lindley-G family of distributions: properties and applications*, Journal of Statistics and Management Systems, 2018, 21(7), 1273–1297.

[55] A. F. Sadek, M. M. El-Din and S. Elmeghawry, *Estimation of stress-strength reliability for quasi Lindley distribution*, Advances in Systems Science and Applications, 2018, 18(4), 39–51.

[56] M. Sankaran, *The discrete Poisson-Lindley distribution*, Biometrics, 1970, 26(1), 145–149.

[57] S. H. Shahbaz, K. Khan and M. Q. Shahbaz, *Acceptance sampling plans for finite and infinite lot size under power Lindley distribution*, Symmetry, 2018, 10.

[58] R. Shanker, *Akash distribution and its applications*, International Journal of Probability and Statistics, 2015, 4(3), 65–75.

[59] R. Shanker, *A quasi Akash distribution*, Assam Statistical Review, 2016a, 30(1), 135–160.

[60] R. Shanker, *The discrete Poisson-Akash distribution*, International Journal of Probability and Statistics, 2016b, 6(1), 1–10.

[61] R. Shanker and A. Mishra, *A two parameter Lindley distribution*, Statistics in Transition New Series, 2013a, 14(1), 45–56.

[62] R. Shanker and A. Mishra, *A quasi Lindley distribution*, African Journal of Mathematics and Computer Science Research, 2013b, 6(4), 64–71.

[63] R. Shanker and K. K. Shukla, *Weighted Akash distribution and its application to model lifetime data*, International Journal of Statistics, 2016, 39(2), 1138–1147.

[64] V. K. Sharma, S. K. Singh, U. Singh and F. Merovci, *The inverse Lindley distribution: a stress-strength reliability model with application to head and neck cancer data*, Journal of Industrial and Production Engineering, 2015, 32(3), 162—173.

[65] L. Tomy, *A retrospective study on Lindley distribution*, Biometrics and Biostatistics International Journal, 2018, 7(2), 163–169.

[66] U. P. Udoudo and E. H. Etuk, *A new extension of quasi Lindley distribution: Properties and applications*, International Journal of Advanced Statistics and Probability, 2019, 7.

[67] L. Zaninetti, *The truncated Lindley distribution with applications in Astrophysics*, Galaxies, 2019, 7(2), 61.

[68] L. Zaninetti, *New probability distributions in Astrophysics: II. The generalized and double truncated Lindley*, International Journal of Astronomy and Astrophysics, 2020, 10, 39–55.

Pramana – J. Phys. (2021) 95:174
https://doi.org/10.1007/s12043-021-02200-2

Study on the structural, optical and dielectric properties of lead tin sulphide nanocrystals

MAYA MATHEW[1] and K C PREETHA[1,2],*

[1]Department of Physics, Payyannur College, Kannur 670 327, India
[2]Sree Narayana College, Varkala, Thiruvananthapuram 695 141, India
*Corresponding author. E-mail: kcpreetha1990@gmail.com

MS received 19 April 2020; revised 12 May 2021; accepted 29 May 2021

Abstract. In this work, a study was done on the structural, optical and dielectric properties of lead tin sulphide (PbSnS) nanocrystals and their thin films, which have got wide range of applications in photovoltaic systems. The nanocrystals of PbSnS were prepared by employing colloidal synthesis technique in which cubic PbSnS were obtained apart from the commonly found orthorhombic form. Nanocrystals of 5.84 nm were obtained which had a high band gap of 3.76 eV and Urbach energy of 0.163 eV. Almost 100% transmittance in the wavelength range of 300–800 nm was found. Nanocrystal thin films of PbSnS were prepared using successive ionic layer adsorption and reaction (SILAR) technique. The preparation of thin film samples by varying the amounts of complexing agent has been investigated. By varying the amount of complexing agents, the crystalline phase changed from cubic to orthorhombic. The lattice strain and dislocation density were found to be lower for the cubic phase. All the samples had high absorption coefficient in the ultraviolet region confirming that the thin films were composed of nanocrystals. There was an increase in transmittance from 60% to 80% with the increase of complexing agent. All the samples had high band gap, high refractive index and large surface roughness which make these PbSnS nanocrystal thin films suitable materials for window layer of solar cells. The cubic and mixed phase structured thin films behaved as polar dielectrics which can find potential applications in the design of efficient capacitors too.

Keywords. Lead tin sulphide; quantum dots; thin films; triethanolamine; window layer; solar cells; polar dielectrics.

PACS Nos 84.60.Jt; 81.05.Hd; 81.15.–z; 78.20.Ci

1. Introduction

Intensive research is going on in the field of photovoltaics to replace the conventionally used silicon solar cells by cost-effective and efficient materials. Binary chalcogenides of copper and lead were studied in this direction. Much studies on PbS and SnS have been made for their photovoltaic properties [1,2]. Techniques such as successive ionic layer adsorption and reaction (SILAR) [3], pulsed laser deposition [6], feasible nebulizer spray technique [4] etc. were used for the synthesis of PbS thin films. Studies on the effect of triethanolamine (TEA) on the structural, morphological and electrical properties were made by Hone and Dejene where the amount of TEA used had direct relation with the material properties [5].

Recently, there have been studies on the doping of tin in lead sulphide to form ternary lead tin sulphide. Combinations of lead tin sulphide with binary lead tellurides are used as efficient thermoelectric materials [7,8]. Kane Norton *et al* used metal dithiocarbamate to produce bulk $Pb_{1-x}Sn_xS$ crystals and liquid phase exfoliation was done to get 2D layers of $Pb_{1-x}Sn_xS$ for important optoelectronic applications [9]. The electrical conductivity of vacuum-evaporated $PbSnS_3$ thin films seems to remain unaffected after doping with chlorides and iodides of cadmium, lead and copper. Conductivity values of 10^{-5} S cm^{-1} were obtained at room temperature which gradually increased at higher temperatures [10]. Annealing of thin films of orthorhombic $Pb_xSn_{1-x}S$ synthesised by hot wall vacuum deposition method was found to have lower lattice strain owing to the increase in crystallite size. Sulphur-deficient films showed p-type conductivity while sulphur-rich films showed n-type conductivity [11]. Nanocrystals

Published online: 16 October 2021

of $PbSnS_3$ in the size range of 3–12 nm were synthesised by mechanical alloying where the elemental precursor powders were mechanically alloyed for 40 h [12]. Thin films of orthorhombic $PbSnS_2$ prepared by spray pyrolysis technique were found to be polycrystalline and showed p-type conductivity [13]. Salem *et al* synthesised $PbSnS_3$ thin films using chemical bath deposition technique in which the films were amorphous which became crystalline orthorhombic upon annealing [14]. Cubic nanocrystals of $Pb_{2-x}Sn_xS_2$ were synthesised using hot injection colloidal synthesis method and the nanocrystals were of cubic NaCl type structure apart from the orthorhombic form [15].

The pH of the chemical bath is a determining factor for the formation of a particular crystal. It also determines the phase of the crystal structure formed [16,17]. This pH is contributed by several factors including the chemical precursors used, the complexing agents, capping agents etc. Complexing agent plays an important role in determining the phase of the crystal structure and there are a few works from literature to cite. The effect of triethanolamine in transforming the morphology of ZnO nanoparticles from the hexagonal nanorods was investigated in [18]. Ming Du *et al* studied the change in morphology of tin sulphide prepared by chemical bath deposition. The morphology changed from nanoflakes to continuous nanoflake films to solid nanospheres at low, medium and high concentration of triethanolamine [19]. Studies on photovoltaic properties of lead tin sulphide (PbSnS) are rare in literature [13]. Also a study on the effect of complexing agent on PbSnS nanocrystals has not been made so far and so this paper intends to analyse the photovoltaic properties of PbSnS and also the change of crystal structure using complexing agent. In the present work, we investigate the effect of the complexing agent, triethanolamine, in changing the phase of PbSnS nanocrystal thin films. We also describe an economic and simple synthesis technique for the preparation of PbSnS nanocrystals and their thin films.

2. Experimental

For the preparation of PbSnS nanocrystals, millimolar solutions of lead acetate ($Pb(COOCH_3)$), tin chloride ($SnCl_2$) and sodium sulphide (Na_2S) were used as the precursors. Triethanolamine (TEA) was used as the complexing agent and cetyl-trimethylammonium bromide (CTAB) was used as the capping agent. The precursors of lead and tin were mixed with constant stirring and CTAB was added to the mixture followed by the addition of sulphur source. The mixture was mixed well and the colour of the solution turned pale brown upon stirring. The solution so formed was decanted to remove the unreacted precursors and larger aggregates of the material. The solution containing nanocrystals of PbSnS was centrifuged multiple number of times to get a gel which was dried and then grinded well. The resultant powder was used for further characterisation. The sample was named ncPTS.

For the preparation of PTS thin films, 60 ml each of millimolar solutions of lead acetate ($Pb(COOCH_3)$), tin chloride ($SnCl_2$), sodium sulphide (Na_2S) and cetyltrimethylammonium bromide (CTAB) were taken separately in beakers alternated by beakers with distilled water. Well cleaned soda lime glass substrates were used for coating. The complexing agent, TEA, was added to each of the cation precursors. Good quality thin films of PbSnS were formed after 20 SILAR cycles. The dipping and rinsing time were set as 5 and 2 min respectively. Three sets of samples were prepared in which the amount of TEA was varied from 1 to 3 ml in steps of 1 ml and the samples were named as PTS1, PTS2 and PTS3.

Structural analyses of the thin film samples were made using Bruker AXS D8 Advance X-ray diffractometer having Cu K_α of wavelength 1.5406 Å. Optical studies were made by Cary 5000 UV-VIS-NIR spectrophotometer. Morphological and compositional analyses were done by a Scanning Electron Microscope of JEOL Model JSM-6390LV. The filament used was tungsten. The thickness of the thin films and other dielectric constants were determined using Variable Angle Spectroscopic Ellipsometric technique (VASE) of Woollen, USA.

3. Results and discussion

3.1 *Structural, optical and morphological analyses of PbSnS nanocrystals*

In general, doping of Sn in PbS crystals gives ternary PbSnS crystals which crystallise in orthorhombic phase. Cubic nanocrystals of rock salt crystal structure can be obtained with the modification of the experimental method used. The stoichiometry corresponding to this structure is $PbSnS_2$ [15]. The XRD pattern of our nanocrystals synthesised using colloidal technique has been found to match well with the cubic form of PbSnS nanocrystals as shown in figure 1. The structural parameters of PbSnS nanocrystals have been tabulated in table 1. The crystallite size is calculated using Scherrer formula (eq. (1)) [20], from the three major peaks corresponding to (111), (002) and (022) diffraction planes and its average value is calculated to be 5.84 nm. The

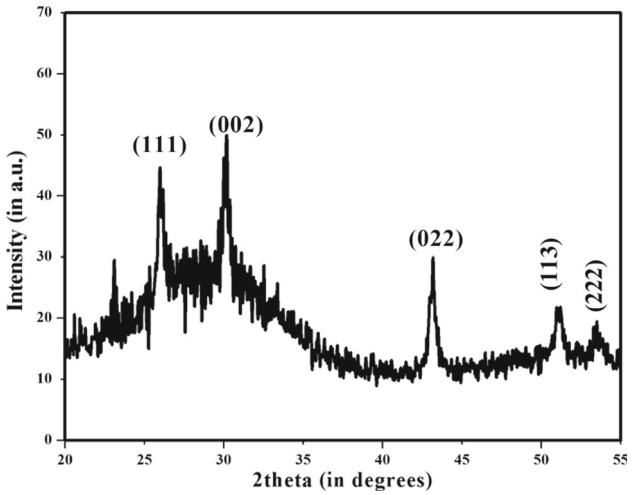

Figure 1. XRD pattern of ncPTS.

Scherrer formula for calculating the crystallite size is given by

$$D = \frac{K\lambda}{\beta \cos\theta}, \tag{1}$$

where K is a constant which is taken as 0.9, λ is the wavelength of X-ray used, β is the full-width at half-maximum in radians and θ is half of the diffraction angle. The calculated value of crystallite size is within the range of Bohr radius [12,15,21] and so the synthesised particles are nanocrystals. The lattice constant is calculated to be 5.93 Å from the formula for cubic crystals using the values of *hkl* and *d*-spacing (eq. (2)) [22] which is written as follows:

$$d = \frac{a}{\sqrt{h^2 + k^2 + l^2}}, \tag{2}$$

where d is the interplanar spacing, a is the lattice constant, h, k and l are the Miller indices. The lattice strain (ε) is calculated using eq. (3):

$$\varepsilon = \frac{\beta}{4\tan\theta}. \tag{3}$$

The dislocation density has been calculated using the formula [23]

$$\text{Dislocation density} = \frac{1}{D^2}, \tag{4}$$

where D is the crystallite size.

The absorption and transmittance spectra of PbSnS nanocrystals are shown in figure 2. The absorption spectrum indicates direct band-gap nature of the nanocrystals [15] with high absorption in the ultraviolet region. Being a nanocrystal, due to quantum size effect, two excitonic peaks are found. Since it is a direct band-gap semiconductor, the band gap (E_g) is found by drawing a tangent from the absorption edge to the x-axis and then converted the value to energy as follows:

$$E_g = \frac{hc}{\lambda} \tag{5}$$

where h is the Planck's constant, c is the velocity of light and λ is the wavelength indicated by the tangent. According to this, two wide band gaps of 3.76 eV and 4.88 eV were obtained, corresponding to 1Se–1Sh and 1Pe–1Ph transitions respectively. Band gaps can also be found from Tauc plots where tangents indicated from linear portions of $(\alpha h\nu)^2 - h\nu$ graphs are used to find the energy gap. Almost 100% constant transmittance has been found for these nanocrystals in the ultraviolet, visible and near infrared regions, particularly in the region 300–800 nm. Urbach energy is a measure of low crystallinity and disorder in the crystalline material. The Urbach plot for PbSnS nanocrystals is shown in figure 2c. The exponential part near the first excitonic peak in the low energy region was considered for the plot. The slope of the linear region gave Urbach energy of 0.163 eV. The equation for calculating Urbach energy is shown as follows:

$$\alpha = \alpha_0 \exp\left(\frac{h\nu}{E_U}\right), \tag{6a}$$

$$\ln\alpha = \ln\alpha_0 + \frac{h\nu}{E_U}, \tag{6b}$$

where α and α_0 are absorption coefficients, h is the Planck's constant, ν is the frequency of incident radiation and E_U is the Urbach energy. α_0 is the intercept and E_U^{-1} is the slope of the graph.

Scanning electron microscopy (SEM) images of PbSnS nanocrystals in powder form at two different magnifications of 645× and 1.4k× are shown in figure 3. As the nanocrystals are found to be agglomerated, the size of the particles cannot be determined from SEM images and rather particle morphology can be seen.

3.2 *Structural and optical analyses of PbSnS thin films*

The XRD patterns of PTS1, PTS2 and PTS3 are shown in figure 4. There has been a mixture of phases and also a change in phase of PbSnS crystals with the addition of TEA. In PTS1, the XRD pattern matched well with cubic PbSnS [15], with one peak due to the diffraction from (212) plane corresponding to orthorhombic $PbSnS_2$ (shown in asterisk). With further addition of TEA, in PTS2, two peaks from orthorhombic $PbSnS_2$ nanocrystals (JCPDS 14-618) have been observed corresponding to diffraction from (112) and (212) planes (shown in asterisk) while the rest of the diffractions are from cubic PbSnS. With the addition of greater amount

Table 1. Structural parameters of the PTS nanocrystals.

2θ (°)	*hkl*	FWHM	*D* (nm)	*d*-spacing (Å)	Lattice constant (*a*) (Å)	Lattice strain	Dislocation density (nm^{-2})
25.95	(111)	3.141	5.19	3.431	5.942	0.029	0.037
30.16	(002)	3.526	4.67	2.961	5.922	0.028	0.045
43.17	(022)	2.232	7.65	2.094	5.922	0.012	0.017

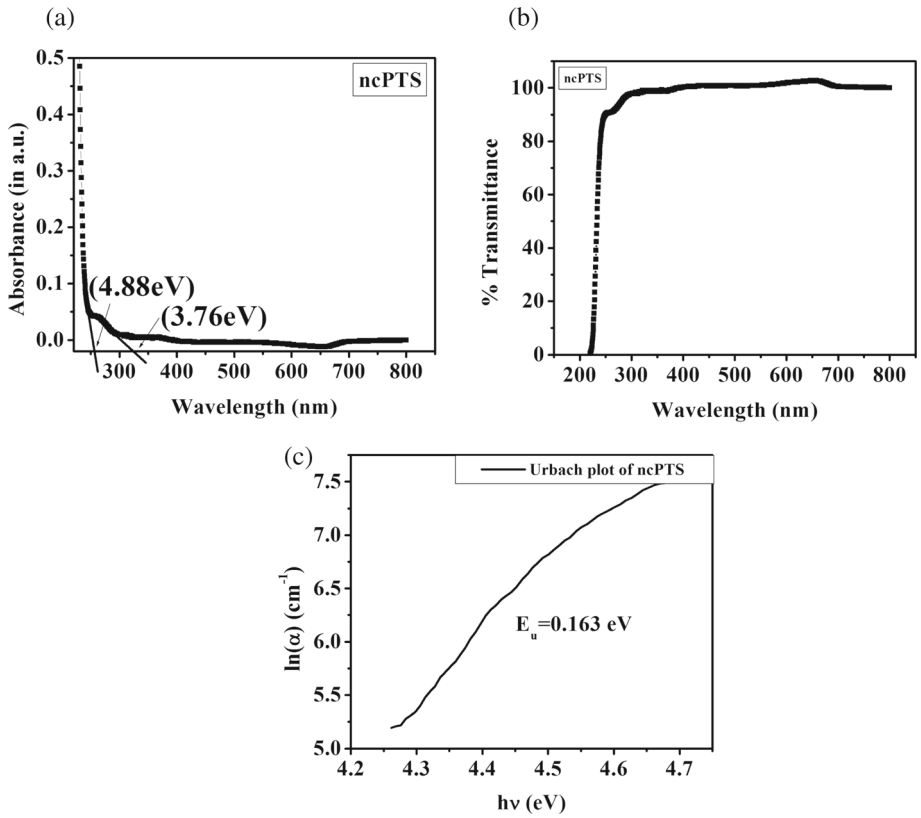

Figure 2. (**a**) Absorbance and (**b**) transmittance spectra of ncPTS. (**c**) Urbach plot for ncPTS.

of TEA, the phase of the PbSnS nanocrystals completely changed from cubic phase to purely orthorhombic phase as seen in the XRD pattern of PTS3. All the peaks matched well with the orthorhombic phase of $PbSnS_3$ nanocrystals [12]. The addition of TEA also affected the crystallinity of the thin film samples. Minimal use of TEA retained the crystallinity of the nanocrystals while use of additional amount of TEA decreased the crystallinity of the sample to a considerable extent. It is assumed that, with further addition of TEA, the samples might become amorphous.

The structural parameters of PTS1, PTS2 and PTS3 thin films are tabulated in table 2. The second set of diffraction angles are those of the orthorhombic phase. PTS1 has an average crystallite size of 44.5 nm, except for the (212) peak which belongs to the orthorhombic phase and has a higher value of crystallite size. Lattice strain is higher for the cubic phase than for the orthorhombic phase due to the smaller value of crystallite size for the former. The same is the case with the values for dislocation density. The crystallite size of PTS2 is lower than that of the cubic crystals, with an average value of 31.5 nm, as the increase in alkalinity of the reaction medium with the addition of TEA decreased the average particle size. However, the size of the cubic crystals in the mixed phase is lower than that of the orthorhombic ones. Consequently, the lattice strain is larger for the cubic crystallites than for the orthorhombic ones. In PTS3, the crystallite size is smaller (compared to PTS1) due to the increase in alkalinity of the reaction medium but the crystallinity of the sample has decreased much. As the size of the nanocrystals is less, the lattice strain is considerable in this sample and also dislocation density. The difference found in the values of crystallite size for PTS2 and PTS3 is probably due to the change in crystal structure. Generally speaking, the cubic form

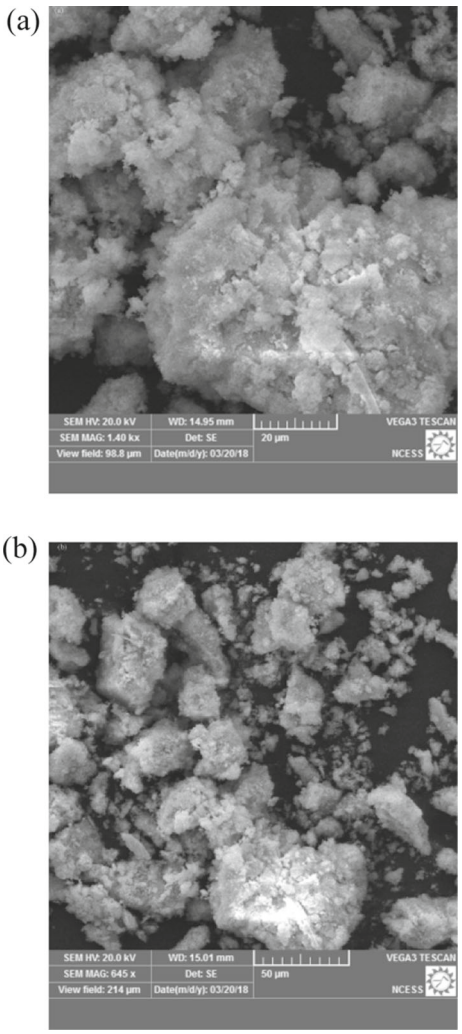

Figure 3. SEM images of ncPTS at magnifications of (**a**) 1.4k× and (**b**) 645×.

of PbSnS is more stable than the orthorhombic form, although the orthorhombic form is commonly found. A graph illustrating this general behaviour is plotted in figure 5.

The absorption spectra of PTS1, PTS2 and PTS3 are shown in figure 6a. PTS1 and PTS2 have absorptions in the ultraviolet and visible regions but the absorption of PTS3 is restricted in the ultraviolet region alone. Only the absorbing regions have changed with the addition of TEA while the absorbance remained almost the same in the three samples. The band gaps of the three samples are found from their absorbance plots which are shown in figure 7. All three samples have sharp absorptions indicating the presence of direct band gap for these materials. So the band gaps have been determined by drawing tangents to the x-axis and then finding their corresponding energies. Due to the formation of nanocrystals, there are multiple band gaps due to 1Se–1Sh and 1Pe–1Ph transitions and these are tabulated in table 3. Band gaps are lower for the cubic phase and still lower for the orthorhombic phase while the mixed phase is found to be of higher band gap. All the three samples are transmitting in the visible and near infrared regions as shown in figure 6b. The transmittance becomes higher and constant with the further addition of TEA.

The Urbach plots of the three samples were also plotted as shown in figure 8. The Urbach energies of the samples were determined from their slopes. For PTS1, the Urbach energy was found to be 0.648 eV while that of PTS2 was 0.778 eV and PTS3 was 0.343 eV. Since the Urbach energy is related to the disorder in the crystalline system, it can be concluded that PTS2 is comparatively more disordered than PTS1 and PTS3. Higher value of Urbach energy shows how disordered the crystalline system is. This finding agrees closely well with the lattice strain and dislocation density found for PTS2 in the XRD analysis. There is a slight discrepancy in the case of PTS1 and PTS3. This discrepancy arises because band tailing found in PTS3 is less than that in PTS1 leaing to the decrease in Urbach energy value for PTS3.

Thin film parameters such as film thickness, dispersion of dielectric constant and surface roughness can be determined with the help of an ellipsometric technique called variable angle spectroscopic ellipsometric (VASE) technique. The optical parameters are obtained by measuring the change in polarisation of the incident wave and also the phase change as it reflects off the sample surface. The fundamental relation used here is

$$\rho = \frac{R_p}{R_s} = \tan\Psi e^{i\Delta}, \tag{7}$$

where R_p and R_s are the intensities of the p and s components of the incident wave, p and s are the polarisation states of the incident wave, where p is the component parallel to the plane of incidence and s is the component perpendicular to the plane of incidence. The amplitude change upon reflection is tan Ψ and Δ is the phase shift. The thin film samples were analysed for optical parameters using VASE technique. The dependence of psi (Ψ) and delta (Δ) with wavelength is plotted in figure 9. The optical parameters obtained are tabulated in table 4. PTS1 with cubic phase is found to have larger film thickness while PTS2, with mixed phases of cubic and orthorhombic has lesser film thickness and then the film thickness increases for PTS3 which has purely orthorhombic phase. The band gap is related to the thin film thickness of the material as thinner films have smaller grains and thicker films have larger grains. So, PTS2 has higher band gap than PTS1 and PTS3. The thickness of the films can also be simultaneously related to the lattice strain experienced by the crystals.

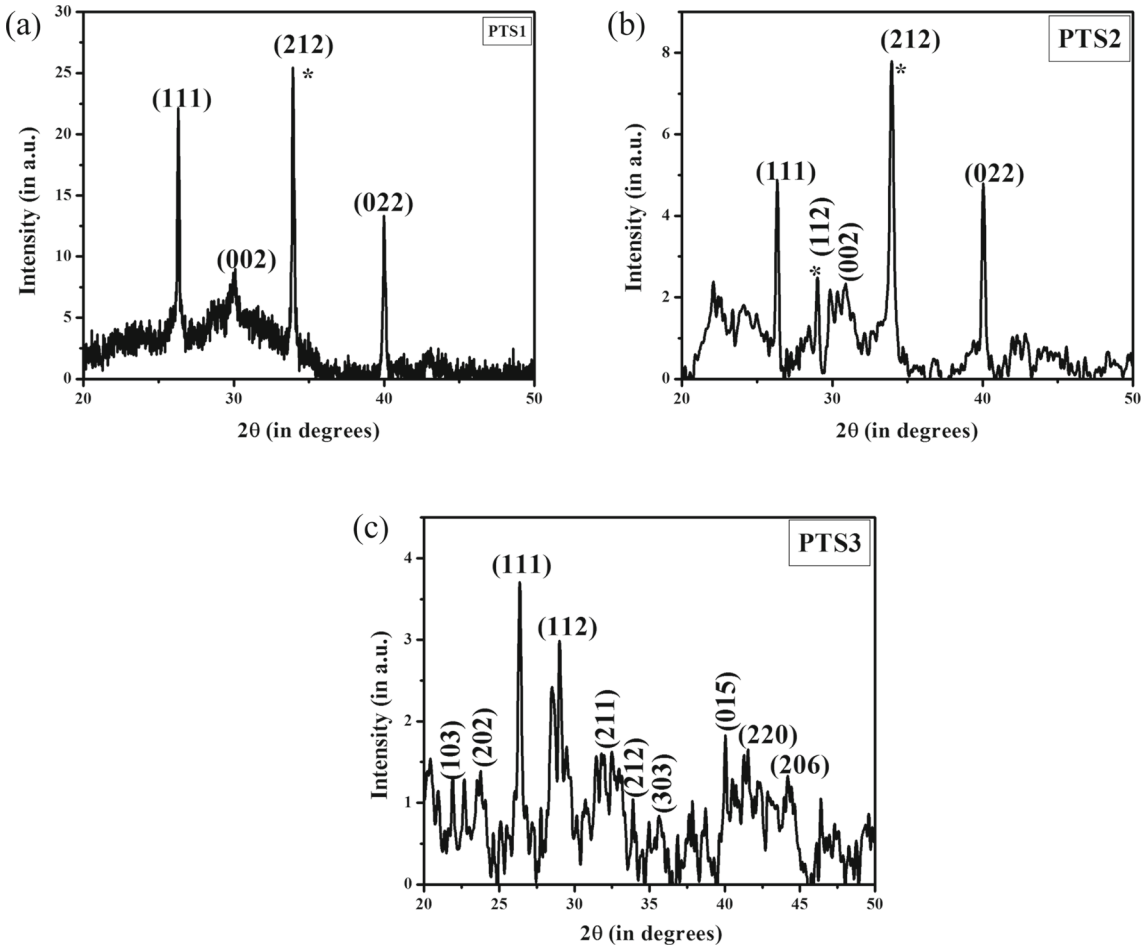

Figure 4. XRD spectra of (**a**) PTS1, (**b**) PTS2 and (**c**) PTS3.

The samples with larger film thickness such as PTS1 and PTS3 were found to have lower strain values than that for PTS2 which has lower film thickness. Surface roughness is found to be the least in the case of PTS3 while the other two samples have quite large surface roughness, probably due to the lack of secondary phases in PTS3.

At high frequencies, refractive index and permittivity are related as follows:

$$n = \frac{c}{v}, \tag{8a}$$

$$n = \sqrt{\frac{\mu\varepsilon}{\mu_0\varepsilon_0}}, \tag{8b}$$

where n is the refractive index, μ and μ_0 are the permeabilities of the material and vacuum respectively, ε and ε_0 are the permittivities of the medium and the free space respectively. Without considering the magnetic field effects, the equation for the refractive index can be rewritten as

$$n = \sqrt{\frac{\varepsilon}{\varepsilon_0}}, \tag{9a}$$

$$n = \sqrt{\kappa}, \tag{9b}$$

where κ is the dielectric constant which is the ratio of permittivities in the medium and in vacuum. Refractive index is higher for the mixed phase system of PTS2 while PTS3 has altogether different refractive index due to the difference in the atomic arrangements. Surface roughness has an important role to play in the absorption, scattering and reabsorption of incident light. PTS1 and PTS2 have higher surface roughness enabling reabsorption of incident light upon scattering from the uneven surfaces, thereby decreasing the amount of light lost due to surface reflection.

The plots of dielectric constant with wavelength for all the three samples are shown in figure 10. The wavelength dependence of both real ($e1$) and imaginary ($e2$) components are plotted separately. All the samples show

Table 2. Structural parameters of PTS1, PTS2 and PTS3.

Sample	2θ (°)	*hkl*	FWHM	D (nm)	d-spacing (Å)	Lattice constant (Å)	Lattice strain	Dislocation density (nm^{-2})
PTS1	26.3	(111)	0.183	44.526	3.386	5.865	0.0034	0.0005
	33.93	(212)	0.150	55.290	2.640		0.0021	0.0003
PTS2	26.32	(111)	0.259	31.500	3.383	5.860	0.0050	0.0001
	28.96	(112)	0.161	50.849	3.081		0.0027	0.0004
PTS3	26.3	(111)	0.216	37.778	3.386		0.0040	0.0007
						$a = 8.988, b = 3.814, c = 12.818$		

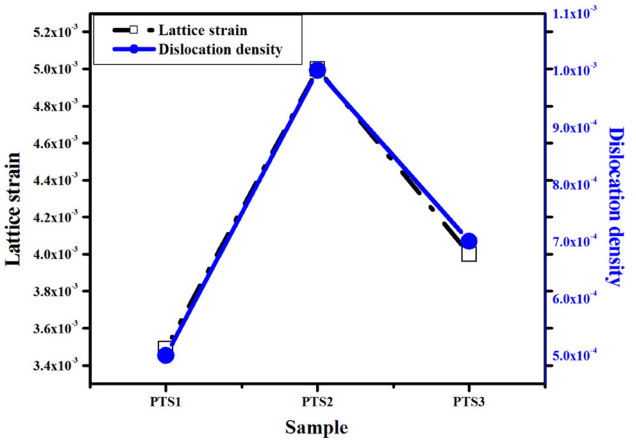

Figure 5. Graph comparing lattice strain and dislocation density of the three samples.

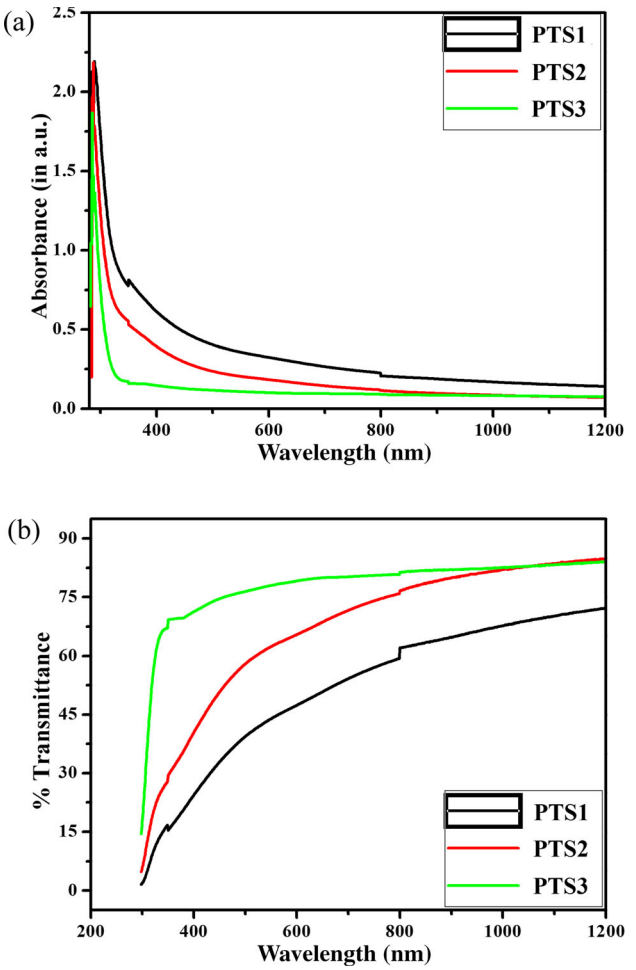

Figure 6. (**a**) Absorption spectra and (**b**) transmittance spectra of PTS quantum dot thin films.

dielectric dispersion. The variation for each of the sample is different due to their structural changes. The real part of the dielectric constant is directly related to the polarisability of the sample while the imaginary part is

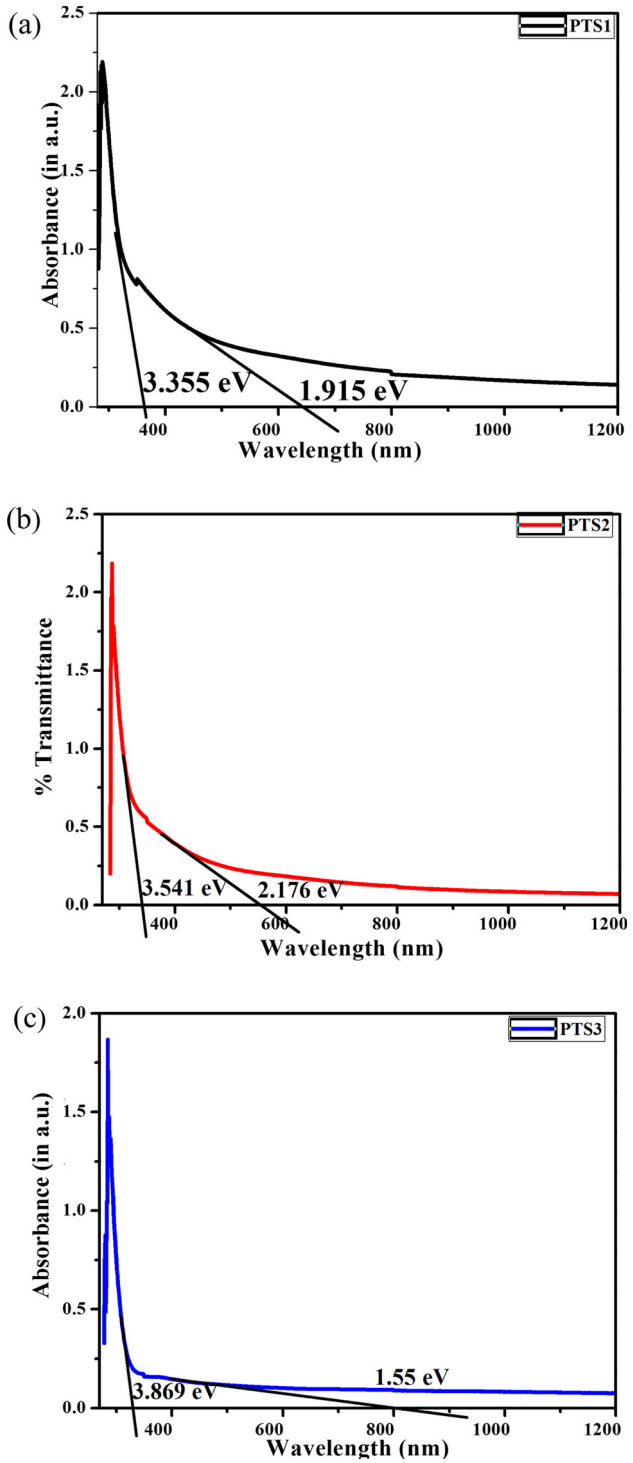

Figure 7. Band gaps of (**a**) PTS1, (**b**) PTS2 and (**c**) PTS3.

related to the dielectric loss or the amount of energy lost as heat. The samples show increase in polarisation with the increase in frequency of incident radiation which is a clear case of polar dielectrics. A semiconductor behaves as a polar dielectric when it consists of polar molecules whose centres of positive and negative charges do not coincide. Here the polar molecule which creates such an environment is the –OH group from TEA. The –OH group creates polarity within the film and with the application of electric field, the dipoles reorient themselves and give higher permittivity. PTS1, which has just 1 ml of TEA, behaves as a polar dielectric but at very high frequencies, due to higher dielectric loss (heating effect), the dipoles disorient themselves leading to a drop in permittivity values. PTS2, when there is higher concentration of TEA, behaves like a polar dielectric and drops off only at a very low wavelength of 400 nm. The case of PTS3 is quite different from the previous two cases because of the drastic change in crystal structure from cubic to orthorhombic. The lower value of permittivity is indicated by the lower value of refractive indices for PTS3. The dispersion of PTS3 has to be considered entirely different from the other two samples because PTS3 is purely orthorhombic in nature. Apart from the effect of –OH group from TEA, the lower refractive index of PTS3 is primarily due to lower thin film density. Considering mass and area of the thin films to be constant, the thickness of PTS3 thin film is greater (not considering PTS1 due to cubic structure), owing to orthorhombic structure formation, and so the density is lower for PTS3. Materials with lower density tend to have lower refractive indices. Similar relation between thickness of the film and the refractive index are found to be true for PTS1 and PTS2 also. However, the dielectric loss for PTS3 approaches zero at these frequencies.

Table 3. Band gaps of PTS samples.

Sample	Band gaps (eV) 1Se–1Sh transition	1Pe–1Ph transition
PTS1	1.915	3.355
PTS2	2.176	3.541
PTS3	1.55	3.869

4. Conclusion

Through this work, we have achieved the synthesis of nanocrystals and nanocrystal thin films of lead tin sulphide (PbSnS) by economic preparation techniques. An investigation on the effect of varying amount of complexing agent on the structural, optical and dielectric properties of PbSnS thin films has also been made. The nanocrystals of PbSnS were found to be cubic in nature while the nanocrystal thin films showed cubic, orthorhombic and mixed phases with the addition of complexing agent. With high band gap, high refractive index, high and constant transmittance (>80%) and high

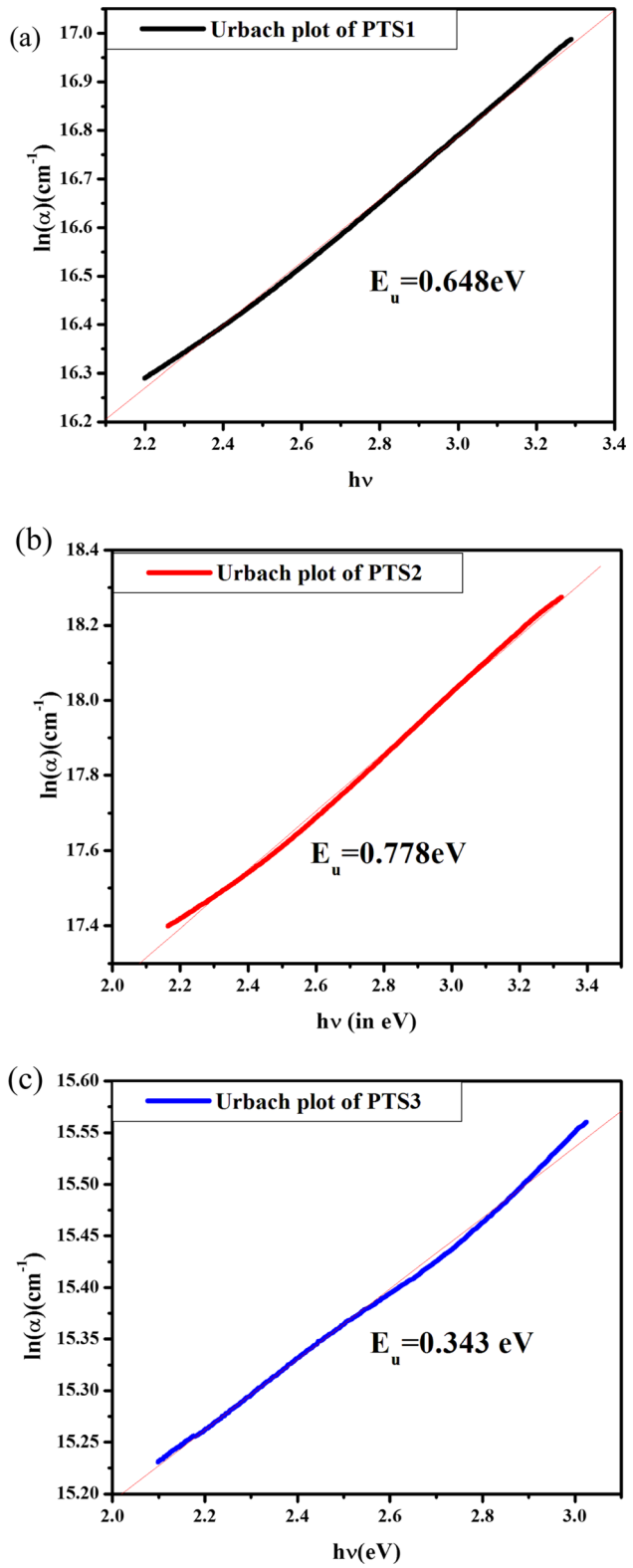

Figure 8. Urbach plots of (**a**) PTS1, (**b**) PTS2 and (**c**) PTS3.

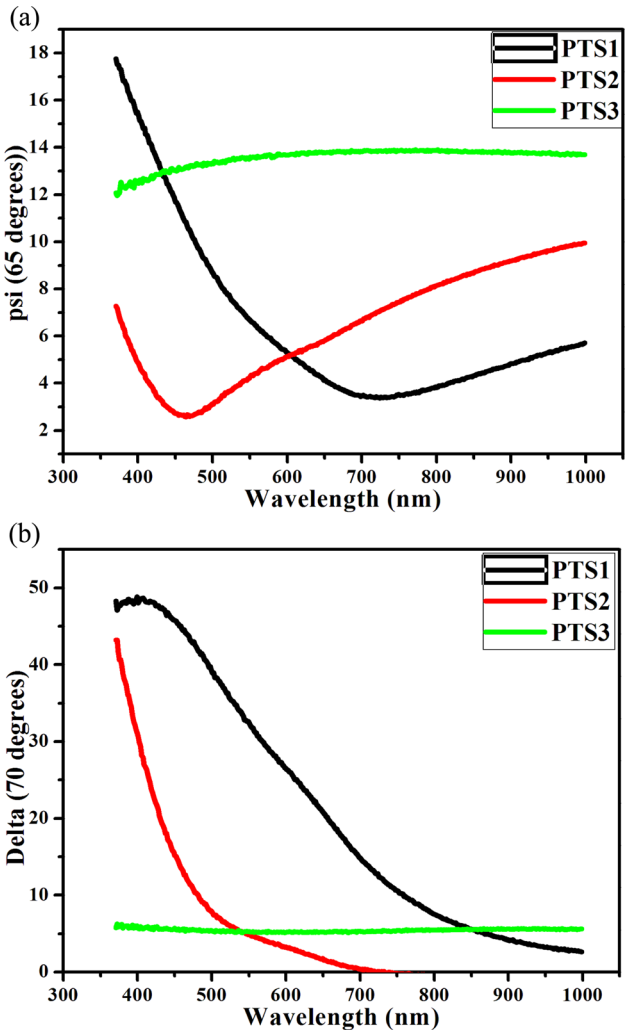

Figure 9. (**a**) Psi and (**b**) delta curves of PTS thin films at an incident angle of 70°.

Table 4. Optical parameters of PTS1, PTS2 and PTS3.

Sample	Thin film thickness (nm)	Surface roughness (nm)	Refractive index
PTS1	67.32	45.84	2.056
PTS2	12.45	50.00	2.439
PTS3	57.42	10.74	1.489

surface roughness (45–50 nm), these nanocrystals can be potentially used as good transmitters of incident radiation for the efficient absorption of light in solar cells.

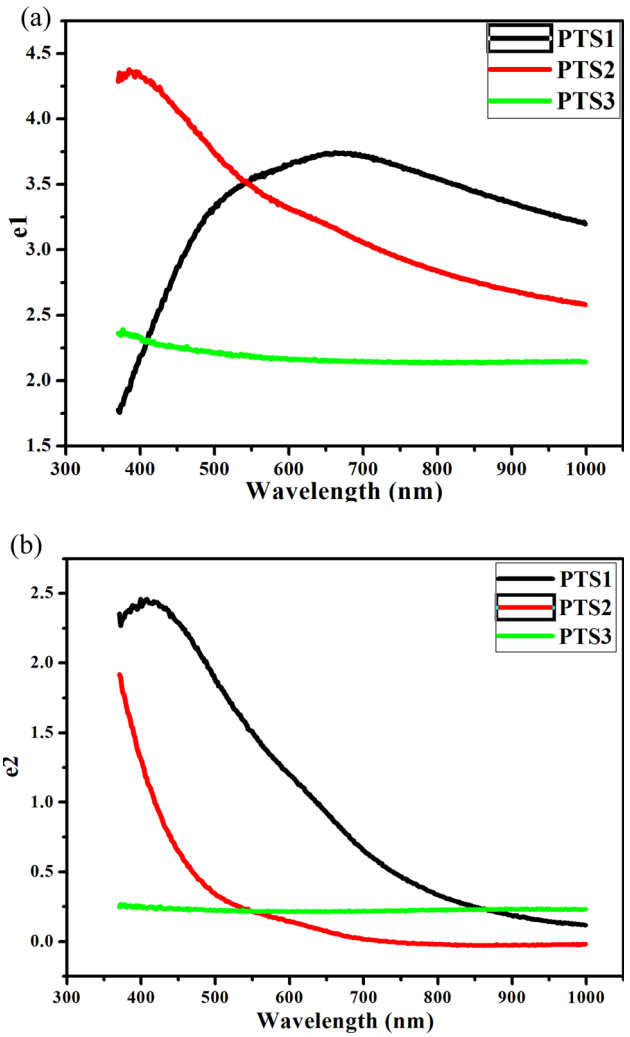

Figure 10. (**a**) $e1$ and (**b**) $e2$ of PTS thin films at an incident angle of 70°.

Acknowledgements

The authors thank STIC Cochin for the XRD and UV analyses, NCESS, Trivandrum for the SEM analysis and KUSICC, Kariavattom campus, Kerala University for the ellipsometric analyses. The authors also thank the University Grants Commission for the Junior Research Fellowship for the successful completion of this project.

References

[1] A J Ragina, K V Murali, K C Preetha, K Deepa and T L Remadevi. *J. Mater. Sci.: Mater. Electron.* **23**(**12**), 2264 (2012)
[2] K C Preetha and T L Remadevi, *J. Mater. Sci.: Mater. Electron.* **25**(**4**), 1783 (2014)
[3] C E Pérez-García, S Meraz-Dávila, G Arreola-Jardón, F de Moure-Flores, R Ramírez-Bon and Y V Vorobiev, *Mater. Res. Exp.* **7**(**1**), 015530 (2020)
[4] T V Beatriceveena, E Prabhu, V Jayaraman and K I Gnanasekar, *Mater. Lett.* **238**, 324 (2019)
[5] Rosario, S Rex, I Kulandaisamy, K Deva Arun Kumar, A M S Arulanantham, S Valanarasu, Maha A Youssef and Nasser S Awwad, *Physica B* **575**, 411704 (2019)
[6] Fekadu Gashaw Hone and Francis Birhanu Dejene, *Inorg. Chem. Commun.* **111**, 107583 (2020)
[7] Chrysoula Ioannidou, Christos B Lioutas, Nikolaos Frangis, Steven N Girard and Mercouri G Kanatzidis, *Chem. Mater.* **28**(**11**), 3771 (2016)
[8] Jian Zhang, Yang Ye, Chao Li, Jun Yang, Huiwen Zhao, Xiaoxuan Xu, Rong Huang, Lin Pan, Chunhua Lu and Yifeng Wang, *J. Alloys Compd* **696**, 1342 (2017)
[9] Kane Norton *et al*, *Chem. Sci.* **10**(**9**), 2843 (2019)
[10] T A Kuku, S O Azi and O Osasona, *J. Mater. Sci.* **41**(**4**), 1067 (2006)
[11] S A Bashkirov, V F Gremenok, V A Ivanov, K Bente, P P Gladyshev, T Yu Zelenyak, A M Saad and M S Tivanov, *Thin Solid Films* **616**, 773 (2016)
[12] Juan Fang, Debesh Devadutta Mishra, Weiquan Cai and Guolong Tan, *Mater. Sci. Semicond. Process.* **68**, 58 (2017)
[13] B Thangaraju and P Kaliannan, *J. Exp. Ind. Crystallogr.* **35**(**1**), 71 (2000)
[14] A M Salem and M O Abou-Helal, *Mater. Chem. Phys.* **80**(**3**), 740 (2003)
[15] Ronald B Soriano, Christos D Malliakas, Jinsong Wu and Mercouri G Kanatzidis, *J. Am. Chem. Soc.* **134**(**6**), 3228 (2012)
[16] Gul Amin, M H Asif, Ahmed Zainelabdin, Siama Zaman, Omer Nur and Magnus Willander, *J. Nanomater.* **96**, 2200 (2011)
[17] Fekadu Gashaw Hone and Francis Birhanu Dejene, *J. Mater. Res. Technol.* **8**(**1**), 467 (2019)
[18] Md Azimul Haque and S Mahalakshmi, *Mater. Focus* **2**(**6**), 469 (2013)
[19] Ming Du, Xuesong Yin and Hao Gong, *Mater. Lett.* **152**, 40 (2015)
[20] Chengzhi Ruan, Jiahua Tao, Chengyun Zhu and Chen Chen, *J. Mater. Sci.: Mater. Electron.* **29**(**15**), 12824 (2018)
[21] Hao Wei, Yanjie Su, Shangzhi Chen, Yang Lin, Zhi Yang, Huai Sun and Yafei Zhang, *CrystEngComm* **13**(**22**), 6628 (2011)
[22] Charles Kittel, Paul McEuen and Paul McEuen, *Introduction to solid state physics* (Wiley, New York, 1996) Vol. 8
[23] Jariya Rakspun, Nathakan Kantip, Veeramol Vailikhit, Supab Choopun and Auttasit Tubtimtae, *J. Phys. Chem. Solids* **115**, 103 (2018)

Covid-19 Pandemic – Revisiting Gandhi's Village Republic

Mary Philip

Assistant Professor, Department of Political Science
Carmel College, University of Calicut, Thrissur India

Abstract

With the world dreading the third wave of the Covid-19 pandemic, countries such as India, have a lot of rethinking and introspection to do before they decide on their strategy to handle the problems caused as a result of the outbreak of the pandemic. Just as some countries are able to cope with difficult times in a better way than so many others, similarly, some states are better equipped than others in arresting the disastrous effects of the same. A closer study of the system which is in place reveal that at least in case of states like Kerala, the functionality of Panchayati Raj system and the effective use of the locally available services, is the reason for the comparatively stronger resistance to the pandemic. Gandhian philosophy of independent and self-sufficient village republic seems to be the answer.

Keywords :- Gandhi, pandemic, self- sufficiency, village republic

Introduction

The countries of the world have often been faced with numerous challenging situations both at the national and international level. They have managed to find solutions either by themselves or with the help of others. However, the Covid-19 pandemic has left almost all the world leaders clueless about a durable solution to this crisis. The pandemic forced the people to remain indoors and to shut down all kind of activity and movement. The rat race for success had to be halted and spending time with family which seemed a rare possibility had now become the new normal. A sudden and changed lifestyle brought with it a host of other problems which were political, social and economic. The established patterns of life and work were altered completely. The result in many instances was the rethinking or revisiting of the past experiences. The prolonged lockdown of businesses and restriction of movement, compelled people to think of alternate ways to earn an income and sustain themselves. Such a situation set the backdrop for revisiting Gandhian ideology and principles that advocated the creation of independent and self-sufficient villages that showcased a balance of inputs and outputs.

Year 2021, the second consecutive year in which the Covid-19 pandemic has refused to die down. What seemed to be perhaps a matter of a few months, is now definitely here to stay

ISSN: 2349-0217

for a much longer time. The initial days and months were filled with fear and anxiety regarding the pandemic and the resulting lockdown. However, gradually the severity and the forced continuity of the quarantine began to seep into the individuals and systems. The first phase of the onset of the pandemic generated different reactions, from different sections of the masses. For some, it was unexpected family reunion where after a very long time family members got to sit and dine together. For some, it was like a festival bonus since they could continue to do their work online while being able to avoid the tiring travel to and from the work place. Children of working parents were overjoyed to have them by their side just like at the time of their birth. Happiness could be witnessed among certain sections of the society for more reason than one. However it cannot be over looked that there was another section of the society that was suddenly rendered jobless, homeless and futureless. The sudden influx of migrant labourers as part of the reverse migration and triggered by the notion that one will be safer in his or her native country or home town even if one had to make to do with limited amenities was witnessed in most parts of the world. A few more months into the pandemic, the fact that sitting at home also meant too many dependants and very little resources began to make people uncomfortable. Joblessness had become a problem not only in the distant work places, but also a pertinent problem in the immediate neighbourhood. Unemployment soon

proved to be the tip of the iceberg. The pandemic laid bare the fact that when struck by a problem such as this, we are in no way prepared to provide solutions. Shortage of food, accommodation and the ability of the health, educational and other facilities to make the necessary alterations and handle the situation proved to be unequipped. But very soon all came to the realisation that Gandhi's idea of decentralised economy and exploitation free equitable distribution of resources are the only answers to a system that has suddenly come to a standstill.

Let us try and analyse the different areas where Gandhi spoke of decentralisation;

Employment: The COVID-19 pandemic has triggered one of the worst job crises since the Great Depression. There is a real danger that the crisis will increase poverty and widen inequalities, with an impact that could be felt for years to come. Countries now need to do everything they can to stop this job crisis from turning into a social crisis. Reconstructing a better and more resilient labour market is an essential investment in the future and future generations. According to Gandhi, self-sufficiency was the only permanent solution to problems of unemployment, under employment, etc. He was in favour of indigenous cottage and small scale industries simply because they are capital saving and labour using. When forced to sit at home during lockdown, with few or no savings in hand, a large

ISSN: 2349-0217

number of families were able to survive by adopting small, yet innovative and indigenous ways of earning income through activities as diverse as cooking to entertainment videos, music and dance class and so on. Perhaps for the first time, each and every individual had started thinking of ways to contribute to the income and savings irrespective of their age. In fact knowingly or unknowingly a division of labour began to be followed, sometimes irrespective of the gender differences.

Education: Though the shift from offline education to online education was marked by a few hiccups in the beginning, the free access to numerous online sources of information has made the comparatively tech savvy generation free to explore the cyber space. The freedom could be quite liberating and at the same time very dangerous too. Previously, e-learning, distance education and correspondence courses were popularly considered as the part of non-formal education, but as of now, it seems that it would gradually replace the formal education system if the circumstances enduringly persist over time. The education ecosystem of India, already weighed down by myriad issues such as school dropouts, learning deficiencies, teacher absenteeism, gender disparity and lack of infrastructure, now faces yet another big challenge-the widening digital divide. The situation is simple and complicated at the same time in different parts of the country. For the younger generations, whether they

ISSN: 2349-0217

like it or not, they are living through the process of education either in the presence of their parents or grandparents or their siblings. Parents and children had to go through a structural re-adjustment in order to accept and accommodate the other in their otherwise personal affair. After a long time both parties are forced to communicate with each other so as to avoid any calls or corrective actions from the educational institutions. Here again, Gandhi's emphasis on the role and importance of family and society on the education and upbringing of a child can be recollected. In many families pandemic brought together joint-family structure where parents went back to the jobs either online or offline and children were entrusted with their siblings, grand parents or other guardians.

Healthcare: The state government's prompt response to COVID-19 can be attributed to its experience and investment made in emergency preparedness and outbreak response in the past during Kerala floods in 2018 and especially, the NIPAH outbreak in 2019. The state used innovative approaches and its experience in disaster management planning came in handy to quickly deploy resources and put up a timely and comprehensive response in collaboration with key stakeholders. Active surveillance, setting up of district control rooms for monitoring; capacity-building of frontline health workers, risk communication and strong community engagement, and

addressing the psychosocial needs of the vulnerable population are some of the key strategic interventions implemented by the state government that kept the disease in control.Globally, health systems have been challenged by the overwhelming demands of the COVID-19 pandemic. Resources and staff are being diverted to test and provide treatment for people with presumed or diagnosed COVID-19, and supplies are limited. Some healthcare services are being compromised in order to meet the demands of caring for COVID-19 patients, and many people fear accessing healthcare facilities due to fear of acquiring the virus. The pandemic situation brought the focus on the healthcare system of the state. The chain of primary health care centres, government and private hospitals, labs and specialised institutions and agencies were very much in place to cater to the affected patients and also to monitor those in quarantine. The services of the doctor and specialist would have gone in vain if the Asha workers, nurses, ambulance drivers and other staff in the health sector had not worked round the clock to contain the virus. The registration and distribution of vaccines is also being handled efficiently by the system. Clusters and high TPRs and deaths sometimes dampen our efforts. But an effective and always responsive system of administration had earned appreciation worldwide. Gandhi was a strong advocate of investment in healthcare sector and as far as the state is

concerned. The state is reaping the benefits of the timely investment in the sector to a great extent.

State Ownership of Means of Production and Distribution: The 'Kit' made available to the households through the public distribution system is considered by many as one of the most important reasons why the present government was able to make history by being elected for the second term. The essentials that reached the households were able to feed a large population that would have otherwise suffered due to absence of income. After a long time many people began to venture out into their backyard, farms and kitchen gardens and sowing seeds and saplings for daily use and medicinal plants that were being recommended as very effective in curing and preventing the spread of Covid 19.

Localisation and Indigenisation: This is another important aspect of Gandhi's idea of development and progress. He was of the opinion that the village and the country should be able to identify its needs, the available talents and resources and develop technology with a purpose. According to him the right type of technology creates more jobs (Covid-19 acted as a catalyst in India's quest for self-sufficiency. India, though for a short period was able to provide leadership in containing the spread of the disease, export of vaccine, etc.)An awareness campaign 'Break the Chain' was successful in promoting the

ISSN: 2349-0217

importance of hand hygiene, physical distancing and cough etiquette. Hand washing stations were installed in strategic locations, including exit and entry points of railway stations etc. to instill a behaviour change. The Kerala Arogyam portal was launched by the Department of Health and Family Welfare with comprehensive information on COVID-19. CovidJagratha portal and Directorate of Health Services website was launched by the Department of Health and Family Welfare with comprehensive information on COVID-19.The high literacy rate in the state and the empowered women self-help groups - Kudumbashree helped the cause in a big way. Kudumbashree formed close to 1.9 lakh WhatsApp groups with 22 lakh neighbourhood groups (NHGs) to educate on key safety measures as advocated by the government during lockdown.Community Kitchen initiative through the Local Self Government Department (LSGD) with the support of Kudumbasree has provided more than 8 651 627 free meals to the labourers, those who are in quarantine, isolation, destitutes and other needy persons. Distribution of millions of cooked meals and provision of free ration under the Public Distribution Scheme to those in need is reflective of a well-thought and a caring response and relief strategy.

All kinds of programmes and assistance being announced and provided by the government and all the other individuals,

organisations and institutions were able to yield the desired results only because of the selfless services of the numerous local self-governing bodies and the PHCs, Asha workers and an army of government officials, NGOs, volunteers, etc. who worked in tandem. The most important aspect of the control of the pandemic was the timely identification, reporting, isolation and treatment and monitoring of not only the affected people but also of the possible carriers too. It is a noteworthy feature that in spite of the heavy population and density of population, the state was able to maintain low death rates, avoid hunger deaths, provide adequate health care facilities not only to the natives but also to a large number of migrant labourers who chose to continue to stay back in the state in spite of the high degree of reverse migration witnessed in different parts of the country. In short, the reason why the state has been ableto hold on in these testing times, is because we have kept alive to a great extend the basic tenets of a village economy or the Gandhian idea of self - sufficiency through our local self- governing bodies. No doubt, there is still a lot to be done. Yet the right path is gradually unfolding before us. We need to strengthen our government mechanisms and also identify the organs that are inefficient or non-performing.

Conclusion

Two years on since the country's first positive case of Novel Coronavirus Disease (COVID-19) was reported in

ISSN: 2349-0217

Kerala, the state with over a population of 35 million, has reported an impressive recovery rate. The leadership helmed a robust response to the novel coronavirus disease very early, following the news of outbreak in China in January 2020.The enabling environment owing to the high literacy rate in the state and high-level political and administrative commitment provided the much-needed impetus in the fight against this pandemic. When the entire country was struggling to hide the frightening and fast increasing death rates, Kerala was able to keep those numbers under control. A major role was played by the decentralised mode of functioning of the government mechanisms that allowed the proper flow of information and resources. The Kerala model has once again proved to be the best available answer to the present crisis. Being rooted in Mahatma Gandhi's vision of self-sufficient villages,it can be seen as a model that could be followed by other nations of the world without falling into any kind of debt-trap which comes as a result of the help that they seek from other nations.

References:-

1. Chadha,.Y. (1997) Rediscovering Gandhi, London: entury.
2. Gandhi, M. K. (1977) The Collected Works, Ahmadabad: Navajivan.
3. Gandhi, M. K. (1997) Hind Swaraj and Other Writings, Cambridge: Cambridge University Press.

4. Kumar Ajit (1991): A Holistic Study of Rural Energy Systems, PhD Thesis, IIT Delhi.

5. Kumar, K. (1994) 'Mohandas Karamchand Gandhi' in Z. Morsy (ed.) Thinkers on Education Volume 2, Paris: UNESCO.

6. Markovits, Claude. (2004). TheUngandhian Gandhi, New Delhi.

7. Nehru (1958). A Bunch of Old Letters

8. Nehru, J (1994). The Discovery of India, Delhi.

9. Nature 591, S15 (2021)

Sciencia Acta Xaveriana
An International Science Journal
ISSN. 0976-1152

Vol. 13 No. 1
pp. 45-51
March 2022

NUMERICAL TAXONOMY STUDIES IN SOME SPECIES OF GENUS CROTALARIA FROM KERALA & TAMILNADU AND SELECTION OF AN APPROPRIATE CP-DNA REGION FOR DERIVING PHYLOGENY BY COMPARING RBCL and TRNL-F IGS SEQUENCES FROM NCBI GENBANK.

Sheersha P [1], Joelri Michael Raj L[1], Leon Stephan Raj T[1], and Kochuthressia K P[2]

[1] Department of Botany, St. Xavier's College, (Autonomous), Palayamkottai, Tamilnadu, India.

[1]Carmel College, Mala, Thrissur 680732, Kerala, India.

Received : Jan 2022 *Accepted : March 2022*

Abstract. Numerical analysis on 48 morphological characters of seven accessions collected from a part of Malabar region of Kerala and south Tamilnadu belonging to the genus *Crotalaria* was done by calculating Jaccards similarity coefficient, UPGMA dendrogram based on the similarity values and PCO analysis. The phenetic study brought out many interesting characters for discrimination of the species like Reddish brown stripes under the keel petals and trifoliate leaves. A Comparative analysis of rbcL and trnL-F intergenic spacer regions in the genus *Crotalaria* was done by retrieving sequences from the NCBI gen bank database. The analysis was performed using MEGA 7.0 which revealed only 5 parsimony informative sites for rbcL gene, whereas 156 parsimony informative sites for trnL-F IGS showing its discriminative power to be better than rbcL gene at intrageneric level for this genus. The study suggests the potential of trnL-F IGS in deriving phylogeny of the genus *Crotalaria*.

1. INTRODUCTION

Crotalaria is a genus of flowering plants in the legume family Leguminosae (sub family papilionoideae). The sub family includes approximately 478 genera and 13,800 species grouped in 28 tribes. The genus Crotalaria L. is the third largest genus of Papilionoideae. Crotalarieae (Benth.) Hutch. is a tribe of legumes that currently comprises 11 genera and ca. 1204 species [15]. According to [1, 2, 10, 16, 17] *Crotalaria* is the largest Fabaceae genus in India with 92 species. A detailed description of 42 species that occurs in China is also reported [5].

Numerical analysis of 58 morphological characters of 12 accessions belonging to *Crotalaria* has revealed potential characters and phylogeny in some species of *Crotalaria* from Carnatic regions and Palni hills [8]. The present phenetic study had also picked out phylogenetically important characters for species identification within the genus especially from parts of Tirunelveli (South Tamilnadu) and Kerala and had also posed a resolved phylogenetic tree of evolutionary significance.

2. MATERIALS AND METHODS

The present investigation aims at the determination of the taxonomic relationship by using numerical analysis of seven taxa at interspecific (infrageneric) levels. The phenetic study presented in this thesis is a study covering seven species of *Crotalaria* from Malabar region of Kerala and Tirunelveli district of Tamilnadu. (Table -1, Plate -1). Coding of results is done based on Multistate coding. 7 OTUs were scored for 48 characters, out of which 26 are qualitative characters and 22 are quantitative characters. The choice of characters was taken and modified from a phenetic study on the same genus from parts of Palni hills and Carnatic regions of Tamilnadu [8]. The data were analysed using MVSP 3.1 (Multi Variate Statstical Package) for calculating Jaccards similarity coefficient and UPGMA dendrogram based on the similarity values. Squared Euclidean distances were calculated and PCO analysis was done based on the Euclidean distances. The selection of an appropriate cpDNA gene was done by doing a comparative study of ten randomly picked sequences of Ribulose Bis-Phosphate Carboxylase gene (rbcL) region and the intergenic spacer between the trnL (UAA) 3 exon and the trnF (GAA) gene (trnL-F intergenic spacer) region of the genus *Crotalaria* from NCBI genbank database. The sequences retrieved from the genbank were analysed using MEGA 7.0.

3. RESULTS AND DISCUSSION

3.1. **Phenetic Study on Crotalaria:** The Multistate coding was done for 26 qualitative characters and 22 quantitative characters based on the field observations. The dendrogram was first generated from Cluster Analysis of both qualitative datasets using Jaccards similarity coefficient and UPGMA. The dendrogram clustered the six species C. *juncea*, C.*retusa*, C. *nummularia*, C.*verrucosa*, C. *incana* and C. *pallida*, whereas C. *laburnifolia* was singled out. The dendrogram from qualitative characters alone was not able to resolve the relationships in *Crotalaria* species studies. So, twenty-two quantitative characters were added to the analyses and a dendrogram was generated. (Figure 8). This dendrogram was able to separate the seven species in to two major clusters. Cluster I contained C.*nummularia*, C.*retusa*, C. *juncea* and C.*verrucosa* where C. *juncea*, C.*retusa* and C.*verrucosa* formed a Sub - Cluster IA within *Cluster* I. C.*pallida* and C. *incana* formed a separate group as Cluster II. C. *laburnifolia* was singled out showing it as a highly divergent species.

The dendrogram has clearly distinguished the seven species based on the geographical variations, where C. *juncea*, C. retusa and C.*verrucosa* occurs normally in plains, but rarely some of

their wild varieties are found at higher altitudes with some phenotypic plasticity. C. *pallida* and C. *incana* are mostly found in distinct geographical areas [11, 12]. Another important morphological character that is similar to C. pallida & C. incana is reddish stripes under the keel petals and moreover both are trifoliate varieties [2]. So, both these characters can be considered as evolutionarily important characters [11, 12]. However, C. *laburnifolia* is also a trifoliate species but it is singled out separately. This means a single character cannot be used to segregate the species and only collection of characters can give a resolved phylogenetic relationship and that is where the phenetic study done here in this thesis proves its utility, since it is done for nearly 48 characters since it is known that more characters taken for study, the more resolved is our phylogeny based on numerical taxonomic studies [9].

The Similarity matrix based on UPGMA, Jaccard's Coefficient analysing 48 variables (26 Qualitative & 22 Quantitative Characters) is presented in Table 2. The maximum similarity value 0.991 was observed between C.*juncea* & C. *verrucosa*. A similarity value 0.977 was observed C. *retusa* and C. *juncea*. Interesting feature is C.*juncea*, C. *verrucosa* and C. *retusa* are simple leaf varieties. Similarly, C. pallida and C. *incana* has a closer similarity matrix of 0.957 and are trifoliate varieties. This gives some information about closely related species and the presence of simple or compound leaf as a phylogenetically important character. However, C. *laburnifolia* a trifoliate variety was found to be very distinct and was singled out. This shows that the species has an exclusive genetic makeup.

The overall Shannons diversity index generated by 48 morphological markers for seven species is 1.78 indicating high diversity. Among the 48 characters seed number had the highest diversity index of 1.934 showing that it is a character of phylogenetic significance. The Principal Coordinate Analysis (PCoA) grouped C. *nummularia*, C.*retusa* and C. *juncea* where all the three are simple leafed varieties. So again, Simple leaf and compound leaf finds its importance in revealing phylogenetic relationships [16].

3.2. **Comparative analysis of rbcL and trnL-F IGS regions:** Selection of gene for Angiosperm taxonomy is very essential and hence a suitable gene was chosen based on sequence analysis of already submitted sequences in the genus *Crotalaria* from the NCBI gen bank database. The CLUSTAL W alignment using MEGA 7.0 for ten rbcL sequences revealed 413/ 420 conserved sites, 7/ 420 variable sites and 5 parsimony informative sites, whereas the CLUSTAL W alignments for ten trnL-F intergenic spacer regions showed 208/400 conserved sites, 189/400 variable sites and 156 parsimony informative sites which is very promising to differentiate species at infrageneric level.

Estimates of Evolutionary Divergence between Sequences were conducted using the Maximum Composite Likelihood model. The analysis involved ten rbcL nucleotide sequences where all positions containing gaps and missing data were eliminated. There was a total of 420 positions in the final dataset. The average distance observed in the distance matrix is 0.007. The same was observed for trnL-F intergenic spacer sequences for ten nucleotide sequences. There were a total of 311 positions in the final dataset. The average distance observed in the distance matrix is 0. 453. (Table 3). Thus trnL-F intergenic spacer showed a better diversity than rbcL

sequences [7]. Moreover, rbcL is a genic region where the evolution rate is very less when compared to intergenic spacer region. So trnL-F intergenic spacer was selected based on the analysis as a better region to resolve the phylogeny at intrageneric level in the genus *Crotalaria* - Leguminosae [14]. The combined study of morphology and sequences will result in deriving a meaningful phylogeny[4].

4. SUMMARY AND CONCLUSION

The Phenetic study using the combination of 26 qualitative characters and 22 quantitative characters gave a resolved dendrogram, rather than using only qualitative characters. The cluster diagrams and similarity values have identified closely related species, where simple leaf varieties like C.juncea, C. verrucosa C. retusa and C. nummularia were found to be very closely related with high similarity index. Similarly, trifoliate varieties like C. pallida and C. incana were separately clustered. C. laburnifolia was singled out in the dendrogram showing it as a distinct species. The study has also picked out some phylogenetically important characters like simple/compound leaves, Reddish brown stripes under the keel petal, Seed number and many other qualitative and quantitative characters for differentiating Crotalaria sp. Selection of gene by analysing ten randomly picked rbcL sequences and trnL-F sequences have revealed trnL-F intergenic spacer region as a good target to differentiate Crotalaria sp. where trnL-F intergenic spacer region showed 156 parsimony informative sites. The study has revealed evolutionarily relevant taxonomic characters for studying Crotalaria sp. and also has brought out the importance trnL-F intergenic spacer region in deriving phylogeny in the genus Crotalaria. This study opens the way to further explore the phylogeny in this genus by collecting more species and the combined analysis of morphology and sequences would bring out new evolutionarily important characters in this genus and propose a revised taxonomic key based on phylogenetically important characters in future.

Fig – 1 *Crotalaria pallida*

Fig – 2 *Crotalaria incana*

Fig – 3 *Crotalaria verrucosa*

Fig – 4 *Crotalaria nummularia*

Fig – 5 *Crotalaria laburnifolia*

Fig – 6 *Crotalaria retusa*

Fig – 7 *Crotalaria juncea*

Note: a - Habit.; b - Leaf.; c - Inflorescenc

Table 1: List of Species in the genus Crotalaria taken for study (Refer Plate 1)

S. No	Botanical Name	Latitude	Longitude	Location and Altitude
1	C.pallida	11.8697281	75.6037985	Ayithara, Kerala 32m
2	C.incana	11.8792075	75.5807954	Neerveli, Kerala 27m
3	C.verrucosa	9.0497453	77.4694801	Vellalankulam, Tamil Nadu 145m
4	C.nummularia	8.6716	77.7382	Reddiarpatti, Tirunelveli 58m
5	C.laburnifolia	9.0497453	77.4694801	Vellalankulam, Tamil Nadu 145m
6	C.retusa	11.8860997	75.592	Kanhileri, Kerala 62m
7	C.juncea	8.7500101	77.7578319	Keezhanatham,RC street, Tirunelveli 42m

Table 2: Similarity matrix based on UPGMA, Jaccard's Coefficient analysing 48 variables (26 Qualitative and 22 Quantitative Characters)

	C.pallida	C.incana	C.verrucosa	C.nummularia	C.laburnifolia	C.retusa	C.juncea
C.pallida	1						
C.incana	0.956	1					
C.verrucosa	0.872	0.87	1				
C.nummularia	0.872	0.87	0.955	1			
C.laburnifolia	0.894	0.851	0.851	0.851	1		
C.retusa	0.894	0.891	0.977	0.977	0.872	1	
C.juncea	0.872	0.87	0.991	0.955	0.851	0.977	1

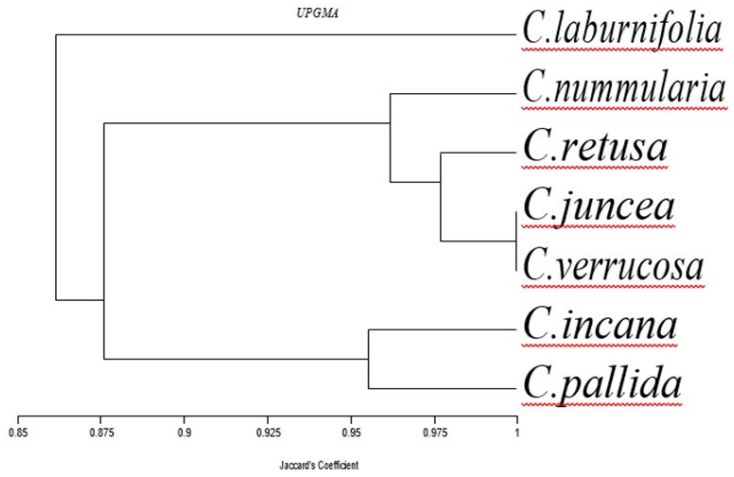

Figure 8: Dendrogram based on 26 qualitative characters and 22 quantitative (48Characters) using Jaccard's Coefficient

Table 3: Distance Matrix for 10 trnL-F intergenic sequences of genus Crotalaria retrieved from NCBI genbank generated by MEGA7.0

KP691136.1_Crotalaria_pallida_var._obovata_voucher_S.Sub_A.K.Pan_1048									
KP691135.1_Crotalaria_pallida_voucher_ S.Sub_A.K.Pan _1010a	0.000								
KP691126.1_Crotalaria_verrucosa_voucher_ S.Sub_A.K.Pan _1009b	0.030	0.030							
KP691093.1_Crotalaria_retusa_voucher_ S.Sub_A.K.Pan _1005	0.043	0.043	0.020						
HM996999.1_Crotalaria_verrucosa_voucher_RHT56074	0.802	0.802	0.816	0.848					
JF304312.1_Crotalaria_juncea_voucher_RHT56079	0.799	0.799	0.812	0.845	0.020				
HM997000.1_Crotalaria_retusa_voucher_RHT56075	0.814	0.814	0.828	0.861	0.020	0.020			
HM996998.1_Crotalaria_pallida_var._obovata_voucher_RHT56073	0.828	0.828	0.831	0.873	0.037	0.050	0.043		
KP691124.1_Crotalaria_verrucosa_voucher_ S.Sub_A.K.Pan _1014b	0.033	0.033	0.003	0.023	0.804	0.801	0.816	0.819	
KP691137.1_Crotalaria_incana_voucher S.Sub_A.K.Pan _1008	0.016	0.016	0.033	0.047	0.830	0.826	0.842	0.856	0.036

Table. Estimates of Evolutionary Divergence between Sequences. The number of base substitutions per site from between sequences are shown. Analyses were conducted using the

Maximum Composite Likelihood model[16]. The analysis involved 10 nucleotide sequences. All positions containing gaps and missing data were eliminated. Overall distance d = 0.453 There were a total of 311 positions in the final dataset. Evolutionary analyses were conducted in MEGA7 [17].

REFERENCES

[1] Ansari AA. (2002) Taxonomic studies on the genus Crotalaria L. in India I. In: Rao RR, Chowdhary HJ, eds. Advances in Legume Research in India. Dehra Dun: Bishan Singh Mahendra Pal Singh, 157-167

[2] Ansari, A.A., (2006). Taxonomic studies on the genus Crotalaria L. in India II Infragenetic classification J. Econ.Taxon.Bot, 30 (3): 570 582.

[3] Ansari, A.A. (2008). Crotalaria L. in India. Dehra-Dunn: Bishen Singh Mahendra Pal Singh.

[4] Boatwright, J.S., Le Roux, M.M., Wink, M., Morozova, T. and Van Wyk, B.-E. (2008). Phylogenetic relationships of tribe Crotalarieae (Fabaceae) inferred from DNA sequences and morphology. Systematic Botany 33: 752761.

[5] Jianqiang, L., Sun, H., Polhill, R.M. and Gilbert, M.G. (2010). Crotalarieae: Crotalaria. In: Z.Y. Wu, P.H. Raven, D.Y. Hong (ed), Flora of China 10 (Fabaceae). Beijin: Science Press and St. Louis: Missouri Botanical Garden Press, pp.105-117.

[6] Kumar S., Stecher G., and Tamura K. (2016). MEGA7: Molecular Evolutionary Genetics Analysis version 7.0 for bigger datasets.Molecular Biology and Evolution 33:1870-1874.

[7] Pierre Taberlet , Eric Coissac, Franois Pompanon, Ludovic Gielly, Christian Miquel, Alice Valentini, Thierry Vermat, Grard Corthier, Christian Brochmann, Eske Willerslev (2010).Power and limitations of the chloroplast trnL (UAA) intron for plant DNA barcoding. Nucleic Acids Res. 2007 Feb; 35(3): e14.

[8] Raj L.J.M., John Britto S., Prabhu S., & Senthilkumar S.R. (2011). Identification of agronomically valuable species of Crotalaria based on phenetics: Agric. Biol. J. N. Am, 2(5): 840-847

[9] Rohlf, F.J. (1990). Morphometrics. Ann. Rev. Ecol. Syst. 21: 299-316.

[10] Sibichen M.T. and S. Nampy , 2007. Crotalaria kurisumalayana Sibichen & Nampy(Fabaceae), a new species from India. Condollea, 62: 105-108.

[11] Subramanian, S (2013). Taxonomy and phylogeny of the genus Crotalaria (Fabaceae): An Overview. Acta Biologica Indica, 2(1) 253-264.

[12] Subramanian S, Arun K. Pandey, R. Geeta and Mark E. Mort (2013). Molecular systematics of Indian Crotalaria (Fabaceae) based on analyses of nuclear ribosomal ITS DNA sequences.. Plant Systematics and Evolution 299(6):1089-1106

[13] Tamura K., Nei M., and Kumar S. (2004). Prospects for inferring very large phylogenies by using the neighbor-joining method. Proceedings of the National Academy of Sciences (USA) 101:11030-11035.

[14] Tomoyuki Nemotoa, Jun Yokoyamab , Tatsuya Fukudac , Yu Iokawad and Hiroyoshi Ohashi (2010). Phylogeny of Lespedeza (Leguminosae) Based on Chloroplast trnL-trnF Sequences. J. Jpn. Bot. 85: 213229 (2010).

[15] Van Wyk, B.-E., Venter, M.& Boatwright, J.S. (2010). A revision of the genus Bolusia (Fabaceae, Crotalarieae). South African Journal of Botany 76: 8694.

[16] Wojciechowski, M. F. (2003). Reconstructing the phylogeny of legumes (Leguminosae): an early 21st century perspective. Advances in Legume Systematics, part 10, higher level systematics (B. B. Klitgaard and A. Bruneau, eds.). Royal Botanic Gardens, Kew, UK. Pages 5- 35

[17] Wojciechowski M. F., Lavin M., and Sanderson M. J. (2004). A phylogeny of legumes (Leguminosae) based on analysis of the plastid matK gene resolves many well-supported subclades within the family. American J. Botany 91: 1846-186

Journal of Mathematical Extension
Journal Pre-proof
ISSN: 1735-8299
URL: http://www.ijmex.com

Power Modified Lindley Distribution: Theory and Applications

C. Chesneau*
Université de Caen

L. Tomy
Deva Matha College, Kuravilangad

M. Jose
Carmel College Mala, Thrissur

Abstract. The power version of the modified Lindley distribution is introduced in this paper, offering a new two-parameter lifetime distribution. As a main interest, it provides a motivated alternative to the Weibull and power Lindley distributions. We discuss its main characteristics and properties, including shapes of the probability density and hazard rate functions, incomplete moments, crude moments, variance, skewness, kurtosis and order statistics. Then, a statistical study of the model is developed. The parameters are estimated by the maximum likelihood method. A simulation study examines the numerical comportment of the bias and mean square error of the maximum likelihood estimates of the parameters. Application of the new model to three data sets is presented, showing that the model has a better fit behavior in comparison to some other well-known lifetime models, including the Weibull and power Lindley models.

AMS Subject Classification: 60E05; 62E15; 62F10
Keywords and Phrases: Lindley distribution, Power Lindley distribution, Moments, Maximum likelihood estimation, Data analysis

Received: September 2020; Accepted: June 2021
*Corresponding Author

1 Introduction

The Lindley distribution pioneered by [24] has received a lot of attention during the last decades. Its primary characterization is the cumulative density function (cdf), which is defined as

$$G(x;\theta) = 1 - \left[1 + \frac{\theta x}{1+\theta}\right] e^{-\theta x}, \quad x > 0, \tag{1}$$

where $\theta > 0$, and $G(x;\theta) = 0$ for $x \leq 0$. The Lindley distribution is considered as a mixture of exponential distribution (with parameter θ) and gamma distribution (with shape parameter 2 and rate parameter θ). [17] have conducted a detailed study of various properties and applications of the Lindley distribution in reliability analysis. It was discovered that it may provide a better fit than the exponential distribution, among the most important facts.

Because of having only one parameter, there are some situations where the Lindley distribution does not provide enough flexibility for analyzing different types of lifetime data. Many researchers have proposed modified or generalized forms of the one-parameter Lindley distribution to address this issue. Some of these modifications or generalizations are the discrete Poisson-Lindley distribution by [28], zero-truncated Poisson-Lindley distribution by [18], size-biased Poisson-Lindley distribution by [16], negative binomial Lindley distribution by [36], two-parameter weighted Lindley distribution by [19], two-parameter Lindley distribution by [31], quasi Lindley distribution by [32], inverse Lindley distribution by [34], gamma Lindley distribution by [37], transmuted Lindley distribution by [26], extended Lindley distribution by [8], Akash distribution by [29], quasi Akash distribution by [30], weighted Akash distribution by [33], three-parameter generalized Lindley distribution by [15], new weighted Lindley distribution by [7], wrapped modified Lindley distribution by [14], Weibull Marshall-Olkin Lindley distribution by [2], inverted modified Lindley distribution by [12], and sum and difference of two Lindley distributions by [13]. In addition, [35] provided a review study on the Lindley distribution and its generalizations.

In particular, a generalization of the Lindley distribution, called power Lindley (PL) distribution, introduced by [20] aims to apply the

power function x^α in the cdf given as (1) in order to increase its overall flexibility. Thus, the considered cdf is defined by

$$G(x;\alpha,\theta) = G(x^\alpha;\theta) = 1 - \left[1 + \frac{\theta x^\alpha}{1+\theta}\right] e^{-\theta x^\alpha}, \quad x > 0, \tag{2}$$

with $\alpha > 0$, and $G(x;\alpha,\theta) = 0$ for $x \leq 0$. This cdf is such that, if X denotes a random variable following the Lindley distribution, then $X^{1/\alpha}$ follows the PL distribution. The probability density function (pdf) of the PL distribution is a two-component mixture of a Weibull distribution (with shape parameter α and rate parameter θ), and a generalized gamma distribution (with shape parameter 2α and rate parameter θ). Then, it is shown in [20] that the parameter α can have an important role in the pliant properties of some crucial functions, such as the corresponding pdf and hazard rate function (hrf). The PL distribution has been studied and generalized by many authors in recent years. The developments include the generalized power Lindley distribution by [25], exponentiated power Lindley distribution by [6], extended power Lindley distribution by [3], alpha power transformed power Lindley distribution by [21] and exponentiated generalized power Lindley distribution by [27].

On the other hand, a weighted modification of the former Lindley distribution, called the modified Lindley (ML) distribution, has been proposed by [11]. It is defined by the following cdf:

$$F(x;\theta) = 1 - \left[1 + \frac{\theta x}{1+\theta} e^{-\theta x}\right] e^{-\theta x}, \qquad x > 0,$$

with $\theta > 0$, and $F(x;\theta) = 0$ for $x \leq 0$. In some sense, in comparison to the former Lindley distribution, the polynomial function x in the bracket is weighted by the one-parameter exponential function $e^{-\theta x}$ in such a way that (i) the definition of the cdf remains manageable and (ii) the following stochastic ordering holds: $G(x;\theta) \leq F(x;\theta) \leq H(x;\theta)$, where $G(x;\theta)$ and $H(x;\theta)$ are the cdfs of the Lindley and exponential distributions with parameter θ, respectively. Thus, it provides a motivated alternative to the Lindley and exponential distributions, keeping only one parameter and an overall simplicity. In [11], the fitting behavior of the ML model is illustrated by the consideration of three popular real data sets, outperforming the Lindley and exponential models in this regard.

In this study, as the PL distribution is for the Lindley distribution, we propose a new generalization of the ML distribution by the use of the one-parameter power function x^α; we consider the cdf given as $F(x;\alpha,\theta) = F(x^\alpha;\theta)$. The corresponding distribution is called the power modified Lindley (PML) distribution. That is, if X denotes a random variable following the ML distribution, then $X^{1/\alpha}$ follows the PML distribution. We thus defined a new two-parameter lifetime distribution satisfying the following desirable stochastic ordering property: $G(x;\alpha,\theta) \leq F(x;\alpha,\theta) \leq H(x;\alpha,\theta)$, where $G(x;\alpha,\theta)$ and $H(x;\alpha,\theta)$ are the cdfs of the PL and Weibull distributions with parameters α and θ, respectively. In this way, we develop an intermediate model between the Weibull and PL models, both well known for their relevance in data fitting. As a first objective, we describe the main properties of the PML distribution, with an emphasis on the moments. Then, the inferential properties of the related model are examined by the use of the maximum likelihood method. Application is provided to three real data sets, showing that it can be more suitable to fit data in comparison to the former Weibull, PL, exponentiated power Lindley and three-parameter generalized Lindley models.

We organize the rest of the paper as follows. Sect. 2 completes the presentation of the PML distribution by expressing some functions of interest. Sect. 3 is devoted to some of its important properties. The inferential aspect of the PML distribution is discussed in Sect. 4, with a simulation study and application of the associated model to three real data sets. Some conclusions are drawn in Sect. 5.

2 Power Modified Lindley Distribution

The fundamentals of the PML distribution are now presented, beginning with the main related functions of interest.

2.1 Functions of interest

First, we recall that the PML distribution is specified by the following cdf:

$$F(x;\alpha,\theta) = 1 - \left[1 + \frac{\theta x^{\alpha}}{1+\theta} e^{-\theta x^{\alpha}}\right] e^{-\theta x^{\alpha}}, \quad x > 0, \tag{3}$$

with $\alpha > 0$ and $\theta > 0$, and $F(x;\alpha,\theta) = 0$ for $x \leq 0$. It is constructed by the composition of the cdf of the former ML distribution and the power function x^{α}. The expression of the survival function immediately follows:

$$S(x;\alpha,\theta) = 1 - F(x;\alpha,\theta) = \left[1 + \frac{\theta x^{\alpha}}{1+\theta} e^{-\theta x^{\alpha}}\right] e^{-\theta x^{\alpha}}, \qquad x > 0, \tag{4}$$

and $S(x;\alpha,\theta) = 1$ for $x \leq 0$. Also, upon differentiation of $F(x;\alpha,\theta)$ with respect to the variable x, the corresponding pdf is given by

$$f(x;\alpha,\theta) = \frac{\theta\alpha}{1+\theta} x^{\alpha-1} e^{-2\theta x^{\alpha}} \left[(1+\theta) e^{\theta x^{\alpha}} + 2\theta x^{\alpha} - 1\right], \quad x > 0, \tag{5}$$

and $f(x;\alpha,\theta) = 0$ for $x \leq 0$. The corresponding hrf is given as

$$h(x;\alpha,\theta) = \frac{f(x;\alpha,\theta)}{S(x;\alpha,\theta)} = \alpha\theta x^{\alpha-1} \left[\frac{\theta x^{\alpha} - 1}{(1+\theta) e^{\theta x^{\alpha}} + \theta x^{\alpha}} + 1\right], \quad x > 0, \tag{6}$$

and $h(x;\alpha,\theta) = 0$ for $x \leq 0$. The functions $F(x;\alpha,\theta)$ and $S(x;\alpha,\theta)$ fully characterize the PML distribution. The functions $f(x;\alpha,\theta)$ and $h(x;\alpha,\theta)$ play complementary roles; they are useful for identifying some crucial statistical features of the lifetime PML model. Further characteristics on these functions are given below.

2.2 Analysis of the pdf

This part is devoted to the pdf of the PML distribution, $f(x;\alpha,\theta)$, as described in (5). A remark on the structure of $f(x;\alpha,\theta)$ is given below. It can be expressed as a linear combination of listed pdfs of the literature.

Indeed, for $x > 0$, we can write

$$f(x;\alpha,\theta) = \theta\alpha x^{\alpha-1}e^{-\theta x^{\alpha}} + \frac{1}{2(1+\theta)}\left[(2\theta)^2\alpha x^{2\alpha-1}e^{-2\theta x^{\alpha}} - 2\theta\alpha x^{\alpha-1}e^{-2\theta x^{\alpha}}\right], \quad (7)$$

and, more explicitly,

$$f(x;\alpha,\theta) = f_1(x;\alpha,\theta) + \frac{1}{2(1+\theta)}\left[f_2(x;\alpha,\theta) - f_3(x;\alpha,\theta)\right],$$

where $f_1(x;\alpha,\theta) = \theta\alpha x^{\alpha-1}e^{-\theta x^{\alpha}}$, $x > 0$, is the pdf of the Weibull distribution with parameters α and θ, $f_2(x;\alpha,\theta) = (2\theta)^2\alpha x^{\alpha-1}x^{\alpha}e^{-2\theta x^{\alpha}}$, $x > 0$ is the pdf of the generalized gamma distribution with parameters 2, 2θ and α, and $f_3(x;\alpha,\theta) = 2\theta\alpha x^{\alpha-1}e^{-2\theta x^{\alpha}}$, $x > 0$, is the pdf of the Weibull distribution with parameters 2θ and α, with standard zero values for these pdfs for $x < 0$. Thus, we can use this linear representation to provide some properties of the PML distribution, an approach that we will consider in Section 3.

An asymptotic study gives

$$\lim_{x\to 0} f(x;\alpha,\theta) = \begin{cases} +\infty & \text{if } \alpha < 1 \\ \dfrac{\theta^2}{1+\theta} & \text{if } \alpha = 1 \\ 0 & \text{if } \alpha > 1 \end{cases}, \quad \lim_{x\to+\infty} f(x;\alpha,\theta) = 0.$$

We see that α plays a determinant role in these limits, mainly when x tends to 0. Also, the critical point(s) for $f(x;\alpha,\theta)$ is(are) given as the solution(s) of the following equation: $\{\log[f(x;\alpha,\theta)\}' = 0$, which can be reduced to

$$(\alpha-1)\frac{1}{x} + \alpha\theta x^{\alpha-1}\left[\frac{(1+\theta)e^{\theta x^{\alpha}}+2}{(1+\theta)e^{\theta x^{\alpha}}+2\theta x^{\alpha}-1} - 2\right] = 0.$$

The maximum point(s) represent(s) the mode(s) of the PML distribution. These critical points or mode(s) can be approximated numerically by the use of any mathematical software.

We conclude this part by showing some plots for $f(x;\alpha,\theta)$ for selected values of the parameters in Figure 1.

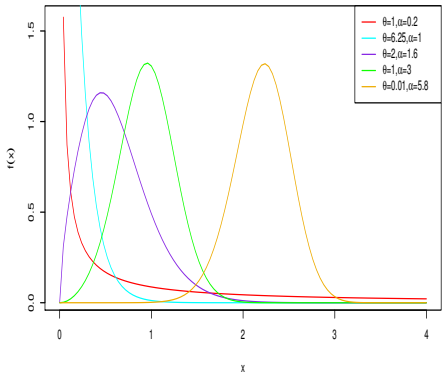

Figure 1: Curves of the pdf of the PML distribution for various values of α and θ

.

Figure 1 shows a variety of non-monotonic shapes, including reverse J-shaped, symmetric, skewed to the left or the right, and unimodal shapes.

2.3 Analysis of the hrf

Here, we focus on the hrf of the PML distribution, $h(x;\alpha,\theta)$, as described in (6). First, the following limits are obtained:

$$\lim_{x\to 0} h(x;\alpha,\theta) = \begin{cases} +\infty & \text{if } \alpha < 1 \\ \dfrac{\theta^2}{1+\theta} & \text{if } \alpha = 1 \\ 0 & \text{if } \alpha > 1 \end{cases},$$

$$\lim_{x\to +\infty} h(x;\alpha,\theta) = \begin{cases} 0 & \text{if } \alpha < 1 \\ \theta & \text{if } \alpha = 1 \\ +\infty & \text{if } \alpha > 1 \end{cases}.$$

The influence of α on these limits is therefore unequivocal.

Also, the critical point(s) for $h(x;\alpha,\theta)$ is(are) given as the solution(s) of the following equation: $\{\log[h(x;\alpha,\theta)\}' = 0$, which can be reduced to

$$(\alpha-1)\frac{1}{x} + \alpha\theta x^{\alpha-1}\left[\frac{(1+\theta)e^{\theta x^\alpha}+2}{(1+\theta)e^{\theta x^\alpha}+2\theta x^\alpha-1} + \frac{\theta x^\alpha-1}{(1+\theta)e^{\theta x^\alpha}+\theta x^\alpha}\right] - \alpha\theta x^{\alpha-1} = 0.$$

Since this equation is complicated to solve analytically, mathematical software is needed to approximate these critical points.

Figure 2 depicts some plots for $h(x;\alpha,\theta)$ for selected values of the parameters.

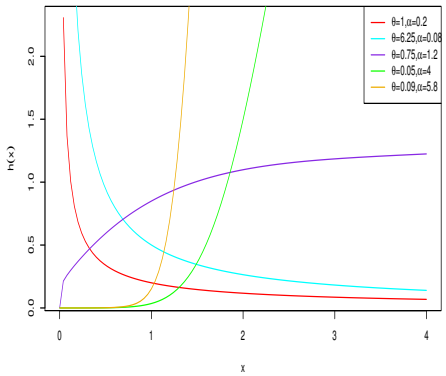

Figure 2: Curves of the hrf of the PML distribution for various values of α and θ

.

Figure 2 shows a variety of monotonic shapes, such as decreasing, increasing, and reverse bathtub shapes. Thus, the hrf of the PML distribution is much more flexible than the hrf of the former ML distribution, only showing unimodal curves (see [11]).

3 Properties

This section is devoted to some important properties of the PML distribution.

3.1 Incomplete moments with application

Here, let us consider a random variable X following the PML distribution, i.e., with the cdf given by (3) or equivalently, with the pdf given as (5). First, we investigate the incomplete moment of X, which are the main ingredients to define important measures and functions that will be discussed later.

Proposition 3.1. *For any positive integer r and positive t, the r^{th} incomplete moment of X taking at t is obtained as*

$$\mu'_r(t) = \theta^{-r/\alpha}\left\{\gamma\left(\frac{r}{\alpha}+1,\theta t^{\alpha}\right)+\frac{r2^{-r/\alpha-1}}{\alpha(1+\theta)}\gamma\left(\frac{r}{\alpha}+1,2\theta t^{\alpha}\right)\right\} - \frac{\theta}{1+\theta}t^{r+\alpha}e^{-2\theta t^{\alpha}},$$

where $\gamma(a,x)$ denotes the lower incomplete gamma function (i.e., $\gamma(a,x) = \int_0^x t^{a-1}e^{-t}dt$, $a,x>0$).

Proof. First of all, let us recall that $\mu'_r(t) = \mathbb{E}(X^r I\{\{X \le t\}\}) = \int_0^t x^r f(x;\alpha,\theta)dx$, where $I(A)$ denotes the indicator function over a certain event denoted by A and $f(x;\alpha,\theta)$ is the pdf given as (5). Now, owing to (7) and the changes of variable $y = \theta x^{\alpha}$, i.e., $x = (y/\theta)^{1/\alpha}$, or $y = 2\theta x^{\alpha}$, i.e., $x = [y/(2\theta)]^{1/\alpha}$, depending on the definition of the

integral, we get

$$\begin{aligned}
\mu_r'(t) &= \int_0^t x^r \theta\alpha x^{\alpha-1} e^{-\theta x^\alpha} dx \\
&+ \frac{1}{2(1+\theta)} \left[\int_0^t x^r (2\theta)^2 \alpha x^{2\alpha-1} e^{-2\theta x^\alpha} dx - \int_0^t x^r 2\theta\alpha x^{\alpha-1} e^{-2\theta x^\alpha} dx \right] \\
&= \theta^{-r/\alpha} \int_0^{\theta t^\alpha} y^{r/\alpha} e^{-y} dy + \frac{1}{2(1+\theta)} \left[(2\theta)^{-r/\alpha} \int_0^{2\theta t^\alpha} y^{r/\alpha+1} e^{-y} dy \right] \\
&- \frac{(2\theta)^{-r/\alpha}}{2(1+\theta)} \int_0^{2\theta t^\alpha} y^{r/\alpha} e^{-y} dy \\
&= \theta^{-r/\alpha} \left\{ \gamma\left(\frac{r}{\alpha}+1, \theta t^\alpha\right) + \frac{2^{-r/\alpha-1}}{1+\theta} \left[\gamma\left(\frac{r}{\alpha}+2, 2\theta t^\alpha\right) \right] \right\} \\
&- \frac{\theta^{-r/\alpha} 2^{-r/\alpha-1}}{1+\theta} \left[\gamma\left(\frac{r}{\alpha}+1, 2\theta t^\alpha\right) \right]. \qquad (8)
\end{aligned}$$

Now, as a known result, the lower incomplete gamma function satisfies the relation: $\gamma(a+1,x) = a\gamma(a,x) - x^a e^{-x}$. Therefore, the term in brackets in (8) can be expressed as

$$\begin{aligned}
&\gamma\left(\frac{r}{\alpha}+2, 2\theta t^\alpha\right) - \gamma\left(\frac{r}{\alpha}+1, 2\theta t^\alpha\right) \\
&= \left(\frac{r}{\alpha}+1\right) \gamma\left(\frac{r}{\alpha}+1, 2\theta t^\alpha\right) - (2\theta t^\alpha)^{r/\alpha+1} e^{-2\theta t^\alpha} - \gamma\left(\frac{r}{\alpha}+1, 2\theta t^\alpha\right) \\
&= \frac{r}{\alpha} \gamma\left(\frac{r}{\alpha}+1, 2\theta t^\alpha\right) - (2\theta t^\alpha)^{r/\alpha+1} e^{-2\theta t^\alpha}. \qquad (9)
\end{aligned}$$

We end the proof of Proposition 3.1 by putting (9) into (8). □

Several results follow from Proposition 3.1, including the expression of the first incomplete moment given as

$$\begin{aligned}
\mu_1'(t) &= \theta^{-1/\alpha} \left\{ \gamma\left(\frac{1}{\alpha}+1, \theta t^\alpha\right) + \frac{2^{-1/\alpha-1}}{\alpha(1+\theta)} \gamma\left(\frac{1}{\alpha}+1, 2\theta t^\alpha\right) \right\} \\
&- \frac{\theta}{1+\theta} t^{1+\alpha} e^{-2\theta t^\alpha}.
\end{aligned}$$

This function with respect to t is involved in the definitions of various important measures and functions in probability and statistics, including

various types of mean deviation, mean residual life functions and income curves, among others.

Also, by applying $t \to +\infty$ in Proposition 3.1, we can derive the crude moments of X. Indeed, the r^{th} crude moment of X is obtained as

$$\mu'_r = \mathbb{E}(X^r) = \lim_{t\to+\infty} \mu'_r(t) = \theta^{-r/\alpha} \left[1 + \frac{r2^{-r/\alpha-1}}{\alpha(1+\theta)}\right] \Gamma\left(\frac{r}{\alpha}+1\right),$$

where $\Gamma(a)$ denotes the (standard) gamma function (i.e., $\Gamma(a) = \int_0^{+\infty} t^{a-1}e^{-t}dt$, $a > 0$). By taking $\alpha = 1$, using $\Gamma(r+1) = r!$, we rediscover the r^{th} crude moments related to the former ML distribution (see [11]). One can also remark that μ'_r is a decreasing function with respect to θ, which tends to 0 when θ tends to $+\infty$. When μ'_r is viewed as a function of α, its behavior becomes more complicated, depending on $\theta \in (0,1)$ or $\theta > 1$. In all cases, if θ is fixed, μ'_r tends to 1 when α tends to $+\infty$.

The first four crude moments of X can be easily deduced as follows:

$$\mu = \mu'_1 = \theta^{-1/\alpha} \left[1 + \frac{2^{-1/\alpha-1}}{\alpha(1+\theta)}\right] \Gamma\left(\frac{1}{\alpha}+1\right),$$

$$\mu'_2 = \theta^{-2/\alpha} \left[1 + \frac{2^{-2/\alpha}}{\alpha(1+\theta)}\right] \Gamma\left(\frac{2}{\alpha}+1\right),$$

$$\mu'_3 = \theta^{-3/\alpha} \left[1 + \frac{32^{-3/\alpha-1}}{\alpha(1+\theta)}\right] \Gamma\left(\frac{3}{\alpha}+1\right)$$

and

$$\mu'_4 = \theta^{-4/\alpha} \left[1 + \frac{2^{-4/\alpha+1}}{\alpha(1+\theta)}\right] \Gamma\left(\frac{4}{\alpha}+1\right).$$

Based on μ and μ'_2, the variance of X is given by

$$\sigma^2 = \theta^{-2/\alpha} \left\{ \left[1 + \frac{2^{-2/\alpha}}{\alpha(1+\theta)}\right] \Gamma\left(\frac{2}{\alpha}+1\right) - \left[1 + \frac{2^{-1/\alpha-1}}{\alpha(1+\theta)}\right]^2 \Gamma\left(\frac{1}{\alpha}+1\right)^2 \right\}.$$

Owing to the standard binomial theorem, the r^{th} central moment of X is given by the following finite linear representation:

$$\begin{aligned}\mu_r &= \mathbb{E}[(X-\mu)^r] \\ &= \sum_{k=0}^{r} \binom{r}{k} (-1)^{r-k} \mu^{r-k} \theta^{-k/\alpha} \left[1 + \frac{k 2^{-k/\alpha-1}}{\alpha(1+\theta)}\right] \Gamma\left(\frac{k}{\alpha}+1\right).\end{aligned}$$

The general coefficient of X is deduced as $C_r = \mu_r/\sigma^r$, covering the skewness and kurtosis coefficients of X given by $\sqrt{\beta_1} = C_3$ and $\beta_2 = C_4$.

Table 1 indicates numerical values for the first four crude moments of X, $\sqrt{\beta_1}$ and β_2, for selected values for α and θ. In particular, in Table 1, one can see that the PML distribution can be left and right skewed, and symmetric. This last aspect is illustrated in the table with the special values $\alpha = 3.49005$ and $\theta = 10$ for which the skewness is near equal to zero, i.e., $\sqrt{\beta_1} \approx 9.1800 \times 10^{-7}$. Also, the PML distribution has a versatile kurtosis; it can be platykurtic (corresponding to $\beta_2 < 3$), mesokurtic (corresponding to $\beta_2 = 3$, near attained in the table with the values $\alpha = 3.65$ and $\theta = 0.01$) and leptokurtic (corresponding to $\beta_2 > 3$).

3.2 Order statistics

From the modeling of various real-life phenomena involving the mixing of minimum and maximum random variables, the concept of order statistics is born. We may refer the reader to [9] and [5]. Here, we discuss some properties of the order statistics of the PML distribution. Firstly, the pdf of the m^{th} order statistic the PML distribution, denoted by $X_{(m)}$, is defined as

$$f_{X_{(m)}}(x;\alpha,\theta) = n\binom{n-1}{m-1} f(x;\alpha,\theta) F(x;\alpha,\theta)^{m-1} S(x;\alpha,\theta)^{n-m}, \quad x \in \mathbb{R}.$$

Table 1: Numerical values for the first four crude moments of X, $\sqrt{\beta_1}$ and β_2 for various choices of parameters

Parameters	μ	μ'_2	μ'_3	μ'_4	$\sqrt{\beta_1}$	β_2
$\alpha = 0.5$ $\theta = 3$	0.2361	0.3055	0.9992	6.1694	6.48045	85.2287
$\alpha = 1.6$ $\theta = 2$	0.6206	0.5181	0.5289	0.6308	0.8743	3.9639
$\alpha = 5.8$ $\theta = 0.01$	2.2036	4.9504	11.3199	26.3129	-0.1936	3.1293
$\alpha = 30$ $\theta = 10$	0.9106	0.8306	0.7589	0.6944	-0.9853	4.7209
$\alpha = 3.5$ $\theta = 10$	0.47099	0.2431	0.1345	0.0787	-0.0025	2.7445
$\alpha = 10$ $\theta = 5$	0.8162	0.6751	0.5650	0.4778	-0.6910	3.7484
$\alpha = 3.49005$ $\theta = 10$	0.4700	0.2422	0.1338	0.0783	9.18×10^{-7}	2.7440
$\alpha = 5$ $\theta = 1$	0.9581	0.9545	0.9819	1.0384	-0.3614	3.2298
$\alpha = 3.65$ $\theta = 0.01$	3.5417	13.1392	50.7832	203.6499	0.0663	3.0008

That is, owing to (3), (4) and (5), for $x > 0$, we have

$$f_{X_{(m)}}(x;\alpha,\theta) = n\binom{n-1}{m-1}\frac{\theta\alpha}{1+\theta}x^{\alpha-1}\left[(1+\theta)e^{\theta x^\alpha} + 2\theta x^\alpha - 1\right] \times \left\{1 - \left[1 + \frac{\theta x^\alpha}{1+\theta}e^{-\theta x^\alpha}\right]e^{-\theta x^\alpha}\right\}^{m-1}\left[1 + \frac{\theta x^\alpha}{1+\theta}e^{-\theta x^\alpha}\right]^{n-m} \times e^{-\theta(n-m+2)x^\alpha}, \quad x > 0,$$

and $f_{X_{(m)}}(x;\alpha,\theta) = 0$ for $x < 0$.

In particular, for $x > 0$, the pdf of $X_{(1)} = \inf(X_1,\ldots,X_n)$ is given as

$$f_{X_{(1)}}(x;\alpha,\theta) = n\frac{\theta\alpha}{1+\theta}x^{\alpha-1}\left[(1+\theta)e^{\theta x^\alpha} + 2\theta x^\alpha - 1\right] \times \left[1 + \frac{\theta x^\alpha}{1+\theta}e^{-\theta x^\alpha}\right]^{n-1} e^{-\theta(n+1)x^\alpha},$$

and the pdf of $X_{(n)} = \sup(X_1,\ldots,X_n)$ can be set as

$$f_{X_{(n)}}(x;\alpha,\theta) = n\frac{\theta\alpha}{1+\theta}x^{\alpha-1}e^{-2\theta x^\alpha}\left[(1+\theta)e^{\theta x^\alpha} + 2\theta x^\alpha - 1\right] \times \left\{1 - \left[1 + \frac{\theta x^\alpha}{1+\theta}e^{-\theta x^\alpha}\right]e^{-\theta x^\alpha}\right\}^{n-1}.$$

Furthermore, $X_{(1)}$ enjoys a singular asymptotic distribution result as described below. First, note that, for $x > 0$,

$$\lim_{\epsilon\to 0}\frac{F(\epsilon x;\alpha,\theta)}{F(\epsilon;\alpha,\theta)} = \lim_{\epsilon\to 0}\frac{xf(\epsilon x;\alpha,\theta)}{f(\epsilon;\alpha,\theta)} = x^\alpha \lim_{\epsilon\to 0}\frac{e^{-2\theta\epsilon^\alpha x^\alpha}\left[(1+\theta)e^{\theta\epsilon^\alpha x^\alpha} + 2\theta\epsilon^\alpha x^\alpha - 1\right]}{e^{-2\theta\epsilon^\alpha}\left[(1+\theta)e^{\theta\epsilon^\alpha} + 2\theta\epsilon^\alpha - 1\right]} = x^\alpha.$$

It follows from [5, Theorem 8.3.6(ii)] that the minimal domain of attraction of the PML distribution is the standard Weibull distribution with parameters 1 and α, i.e., with cdf $K(x;\alpha) = 1 - e^{-x^\alpha}$ for $x > 0$, and $K(x;\alpha) = 0$ for $x < 0$.

4 Parametric Estimation and Application

This section is devoted to the practical features of the PML model. First, we investigate the estimation of the parameters θ and α, along with a simulation study, then applications are given for three different data sets.

4.1 Parametric estimation

Here, the parameters α and θ are assumed to be unkown. For estimating them, we propose the method of maximum likelihood. Thus, let $x_1, \ldots, x_n$ be a n independent observations from the PML distribution with unknown parameters α and θ, corresponding to data. Then, the likelihood function is given by

$$\begin{aligned} L(\alpha,\theta) &= \prod_{i=1}^{n} f(x_i;\alpha,\theta) \\ &= \frac{\theta^n \alpha^n}{(1+\theta)^n} e^{-2\theta\sum_{i=1}^{n} x_i^{\alpha}} \left(\prod_{i=1}^{n} x_i\right)^{\alpha-1} \prod_{i=1}^{n} \left[(1+\theta)e^{\theta x_i^{\alpha}} + 2\theta x_i^{\alpha} - 1\right]. \end{aligned}$$

The log-likelihood function follows immediately as

$$\begin{aligned} \ell(\alpha,\theta) &= \log\left[L(\alpha,\theta)\right] = n\log(\theta) + n\log(\alpha) - n\log(1+\theta) \\ &\quad - 2\theta\sum_{i=1}^{n} x_i^{\alpha} + (\alpha-1)\sum_{i=1}^{n}\log(x_i) + \sum_{i=1}^{n}\log\left[(1+\theta)e^{\theta x_i^{\alpha}} + 2\theta x_i^{\alpha} - 1\right]. \end{aligned}$$

The maximum likelihood estimates (MLEs) for α and θ, say $\hat{\alpha}$ and $\hat{\theta}$ are defined as $(\hat{\alpha},\hat{\theta}) = \arg\max_{(\alpha,\theta)\in(0,+\infty)^2} L(\alpha,\theta)$ or, equivalently, $(\hat{\alpha},\hat{\theta}) = \arg\max_{(\alpha,\theta)\in(0,+\infty)^2} \ell(\alpha,\theta)$. One can obtained these estimates by solving $\partial\ell(\alpha,\theta)/\partial\alpha = 0$ and $\partial\ell(\alpha,\theta)/\partial\theta = 0$ (simultaneously) according to α and θ, equations which can be expressed analytically as

$$\frac{n}{\alpha} - 2\theta\sum_{i=1}^{n} x_i^{\alpha}\log(x_i) + \sum_{i=1}^{n}\log(x_i) + \theta\sum_{i=1}^{n}\frac{x_i^{\alpha}\log(x_i)\left[(1+\theta)e^{\theta x_i^{\alpha}} + 2\right]}{(1+\theta)e^{\theta x_i^{\alpha}} + 2\theta x_i^{\alpha} - 1} = 0$$

and

$$\frac{n}{\theta} - \frac{n}{1+\theta} - 2\sum_{i=1}^{n} x_i^{\alpha} + \sum_{i=1}^{n}\frac{e^{\theta x_i^{\alpha}}\left[(1+\theta)x_i^{\alpha} + 1\right] + 2x_i^{\alpha}}{(1+\theta)e^{\theta x_i^{\alpha}} + 2\theta x_i^{\alpha} - 1} = 0.$$

These equations are complicated to solve analytically. One can use mathematical software to get numerical solutions. Under regularity conditions, the bi-dimensional normal distribution $\mathcal{N}_2((\alpha,\theta), J^{-1}(\hat{\alpha},\hat{\theta}))$ can approximate the underlying distribution of $(\hat{\alpha},\hat{\theta})$, where $J(\alpha,\theta)$ denote the following 2×2 matrix:

$$J(\alpha,\theta) = -\begin{pmatrix} \dfrac{\partial^2 \ell(\alpha,\theta)}{\partial \alpha^2} & \dfrac{\partial^2 \ell(\alpha,\theta)}{\partial \alpha \partial \theta} \\ \dfrac{\partial^2 \ell(\alpha,\theta)}{\partial \theta \partial \alpha} & \dfrac{\partial^2 \ell(\alpha,\theta)}{\partial \theta^2} \end{pmatrix},$$

whose components can be expressed analytically with mathematical developments. This asymptotic result can be used to generate asymptotic confidence intervals, statistical tests, and so on.

4.2 Simulation study

Here, we perform a simulation study evaluating the performance of the MLEs presented above for the PML model for selected values of the parameters α and θ. The simulation experiment was repeated 1000 times each with sample sizes of 20, 50, 100, 200, and the parameter combinations are as follows:
I) $\alpha = 1.95$ and $\theta = 0.85$, II) $\alpha = 0.2$ and $\theta = 0.1$, III) $\alpha = 1.5$ and $\theta = 0.5$, IV) $\alpha = 2$ and $\theta = 1$.
The algorithm for the simulation study is formalized as follows:

Step 1: Set the number of replications denoted by N.

Step 2: Set the sample size denoted by n and the values of the parameters α and θ.

Step 3: Set the initial value for the random start, denoted by x_0.

Step 4: For $j = 1, \ldots, n$, generate u_j from a random variable U_j following the unit uniform distribution.

Step 5: Update x_0 by x^* by using the Newton's formula as follows:

$$x^* = x_0 - \left\{ \frac{F(x_0;\alpha,\theta) - u_j}{f(x_0;\alpha,\theta)} \right\},$$

where $F(x_0;\alpha,\theta)$ and $f(x_0;\alpha,\theta)$ are the cdf and pdf of the PML distribution at $x = x_0$ as given by (3) and (5), respectively.

Step 6: If $|x_0 - x^*| \leq \epsilon$ for small $\epsilon > 0$, ϵ being considered as a tolerance limit, then $x = x^*$ is considered as a generated value from the PML distribution with parameter α and θ, else set $x_0 = x^*$ and go to Step 5.

Step 7: Repeat Steps 4 to 6 for $j = 1, \ldots, n$ to obtain n values $x_1, \ldots, x_n$.

Step 8: Compute the MLEs of α and θ from $x_1, \ldots, x_n$.

Step 9: Repeat Steps 2 to 8, N times.

Step 10: Compute the average estimate (AE), Bias and mean square error (MSE) for each parameter, defined as

$$\text{AE}(\alpha) = \frac{1}{N}\sum_{i=1}^{N}\hat{\alpha}_i, \quad \text{Bias}(\alpha) = \frac{1}{N}\sum_{i=1}^{N}(\hat{\alpha}_i - \alpha),$$

$$\text{MSE}(\alpha) = \frac{1}{N}\sum_{i=1}^{N}(\hat{\alpha}_i - \alpha)^2,$$

$$\text{AE}(\theta) = \frac{1}{N}\sum_{i=1}^{N}\hat{\theta}_i,$$

$$\text{Bias}(\theta) = \frac{1}{N}\sum_{i=1}^{N}(\hat{\theta}_i - \theta), \quad \text{MSE}(\theta) = \frac{1}{N}\sum_{i=1}^{N}(\hat{\theta}_i - \theta)^2,$$

where $\hat{\alpha}_i$ and $\hat{\theta}_i$ are the MLEs of α and θ, respectively, obtained at the i^{th} replication.

Table 2 presents the AEs, Bias and MSEs values of parameters for different sample sizes. Figures 3 and 4 give the graphical representations of the Bias and MSE related to the two parameters.

Table 2: Numerical values for the AEs, Bias and MSE of the parameters based on 1000 simulations in the setting of the PML model

	n	Parameters	AEs	Bias	MSE
I	20	α	2.038336	0.08833574	0.2176643
		θ	0.8708443	0.02084432	0.03701037
	50	α	1.996429	0.04642946	0.08285901
		θ	0.8572819	0.00728185	0.01355176
	100	α	1.96219	0.01219701	0.06173568
		θ	0.8453169	-0.004683061	0.00622736
	200	α	1.951196	0.001195866	0.04729822
		θ	0.8455547	-0.004445285	0.003326896
II	20	α	0.2138739	0.01387395	0.001786709
		θ	0.09174396	-0.008256044	0.003104728
	50	α	0.2049212	0.00492118	0.0005953382
		θ	0.09577495	-0.00422505	0.001230094
	100	α	0.2017429	0.001742857	0.0001910657
		θ	0.09837379	-0.001626206	0.0007620415
	200	α	0.200525	0.0005250294	8.89×10^{-6}
		θ	0.09927519	-0.0007248077	1.50×10^{-5}
III	20	α	1.592697	0.09269666	0.100596
		θ	0.4914032	-0.008596789	0.01619796
	50	α	1.526672	0.0266715	0.04286805
		θ	0.4986687	-0.00133133	0.00605377
	100	α	1.50961	0.009610091	0.03863887
		θ	0.49886	-0.001139978	0.003621219
	200	α	1.493986	-0.006014323	0.03088576
		θ	0.5006133	0.0006133199	0.001788008
IV	20	α	2.112133	0.1121327	0.2631284
		θ	1.021017	0.02101712	0.05205832
	50	α	2.049721	0.04972109	0.08723618
		θ	1.005752	0.005751939	0.01899681
	100	α	2.012916	0.01291555	0.06636949
		θ	0.9978486	-0.002151383	0.008961524
	200	α	2.003441	0.003441277	0.0336673
		θ	1.000845	0.0008452682	0.004373854

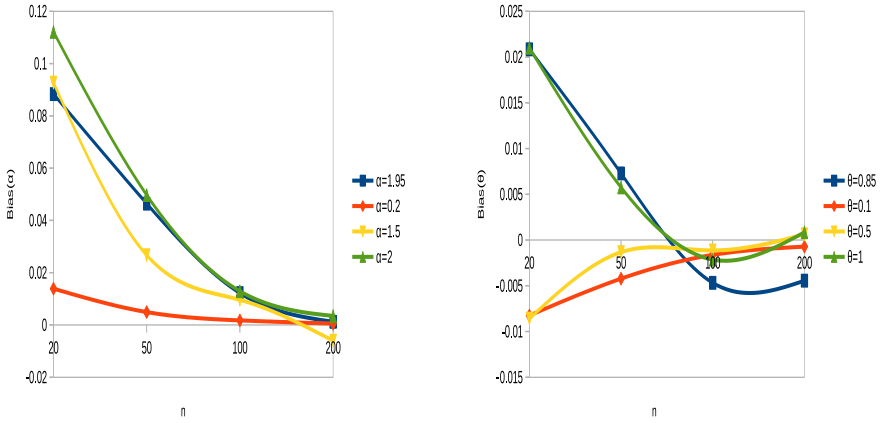

(a) (b)

Figure 3: Curves of the Bias for the estimates of (a) α and (b) θ for various sample sizes

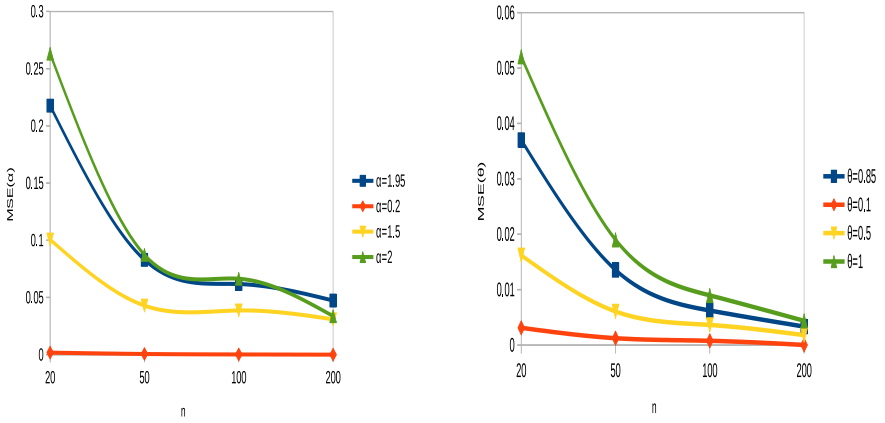

(a) (b)

Figure 4: Curves of the MSE for the estimates of (a) α and (b) θ for various sample sizes

From Table 2, and Figures 3 and 4, it can be noted that, as sample size increases, the Bias decays towards zero and MSE decreases. That is, this illustrates the fact that the parent estimators are asymptotically unbiased and consistent. Hence, the maximum likelihood method works quite well to estimate the parameters of the PML model.

4.3 Application

Now, we use the previous parametric estimation for data fitting purposes. We fit the PML distribution to three data sets and compare the results with those of the fitted Weibull (W), PL, exponentiated power Lindley (EPL) and three-parameter generalized Lindley (TGL) distributions. The corresponding pdfs of these competitors are recalled below.

- For the W distribution:

$$f(x;\alpha,\theta)=\frac{\alpha}{\theta}\left(\frac{x}{\theta}\right)^{\alpha-1}e^{-(x/\theta)^{\alpha}},\quad x>0,$$

  with $\alpha>0$ and $\theta>0$, and $f(x;\alpha,\theta)=0$ for $x<0$.

- For the PL distribution:

$$f(x;\alpha,\theta)=\frac{\alpha\theta^2}{\theta+1}(1+x^{\alpha})x^{\alpha-1}e^{-\theta x^{\alpha}},\quad x>0,$$

  with $\alpha>0$ and $\theta>0$, and $f(x;\alpha,\theta)=0$ for $x<0$.

- For the EPL distribution:

$$f(x;\alpha,\beta,\theta)=\frac{\alpha\theta^2\beta x^{\beta-1}}{\theta+1}(1+x^{\beta})e^{-\theta x^{\beta}}\left[1-\left(1+\frac{\theta x^{\beta}}{\theta+1}\right)e^{-\theta x^{\beta}}\right]^{\alpha-1},$$

  $x>0$ with $\alpha>0$, $\beta>0$ and $\theta>0$, , and $f(x;\alpha,\beta,\theta)=0$ for $x<0$.

- For the TGL distribution

$$f(x;\alpha,\beta,\theta)=\frac{\alpha\theta^2(\beta+x^{\alpha})x^{\alpha-1}e^{-\theta x^{\alpha}}}{1+\theta\beta},\quad x>0,$$

  with $\alpha>0$, $\beta>0$ and $\theta>0$, and $f(x;\alpha,\beta,\theta)=0$ for $x<0$.

We estimate the unknown parameters of each model by the maximum likelihood method of estimation. In order to compare the five models, we consider criteria like the statistic log-likelihood ($\hat{\ell}$), Akaike information criterion (AIC), Bayesian information criterion (BIC), corrected Akaike information criterion (AICc), Hannan-Quinn information criterion (HQIC) and the values of the Kolmogorov-Smirnov (K-S) statistic, and the corresponding p-values (p-V) for the three different data sets.

The model with the lowest AIC, BIC, AICc, HQIC and K-S and the largest p-V is considered the best.

Bladder cancer patients data

According to [23], the data represent the remission times (in months) of a random sample of 128 bladder cancer patients. The data are as follows.
{0.08, 2.09, 3.48, 4.87, 6.94, 8.66, 13.11, 23.63, 0.2, 2.23, 0.26, 0.31, 0.73, 0.52, 4.98, 6.97, 9.02, 13.29, 0.4, 2.26, 3.57, 5.06, 7.09, 11.98, 4.51, 2.07, 0.22, 13.8, 25.74, 0.5, 2.46, 3.64, 5.09, 7.26, 9.47, 14.24, 19.13, 6.54, 3.36, 0.82, 0.51, 2.54, 3.7, 5.17, 7.28, 9.74, 14.76, 26.31, 0.81, 1.76,8.53, 6.93, 0.62, 3.82, 5.32, 7.32, 10.06, 14.77, 32.15, 2.64, 3.88, 5.32, 3.25, 12.03, 8.65, 0.39, 10.34, 14.83, 34.26, 0.9, 2.69, 4.18, 5.34, 7.59, 10.66, 4.5, 20.28, 12.63, 0.96, 36.66, 1.05, 2.69, 4.23, 5.41, 7.62, 10.75, 16.62, 43.01, 6.25, 2.02, 22.69, 0.19, 2.75, 4.26, 5.41, 7.63, 17.12, 46.12, 1.26, 2.83, 4.33, 8.37, 3.36, 5.49, 0.66, 11.25, 17.14, 79.05, 1.35, 2.87, 5.62, 7.87, 11.64, 17.36, 12.02, 6.76, 0.4, 3.02, 4.34, 5.71, 7.93, 11.79, 18.1, 1.46, 4.4, 5.85, 2.02, 12.07}

Tables 3 and 4 give the relevant numerical values for all the fitted models based on the bladder cancer patients data set. Figure 5 gives the graphs of the estimated pdfs and cdfs of the fitted models for the bladder cancer patients data set.

Table 3: Estimated values, $\hat{\ell}$, AIC and BIC for the bladder cancer patients data set

Distributions	Estimates	$-\hat{\ell}$	AIC	BIC
PML	$\boldsymbol{\hat{\alpha} = 0.7290}$ $\boldsymbol{\hat{\theta} = 0.2775}$	**401.2802**	**806.5603**	**812.2644**
W	$\hat{\alpha} = 0.9229$ $\hat{\theta} = 8.2290$	402.1907	808.3814	814.0854
PL	$\hat{\alpha} = 0.7442$ $\hat{\theta} = 0.3855$	402.2373	808.4745	814.1786
EPL	$\hat{\alpha} = 1.8412$ $\hat{\beta} = 0.5785$ $\hat{\theta} = 0.7252$	401.0833	808.1666	816.7227
TGL	$\hat{\alpha} = 0.9196$ $\hat{\beta} = 102.6147$ $\hat{\theta} = 0.1528$	402.2331	810.4661	819.0222

Table 4: AICc, HQIC and K-S with p-V for the bladder cancer patients data set

Distributions	AICc	HQIC	K-S	p-V
PML	**806.6563**	**808.878**	**0.0428**	**0.9732**
W	808.4774	810.699	0.0518	0.8817
PL	808.5705	810.7922	0.0458	0.9512
EPL	808.3601	811.643	0.0480	0.93
TGL	810.6596	813.9426	0.0524	0.8736

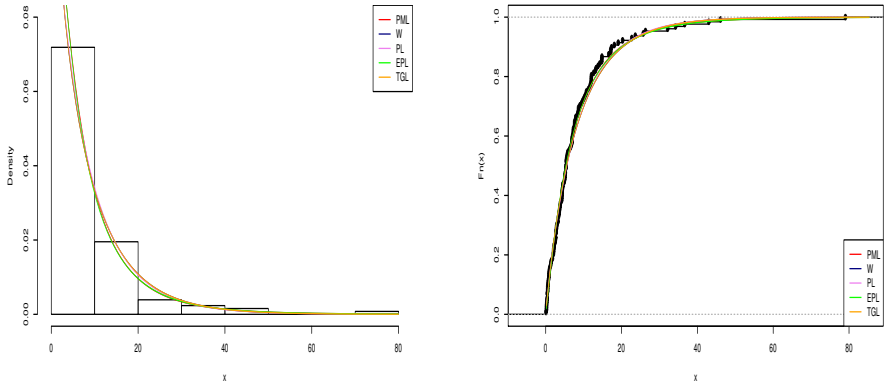

(a) (b)

Figure 5: Curves of the estimated (a) pdfs and (b) cdfs of the fitted models for the bladder cancer patients data set

Fatigue fracture data set

This data represents the life of fatigue fracture of Kevlar 373/epoxy subjected to constant pressure at 90% stress level until all had failed. The data was extracted from [1] and was previously used by [4] and [10]. The data are as follows.
{0.0251, 0.0886, 0.0891, 0.2501, 0.3113, 0.3451, 0.4763, 0.5650, 0.5671, 0.6566, 0.6748, 0.6751, 0.6753, 0.7696, 0.8375, 0.8391, 0.8425, 0.8645, 0.8851, 0.9113, 0.9120, 0.9836, 1.0483, 1.0596, 1.0773, 1.1733, 1.2570, 1.2766, 1.2985, 1.3211, 1.3503, 1.3551, 1.4595, 1.4880, 1.5728, 1.5733, 1.7083, 1.7263, 1.7460, 1.7630, 1.7746, 1.8275, 1.8375, 1.8503, 1.8808, 1.8878, 1.8881, 1.9316, 1.9558, 2.0048, 2.0408, 2.0903, 2.1093, 2.1330, 2.2100, 2.2460, 2.2878, 2.3203, 2.3470, 2.3513, 2.4951, 2.5260, 2.9911, 3.0256, 3.2678, 3.4045, 3.4846, 3.7433, 3.7455, 3.9143, 4.8073, 5.4005, 5.4435, 5.5295, 6.5541, 9.0960}

Tables 5 and 6 give the relevant numerical summaries for all the fitted models based on fatigue fracture data sets. Figure 6 gives the graphs of the estimated pdfs and cdfs of the fitted models for the fatigue

Table 5: Estimated values, $\hat{\ell}$, AIC and BIC for the fatigue fracture data set

Distributions	Estimates	$-\hat{\ell}$	AIC	BIC
PML	$\boldsymbol{\hat{\alpha} = 1.1182}$ $\boldsymbol{\hat{\theta} = 0.5324}$	**121.2194**	**246.4389**	**251.1004**
W	$\hat{\alpha} = 1.3257$ $\hat{\theta} = 2.1328$	122.5264	249.0529	253.7144
PL	$\hat{\alpha} = 0.7047$ $\hat{\theta} = 1.1423$	122.4018	248.8037	253.4652
EPL	$\hat{\alpha} = 1.5375$ $\hat{\beta} = 0.9495$ $\hat{\theta} = 1.0215$	121.8682	249.7364	256.7286
TGL	$\hat{\alpha} = 0.9931$ $\hat{\beta} = 0.1478$ $\hat{\theta} = 0.9635$	121.6506	249.3011	256.2933

Table 6: AICc, HQIC and K-S with p-V for the fatigue fracture data set

Distributions	AICc	HQIC	K-S	p-V
PML	**246.6033**	**248.3017**	**0.0964**	**0.4516**
W	249.2173	250.9157	0.1099	0.2954
PL	248.9681	250.6665	0.1123	0.2722
EPL	250.0697	252.5308	0.0992	0.4156
TGL	249.6344	252.0956	0.1020	0.3822

fracture data set.

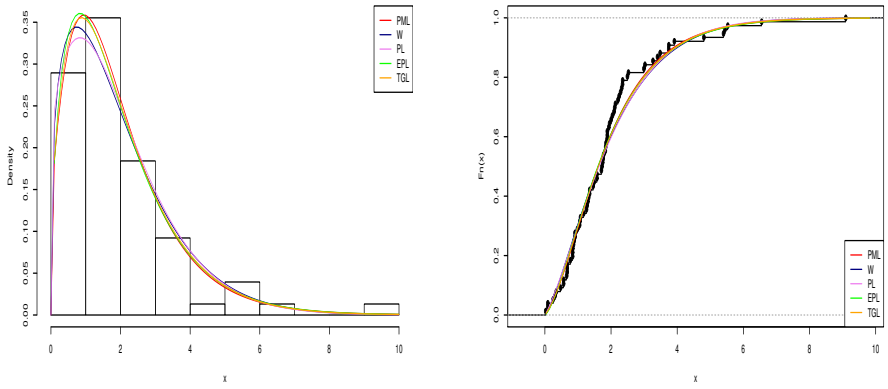

(a) (b)

Figure 6: Curves of the estimated (a) pdfs and (b) cdfs of the fitted models for the fatigue fracture data set

March precipitation data set

This real data set represents 30 successive values of march precipitation (in inches) in Minneapolis/St Paul given by [22] and the data are as given below.
{0.77, 1.74, 0.81, 1.2, 1.95, 1.2, 0.47, 1.43, 3.37, 2.2, 3, 3.09, 1.51, 2.1, 0.52, 1.62, 1.31, 0.32, 0.59, 0.81, 2.81, 1.87, 1.18, 1.35, 4.75, 2.48, 0.96, 1.89, 0.9, 2.05}.

Tables 7 and 8 provide the relevant numerical summaries for all the fitted models based on the march precipitation data set.

Figure 7 gives the graphs of the estimated pdfs and cdfs of the fitted models for the march precipitation data set.

Table 7: Estimated values, $\hat{\ell}$, AIC and BIC for the march precipitation data set

Distributions	Estimates	$-\hat{\ell}$	AIC	BIC
PML	$\boldsymbol{\hat{\alpha} = 1.4739}$ $\boldsymbol{\hat{\theta} = 0.4923}$	**38.5278**	**81.0556**	**83.8579**
W	$\hat{\alpha} = 1.8087$ $\hat{\theta} = 1.8924$	38.64328	81.28657	84.08896
PL	$\hat{\alpha} = 1.5263$ $\hat{\theta} = 0.6460$	38.8729	81.74579	84.54819
EPL	$\hat{\alpha} = 3.4070$ $\hat{\beta} = 0.9235$ $\hat{\theta} = 1.6304$	38.10625	82.2125	86.41609
TGL	$\hat{\alpha} = 1.8103$ $\hat{\beta} = 358.0827$ $\hat{\theta} = 0.3179$	38.6435	83.287	87.49059

Table 8: AICc, HQIC and K-S with p-V for the march precipitation data set

Distributions	AICc	HQIC	K-S	p-V
PML	**81.5000**	**81.9521**	**0.0526**	**1**
W	81.73101	82.18307	0.0689	0.9988
PL	82.19023	82.64231	0.0682	0.999
EPL	83.13558	83.55727	0.0624	0.9998
TGL	84.2100	84.6318	0.0688	0.9989

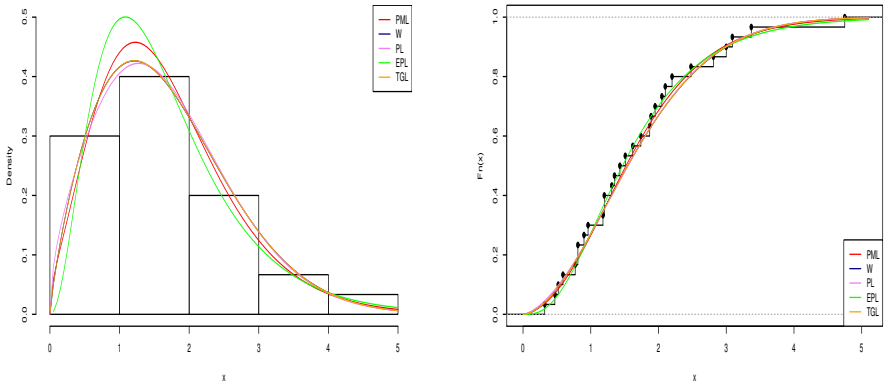

(a) (b)

Figure 7: Curves of the estimated (a) pdfs and (b) cdfs of the fitted models for the march precipitation data set

Thus, in Tables 3, 4, 5, 6, 7 and 8, the parameter estimates for the PML, W, PL, EPL and TGL models are calculated by using the maximum likelihood method. Also, $-\hat{\ell}$, AIC, BIC, AICc, HQIC and K-S with p-V are presented for the three different data sets. For all of them, based on the lowest values of the AIC, BIC, AICc, HQIC and K-S with p-V, the PML model turns out to be a better model than the W, PL, EPL and TGL models. Figures 5, 6 and 7 show the closeness of the fitted pdfs with the empirical histogram and fitted cdfs with empirical cdfs for different data sets. Based on the observations of these plots, the proposed model provides a closer fit to these data sets.

5 Conclusions

In this paper, a new two-parameter distribution, namely, PML distribution, is proposed based on power transformation over the modified Lindley distribution. We have exhibited its moments, incomplete moments, skewness, kurtosis, and order statistics. In the setting of the PML model, the unknown parameters were estimated by the maximum

likelihood method of estimation. A simulation study was carried out to evaluate the bias and mean square error of the maximum likelihood estimates of the parameters. We have shown by means of three applications to real data that the proposed model can yield better fits than the famous W, PL, EPL and TGL models.

Acknowledgements
The authors would like to express their gratitude to the reviewer for his or her detailed comments on the manuscript, which helped to improve it in several ways.

References

[1] I. B. Abdul-Moniem and M. Seham, Transmuted Gompertz distribution, *Computational and Applied Mathematics*, 1 (2015) , 88-96.

[2] A.Z. Afify, M. Nassar, G.M. Cordeiro and D. Kumar, The Weibull Marshall-Olkin Lindley distribution: properties and estimation, *Journal of Taibah University for Science*, 14 (2020), 192-204.

[3] S. H. Alkarni, Extended power Lindley distribution: a new statistical model or non -monotone survival data, *European Journal of Statistics and Probability*, 3 (2015), 19-34.

[4] D. F. Andrews and A. M. Herzberg, *Data: a collection of problems from many fields for the student and research worker* , Springer Series in Statistics, New York (1985).

[5] B. C. Arnold, N. Balakrishnan and H. N. Nagaraja, *A First Course in Order Statistics*, John Wiley and Sons, New York (1992).

[6] S. K. Ashour and M.A. Eltehiwy, Exponentiated power Lindley distribution, *Journal of Advanced Research*, 6 (2015), 895-905.

[7] A. Asgharzadeh, H. S. Bakouch, , S. Nadarajah and F. Sharafi, A new weighted Lindley distribution with application, *Brazilian Journal of Probability and Statistics*, 30 (2016), 1-27.

[8] H. S. Bakouch, B. M. Al-Zahrani, A. A. Al-Shomrani, V. A. A. Marchi and F. Louzada, An extended Lindley distribution, *Journal of the Korean Statistical Society*, 41 (2012), 75-85.

[9] N. Balakrishnan and A. C Cohen, *Order Statistics and Inference*, Academic Press , New York (1991).

[10] R. E. Barlow, R.H. Toland and T. Freeman, A Bayesian analysis of stress rupture life of Kevlar 49/epoxy sphere-cal pressure vessels, *In 'Proc. Conference on Applications of Statistics, Marcel Dekker, New York* (1984).

[11] C. Chesneau, L. Tomy and J. Gillariose, A new modified Lindley distribution with properties and applications, *Journal of Statistics and Management Systems*,Journal of Statistics and Management Systems, (2021), 1-21.

[12] C. Chesneau, L. Tomy and J. Gillariose, The inverted modified Lindley distribution, *Journal of Statistical Theory and Practice*, 14 (2020), 1-17.

[13] C. Chesneau, L. Tomy and J. Gillariose, On a sum and difference of two Lindley distributions: theory and applications, *REVSTAT–Statistical Journal*, 18(2020), 673-695.

[14] C. Chesneau, L. Tomy and M. Jose, Wrapped modified Lindley distribution, *Journal of Statistics and Management Systems*, (2021), 1-16.

[15] N. Ekhosuehi and F. Opone, A three-parameter generalized Lindley distribution: properties and application, *Statistica*, 78 (2018), 233-249.

[16] M. E. Ghitany and D. K. Al-Mutairi, Size-biased Poisson-Lindley distribution and its applications, *Metron- International Journal of Statistics*, 66 (2008), 299-311.

[17] M. E. Ghitany, B. Atieh and S. Nadarajah, Lindley distribution and its applications, *Mathematics and Computers in Simulation*, 78 (2008a), 493-506.

[18] M. E. Ghitany, D. K. Al-Mutairi and S. Nadarajah, Zero-truncated Poisson-Lindley distribution and its applications, *Mathematics and Computers in Simulation*, 79 (2008b), 279-287.

[19] M. E. Ghitany, F. Alqallaf, D. K. Al-Mutairi and H. A. Husain,A two-parameter weighted Lindley distribution and its applications to survival data, *Mathematics and Computers in Simulation*, 81(2011), 1190-1201.

[20] M. E. Ghitany, D. K. Al-Mutairi, N. Balakrishnan and L. J. Al-Enezi, Power Lindley distribution and associated inference, *Computational Statistics and Data Analysis*, 64 (2013), 20-33.

[21] A. S. Hassan, M. Elgarhy, R. E. Mohamd and S. Alrajhi, On the alpha power transformed power Lindley distribution, *Journal of Probability and Statistics*, 2019 (2019).

[22] D. Hinkley, On quick choice of power transformations, *Applied Statistics*, 26 (1977), 67-69.

[23] E. T. Lee and J. W. Wang , *Statistical Methods for Survival Data Analysis*, Wiley, New York (2003).

[24] D. V. Lindley, Fiducial distributions and Bayes' theorem, *Journal of the Royal Statistical Society, Series A*, 20 (1958), 102-107.

[25] G. W. Liyanage and M. Parai, The generalized power Lindley distribution with its applications, *Asian Journal of Mathematics and Applications*, 2014 (2014), 1-23.

[26] F. Merovci, Transmuted Lindly distribution, *International Journal of Open Problems in Computer Science and Mathematics*, 238 (2013), 1-20.

[27] S. M. T. K. MirMostafaee, M. Alizadeh, E. Altun and S.Nadarajah, The exponentiated generalized power Lindley distribution: Properties and applications, *Applied Mathematics-A Journal of Chinese Universities*, 34 (2019), 127-148.

[28] M. Sankaran, The discrete Poisson-Lindley distribution, *Biometrics*, 26 (1970), 145-149.

[29] R. Shanker, Akash distribution and Its Applications, *International Journal of Probability and Statistics*, 4 (2015), 65-75.

[30] R. Shanker, A quasi Akash distribution. itAssam Statistical Review, 30 (2016), 135-160.

[31] R. Shanker, A. Mishra, A two parameter Lindley distribution, *Statistics in Transition New Series*, 14 (2013a), 45-56.

[32] R. Shanker, A. Mishra. A quasi Lindley distribution, *African Journal of Mathematics and Computer Science Research*, 6 (2013b), 64-71.

[33] R. Shanker and K. K Shukla, Weighted Akash distribution and its application to model lifetime data, *International Journal of Statistics*, 39 (2016), 1138-1147.

[34] V. K. Sharma, S. K. Singh, U. Singh, and F. Merovci, The inverse Lindley distribution: a stress-strength reliability model with application to head and neck cancer data, *Journal of Industrial and Production Engineering*, 32 (2015), 162-173.

[35] L. Tomy, A retrospective study on Lindley distribution, *Biometrics and Biostatistics International Journal*, 7 (2018), 163-169.

[36] H. Zamani and N. Ismail, Negative binomial-Lindley distribution and its application, *Journal of Mathematics and Statistics*, 6 (2010), 4-9.

[37] H. Zeghdoudi and S. Nedjar, Gamma-Lindley distribution and its application, *Journal of Applied Probability and Statistics*, 11 (2016), 129-138.

Christophe Chesneau
Department of Mathematics
Assistant Professor of Mathematics
LMNO, University of Caen- Normandie
Caen, France
E-mail: christophe.chesneau@gmail.com

Lishamol Tomy
Department of Statistics
Assistant Professor of Mathematics
Deva Matha College, Kuravilangad
Kerala, India
E-mail: lishatomy@gmail.com

Meenu Jose
Department of Statistics
Assistant Professor of Mathematics
Carmel College Mala
Thrissur, India
E-mail: meenusgc@gmail.com

Phytotaxa 512 (2): 097–106
https://www.mapress.com/j/pt/

Article

ISSN 1179-3155 (print edition)
PHYTOTAXA
ISSN 1179-3163 (online edition)

https://doi.org/10.11646/phytotaxa.512.2.2

Revisiting the taxonomy of *Strobilanthes homotropa* (Acanthaceae) and a new species *Strobilanthes pradeepiana* from the Western Ghats, India

SINJUMOL THOMAS[1], SUSAI JOHN BRITTO[2] & BINCE MANI[3]*

[1] *Department of Botany, Carmel College, Mala, Thrissur-680732, India.*
sunithatom@gmail.com; https://orcid.org/0000-0003-4907-9197

[2] *The Rapinat Herbarium and Centre for Molecular Systematics, St. Joseph's College (Autonomous), Tiruchirappalli-620002, India.*
sjohnbritto@hotmail.com; https://orcid.org/0000-0002-0501-4271

[3] *Department of Botany, St. Thomas College Palai, Kottayam-686574, India.*
binsnm@gmail.com; https://orcid.org/0000-0002-6076-4622

**Corresponding author: binsnm@gmail.com*

Abstract

Strobilanthes homotropa is an intricate species reported from Nilgiris, India. This taxon was treated in various ways leading to ambiguity in its taxonomic recognition. The present study revisits the taxonomy of *S. homotropa* and provides an amended description for the species. While doing so, *S. homotropa* is segregated from the puzzling species *S. sexennis* and a new species *S. pradeepiana* is recognized.

Keywords: Kerala, Nilgiris, Ootacamund, *Strobilanthes sexennis*, *S. gracilis*

Introduction

Strobilanthes Blume (1826:781) is one of the largest and diverse genera in the family Acanthaceae mainly distributed in tropical and subtropical regions of Asia and Melanesia (Carine & Scotland 2002, Tripp *et al*. 2013, Chen *et al*. 2019, Deng 2019, Chen *et al*. 2020) and comprises about 450 species (Mabberley 2017). In India, the genus is represented by more than 150 species (Karthikeyan *et al*. 2009; Thomas *et al*. 2020), of which approximately 70 species occur in south India alone (Carine & Scotland 2002, Venu, 2006, Krishnapillai 2020). Due to their plietesial flowering pattern and narrow distribution, species delimitation remains problematic in *Strobilanthes* (Wood & Scotland 2009). A comprehensive and critical study of *Strobilanthes* is challenging because many species are inadequately known and seldom disparagingly collected. In the present study, the taxonomy of the complex species *S. homotropa* Nees (1847:187) is re-examined.

Strobilanthes sexennis Nees (1836:312) was described based on the material *Walker s.n.* (*Walker in Herb. Arnott*) collected from Sri Lanka (Ceylon). Eleven years later, along with a detailed description of *S. sexennis*, Nees (1847) described another related species, *S. homotropa* Nees (1847:187), from Nilgiris (Utacamund/Ootacamund), India based on the gathering *Perrottet 119*. The specimens of *S. homotropa* were wrongly treated by some authors resulting in the erroneous treatment of these materials to date. Besides, Nees (1836; 1847) and Wight (1849), one of the major accounts on Indian Acanthaceae was given by Anderson (1867). Anderson, however, excluded *S. homotropa* in his treatments. Meanwhile, a gathering from Nilgiris (*Hohenacker 1432*) was erroneously named *S. interrupta* Benth. ex Clarke (1884: 474) by Bentham (Clarke, 1884). In his '*Icones Plantarum Indiae Orientalis*', Beddome (1874) provided the description and line drawings of *S. sexennis* with synonymy of *S. homotropa* Nees, and stated that *S. sexennis* is common in Nilgiris, Ceylon (Sri Lanka), and Pulneys (Palani). Clarke (1884) re-instated *S. homotropa* as a distinct species from *S. exennis*, and merged *S. interrupta* with *S. sexennis* Nees. Thus, both *S. sexennis* and *S. homotropa* were recorded in Nilgiris (to large extent South India). The erroneous treatments of Nilgiri (Ooty/Ootacamund) specimens by Bentham, Beddome, and Clarke would largely mislead the botanists on the further recognition of these specimens. Therefore, in most of the later floristic accounts, *S. homotropa* Nees was treated as either *S. sexennis* (Trimen 1895, Fyson 1915, Venu 2006, Pradeep 2015), and a related specimen in Travancore high ranges (Munnar, Idukki) as *S. homotropa* (Venu 2006, Pradeep 2015, Augustine 2018) or *S. sexennis* var. *homotropa* (Wood 1995, Wood 1998).

Accepted by Yunfei DENG: 29 Jun. 2021; published: 22 Jul. 2021

Remarkably, the specimen similar to *S. homotropa* Nees and *S. sexennis* Nees found in Travancore high ranges of Idukki (Vagavurai hills, Munnar) is incorrectly recognized yet. It is documented as *S. homotropa* in some literature (Venu 2006, Pradeep 2015, Augustine 2018). This specimen brought our attention during the documentation and critical study of *Strobilanthes* in Munnar, Idukki. A detailed analysis proved that this specimen is totally different from *S. homotropa*, *S. sexennis*, or any known species of *Strobilanthes* in vegetative and floral morphology. Therefore, we treated it as a new species, *Strobilanthes pradeepiana*, described below.

At present, *Strobilanthes homotropa* Nees is treated as a distinct species in the Kew herbarium database (POWO 2020). However, the description for the species in various literature is mixed with the characters of different species (Wood 1995, Wood 1998, Venu 2006, Pradeep 2015, Augustine 2018). Therefore, it is quite necessary to separate *S. homotropa* from its allied species. A detailed study of the life history strategy, herbarium materials (*Perrottet 119, Perrottet s.n., Perrottet 877, Hohenacker 1432*, etc.) and live collections concluded that *S. homotropa* differs from *S. sexennis* and *S. pradeepiana*, and could be a distinct species. Particularly, the south Indian species of the *S. sexennis*-*S. homotropa* allies could easily be set apart by its plietesial life history strategy of 10 years (Pradeep 2018) from Sri Lankan species, which is having 12 years of plietesial life history pattern (Wood 1995, Wood 1998). Besides, it is presumed that *S. homotropa* is a south Indian endemic whereas *S. sexennis* is a Sri Lankan endemic. The present study scrutinized this matter and an amended description of *S. homotropa* is also provided.

Taxonomy

Strobilanthes pradeepiana B. Mani, Sinj. Thomas & Britto, *sp. nov.* (Figures 1–3)

The new species is allied to *S. sexennis* Nees and *S. homotropa* Nees, but it can be easily distinguished from *S. sexennis* by its 10 years of plietesial life history pattern (vs. 12 years), leaf base auriculate (vs. non-auriculate), apex cuspidate (vs. acute or acuminate), bracts oblong (vs. ovate or elliptic), and corolla boles obrenifrom (vs. ovate), and differs from *S. homotropa* by its stem without transverse ridges (vs. with transverse ridges), leaf apex cuspidate (vs. acute–acuminate), bracts oblong (vs. ovate), corolla lobes obrenifrom (vs. orbicular) and ovary apex glabrous (vs. glandular-pubescent ovary apex).

Type:—INDIA. Kerala: Idukki district, Munnar, Vagavurai, 18 October 2018, *Pradeep 68946* (holotype RHT!, isotypes RHT!, MH!).

Description:—Large shrubs, 3–8 m high. Stems quadrangular, canaliculated, hispid, hairs glandular, transverse ridges not prominent. Leaves slightly anisophyllous, petiolate, one or two uppermost pairs become sessile at flowering; petiole 4–5.5 cm long, lamina decurrent on the petiole, base amplexicaul and auriculate, pubescent; blades elliptic, 17–25.5 × 7–12 cm, pubescent on both surfaces, secondary veins 14–16 on each side of midvein and prominent on both surfaces, base cuneate, margin serrate, apex cuspidate; floral lamina elliptic, 8–13 × 2.5–5 cm, pubescent on both surfaces, secondary veins 10–12 on each side of midvein and prominent on both surfaces, base auriculate, margin serrate, apex acuminate–cuspidate. Inflorescences of terminal and axillary branched spikes, stout, 18–25 cm long; rachis glandular pubescent; bracts oblong, 14–20 × 4–5 mm, equal to or longer than calyx at anthesis, 5-nerved from base, glandular pubescent on both surfaces, acute at apex; bracteoles oblong, 10–12 × 1.5–2.5 mm, glandular pubescent on both surfaces, rounded at apex. Flowers ca. 2 mm long pedicellate. Calyx 12–15 mm long, glandular pubescent, 5-lobed to base; lobes linear, nearly equal, apices obtuse. Corolla 3.1–3.4 cm long, campanulate, purple-white, outer surface glabrous, inside pubescent; tube basally cylindrical, ca. 8 mm long, falcate; throat 23–26 mm long, curved at middle; lobes obreniform, ca. 11 × 12 mm, apices emarginate. Stamens 4, didynamous, included; the united part of filaments villous, shorter pair ca. 3 mm long, short hairs present only at base, longer pair ca. 7 mm long, villous throughout; anther thecae oblong, ca. 4 mm long. Ovary ca. 3 mm long, glabrous; style ca. 21 mm long, villous on the abaxial side. Capsule not seen.

Phenology:—Flowering from October–December. This species shows 10 years of plietesial life history strategy.

Etymology:—*Strobilanthes pradeepiana* is named after A. K. Pradeep (WWI Innovative Solutions, Kottayam) for his outstanding contribution to south Indian *Strobilanthes*. He studied and documented the ecology, diversity and life history pattern of *Strobilanthes* of south India for the last two decades.

Distribution and habitat:—The new species is presently known only from in and around Vagavurai hills, Munnar and most probably a narrow endemic (Figure 4). It is one of the major shola undergrowths at an elevation of 1,900–2,400 m.

Notes:—*Strobilanthes pradeepiana* is an overlooked species, and differs from allied species *S. homotropa* and *S. sexennis* by its stem without transverse ridges (not having ridged stem), hispid lamina with cuspidate apex (not glabrous and having acute-acuminate apex), oblong bracts with acute apex (not ovate or elliptic with obtuse apex), obreniform corolla with emarginated apex (not orbicular with retuse apex or ovate with sub-acute apex). A detailed comparison of diagnostic features of these species are given in Table 1.

TABLE 1. Diagnostic characters of *S. homotropa*, *S. pradeepiana* and *S. sexennis*†.

Characters	***S. homotropa***	***S. pradeepiana***	***S. sexennis***
Periodicity	10 years	10 years	12 years
Stem	Terete	Quadrangular	Quadrangular
Transverse ridges	Conspicuous	Absent	Conspicuous
Pubescence	Glabrous	Hispid, glandular	Glabrous
Leaves	Auriculate	Auriculate and amplexicaul	Non-auriculate
Blade			
Shape	Narrowly elliptic -lanceolate	Elliptic	Narrowly elliptic or ovate or oblong
Base	Attenuate	Cuneate	Cuneate or rounded or cordate
Apex	Acute-acuminate	Cuspidate	Acuminate
Pubescence	Glabrous	Hispid	Glabrous
Petiole	Decurrent, base auriculate	Decurrent, base auriculate	Not decurrent, base not auriculate
Inflorescence	Non-secund	Non-secund	Secund
Bracts			
Shape	Ovate or elliptic, saccate	Oblong	Ovate or elliptic
Apex	Obtuse	Acute	Obtuse
Bracteoles			
Shape	Oblanceolate-spathulate	Oblong	Oblong or Oblanceolate or elliptic or obovate
Calyx			
Lobes	Equal	Subequal	Subequal
Apex	Obtuse-acute	Obtuse	Obtuse
Corolla			
Lobes	Orbicular	Obreniform	Ovate
Apex	Retuse	Emarginate	Sub-acute
Ovary apex	Glandular pubescent	Glabrous	Glabrous

† Wood 1995; Wood 1998

Additional specimens examined (paratypes):—INDIA. Kerala: Idukki, Munnar, Vagavurai hills, 16 September 2008, *Pradeep 68940* (RHT); same locality, 03 September 2018, *Pradeep 68945* (RHT); same locality, 25 November 2018, *Pradeep 68875* (RHT).

FIGURE 1. *Strobilanthes pradeepiana*. A. Inflorescence; B. Bracts; C. Bracteoles; D. Flower; E. Calyx; F. Corolla l. s.; G. Pistil. Illustrated by Philominal Selvi.

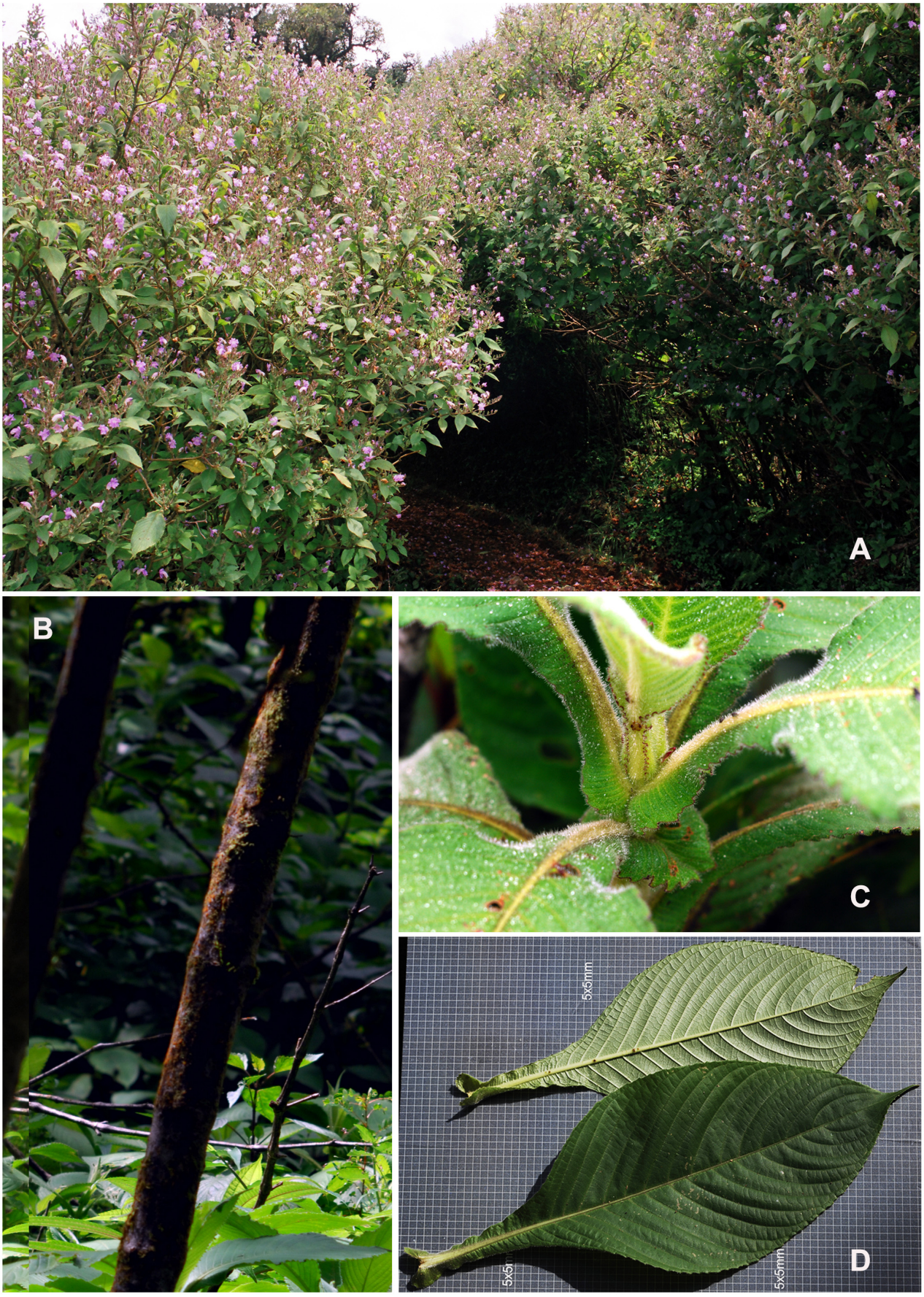

FIGURE 2. *Strobilanthes pradeepiana*. A. Habit; B. Old stem; C. Young stem with amplexicaul leaf base; D. Leaves.

FIGURE 3. *Strobilanthes pradeepiana*. A–B. Inflorescence; C. Bracts; D. Bracteoles; E. Calyx; F. Corolla; G. Corolla opened; H. Pistil; I. Young infructescence.

Strobilanthes homotropa Nees (1847: 187). ≡ *Mackenziea homotropa* (Nees) Bremekamp (1944: 182). ≡ *Strobilanthes sexennis* var. *homotropa* (Nees) Wood (1995: 19). **Type**:—INDIA. Tamil Nadu: Nilgiris, Ootacamund, 1840, *Perrottet 119* (holotype P! P00719346). (Figure 5)

Strobilanthes interrupta Benth. ex Clarke (1884: 474). **Type**:—INDIA. Tamil Nadu: Nilgiris, Doddabetta, *Hohenacker 1432* (holotype K!).

Description:—Large shrubs, 3–8 m high. Stems terete, glabrous, transverse ridges present. Leaves slightly anisophyllous, petiolate, few upper most pairs become sessile at flowering; petiole 5–7 cm long, lamina decurrent on the petiole, base amplexicaul and auriculate, glabrous; blades narrowly elliptic to lanceolate, 17–21 × 5–7 cm, glabrous, secondary veins 8–10 on each side of midvein and prominent on both surfaces, base attenuate, margin serrate, apex acute to acuminate; floral lamina oblong-narrowly elliptic, 7–12 × 2–3 cm, glabrous, secondary veins 5–8 on each side of midvein and prominent on both surfaces, base auriculate, margin serrate, apex acute to acuminate. Inflorescences of terminal and axillary branched spikes, stout, 12–23 cm long; rachis glandular pubescent; bracts ovate, 12–16 × 7–9 mm, equal to or longer than calyx at anthesis, 5-nerved from base, glandular pubescent on both surfaces, obtuse at apex; bracteoles oblanceolate-spathulate, 9–10 × ca. 2.5 mm, glandular pubescent on both surfaces, obtuse at apex. Flowers ca. 1.5 mm long pedicellate. Calyx 10–12 mm long, glandular pubescent, 5-lobed to base; lobes linear, equal, apices obtuse-acute. Corolla 2–2.4 cm long, campanulate, purple-white or white, outer surface glabrous, inside pubescent; tube basally cylindrical, ca. 4 mm long; throat 16–20 mm long, curved at middle; lobes orbicular, ca. 6 × 7 mm, apices retuse. Stamens 4, didynamous, included; filaments villous, shorter pair ca. 2.5 mm long, longer pair ca. 7 mm long; anther thecae oblong, ca. 3.5 mm long. Ovary ca. 2 mm long, glandular pubescent at apex; style ca. 22 mm long, villous on the abaxial side. Capsule not seen.

Phenology:—Flowering from October–December, every 10 years.

Distribution and habitat:—This species is chiefly distributed in different parts of the Nilgiris especially in the Doddabetta hills, Tamil Nadu. Its distribution extends up to southern parts of Anamalai hill ranges in the south (Figure 4). It is one of the major shola species in this region and found at an elevation of 2,000–2,630 m.

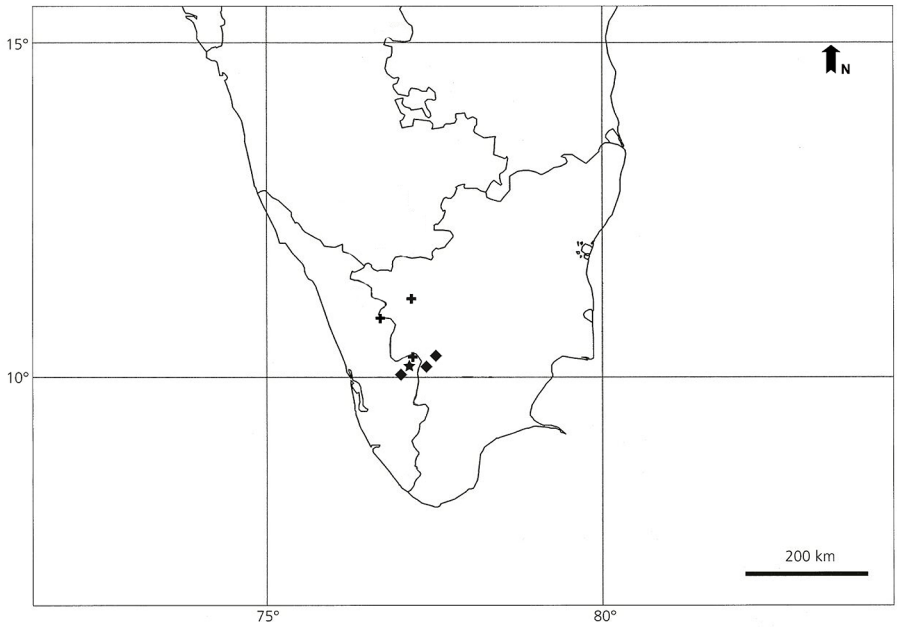

FIGURE 4. Distribution of *Strobilanthes homotropa* (✚), *S. pradeepiana* (★) and *S. gracilis* (◆).

Notes:—*Strobilanthes homotropa* is confusable with *S. gracilis* Beddome (1864:55) by the transversely ridged stems and glossy leaves. The latter species is found in the Anamalai hills, Palani (Pulney) hills, and Travancore hills (Gamble 1924) of south India. The occurrence of *S. sexennis* in south India shall be a mistake by Beddome (1874), who might also wrongly documented *S. homotropa* in the Nilgiris and few populations of *S. gracilis* in the Palani Hills. It is evident from the floristic account on Palani Hills that it doesn't mention the occurrence of *S. homotropa* in Palani Hills (Matthew 1999). The taxonomic ambiguity regarding the identity of *S. homotropa* might be due to its treatments that were mainly based on herbarium specimens and also failed to observe the live materials. *Strobilanthes homotropa* can be easily distinguished from *S. sexennis* by the characteristics of plietesial life history strategy of 10 years (not

twelve years), lamina auriculate (not non-auriculate), non-secund inflorescences (not secund inflorescences), flowers pedicellate (not sessile), and ovary glandular-pubescent at apex (not glabrous). The comparison between *S. homotropa* and *S. sexennis* is shown in Table 1.

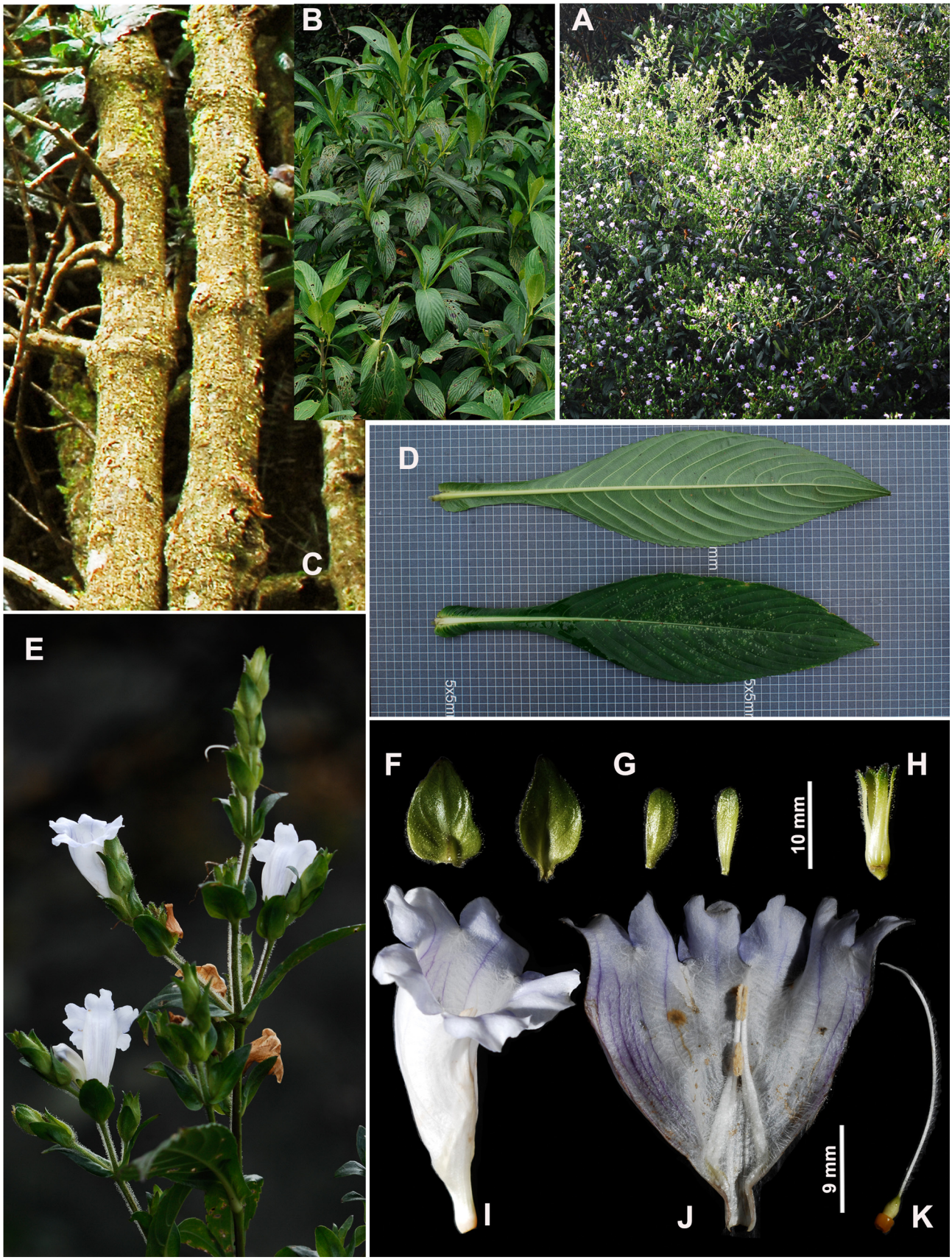

FIGURE 5. *Strobilanthes homotropa*. A–B. Habit; C. Stem with transverse ridges; D. Leaves; E. Inflorescence; F. Bract; G. Bracteole; H. Calyx; I. Corolla; J. Corolla opened; K. Pistil.

Specimens examined

Strobilanthes homotropa:—INDIA. **Kerala**: Idukki, Munnar, 08 October 2010, *Pradeep 68942* (RHT); 31 October 2020, *Pradeep 68948* (RHT). **Tamilnadu**: Nilgiris, 20 October 2007, *Pradeep 68943* (RHT); 06 December 2017, *Pradeep 68944* (RHT); Nilgiris, 1875, *Beddome s. n.* (MH); Ootacamund, 1840, *Perrottet 119* (P); Nilgiris, *Perrottet 877* (P, K); *Perrottet s.n.* (GZU); Doddabetta, *Hohenacker 1432* (K, US, P, L); Dodabetta, 8000 ft., October 1883, *Gamble 12950* (MH); Dodabetta, *Metz 1848* (P); Conoor, *Perrottet s.n.* (P); Sispara, April 1884, *Beddome 28* (MH); Sispara, November 1883, *Gamble 13386* (MH); January 1884, *Gamble 14254* (MH); 5000 ft., May 1884, *Gamble 14254* (MH).

Strobilanthes sexennis* var. *sexennis:—SRI LANKA. *Walker s.n.* (holotype E-GL); *Walker 107* (K); Nuwara Eliya district: Shanthipura, 03 November 1994, *Scotland & Jayaselsara 19* (L); Trail up Pidurutalagala, 20 September 1975, *Foster 5010* (US); Horton Plains, 30 October 1976, *Jayasuriya 2384* (US); along trail from Big World's End, Horton Plains to tea estate bungalow near Galagama Falls, 27 December 1970, *Theobald & Krahulik 2831* (US); Horton Plains, 20 October 1993, *Cramer, Jayasekera & Samarasinghe 6862* (US); on the track between Big World's End and bungalow above Nonpareil Estate, Montane Forest, 05 March 1977, Bremer 970 (US).

Strobilanthes sexennis* var. *cerinthoides:—SRI LANKA. *Walker s.n.* (holotype K); *Walker s.n.* (E-GL); 1854, *Thwaites C P 66* (P) 1853, *Thwaites C P 2594* (K); 1839, *MacKenzie s.n.* (K); De Carney ad Adam's Peak, 07 December 1975, *Bernardi 15794* (US); Maskaliya: de Tanna ad Adam's Peak, 12 December 1975, *Bernardi 15935* (US).

Strobilanthes sexennis* var. *hirsutissima:—SRI LANKA. *Walker s.n.* (E-GL); *Walker 195* (K). **Nuwara Eliya District**: on steep ascent from Pattipola to Horton Plains, 26 December 1970, *Theobald & Krahulik 2826* (US); Trail up Pidurutalagala, 21 September 1975, Foster 5009 (US); open shrubby area near edge of small stream along A-5 Highway, Westward Ho tea estate north of Nuwara Eliya, 02 December 1970, *Theobald & Krahulik 2724* (US).

Strobilanthes sexennis* var. *arguta:—SRI LANKA. *Walker s.n.* (K); *Walker 107* (K). **Nuwara Eliya District**: Horton Plains, in undergrowth along embankments of Pattipola-Horton Plains road, 20 October 1993, *Cramer 6860* (US); Hakgala, 23 April 1970, *Cramer 2921* (US); on steep ascent from Pattipola to Horton Plains, 26 December 1970, *Theobald & Krahulik 2827* (US); Pedro, 19 August 1970, *Cramer 3129* (US).

Strobilanthes sexennis* var. *cordata:—SRI LANKA. 1860, *Thwaites C P 3626* (K).

Strobilanthes sexennis* var. *glaberrima:—SRI LANKA. **Matale District**: Laggala, 10 November 1978, *Cramer 5231* (K, US).

Strobilanthes sexennis* var. *oblongifolia:—SRI LANKA. Rasamalayi, Gartmore, July 1925, *Stockdale s.n.* (holotype K); *Stockdale 73* (K).

Strobilanthes gracilis:—INDIA. **Kerala**: Idukki, Munnar, Vagavurai, 10 November 2008, *Pradeep 68941* (RHT); 17 December 2018, *Pradeep 68947* (RHT).

Acknowledgments

The authors are grateful to the authorities of Carmel College Mala, Rapinat Herbarium, St. Joseph's College (Autonomous), Tiruchirappalli and St. Thomas College Palai for providing research facilities. We would like to thank the curators of various herbaria (CAL, E, GZU, K, MH, P, RHT, and US) for providing access to the specimens.

References

Anderson, T. (1867) An enumeration of the Indian species of Acanthaceae. *The Journal of the Linnean Society, Botany* 9: 425–526. https://doi.org/10.1111/j.1095-8339.1867.tb01308.x

Augustine, J. (2018) *Strobilanthes Blume in the Western Ghats, India*. Malabar Natural History Society, Kozhikode, 152 pp.

Beddome, R.H. (1864) Contributions to the Botany of Southern India. *The Madras Journal of Literature and Science*, *Ser.3* 1: 55. [https://www.biodiversitylibrary.org/item/164965]

Beddome, R.H. (1874) *Icones Plantarum Indiae Orientalis*, vol. 1. Gantz Brothers, Madras, 70 pp., 300 t. [https://www.biodiversitylibrary.org/item/262606]

Blume, C.L. (1826) *Bijdragen tot de Flora van Nederlandsch Indie* 14. Ter Lands Drukkerij, Batavia, pp. 780–807. https://doi.org/10.5962/bhl.title.395

Carine, M.A. & Scotland, R.W. (2002) Classification of *Strobilanthinae* (Acanthaceae): trying to classify the unclassifiable? *Taxon* 51: 259–279.
https://doi.org/10.2307/1554897

Chen, J-T., Huang, X-H., Lv, Z-Y., Kuang, T.-H., Luo, J., Deng, Y.F. & Deng, T. (2020) *Strobilanthes sunhangii* (Acanthaceae), a new species from Tibet, China. *PhytoKeys* 166: 117–127.
https://doi.org/10.3897/phytokeys.166.58831

Chen, F.L., Deng, Y.F., Xiong, Z.B. & Ran, J.C. (2019) *Strobilanthes hongii*, a new species of Acanthaceae from Guizhou, China. *Phytotaxa* 388 (1): 135–144.
https://doi.org/10.11646/phytotaxa.388.1.7

Clarke, C.B. (1884) Acanthaceae. *In*: Hooker, J.D. (Ed.) *Flora of British India* 4. L. Reeve, London. pp. 387–558.
https://www.biodiversitylibrary.org/item/13817

Deng, Y.F. (2019) Transfer of the Philippine species of *Hemigraphis* Nees to *Strobilanthes* Blume (Acanthaceae). *Phytotaxa* 404 (5): 203–208.
https://doi.org/10.11646/phytotaxa.404.5.3

Fyson, P.F. (1915) *The Flora of the Nilgiri and Pulney Hill-tops*1. The Superintendent, Govt. Press, Madras, pp. 312–314.
https://doi.org/10.5962/bhl.title.10798

Gamble, J.S. (1924) *Flora of the Presidency of Madras* 2. West, Newman & Adlard, London, pp. 1025–1044.
https://www.biodiversitylibrary.org/item/10372

Karthikeyan, S., Sanjappa, M. & Moorthy, S. (2009) *Flowering Plants of India, a check-list of Dicotyledones*, vol. 1. Botanical Survey of India, Kolkata, India, pp. 41–60.

Krishnapillai, P.A., Thomas, S., Britto, S.J. & Mani, B. (2020) Amending *Strobilanthes gamblei* (Acanthaceae) and an overlooked new species *Strobilanthes bourdillonii* from the Western Ghats, India. *Phytotaxa* 472 (1): 49–55.
https://doi.org/10.11646/phytotaxa.472.1.6

Mabberley, D.J. (2017) *Mabberley's Plant-book: A portable dictionary of plants, their classification and uses*, 4th Ed. Cambridge University Press. Cambridge, UK, 1102 pp.
https://doi.org/10.1017/9781316335581

Matthew, K.M. 1999. *The Flora of the Palni Hills, South India* 2. The Rapinat Herbarium, Tiruchirapalli, India, pp. 576–1196.

Nees Von Esenbeck, C.G. (1836) Characters of new species of Indian Acanthaceae. *Companion to the Botanical Magazine* 2: 310–313. [https://www.biodiversitylibrary.org/item/107303]

Nees Von Esenbeck, C.G. (1847). Acanthaceae. *In*: De Candolle, A. (Ed.) *Prodromus systematis naturalis regni vegetabilis* 11. Masson, Paris, pp. 46–519.
https://www.biodiversitylibrary.org/item/7160

POWO (2020) Plants of the world online, Facilitated by the Royal Botanic Gardens, Kew. Available from: http://www.plantsoftheworldonline.org/taxon/urn:lsid:ipni.org:names:55733-1 (accessed 25 December 2020)

Pradeep, A.K. (2015) *Kurinji field guide: Eravikulam National Park* 1. Anamudi Forest Development Agency, Wildlife Division, Munnar, 70 pp.

Pradeep, A.K. (2018) *Kurinji field guide: Eravikulam National Park* 2. Anamudi Forest Development Agency, Wildlife Division, Munnar, 70 pp.

Thomas, S., Mani, B., Britto, S.J., Deng, Y.F., Pradeep, A.K. & Santhosh Kumar, E.S. (2020) Notes on *Strobilanthes cuspidata* with reinstatement of *Endopogon versicolor* (Acanthaceae). *Plant Science Today* 7: 29–38.
https://doi.org/10.14719/pst.2020.7.1.627

Trimen, H. (1895) *A handbook to the flora of Ceylon*. Dulau & Co., London, 477 pp.

Tripp, E.A., Daniel, T.F., Fatimah, S. & McDade, L.A. (2013) Phylogenetic relationships within Ruellieae (Acanthaceae) and a revised classification. *International Journal of Plant Sciences* 174: 97–137.
https://doi.org/10.1086/668248

Venu, P. (2006) *Strobilanthes Blume (Acanthaceae) in Peninsular India*. Botanical Survey of India, Kolkata, 216 pp.

Wight, R. (1849) *Icones Plantarum Indiae Orientalis* 4. J.B. Pharoah, Madras, 74 pp., 458 t. [https://www.biodiversitylibrary.org/item/1859]

Wood, J.R.I. (1995) Notes on *Strobilanthes* (Acanthaceae) for the Flora of Ceylon. *Kew Bulletin* 50 (1): 1–24.
https://doi.org/10.2307/4114605

Wood, J.R.I. (1998) *Strobilanthes*. *In*: Dassanayake, M.D. & Clayton, W.D. (Eds.) *A revised hand book to the flora of Ceylon* 12. A.A. Balkema, Netherlands, pp. 21–65.

Wood, J.R.I. & Scotland, R.W. (2009) New and little-known species of *Strobilanthes* (Acanthaceae) from India and South East Asia. *Kew Bulletin* 64: 3–47.
https://doi.org/10.1007/s12225-009-9098-2

Wrapped modified Lindley distribution

Article · April 2021

DOI: 10.1080/09720510.2020.1796313

CITATION
1

READS
40

3 authors:

Christophe Chesneau
Université de Caen Normandie
289 PUBLICATIONS **1,250** CITATIONS
SEE PROFILE

Lishamol Tomy
Deva Matha College Kuravilangad, kottayam, Kerala, India
39 PUBLICATIONS **89** CITATIONS
SEE PROFILE

Meenu Jose
3 PUBLICATIONS **1** CITATION
SEE PROFILE

Journal of Statistics and Management Systems

ISSN: (Print) (Online) Journal homepage: https://www.tandfonline.com/loi/tsms20

Wrapped modified Lindley distribution

Christophe Chesneau, Lishamol Tomy & Meenu Jose

To cite this article: Christophe Chesneau, Lishamol Tomy & Meenu Jose (2021): Wrapped modified Lindley distribution, Journal of Statistics and Management Systems, DOI: 10.1080/09720510.2020.1796313

To link to this article: https://doi.org/10.1080/09720510.2020.1796313

Published online: 18 Apr 2021.

Journal of Statistics & Management Systems
ISSN 0972-0510 (Print), ISSN 2169-0014 (Online)
DOI : 10.1080/09720510.2020.1796313

Taylor & Francis
Taylor & Francis Group

Wrapped modified Lindley distribution

Christophe Chesneau*
Department of Mathematics
Université de Caen
LMNO
Campus II
Science 3
Caen 14032
France

Lishamol Tomy†
Department of Statistics
Deva Matha College
Kuravilangad 686633
Kerala
India

Meenu Jose§
Department of Statistics
Carmel College, Mala
Thrissur 680732
Kerala
India

Abstract

To model data in angular form, circular distributions are the most appropriate mathematical tools. In this paper, we introduce a new one-parameter circular distribution based on the wrapping method, called the wrapped modified Lindley distribution. Characteristic function and fundamental properties of this distribution are described. Method of maximum likelihood estimation is used for the estimation of the parameter. The proposed model is applied to two real-life datasets, and its performance is compared with

*E-mail: christophe.chesneau@gmail.com (Corresponding Autor)
†E-mail: lishatomy@gmail.com
§E-mail: meenusgc@gmail.com

that of the wrapped Lindley, wrapped exponential and transmuted wrapped exponential models.

Subject Classification: *60E05, 62E15, 62F10.*

Keywords: *Modified Lindley distribution, Wrapped Lindley distribution, Trigonometric moments, Characteristic function, Method of maximum likelihood, Data analysis.*

1. Introduction

When the data points are distributed on a circle instead of the real line (or part of it), the related phenomenon can be not modeled by a random variable having standard distributions, motivating the emergence of the so-called circular distributions. In contemporary scenarios, the use of circular distributions has been relevant in various circumstances like astronomy, demography, image analysis, geology, meteorology and earth science. For this reason, numerous researchers develop circular distributions with various features, aiming to extend the scope of applications in this setting. Here, arises the scope of study of circular data by using circular models.

As prime definition, a circular distribution is a probability distribution whose total probability is concentrated on an unit circle in the plane, i.e., $\{(\cos(\theta), \sin(\theta));\ \theta \in [0, 2\pi)\}$. Wrapping is one of the methods to create a circular distribution. If X is a random variable defined on a real line, then the corresponding wrapped random variable θ is defined as $\theta = X \pmod{2\pi}$. This method creates a wide class of probability distributions that are flexible to accommodate the different characteristics of circular data. In particular, Levy (1939) proposed wrapped distributions which laid the first stone of this method. Several authors have done extensive works on introducing wrapped distributions and studying their statistical properties and inference procedures. We refer the reader to the wrapped Laplace distribution by Jammalamadaka and Kozubowski (2003), wrapped exponential distribution by Jammalamadaka and Kozubowski (2004), wrapped t family circular distribution by Pewsey *et al.* (2007), wrapped gamma distribution by Coelho (2007), wrapped stable family of distributions by Pewsey (2008), wrapped three-parameter gamma distribution by Roy and Adnan (2010), wrapped chi-square distribution by Adnan and Roy (2011), wrapped weighted exponential distribution by Roy and Adnan (2012), wrapped generalized Gompertz distribution by Roy and Adnan (2012), wrapped geometric distribution by Jacob and Jayakumar (2013) and wrapped variance gamma distribution by Adnan and Roy (2014). Recently, Joshi and Jose (2017) proposed a new

circular distribution by wrapping the Lindley distribution and applied it for biological data. Also, Yilmaz and Bicer (2018) derived transmuted wrapped exponential distribution and studied its properties.

In the last decades, the Lindley distribution and its generalizations have been widely used by different authors. In this regard, we may refer the interested reader to Singh et al. (2016), Elgarhy et al. (2018) and Tomy (2018), and the references therein. As a recent development, Chesneau et al. (2019) derived the modified Lindley distribution, constituting a one-parameter lifetime distribution halfway between the exponential and Lindley distributions with desirable modelling properties. On the other side, circular models that can be generated by wrapping known distributions have wide applications in the present scenario. In this article, we adapt the modified Lindley distribution in view of analyzing circular data by wrapping the modified Lindley probability density function around the circumference of a unit circle. The resulting distribution is called the wrapped modified Lindley distribution. We explore the theoretical and practical properties of this new wrapped distribution. In particular, we show that, in some situations, the wrapped modified Lindley distribution provides a serious alternative to modern distributions using the wrapping technique, such as the transmuted wrapped exponential, wrapped exponential and wrapped Lindley distributions.

The rest of the paper is organized as follows. In Section 2, we introduce the wrapped modified Lindley distribution and, in Section 3, we discuss its different properties, including the trigonometric moments. The maximum likelihood estimator of the unknown parameter is described in Section 4. In Section 5, the analysis of two real data set is presented, illustrating the modeling potential of the wrapped modified Lindley distribution. Finally, the conclusion of the paper appears in Section 6.

2. The wrapped modified Lindley distribution

Recently, Chesneau et al. (2019) proposed a new general family of modified Lindley distributions. It is defined by a cumulative density function (cdf) which is a particular weighted modification of the cdf of the Lindley distribution. The modified Lindley (ML) distribution is a special member of this family, defined with a particular weighted exponential function, making it halfway between the exponential and Lindley distributions. More precisely, the ML distribution with parameter $\lambda > 0$ is characterized by

$$F(x) = 1-\left[1+\frac{\lambda x}{1+\lambda}e^{-\lambda x}\right]e^{-\lambda x}; \qquad x>0. \tag{1}$$

By differentiation of $F(x)$, the corresponding probability density function (pdf) is given by

$$f(x) = \frac{\lambda}{1+\lambda}e^{-2\lambda x}\left[(1+\lambda)e^{\lambda x}+2\lambda x-1\right]; \quad x>0, \lambda>0.$$

An important remark is that we can write $f(x)$ as

$$f(x) = f_1(x)+a(f_2(x)-f_3(x)), \tag{2}$$

where $f_1(x)$ is the pdf of the exponential distribution with parameter λ, i.e., $f_1(x)=\lambda e^{-\lambda x}$, $x>0$, $f_2(x)$ is the pdf of the gamma distribution with parameters $(2,2\lambda)$, i.e., $f_2(x)=(2\lambda)^2 x e^{-2\lambda x}$, $x>0$, $f_3(x)$ is the pdf of the exponential distribution with parameter 2λ, i.e., $f_3(x)=2\lambda e^{-2\lambda x}$, $x>0$, and $a=1/[2(1+\lambda)]\in(0,1/2)$.

Now, we propose a circular (wrapped) form of the ML distribution. Let X be a random variable following the ML distribution with parameter λ. Then, the wrapped modified Lindley (WML) distribution is defined by the one of $\theta = X \pmod{2\pi}$. The random variable θ having the WML distribution is denoted by $\theta \sim \text{WML}(\lambda)$. The rest of this section is devoted to the main functions related to the WML distribution, i.e., its pdf and cdf, with some plots as illustration.

The result above presents the corresponding pdf of the WML distribution.

Proposition 2.1 : The pdf of $\theta \sim WML(\lambda)$ is given by

$$g(\theta) = \frac{\lambda e^{-\lambda\theta}}{1-e^{-4\lambda\pi}}\left\{1+e^{-2\lambda\pi}+\frac{e^{-\lambda\theta}}{1+\lambda}\left[2\lambda\theta-1+\frac{4\lambda\pi e^{-4\lambda\pi}}{1-e^{-4\lambda\pi}}\right]\right\};$$
$$\lambda>0,\ \theta\in[0,2\pi). \tag{3}$$

Proof : As alpha definition, based on (2), the pdf of $\theta \sim \text{WML}(\lambda)$ is given by

$$g(\theta) = \sum_{m=0}^{+\infty} f(\theta+2m\pi) = \sum_{m=0}^{+\infty} f_1(\theta+2m\pi)+$$
$$a\left[\sum_{m=0}^{+\infty} f_2(\theta+2m\pi)-\sum_{m=0}^{+\infty} f_3(\theta+2m\pi)\right].$$

Now, remark that, after some algebra,

$$\sum_{m=0}^{+\infty} f_1(\theta+2m\pi) = \lambda e^{-\lambda\theta}\sum_{m=0}^{+\infty} e^{-2m\lambda\pi} = \frac{\lambda e^{-\lambda\theta}}{1-e^{-2\lambda\pi}},$$

$$\begin{aligned}\sum_{m=0}^{+\infty} f_2(\theta+2m\pi) &= (2\lambda)^2 e^{-2\lambda\theta}\sum_{m=0}^{+\infty}(\theta+2m\pi)e^{-4m\lambda\pi} \\ &= (2\lambda)^2 e^{-2\lambda\theta}\left[\frac{\theta}{1-e^{-4\lambda\pi}} + \frac{2\pi e^{-4\lambda\pi}}{(1-e^{-4\lambda\pi})^2}\right]\end{aligned}$$

and

$$\sum_{m=0}^{+\infty} f_3(\theta+2m\pi) = 2\lambda e^{-2\lambda\theta}\sum_{m=0}^{+\infty} e^{-4m\lambda\pi} = \frac{2\lambda e^{-2\lambda\theta}}{1-e^{-4\lambda\pi}}.$$

Therefore, by putting the above equalities together, we obtain

$$\begin{aligned} g(\theta) &= \sum_{m=0}^{+\infty} f(\theta+2m\pi) \\ &= \frac{\lambda e^{-\lambda\theta}}{1-e^{-2\lambda\pi}} + \frac{1}{2(1+\lambda)}\left[(2\lambda)^2 e^{-2\lambda\theta}\left(\frac{\theta}{1-e^{-4\lambda\pi}} + \frac{2\pi e^{-4\lambda\pi}}{(1-e^{-4\lambda\pi})^2}\right) - \frac{2\lambda e^{-2\lambda\theta}}{1-e^{-4\lambda\pi}}\right] \\ &= \frac{\lambda e^{-\lambda\theta}}{1-e^{-2\lambda\pi}} + \frac{\lambda e^{-2\lambda\theta}}{1+\lambda}\left[\frac{2\lambda\theta-1}{1-e^{-4\lambda\pi}} + \frac{4\lambda\pi e^{-4\lambda\pi}}{(1-e^{-4\lambda\pi})^2}\right] \\ &= \frac{\lambda e^{-\lambda\theta}}{1-e^{-4\lambda\pi}}\left\{1+e^{-2\lambda\pi} + \frac{e^{-\lambda\theta}}{1+\lambda}\left[2\lambda\theta - 1 + \frac{4\lambda\pi e^{-4\lambda\pi}}{1-e^{-4\lambda\pi}}\right]\right\}. \end{aligned}$$

This ends the proof of Proposition 2.1. □

Remark 2.2 : We can write the pdf $g(\theta)$ as a linear combination of wrapped exponential and wrapped gamma pdfs as

$$g(\theta) = g_1(\theta) + a\big(g_2(\theta) - g_3(\theta)\big),$$

where $g_1(\theta)$ is the pdf of the wrapped exponential distribution with parameter λ, i.e., $g_1(\theta) = \lambda e^{-\lambda\theta}/(1-e^{-2\lambda\pi})$, $\theta \in [0, 2\pi)$, $g_2(\theta)$ is the pdf of the wrapped gamma distribution with parameters $(2, 2\lambda)$, i.e., $g_2(\theta) = (2\lambda)^2 e^{-2\lambda\theta}[\theta/(1-e^{-4\lambda\pi}) + 2\pi e^{-4\lambda\pi}/(1-e^{-4\lambda\pi})^2]$, $\theta \in [0, 2\pi)$, $g_3(\theta)$ is the pdf of the wrapped exponential distribution with parameter 2λ, i.e., $g_3(\theta) = 2\lambda e^{-2\lambda\theta}/(1-e^{-4\lambda\pi})$, $\theta \in [0, 2\pi)$, and $a = 1/[2(1+\lambda)]$. This representation will be useful to determine the fundamental properties of the WML distribution.

The cdf of $\theta \sim \text{WML}(\lambda)$ is obtained as follows, after some algebra similar to those in the proof of Proposition 2.1,

$$\begin{aligned} G(\theta) &= \sum_{m=0}^{+\infty}[F(\theta+2m\pi)-F(2m\pi)] \\ &= \sum_{m=0}^{+\infty}\left(\left[1+\frac{2m\lambda\pi}{1+\lambda}e^{-2m\lambda\pi}\right]e^{-2m\lambda\pi}-\left[1+\frac{\lambda(\theta+2m\pi)}{1+\lambda}e^{-\lambda(\theta+2m\pi)}\right]e^{-\lambda(\theta+2m\pi)}\right) \\ &= (1-e^{-\lambda\theta})\frac{1}{1-e^{-2\lambda\pi}}+\frac{2\lambda\pi}{1+\lambda}(1-e^{-2\lambda\theta})e^{-4\lambda\pi}\frac{1}{(1-e^{-4\lambda\pi})^2} \\ &\quad -\frac{\lambda\theta}{1+\lambda}e^{-2\lambda\theta}\frac{1}{1-e^{-4\lambda\pi}}. \end{aligned} \tag{4}$$

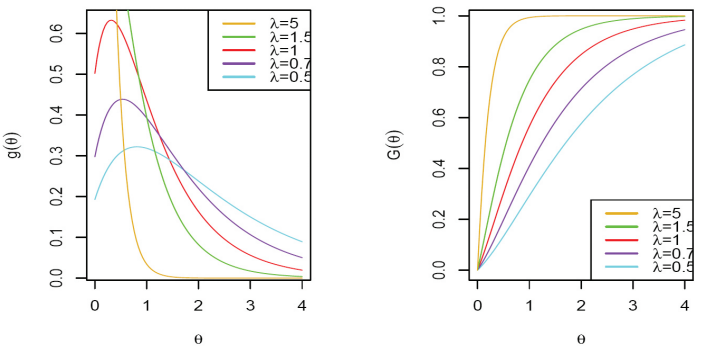

Figure 1

Pdf and cdf of the WML distribution for various values of λ.

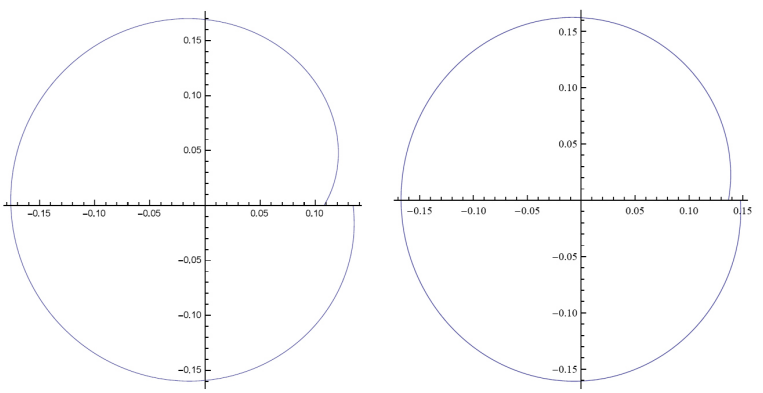

Figure 2

Circular representation of the pdf of the WML distribution for $\lambda = 0.15$ and $\lambda = 0.1$, respectively.

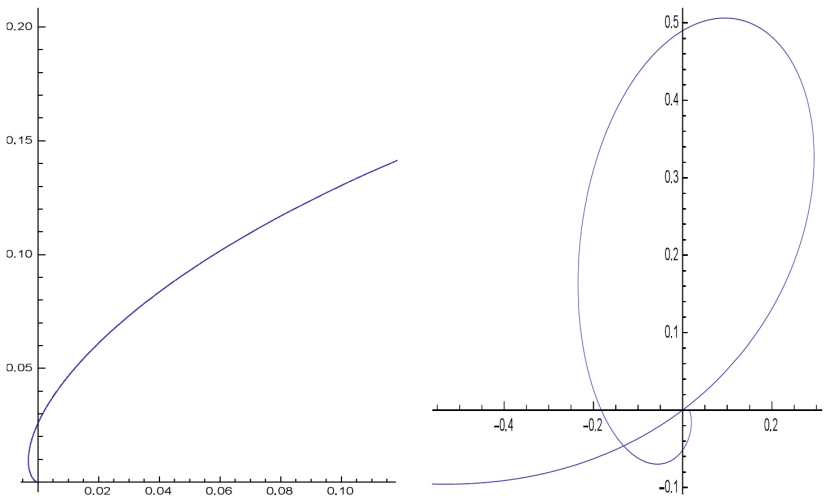

Figure 3

Circular representation of the pdf of the WML distribution for $\lambda = 3$ and $\lambda = 0.65$, respectively.

Figure 1 depicts the behavior of the pdf and cdf of the proposed distribution for different values of λ. The plots indicate that the WML distribution can be reverse J-shaped and left-skewed. Also, the circular presentations of the WML pdf for different parameter values are shown in Figures 2 and 3.

3. Fundamental properties

Here, we present some fundamental properties of the WML distribution, starting with its characteristic function. First of all, by denoting $\mathbb{E}$ the expectation and i the unit imaginary number, let us recall that the characteristic function of the ML distribution is given by

$$\varphi(t) = \mathbb{E}(e^{itX}) = \frac{\lambda}{\lambda - it} + \frac{it\lambda}{(1+\lambda)(2\lambda - it)^2}; \quad t \in \mathbb{R}.$$

After some algebra, we get

$$\varphi(t) = \frac{\lambda^2}{\lambda^2 + t^2} - \frac{4\lambda^2 t^2}{(1+\lambda)(4\lambda^2 + t^2)^2}$$

$$+i\left[\frac{\lambda t}{\lambda^2+t^2}+\frac{4\lambda^3 t}{(1+\lambda)(4\lambda^2+t^2)^2}-\frac{\lambda t^3}{(1+\lambda)(4\lambda^2+t^2)^2}\right].$$

For $p=\pm1,\pm2,\ldots,$ the p^{th} trigonometric moment of θ is given by

$$\varphi_p = \varphi(p)=\alpha_p+i\beta_p,$$

where α_p and β_p are the p^{th} non-central trigonometric moments of the respective distribution

$$\begin{aligned}\alpha_p &= \frac{\lambda^2}{\lambda^2+p^2}-\frac{4\lambda^2p^2}{(1+\lambda)(4\lambda^2+p^2)^2}\\ &= \frac{\lambda^2(16\lambda^5+16\lambda^4+8\lambda^3p^2+4\lambda^2p^2+\lambda p^4-3p^4)}{(1+\lambda)(\lambda^2+p^2)(4\lambda^2+p^2)^2}\end{aligned}$$

and

$$\begin{aligned}\beta_p &= \frac{\lambda p}{\lambda^2+p^2}+\frac{4\lambda^3 p}{(1+\lambda)(4\lambda^2+p^2)^2}-\frac{\lambda p^3}{(1+\lambda)(4\lambda^2+p^2)^2}\\ &= \frac{\lambda^2 p(16\lambda^4+20\lambda^3+8\lambda^2p^2+11\lambda p^2+p^4)}{(1+\lambda)(\lambda^2+p^2)(4\lambda^2+p^2)^2}.\end{aligned}$$

One can remark that $\beta_p \geq 0$. Also, by analogy, note that $\alpha_p=\mathbb{E}(\cos(p\theta))$ and $\beta_p=\mathbb{E}(\sin(p\theta))$, which are the p^{th} cosine and sine moment of θ, respectively.

For $p=\pm1,\pm2,\ldots,$ the p-th trigonometric moment of θ is given by

$$\varphi_p = \rho_p e^{i\mu_p},$$

where

$$\rho_p = \sqrt{\alpha_p^2+\beta_p^2}$$

and, since $\beta_p \geq 0$,

$$\mu_p=\arg(\varphi_p) = \begin{cases}\arctan\left(\dfrac{\beta_p}{\alpha_p}\right)+\pi & \text{if } \alpha_p<0,\ \beta_p\geq 0,\\ \dfrac{\pi}{2} & \text{if } \alpha_p<0,\ \beta_p>0,\\ \arctan\left(\dfrac{\beta_p}{\alpha_p}\right)\text{if} & \text{if } \alpha_p>0,\\ \text{undefined} & \text{if } \alpha_p=0,\ \beta_p=0,\end{cases} \tag{5}$$

After some algebra, we can express μ_p as (5) with the ratio

$$\frac{\beta_p}{\alpha_p} = p\frac{16\lambda^4+20\lambda^3+8\lambda^2p^2+11\lambda p^2+p^4}{16\lambda^5+16\lambda^4+8\lambda^3p^2+4\lambda^2p^2+\lambda p^4-3p^4}$$

and

$$\rho_p = \lambda^2\sqrt{\frac{16\lambda^4+32\lambda^3+8\lambda^2p^2+16\lambda^2+16\lambda p^2+p^4+9p^2}{(1+\lambda)^2(\lambda^2+p^2)(4\lambda^2+p^2)^2}}.$$

The mean direction of θ is given by μ_1. The angular concentration of θ is obtained as

$$\rho_1 = \lambda^2\sqrt{\frac{16\lambda^4+32\lambda^3+24\lambda^2+16\lambda+10}{(1+\lambda)^2(\lambda^2+1)(4\lambda^2+1)^2}}.$$

The circular variance of θ is

$$V = 1-\rho_1 = 1-\lambda^2\sqrt{\frac{16\lambda^4+32\lambda^3+24\lambda^2+16\lambda+10}{(1+\lambda)^2(\lambda^2+1)(4\lambda^2+1)^2}}.$$

The circular standard deviation of θ is obtained as

$$\sigma = \sqrt{-2\log(\rho_1)} = \sqrt{-4\log(\lambda)-\log\left(\frac{16\lambda^4+32\lambda^3+24\lambda^2+16\lambda+10}{(1+\lambda)^2(\lambda^2+1)(4\lambda^2+1)^2}\right)}.$$

The p-th central cosine and sine moment of θ are given by, respectively,

$$\bar{\alpha}_p = \mathbb{E}[\cos(p(\theta-\mu_1))], \quad \bar{\beta}_p = \mathbb{E}[\sin(p(\theta-\mu_1))].$$

By using standard trigonometric formula, we can express them as $\bar{\alpha}_p = \beta_p\sin(p\mu_1)+\alpha_p\cos(p\mu_1)$ and $\bar{\beta}_p = \beta_p\cos(p\mu_1)-\alpha_p\sin(p\mu_1)$.

The skewness and kurtosis coefficients of θ are given by, respectively,

$$\gamma_1 = \frac{\bar{\beta}_2}{V^{3/2}}, \quad \gamma_2 = \frac{\bar{\alpha}_2-\rho_1^4}{V^2}.$$

Table 1 exhibits the numerical values of different characteristics of the WML distribution for various values of the parameter λ. It can be seen that, when λ increases, the circular variance decreases. Similarly, the coefficient of skewness decreases when λ increases. On the other hand, when λ increases, the coefficient of kurtosis increases.

Table 1

Numerical values of different characteristics of the WML distribution for various values of λ.

Characteristics of the WML distribution		$\lambda = 0.25$	$\lambda = 1$	$\lambda = 1.5$	$\lambda = 2$	$\lambda = 5$
Trigonometric moments	α_1	-0.0692	0.42	0.6563	0.7815	0.9599
	α_2	-0.0289	0.075	0.2748	0.4467	0.8559
	β_1	0.1393	0.56	0.5096	0.4346	0.2004
	β_2	0.0400	0.4	0.5155	0.54	0.3596
Circular variance	V	0.8445	0.3	0.1691	0.1057	0.0194
Circular standard deviation	σ	1.9292	0.8446	0.6087	0.4728	0.1979
Mean direction	μ_1	2.0317	0.9273	0.6602	0.5075	0.2058
Central trigonometric moments	$\bar{\alpha}_1$	0.1555	0.7	0.8309	0.892	0.9806
	$\bar{\alpha}_2$	-0.0144	363	0.5675	0.6944	0.9282
	$\bar{\beta}_1$	3.469447e-17	5.511e-17	-5.511e-17	0	2.7755e-17
	$\bar{\beta}_2$	-0.0472	-0.184	-0.1384	-0.0945	-0.0128
Coefficient of skewness	γ_1	-0.0608	-1.1198	-1.9907	-2.7487	-4.75890
Coefficient of kurtosis	γ_2	-0.0210	1.3655	3.1789	4.9080	9.7514

4. Maximum likelihood method

In this section, the WML model is considered and we investigate the estimation of λ by the method of maximum likelihood. Let $\theta_1, \theta_2, \ldots, \theta_n$ be n independent realizations from the WML distribution. Then, the corresponding likelihood function is given by

$$L(\lambda)=\prod_{i=1}^{n}g(\theta_i)=\frac{\lambda^n}{(1-e^{-4\lambda\pi})^n}e^{-\lambda\sum_{i=1}^{n}\theta_i}\prod_{i=1}^{n}\left\{1+e^{-2\lambda\pi}+\frac{e^{-\lambda\theta_i}}{1+\lambda}\left[2\lambda\theta_i-1+\frac{4\lambda\pi}{e^{4\lambda\pi}-1}\right]\right\}$$

and the corresponding log-likelihood function is obtained as

$$\ell(\lambda)=\log[L(\lambda)]$$

$$=n\log(\lambda)-n\log(1-e^{-4\lambda\pi})-\lambda\sum_{i=1}^{n}\theta_i+\sum_{i=1}^{n}\log\left\{1+e^{-2\lambda\pi}+\frac{e^{-\lambda\theta_i}}{1+\lambda}\left[2\lambda\theta_i-1+\frac{4\lambda\pi}{e^{4\lambda\pi}-1}\right]\right\}.$$

The maximum likelihood estimator is obtained by the maximization of $\ell(\lambda)$ with respect to λ. Here, we can obtain it by solving the equation $\partial\ell(\lambda)/\partial\lambda=0$, i.e.,

$$\frac{n}{\lambda}-n\frac{4\pi}{e^{4\pi\lambda\pi}-1}-\sum_{i=1}^{n}\theta_i+\sum_{i=1}^{n}\frac{h(\theta_i;\lambda)}{1+e^{-2\lambda\pi}+\frac{e^{-\lambda\theta_i}}{1+\lambda}\left[2\lambda\theta_i-1+\frac{4\lambda\pi}{e^{4\lambda\pi}-1}\right]}=0,$$

where

$$h(\theta_i;\lambda)=-\frac{2\lambda\theta_i^2e^{-\lambda\theta_i}}{1+\lambda}+\frac{3\theta_ie^{-\lambda\theta_i}}{1+\lambda}-\frac{2\lambda\theta_ie^{-\lambda\theta_i}}{(1+\lambda)^2}-\frac{4\pi\lambda\theta_ie^{-\lambda\theta_i}}{(e^{4\pi\lambda}-1)(1+\lambda)}+\frac{e^{-\lambda\theta_i}}{(1+\lambda)^2}$$
$$-\frac{16\pi^2\lambda e^{4\pi\lambda}e^{-\lambda\theta_i}}{(e^{4\pi\lambda}-1)^2(1+\lambda)}+\frac{4\pi e^{-\lambda\theta_i}}{(e^{4\pi\lambda}-1)(1+\lambda)}-\frac{4\pi\lambda e^{-\lambda\theta_i}}{(e^{4\pi\lambda}-1)(1+\lambda)^2}-2\pi e^{-2\pi\lambda}.$$

The equation above cannot be solved analytically. Thus, different numerical techniques can be performed to get a solution, by the use of any mathematical software (R, Python, Matlab, Mathematica...).

5. Applications

In this section, we illustrate the usefulness of the WML model. We fit the WML distribution to two practical data sets and compare the results with those of the fitted wrapped Lindley (WL), wrapped exponential (WE) and transmuted wrapped exponential (TWE) distributions. We estimate the unknown parameter(s) of each model by the maximum likelihood method. Also, the statistics Akaike information criterion (AIC) and Bayesian information criterion (BIC) are used to compare the four models. We recall that $AIC=2k-2l$ and $BIC=k\log(n)-2l$, where k is the number of parameters, n is the sample size and l is the maximized value of the log-likelihood function under the considered model.

Table 2

Estimated values, log-likelihood, AIC and BIC for the turtle data set

Distribution	Estimates	l	AIC	BIC
WML	$\hat{\lambda} = 0.5605278$	-118.2947	238.5895	240.9202
WL	$\hat{\lambda} = 0.7845654$	-119.805	241.6101	243.9408
WE	$\hat{\lambda} = 0.4228703$	-120.6474	243.2939	245.6256
TWE	$\hat{\lambda} = 0.7476771$ $\hat{\Lambda} = -0.9515879$	-117.9474	239.8949	244.5564

5.1 *The turtle data set*

The turtle data set was given by Rao and Sen Gupta (2001). It contains orientations of 76 turtles laying their eggs. This data set is also considered in Joshi and Jose (2017) with the WL distribution as contribution. The data are as given below.

{8, 9, 13, 13, 14, 18, 22, 27, 30, 34, 38, 38, 40, 44, 45, 47, 48, 48, 48, 48, 50, 53, 56, 57, 58, 58, 61, 63, 64, 64, 64, 65, 65, 68, 70, 73, 78, 78, 78, 83, 83, 88, 88, 88, 90, 92, 92, 93, 95, 96, 98, 100, 103, 106, 113, 118, 138, 153, 153, 155, 204, 215, 223, 226, 237, 238, 243, 244, 250, 251, 257, 268, 285, 319, 343, 350}.

Table 2 gives the relevant numerical summaries for the four fits based on the turtle data set.

Figure 4 gives the graph of estimated pdf and cdf of the considered distributions for the turtle data set.

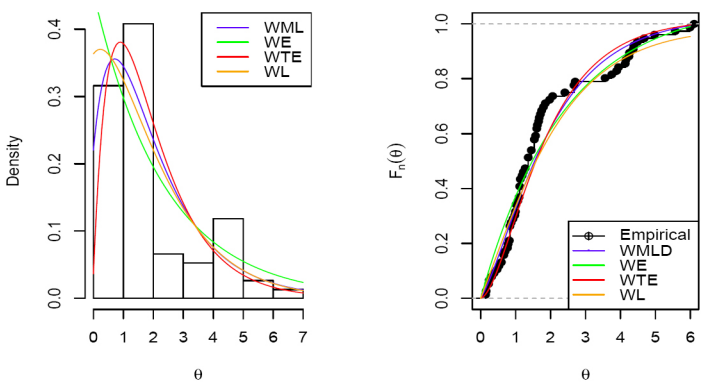

Figure 4

Estimated pdfs and cdfs of the considered distributions for the turtle data set.

Table 3

Estimated values, log-likelihood, AIC and BIC for the feldspar laths data set.

Distribution	Estimates	l	AIC	BIC
WML	$\hat{\lambda} = 0.7131918$	-175.7633	353.5265	356.4093
WL	$\hat{\lambda} = 0.9713978$	-176.87271	355.7454	357.6575
WE	$\hat{\lambda} = 0.61212855$	-182.8546	367.7091	370.5919
TWE	$\hat{\lambda} = 0.8836261$ $\hat{\Lambda} = -0.74378339$	-174.5348	353.0696	358.8352

5.2 *Long-axis orientations of feldspar laths data*

The feldspar laths data set was given by Fisher (1993). It contains the measurements of long-axis orientations of feldspar laths: a data of 133 measurements of feldspar laths in basalt direction in degrees as given below. {176, 162, 49, 174, 174, 49, 54, 63, 59, 61, 66, 104, 97, 58, 121, 5, 178, 3, 168, 0, 18, 39, 140, 63, 55,170, 169, 37, 152, 73, 53, 176, 72, 170, 113, 56, 87, 161, 164, 21, 50, 6, 59, 140, 54, 64, 56, 38, 61, 143, 51, 144, 148, 44, 60, 98, 86, 145, 38, 168, 39, 134, 68, 57, 129, 68, 132, 82, 54, 119, 131, 50, 93, 160, 127, 124, 65, 108, 52, 61, 86, 37, 132, 83, 163, 58, 144, 29, 80, 172, 144, 138, 10, 45, 137, 11, 145, 103, 69, 124, 54, 121, 139, 111, 153, 13, 5, 5, 107, 104, 39, 133, 36, 63, 4, 21, 51, 30, 52, 90, 143, 13, 50, 109, 12, 170, 5, 14, 91, 132, 121}.

Table 3 gives the relevant numerical values for four fits based on long-axis orientations of the feldspar laths data set.

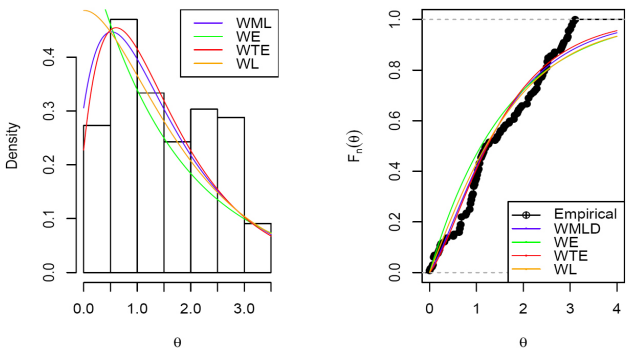

Figure 5

Estimated pdfs and cdfs of the considered distributions for long-axis orientations of the feldspar laths data set.

Figure 5 gives the graph of estimated pdf and cdf of the considered distributions for long-axis orientations of feldspar laths data set.

Thus, in Tables 2 and 3, the maximum likelihood estimates of the parameters for the fitted distributions along with likelihood, AIC and BIC values are presented for two different data sets. Based on the lowest values of the AIC and BIC (excepted the AIC for the TWE model in feldspar laths data set), the WML model turns out to be a better model than the WL, WE and TWE models. A visual comparison of the closeness of the fitted pdfs with the observed histograms of the data and fitted cdfs with empirical cdfs for different data sets are presented in Figures 4 and 5, respectively. These plots indicate that the proposed model provides a closer fit to these data sets.

6. Conclusion

In this article, we used the wrapping method to introduce a new circular distribution, called the WML distribution. A class of basic properties is also found here, including characteristic function, trigonometric moments, circular variance, circular standard deviation, skewness and kurtosis. The maximum likelihood method is employed for estimating the model parameters. Two applications of real life data fitting show good result in favor of the proposed distribution when compared to WL, WE and TWE distributions. Therefore, the proposed distribution may be considered as a good contribution to the existing knowledge.

Acknowledgments

We would like to thank the referee for helpful comments, improving the quality of the manuscript.

References

[1] Adnan, M.A.S. and Roy, S. (2011). Wrapped Chi-square distribution. *Journal of Applied Statistical Science*, 18, 307-317.

[2] Adnan, M.A.S. and Roy, S. (2014). Wrapped variance gamma distribution with an application to wind direction. *Journal of Environmental Statistics*, 6(2), 1-10.

[3] Chesneau, C., Tomy, L. and Gillariose, J. (2019). A new modified Lindley distribution with properties and applications. *Journal of Statistics and Management Systems*, Submitted.

[4] Coelho, C.A. (2007). The wrapped Gamma distribution and wrapped sums and linear combinations of independent Gamma and Laplace distributions. *Statistical Theory and Practice*, 1, 1-29.

[5] Elgarhy, M., Sharma, V.K. and Elbatal, I. (2018). Transmuted Kumaraswamy Lindley distribution with application. *Journal of Statistics and Management Systems*, 21(6), 1083-1104.

[6] Fisher, N.I. (1993). Statistical analysis of circular data. *Cambridge University press, Melbourne*.

[7] Levy, P.L. (1939). Addition des variables aléatoires définies sur une circonfèrence. *Bull Soc Math*, 67, 1-41.

[8] Jacob, S. and Jayakumar, K. (2013). Wrapped geometric distribution: A new probability model for circular data. *Journal of Statistical Theory and Applications*, 12(4), 348-355.

[9] Jammalamadaka, S.R. and Kozubowski, T.J. (2003). A new family of circular models:the wrapped Laplace distributions. *Advances and Applications in Statistics*, 3, 77-103.

[10] Jammalamadaka, S.R. and Kozubowski, T.J. (2004). New families of wrapped distributions for modelling skew circular data. *Communications in Statistics-Theory and Methods*, 33, 2059-2074.

[11] Joshi, S. and Jose, K.K. (2017). Wrapped Lindley Distribution. *Communications in Statistics-Theory and Methods*, 1-9.

[12] Pewsey, A. (2008). The wrapped stable family of distributions as a flexible model for circular data. *Computational Statistics and Data Analysis*, 52(3), 1516-1523.

[13] Pewsey, A., Lewis, T. and Jones, M. C. (2007). The wrapped t family of circular distributions. *Australian and amp; New Zealand Journal of Statistics*, 49(1), 79-91.

[14] Rao, J.S. and Sen Gupta, A. (2001). Topics in circular statistics. *new York:World Scientific*, 5.

[15] Roy, S. and Adnan, M.A.S. (2010). Wrapped Three parameter Gamma distribution. *JSM Vancouver, British Columbia, Canada*.

[16] Roy, S. and Adnan, M.A.S. (2012). Wrapped weighted exponential distributions. *Statistics and Probability Letters*, 82, 77-83.

[17] Roy, S. and Adnan, M.A.S. (2012). Wrapped Generalized Gompertz distribution: an Application to Ornithology. *Journal of Biometrics and Biostatistics*, 3(6), 1-4.

[18] Singh, S.K., Singh, U. and Sharma, V.K. (2016). Estimation and prediction for Type-I hybrid censored data from generalized Lindley distribution. *Journal of Statistics and Management Systems*, 19(3), 367-396.

[19] Tomy, L. (2018). A retrospective study on Lindley distribution. *Biometrics and Biostatistics International Journal*, 7(3), 163-169.

[20] Yilmaz, A. and Bicer, C. (2018). A new wrapped exponential distribution. *Mathematical Sciences*, 12(4), 285-293.

Received December, 2019

Revised April, 2020

THE DREARY LIVES AND DISMAL FUTURE OF TRANSGENDER IN COVID-19 CRISIS

JISHA CHAKKUNNY M
Assistant Professor, Department of Sociology,
Carmel College, Mala.

ABSTRACT

The people of the world are fighting together to survive the intensity of the second wave of Covid-19. The situation of the marginalized in the society is deplorable as social distance and denial of contacts are applied across the country to prevent and combat the spread of the disease. Transgender people who have been excluded from the mainstream of society are frustrated with the loss of livelihoods and security. The main objectives of this study are to analyze the miserable life experiences of transgender individuals who have been plunged into darkness and despair due to the epidemic, and to suggest solutions to overcome this predicament. It draws attention to the collective responsibility of the public and the political authorities surpass the pandemic crisis.

Keywords: Dreary life, Transgender, Economic Crisis, Psychological Effects.

INTRODUCTION

The people of the world are fighting together to survive the intensity of the second wave of Covid-19. The situation of the marginalized in the society is deplorable as social distance and denial of contacts are applied across the country to prevent and combat the spread of the disease. Transgender people who have been excluded from the mainstream of society are frustrated with the loss of livelihoods and security. One of the most important consequences of the Covid-19 epidemic is the changes it has brought to individual lives. The changes that take place in the mental level, emotions, thoughts and actions along with the social alienation are very intriguing, interesting and complex. Transgender people have always received help from community-based organizations, individuals, political parties and governments to move forward in overcoming economic crisis and social isolation. This global health crisis is regulating and controlling our lives and daily routines and shaping our anxiety and hope for the future.

METHODOLOGY

The research work mainly focuses on the dreary lives and dismal future of transgender in covid-19 crisis period. The main objectives of this study are (a) To analyze the miserable life experiences of transgender individuals who have been plunged into darkness and despair due to the epidemic. (b) To assess the role of the Community Based Organizations (CBOs) in the crisis situation (c) To suggests solutions to overcome the covid-19 pandemic predicament. The study was conducted among 50 transgender in Thrissur district, the cultural capital of Kerala. The interview schedule was used for primary data collection. Descriptive research design and snowball sampling method were used for the study. Respondents belonged to the age group of 20 to 50 and were members of the 'Nila' and FICO (Foundation for Innovations and Cultural Organisation), the Community Based Organizations in Thrissur.

LITERATURE REVIEW

In general, transgender people are alienated from the mainstream of society. Besides, they face a number of hardships in life. The following literature reviews help to understand the problems experienced by transgender individuals during the Covid-19 pandemic period.

Banerjee & Rao (2020) in their article "The Graying Minority": Lived Experiences and Psychosocial Challenges of Older Transgender Adults During the COVID-19 Pandemic in India, A Qualitative Exploration- explains elderly transgender people face difficulties due to marginalization, sigma, and disease, as well as multiple survival threats, especially at the physical, emotional, and financial levels. Their emotional and social risk is high during this pandemic. No one takes the needs of older transgender people seriously. Policies required for their welfare should be formulated and implemented. Their health and wellbeing can only be ensured by raising the level of social awareness.

Harris & Moss (2020) reveals Implementing policies designed for the health, welfare and security of the people is a fundamental responsibility of the respective government. These policies also aim at the economic development of the country. Each government faces a number of challenges in overcoming the crises caused by the scourge of corona virus. Most importantly the economic repercussions are very worrying. While trying to work towards prosperity and survival, the high prevalence of the disease is a devastating reality facing all countries.

According to Pillay & Barnes (2020) says that Covid-19 poses new challenges to the nations of the world that are suffering from adverse conditions. It places more burdens on the government. Lockdown restrictions to reduce the spread of the disease create problems such as unemployment, poverty and mental health problems. In such countries, marginalized transgender groups are most affected. For them, this period has created fear; frustration and panic. Losses of employment and financial crisis have disrupted their lives.

Poteat, Reisner *et al* (2020) analyses Covid-19 pandemic has adversely affected transgender women, especially transgender women living with HIV. Difficulties in employment, income, food, and shelter indicate a high risk of violence against these gender minorities. HIV-infected transgender women with Covid-19 Symptoms rarely see the possibility of receiving care in city hospitals. Such hospitals are already overcrowded with Covid-19 patients. Such conditions increase the risk of disease transmission.

SOCIO-ECONOMIC PROFILE OF THE RESPONDENTS

Table: 1 Personal details of the respondents (n=25)

Socio - Economic Status	Category	Frequency	Percentage
Age	Below 20	6	12
	20 to 30	12	24
	31to 40	24	48
	Above 40	8	16
Religion	Hindu	36	72
	Christian	10	20
	Muslim	4	8

Education	Primary	2	4
	High School	8	16
	SSLC	4	8
	Higher Secondary	12	24
	UG	13	26
	PG	8	16
	Diploma	3	6
Occupation	Unemployed	22	44
	Self Employed	4	8
	Working in NGO	4	8
	Courier Service	2	4
	Cleaning Work	4	8
	Sex Work	14	28
Monthly Income	Up to 1000	28	56
	1001 to 3000	8	16
	3001 to 5000	6	12
	Above 5000	8	16
Living Arrangement	Living Alone	4	8
	Living with TG Friends	24	48
	Living with Family	10	20
	Living with Partner	4	8
	Hostel/Lodge	8	16

DISCUSSION

Table: 2 Economic Effects of Covid-19 Pandemic

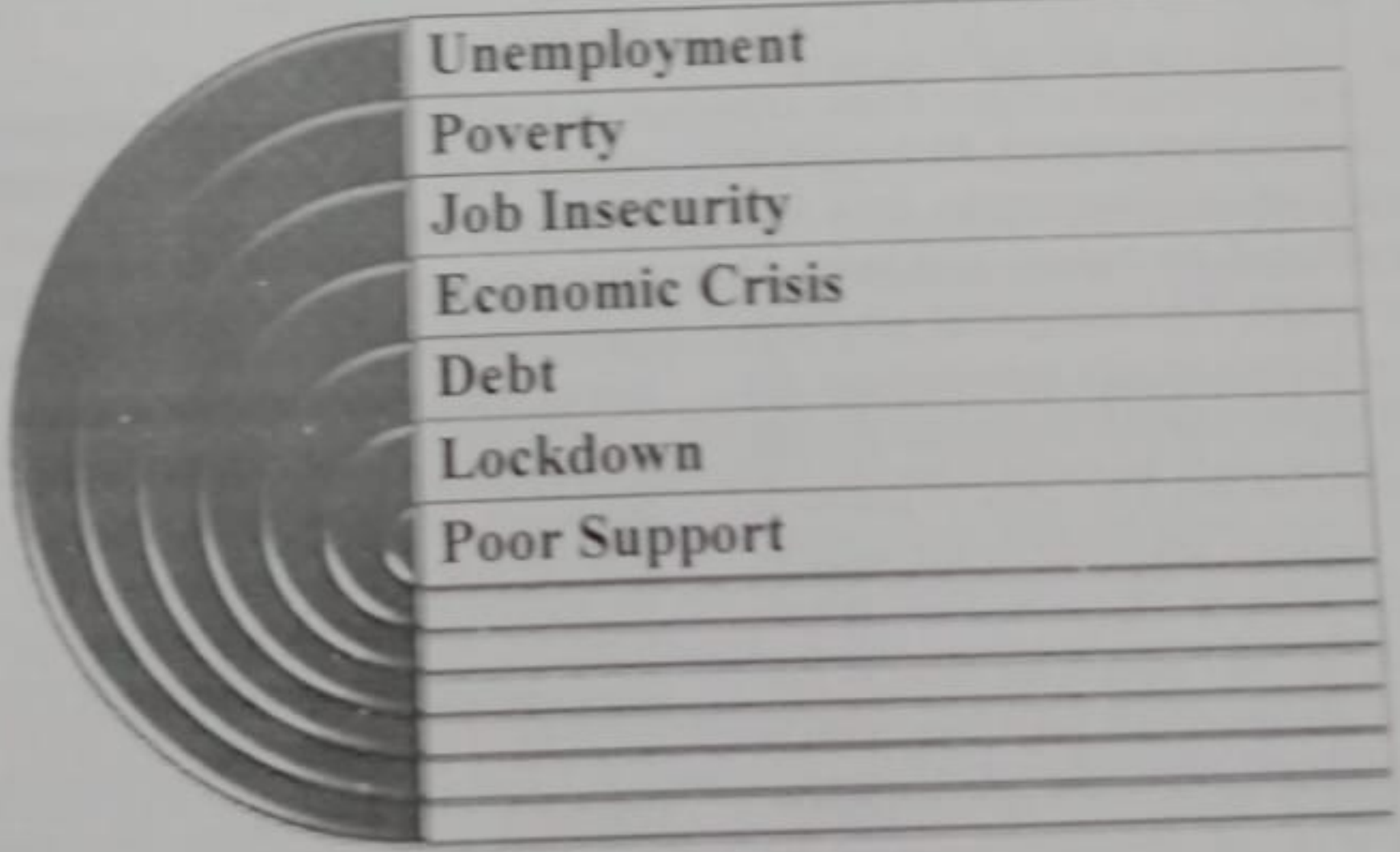

The financial status of transgender people in India is deplorable. Transgender people do not get high paying jobs due to lack of higher education. Therefore, their economic status and standard of living remain very low. They are often unable to raise their living standards due to unemployment and meager income. The literacy rate of transgender people in Kerala is very high compared to other states. However, they have to migrate from villages to cities in search of employment opportunities. In the workplace, transgender people face exploitation and discrimination. During the Covid-19 period, the economic status of transgender people remained very low. The transgender community has suffered from the social isolation, lockdowns and stigma. They are facing a crisis situation in the financial sector. Many transgender people do not have a home. In addition, there are transgender people who find it difficult to rent a living space or even meet basic needs. Many are worried about the loss of livelihoods during the lockdown. Transgender people have a habit of spending more than saving. During the Covid-19 epidemic, transgender people spent all their possessions without any personal collection.

Unemployment, poverty, disease, social stigma and financial vulnerability have also adversely affected the mental well being of transgender people. Few transgender people do not receive the assistance provided by the government due to lack of documents proving their transgender identity. The Covid-19 pandemic poses a formidable challenge to the lives of transgender people. Community Based Organizations are very helpful for them to face this situation with courage. Lockdowns seem to close the windows to the lives of transgender people, but it is only with the help of the government that the unemployed can overcome this crisis. CBOs also enable them to survive this difficult period.

PSYCHOLOGICAL EFFECTS OF COVID-19 PANDEMIC AMONG TRANSGENDER

The global population is fully aware of the spread of Corona virus disease (Covid-19) and its physical symptoms. Everyone has the utmost care to take the necessary precautions against corona virus infection. In addition, everyone has a clear understanding of the disease and the health care that needs to be continued. However, awareness of the psychological consequences of the Covid-19 pandemic is scarce in society. Research shows that this global problem is negatively affecting human thinking, emotions, and behavior. Post-traumatic strain, temper, and confusion are reported in an analysis of the psychological effects of quarantine on covid-19. It has been reported that increasing the duration of the quarantine leads to greater stress and decreased availability of food and water creates constant stress during the quarantine (Brooks et al., 2020).

Covid-19 Pandemic has adversely affected the lives of individuals. The situation of the transgender, a marginalized section of society, is now very deplorable and reprehensible. This is a special period in the history of the world where human beings are forced to live apart from their fellow human beings. The particular situation has adversely affected the mental wellbeing of individuals. Transgender people face this situation along with the misery of isolation, loneliness and their other rejected experiences in normal life. Therefore, it has psychologically far-reaching consequences for them. This circumstance is a threat to the mental well being

of transgender people. The following table describes the psychological distress experienced by transgender people through social isolation, infrequent contact, and other related problems. These are the psychological effects of the Covid-19 pandemic.

Table: 3 Psychological Effects of Covid-19 Pandemic

Psychological Effects		Frequency	Percent
1	Anxiety	50	100
2	Anger or Angry	40	80
3	Boredom	50	100
4	Depression	45	90
5	Fear	40	80
6	Fatigue	48	96
7	Hate	40	80
8	Hopelessness	40	80
9	Irritation	44	88
10	Insomnia	36	72
11	Loneliness	50	100
12	Laziness	46	92
13	Low self esteem	20	40
14	Suicidal tendency	30	60
15	Tension	48	96
16	Stress and Strain	46	92
17	Sadness	40	80
18	Unhappiness	40	80

It is clear from these psychological effects that a pandemic is not just a medical phenomenon and that such conditions abruptly affect individuals' mental state, thoughts, feelings, emotions, and actions. The findings of this study show that individuals should give the same importance to maintaining mental health as they do to physical health, which requires conscious effort on the part of individuals. This Pandemic Period also provides us with the psychological training that we need to be aware of the changes in the mental state of the individual due to the social environment and circumstances. There is a close relationship between the mental wellbeing of transgender individuals and their personal issues. They are neglected and ridiculed in all walks of life.

Transgender people experience personal and internal conflicts and social discrimination. For them, the travel ban, contact ban, celebration ban, isolation caused by social distance and quarantine created by the Covid-19 Pandemic, low level of economic status, insecurity and unemployment are always negatively related. These psychological effects are the result of the interaction of all these factors. The anxieties and difficulties experienced during the pandemic period later come out as negative emotions. These are the common emotions and their expression that occur when even the primary needs are not satisfied. Transgender people face many critical issues due to extreme degree of discrimination. Covid-19 Pandemic deepened it. Fear, anger, irritation and tension are expressed as uncertainty about the future. Lack of financial security creates tension and increases anxiety and loss of happiness. In addition,

ambiguities about the future destroy expectations. Loss of vitality and hope leads to severe depression. Feelings of failure and negative thoughts lower their self-esteem. Loneliness, sadness and guilt lead to suicidal tendencies. Covid-19 Pandemic throws the lives of transgender people into the darkness of despair.

ROLE OF COMMUNITY BASED ORGANIZATIONS IN COVID-19 CRISIS

Community based organizations are the ones that constantly come to the rescue of transgender people in all their difficulties. During the Covid -19 epidemic, the CB0s were at the forefront of providing them with everything they needed. 'Nila' and 'Foundation for Innovations and Cultural Organization' (FICO) are the two main organizations working for TGs in Thrissur district.

- Transgender people often have health problems. But during the lockdown, they had no facilities to go to the hospitals or visit the doctor and get the necessary medical care.In this helpless situation, the CB0 officials took the initiative to conduct an online consultation with the doctor and to buy all the medicines prescribed for them free of cost on time.
- The food kits provided by the government through the Department of Social Justice were taken over by the CBO officials and delivered responsibly to the transgender homes.
- They sought to assist transgender people by maintaining constant contact with well-wishers, organizations, organizations, charitable societies, corporate executives, and public figures. During the lockdown, the CB0s paid special attention to storing and providing essential food grain kits to help transgender people survive without starvation.
- During this Covid-19 period, the government issued food kits three times exclusively for all transgender individuals who applied for an ID card. It was supplied to transgender people through CBOs.
- When the Department of Social Justice took the initiative to vaccinate transgender people against the corona vaccine as a preventive measure, the two CBOs worked together to make the event a success. Fifty-five transgender people were vaccinated that day.
- Under the leadership of CBO "Nila", a webinar on "Corona and Immunization and Transgender Life" was organized to create awareness among the community members.
- To protect the environment, on the occasion of World Environment Day on June 5, the organizations provided an opportunity for transgender people to plant 101 plants.
- The CBOs took special care to organize online meetings of the Executive Committee to coordinate all the activities of the pandemic period.
- With the effective use of social media, organizations have been able to stay in touch with transgender people, even during the lockdown period. Transgender people were greatly relieved to receive assistance through the timely intervention of organizations.
- They suffered from lockdowns and unemployment, and lost even their hormone medicine due to the financial crisis.CB0s

- Give transgender people all the rights and benefits required by the Constitution.
- Appoint a planning committee consisting of experts in the fields of sociology and economics to find out what is needed for the all-round growth of transgender people.
- Form a Planning Committee comprising of transgender representatives.
- Give special consideration to transgender people in the Five Year Plan.
- Provide government appointments for transgender people according to their educational qualifications.
- Implement reservation in government jobs for transgender people.
- The money required for sex reassignment surgery (SRS) should be deposited by the government in the hospital account in a timely manner.
- Give financial assistance to all homeless transgender people to build their own home.
- Provide special protection for transgender people in emergencies such as floods and epidemics.
- Train transgender people to acquire what they need to live with hope, to achieve higher status through self-effort, and to develop skills.
- Disseminate programs on social media in a way that helps to cultivate a positive attitude about transgender people in the public.
- Provide necessary medical care to transgender people.
- Ensure awareness and quarantine facilities on precautionary measure especially for transgender people who are at risk population during the epidemic.
- Take steps to prevent transphobia.
- To prevent discrimination, abuse and gender attacks equip help lines and make transgender people aware of it.
- It is mandatory to include information about different gender identity in school textbooks.
- Provide financial assistance to those who deserve it.
- Make unemployment wage and employment availability for transgender people through employment exchange.
- Include transgender people in health insurance policies.
- Provide counseling and helpline facilities to ensure mental health.
- Build transgender Old Age Homes run by the government.
- Appoint a commission to study the problems faced by transgender people in Kerala.

CONCLUSION

In the most modern age, the whole world is going through the second wave of the Covid-19 pandemic. The experience of being a Global Village is also getting closer to the nations of the world who are fighting for survival in these historically significant days. The plight of transgender people, one of the most marginalized sections of society, is a matter of special concern as the world is on the cusp of spreading the disease caused by the Naval Corona virus. Transgender people are the ones who struggle the most to overcome the challenges posed by the miserable living

conditions of marginalized minorities. Transgender people are doubly affected by the isolation and loneliness created by social distance and lockdowns. Their lives, mixed with despair, helplessness and neglect, are a question mark in the eyes of the world's conscience. We must be able to protect the human rights and constitutional denials that are being destroyed in the lives of transgender people who are melting in the furnace of life experiences. Only then will we enter the freedom of liberation from the framework of sectarianism. It is the responsibility of society to bring the lives of transgender people, who have sunk into the misery of the epidemic, into the light of survival.

REFERENCES

1. Chakrapani, V., Newman, P. A., Sebastian, A., Rawat, S., Shunmugam, M., & Sellamuthu, P. (2021). The Impact of COVID-19 on Economic Well-Being and Health Outcomes Among Transgender Women in India. *Transgender Health*.
2. Harris, P., & Moss, D. (2021).Managing through the Covid second wave: Public affairs and the challenge of Covid vaccination.*Journal of Public Affairs*, *21*(1).
3. Hawke, L. D., Hayes, E., Darnay, K., & Henderson, J. (2021). Mental health among transgender and gender diverse youth: An exploration of effects during the COVID-19 pandemic.*Psychology of Sexual Orientation and Gender Diversity*.
4. Holmes, R., & Hunt, A. (2021). Have social protection responses to Covid-19 undermined or supported gender equality.
5. Kidd, J. D., Jackman, K. B., Barucco, R., Dworkin, J. D., Dolezal, C., Navalta, T. V., ... & Bockting, W. O. (2021). Understanding the impact of the COVID-19 pandemic on the mental health of transgender and gender nonbinary individuals engaged in a longitudinal cohort study. *Journal of Homosexuality*, *68*(4), 592-611.
6. Teixeira da Silva, D., Biello, K., Lin, W. Y., Valente, P. K., Mayer, K. H., Hightow-Weidman, L., & Bauermeister, J. A. (2021). COVID-19 Vaccine Acceptance among an Online Sample of Sexual and Gender Minority Men and Transgender Women. *Vaccines*, *9* (3), 204.
7. Banerjee, D., & Rao, T. S. (2020). "The Graying Minority": Lived Experiences and Psychosocial Challenges of Older Transgender Adults During the COVID-19 Pandemic in India, A Qualitative Exploration. *Frontiers in Psychiatry*, *11*.
8. Banerjee, D., & Nair, V. S. (2020). "The Untold Side of COVID-19": struggle and perspectives of the sexual minorities. *Journal of Psychosexual Health*, *2*(2), 113-120.
9. Gonzales, G., de Mola, E. L., Gavulic, K. A., McKay, T., & Purcell, C. (2020). Mental health needs among lesbian, gay, bisexual, and transgender college students during the COVID-19 pandemic. *Journal of Adolescent Health*, *67*(5), 645-648.
10. Harris, P., & Moss, D. (2020). Covid, pandemics, plague and public affairs: Lessons from history. *Journal of Public Affairs*, *20* (4).
11. Pillay, A. L., & Barnes, B. R. (2020). Psychology and COVID-19: impacts, themes and way forward. *South African Journal of Psychology*, *50*(2), 148-153.

Environmental and Experimental Biology (2021) 19: 161–171
http://doi.org/10.22364/eeb.19.16

Original Paper

Influence of hosts on the production of bioactive compounds in the hemiparasitic plant *Helicanthes elasticus*

ISSN 2255-9582

T.G. Ajithkumar[1], Sinjumol Thomas[2], Lizzy Mathew[3]

[1]Government Arts and Science College for Women, Malappuram, Kerala, India
[2]Department of Botany, Carmel College, Mala, Thrissur, Kerala, India
[3]Department of Botany, St.Teresa's College (Autonomous), Ernakulam, Kerala, India

*Corresponding author, E-mail: ajithgopalakrishnan81@gmail.com

Abstract

Helicanthes elasticus growing on six different hosts produced different gas chromatograph profiles indicating the influence of host on the metabolite production of parasite. 1,2,3-benzenetriol (pyrogallol) and methyl-3,4,5-trihydroxybenzoate (methyl gallate), which were identified in all of the accessions were considered as gas chromatograph marker compounds of the methanolic extract of the parasite. Some assisted marked compounds obtained from this hemi-parasitic plant and their presence were found to differ among the hosts. Occurrence of various other active ingredients particular to the parasite collected from different hosts were also detected. UPGMA cluster analysis based on the 13 different compounds clearly showed the influence of host on the phytochemical production. Parasite-host interaction leads to phytochemical mosaicism in the selected hemiparasitic plant and such a phenomenon is highly significant for their utilization in various fields of the pharmaceutical industries.

Key words: *Helicanthes elasticus*, hemiparasite, GC-MS, 1,2,3-benzenetriol, methyl-3,4,5-trihydroxybenzoate.
Abbreviations: GC, gas chromatography; HEA, *H. elasticus* obtained from *Anacardium occidentale*; HEC, *H. elasticus* obtained from *Citrus maxima*; HEH, *H. elasticus* obtained from *Hevea brasiliensis*; HEM, *H. elasticus* obtained from *Murraya koenigii*; HEN, *H. elasticus* obtained from *Nerium oleander*; HES, *H. elasticus* obtained from *Saraca asoca*; MS, mass spectrometry; RT, retention time.

Introduction

Loranthaceae, the most widely dispersed family of parasitic plants known as mistletoes, has been afflicted by alarming rates of generic and specific level misidentification (Franklin 2017). They are primarily pantropical in distribution, with a range that includes temperate zones in the southern hemisphere (Rajasekaran 2007). The family is particularly interesting because it is a monophyletic group that comprises both terrestrial and aerial root parasites (Wilson, Calvin 2006). Furthermore, despite being a minor component of vegetation in forest and woodland ecosystems, mistletoe has a significant impact on species richness and is regarded as a keystone resource (Watson 2001). Loranthaceae has over 1000 species in 74 genera and is primarily distributed in tropical areas (Barlow et al. 1989). In India, Loranthaceae comprises nine genera and 35 species with *Dendrophthoe, Helicanthes, Macrosolen, Tolypanthes, Helixanthera, Taxillus*, and *Scurulla* being the most extensively spread in South India (Thriveni 2013).

Helicanthes elasticus (Desv.) Danser is a robust parasite with dichotomous branching and subsessile and decussate leaves. Flowers are produced in short axillary fascicles with a very small bract. Their calyx is cupular and corolla lobes are twisted and interlocked after anthesis. Flowers often produce five stamens with narrowly oblong anthers. The style is linear and stigma obovoid. The fruit is a globose berry. The branches are woody and are swollen at nodes (Sasidharan, Sivarajan 1996). It is one of the most delicate mistletoes, and can grow rapidly over the host. When infested, it produces a number of haustoriferous runners or epicortical roots from its base to all sides. Within a short period, the parasite creates a network over the host and it branches profusely, which helps the mistletoe to establish even on the vertical smooth trunks of trees. The dead parasite can be distinguished by the netlike haustorial growth, dichotomous branching and swollen nodes (Shanavaskhan, Sivadasan 2009). *H. elasticus* is a generalist parasite having a capacity to grow on diversified plant species including angiosperms and gymnosperms.

Among the members of Loranthaceae found in Kerala, this parasitic species showed maximum diversity in the number of host trees. A wide variety of plants were infected by this Loranthacean member and each host plant might have some influence on the growth pattern of this parasite. Nearly 73 trees belonging to different families were already reported as hosts of this plant (Sunil Kumar et al. 2015; Ajith Kumar, Mathew 2020). It was reported by Scot (1871) that

trees with bark having acrid, bitter or astringent qualities, and which produce limbid or milky juice, are less affected by Loranthacean members. However, the plant *H. elasticus* can infest the latex-producing *Hevea brasiliensis*, volatile oil-containing *Citrus* species (Shanavaskhan, Sivadasan 2009) and heavy barked trees like *Terminalia* (Sunil Kumar et al. 2015). The morphology, anatomical features, physiological behavior, phytochemical content or even genetic makeup of the parasite could be affected by the host. There are citations in famous Ayurvedic literature about the mistletoes. It was mentioned by Susrutha (ancient Indian physician known today as Father of Surgery) that the properties of this parasitic plant varies between hosts. Also, Raja Nighantu, an ancient Ayurvedic work by Narahari, states that along with the phytochemical properties of the mistletoe, it also shows the properties of host plant in which they grow (Namboothiri 2011). Influence of the host plant on the chemical composition of mistletoe and dependence of its medicinal properties on the host species were shown in the case of *Dendrophthoe falcata* (Indrani, Balasubhramanian 1985). It was reported that *D. falcata* grown on *Calotropis gigantea* improved cognitive function (Warrier et al. 1996) and the same plant infected on *Shorea robusta* was found to be effective in the treatment of paralysis, and the plant obtained from *Tamarindus indica* was used for treating impotency (Jain,1965). The importance of the host's function in the production of biologically active substances by the parasitic plants growing was well explained by these findings.

The major aim of the present study was to analyze the role of host tree in the production of biologically significant compounds in *H elasticus*. For this, gas chromatography-mass spectrometry (GC-MS) was used to determine the differences in the occurrence of such compounds in this hemi-parasitic plant collected from six different hosts. Mass spectroscopy (MS) coupled with gas chromatography (GC) can detect compounds and is used for direct analysis of chemical components present in herbal medicine. It has proved to be highly suitable for the analysis of non-polar components, volatile essential oils, fatty acids, lipids and alkaloids (Betz et al. 1997). Various chemical compounds eluted in the extraction process were identified and quantified based on their retention value and with matching spectra. MS analyzes the compounds eluted at different times to identify their nature and structure. The large compounds break into smaller ones giving different peaks at different m/z ratios. The fingerprint obtained from the analysis consists of different peaks, each denoting a specific compound and the height of the peaks determines their quantity. The fingerprint is the GC chromatogram for a particular extract of a plant, it is unique and hence can be used for the correct identification and authentication of a particular plant or drug. Comparison of the chromatogram and eluted compounds serves as an effective tool to analyze the influence of hosts on them.

Materials and methods

Plant material

Fresh and tender twigs of *Helicanthes elasticus* growing on six host plants (*Nerium oleander, Hevea braziliensis, Citrus maxima, Saraca asoca, Anacardium occidentale* and *Murayya koeinigii*) were collected from various sites places of the Ernakulam District (10.0718°N, 76.5488°E), Kerala, India. The branches of the hosts affected with parasite were also collected at a distance of 50 cm from the point of infection. Both the hosts and parasites collected were identified using reference books (Gamble 1967; Sasidharan, Sivarajan 1996; Nayar et al. 2006). Specimens of *H. elasticus* collected from selected hosts were entered in the herbarium of the Department of Botany, St. Teresa's College (Autonomous), Ernakulam, Kerala. Twigs of *H. elasticus* collected from above six host plants were shade dried for a month and powdered.

Extract preparation

A sample of 20 g powder of parasitic accessions was extracted in 200 mL methanol for 10 h in a Soxhlet apparatus and the extract was concentrated to 10 mL using a rotary evaporator, 2 mL of each were stored in cuvettes and used for GC-MS analysis.

GC-MS analysis

The GC-MS analysis of the extract was performed using a model QP 2010 series Shimadzu, Tokyo, Japan equipped with a Rxi-5Sil MS fused silica capillary column of 30 m length, 0.25 mm diameter and 0.25 μm film thickness. Helium gas was used as the carrier gas at a constant flow rate of 1 mL min^{-1} and 1 μL of the sample was manually injected in split mode. Injection temperature was set at 200 °C, at a flow control mode in linear velocity of 36.3 cm s^{-1}. The oven temperature was programmed from 50 to 280 °C at a rate of 5 °C min^{-1} increase and retained for about 5 min at the end. The total running time of the GC-MS was 51 min. MS parameters were 200 °C ion source temperatures and 280 °C interface temperatures.

Identification of the components in the extracts was assigned by the comparison of their retention indices and mass spectra fragmentation patterns with those stored in the computer library and also with published literature. The relative amount of each compound in percentage was determined by comparing its average peak area to total area. The NIST011s.LIB, WILEY8 LIB library source was used for matching the identified components from the plant materials. This was carried out in order to determine whether the species contain group of compounds or any individual compound that gives proof for its use in current commercial and tradition as a herbal medicine (Manickam, Periyasami 2014).

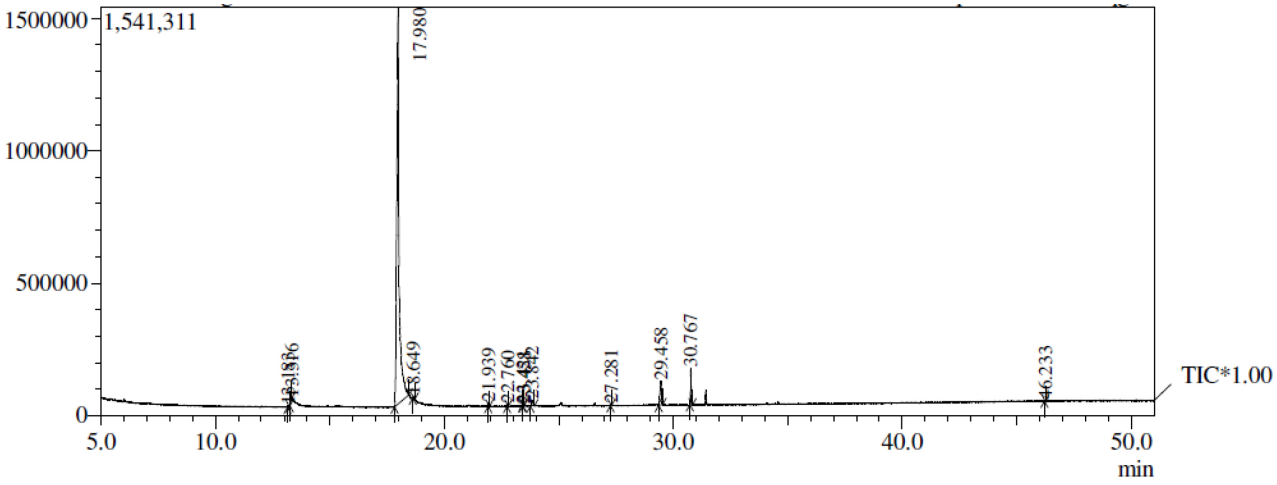

Fig. 1. GC chromatogram of *H. elasticus* growing on *Nerium oleander* (HEN).

Dendrogram construction

Based on the comparative analysis of selected chemical compounds identified in parasitic samples, a Jaccard's similarity index table was produced and an UPGMA tree was constructed based on this index to determine the similarity among the six accessions of *H. elasticus* obtained from six different hosts

Results

H. elasticus growing on *Nerium oleander* (HEN) produced 13 peaks in the chromatogram (Fig. 1) representing 13 different compounds; 1,2,3-benzenetriol with retention time (RT) value 17.980 had a maximum area percentage of 91.76, while the other peaks found were relatively small and had a lower area (Table 1). The parasite on *Hevea brasiliensis* showed the occurrence of 21 different peaks (Fig. 2) and 1,2,3-benzenetriol (74.88%) and 1,3,4,5-tetrahydroxy-cyclohexane carboxylic acid (10.13%) were the most prominent compounds. Other biologically active compounds like hexadecanoic acid, 1,2-benzenediol and nonanoic acid were also present in the *H. elasticus* growing on *Hevea brasiliensis* (Table 2). The *H. elasticus* parasitic on *Citrus maxima* showed 10 peaks with 1,2,3-benezenetriol having the largest area percentage (68.65%) and having RT of 18.036 (Fig. 3, Table 3).

H. elasticus grown on *Saraca asoca* showed 18 peaks (Fig. 4) of which the largest area percentage was shown by 1,2,3 benzenetriol with 51.59% and RT 17.958, followed by 1,3,4,5-tetrahydroxy-cyclohexane carboxylic acid with 33.40% and RT 24.191. Other important compounds found in the extract of the parasite were 1,2-benezenediol, diglycerol, hexadecanoic acid, oxalic acid etc. (Table 4). *H. elasticus* obtained from *Anacardium occidentale* produced 16 peaks (Fig. 5), of which 1,2,3-benzenetriol formed the main compound with 63.36% area, followed by 1,3,4,5 tetrahydroxy-cyclohexane carboxylic acid with 26.67%. Brenzkatechin, 2-amino-succinamic acid, thymine, etc. were also present in the extract (Table 5). Analysis of *H. elasticus* growing on *Murayya koeinigii* (HEM) showed 23

Table 1. GC-MS peak report of methanolic extract of *H. elasticus* obtained from *Nerium oleander* (HEN) with compounds detected

Peak No.	RT	Compound	Area (%)
1	13.183	N-methyl-N-aminosulfonyl-N-methylsulfonylamine	0.09
2	13.316	1,2-Benzenediol	0.47
3	17.980	1,2,3-Benzenetriol	91.76
4	18.649	Cyclohexanone, dimethylhydrazone	0.10
5	21.939	Nonanoic acid, methyl ester	0.29
6	22.760	1-Butanol, 3-methyl-	0.10
7	23.421	3-Nitropentan-2-ol	0.13
8	23.458	Isobutyl alcohol-2-d1	0.06
9	23.842	Butyric acid, 3-methylbutylester	1.08
10	27.281	Butanoic acid	0.10
11	29.458	Methyl 3,4,5-trihydroxybenzoate	3.34
12	30.767	Hexadecanoic acid, methyl ester	2.43
13	46.233	Ethyne, fluoro-	0.04

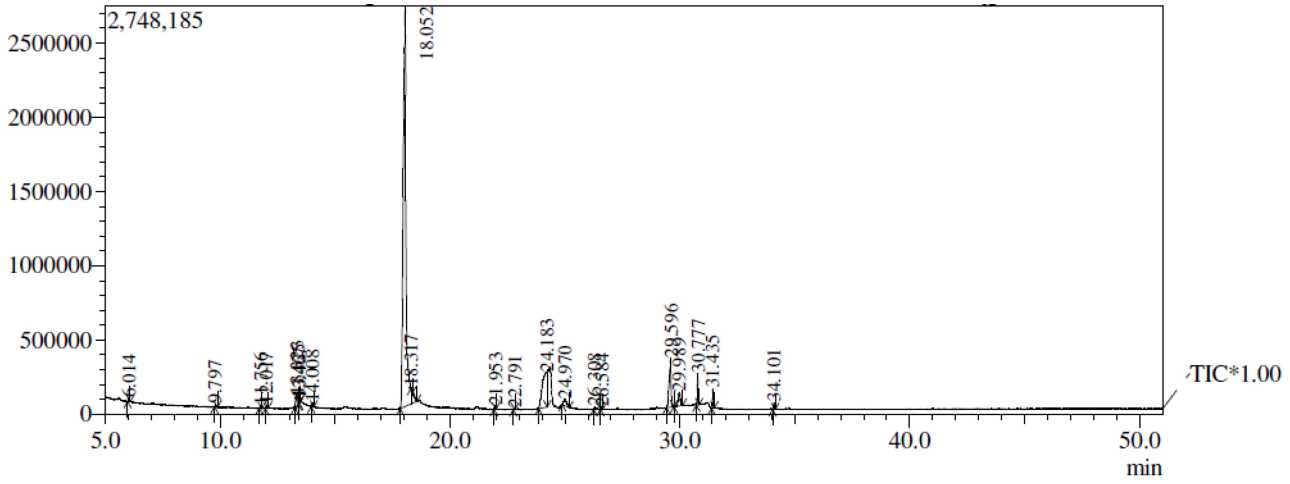

Fig. 2. GC chromatogram of *H. elasticus* growing on *Hevea brasilensis* (HEH).

different peaks (Fig. 6) with 1,2,3-benzenetriol being the main compound with RT 17.955 and 62.74% area. Other important compounds indicated included 1,2-benzenediol, 2-heptamine, propiolic acid, hexadecanoic acid, acetic acid, nitrous acid, heptadecanoic acid, butanoic acid etc. (Table 6).

An UPGMA tree was produced based on the Jaccard's similarity index. It classified the six accessions of *H. elasticus* collected from six different host plants into three clusters (Fig. 7). Cluster I comprised HEN and HEH, Cluster II with HEC and HEM and Cluster III with HES and HEA. The accessions of Cluster II showed maximum similarity of 77% with Cluster III in the bioactive compounds obtained (Table 7) with GC-MS. Cluster I formed a separate branch in the tree and was joined to the other clusters with more similarity with accessions of Cluster II.

Discussion

Parasitic plants, especially the obligate hemiparasites mistletoes, depend on hosts for water and nutrients and differ in their host use preference and specificity (Calder, Bernhardt 1983; Press, Graves 1995). Apart from this, chemical signalling or specific chemical interactions occur

Table 2. GC-MS peak report of methanolic extract of *H. elasticus* obtained from *Hevea brasiliensis* (HEH) with compounds detected

Peak No.	RT	Compound	Area (%)
1	6.014	2,3-Dihydroxy propanal	0.20
2	9.797	Methoxy cyclobutane	0.14
3	11.756	2,3-Dihydro-3,5-dihydroxy-6-methyl-4H-pyran-4-one	0.16
4	12.017	Formic acid, ethenyl ester	0.21
5	13.323	1,2-Benzenediol	1.51
6	13.425	p-Mesyloxyphenol	0.17
7	13.467	2-Furancarboxaldehyde, 5-methyl-	0.12
8	14.008	2-Furancarboxaldehyde, 5-(hydroxymethyl)-	0.20
9	18.052	1,2,3-benzenetriol	74.88
10	18.317	Hexane-1,6-bisurea, n', n"-bis(1,2,4-triazol-3-yl)-	0.04
11	21.953	Tetradecanoic acid, 12-methyl-, methyl ester	0.14
12	22.791	Propanedioic acid, propyl-	0.09
13	24.183	1,3,4,5-Tetrahydroxy-cyclohexanecarboxylic acid	10.13
14	24.970	D-glycero-D-galacto-heptose	1.17
15	26.308	1-Butanol, 3-methyl-	0.25
16	26.584	Nonanoic acid, methyl ester	0.12
17	29.596	Methyl 3,4,5-trihydroxybenzoate	5.80
18	29.989	Beta-D-glucopyranose, 1,6-anhydro-	1.87
19	30.777	Hexadecanoic acid, methyl ester	1.48
20	31.435	Hexadecanoic acid	0.93
21	34.101	Methyl-9-octadecenoate	0.40

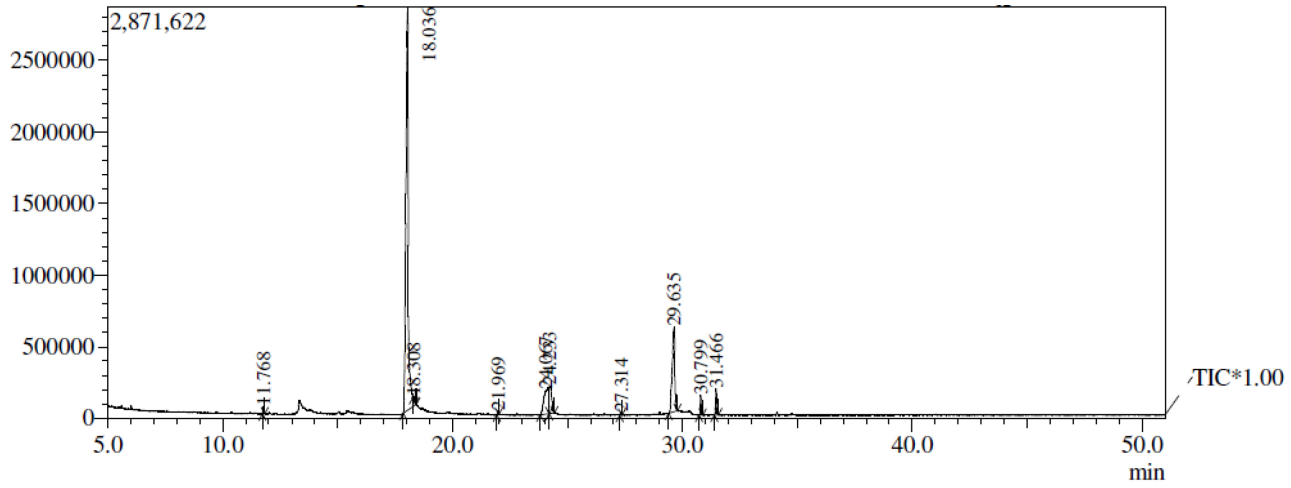

Fig. 3. GC chromatogram of *H. elasticus* growing on *Citrus maxima* (HEC).

Table 3. GC-MS peak report of methanolic extract o*f H. elasticus* obtained from *Citrus maxima* (HEM) with compounds detected

Peak No.	RT	Compound	Area (%)
1	11.768	2,3-Dihydro-3,5-dihydroxy-6-methyl-4H-pyran-4-one	0.43
2	18.036	1,2,3-Benzenetriol	68.65
3	18.308	Methyl 5-oxo-2-pyrrolidinecarboxylate	0.10
4	21.969	Undecanoic acid, methyl ester	0.20
5	24.067	1,3,4,5-Tetrahydroxy-cyclohexanecarboxylic acid	8.42
6	24.233	1,3,4,5-Tetrahydroxy-cyclohexanecarboxylic acid	4.31
7	27.314	Decanoic acid	0.16
8	29.635	Methyl 3,4,5-trihydroxybenzoate	15.12
9	30.799	Hexadecanoic acid, methyl ester	1.03
10	31.466	Hexadecanoic acid	1.59

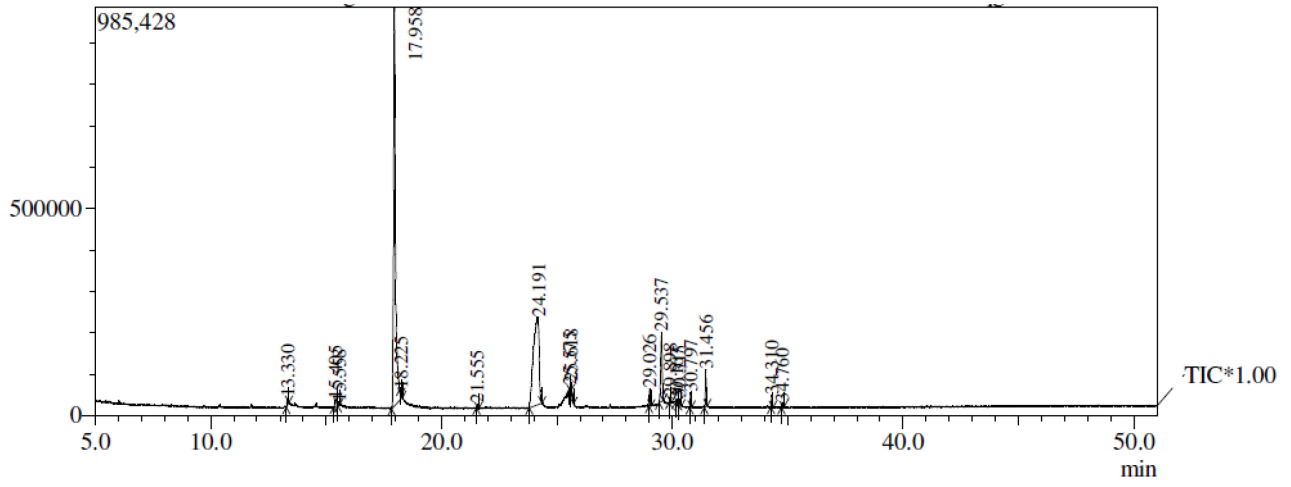

Fig. 4. GC chromatogram of *H. elasticus* growing on *Saraca asoca* (HES).

between mistletoes and their hosts as they require contact signals to recognize a host to initiate the development of the haustorium for its establishment (Desale et al. 2016). Such factors are called haustorium-inducing factors (Jamison, Yoder 2001). Some require chemical signals such as strigolactones for germination of their seeds on the host surface (Xie et al. 2010; Cavar et al 2015). It was reported that haustorium-inducing factors might be species specific and activate specific recognition sites in particular parasites or host plants, which leads to paratite establishment (Tomilov et al. 2006).

The host-parasitic interaction is an ongoing process

Table 4. GC-MS peak report of methanolic extract of *H. elasticus* obtained from *Saraca asoca* (HES) with compounds detected

Peak No.	RT	Compound	Area (%)
1	13.330	1,2-Benzenediol	0.60
2	15.405	2,5-Cyclohexadiene-1,4-dione compound with 1,4-benzenediol	1.04
3	15.558	7-Oxa-1-azabicyclo[3.2.1] octane, 5-methyl-	0.20
4	17.958	1,2,3-Benzenetriol	51.59
5	18.225	l-Proline, 5-oxo-, methyl ester	0.08
6	21.555	2-Tert-butyl-4-(1,1,3,3-tetramethylbutyl) phenol	0.19
7	24.191	1,3,4,5-Tetrahydroxy-cyclohexanecarboxylic acid	33.40
8	25.575	Diglycerol	0.13
9	25.618	Mome inositol	0.91
10	29.026	Butanoic acid, 3,7-dimethyl-6-octenyl ester	0.92
11	29.537	Methyl 3,4,5-trihydroxybenzoate	6.18
12	29.898	9-Dodecen-1-ol (Z)-	0.23
13	30.167	Oxalic acid, cyclobutyl ethyl ester	0.29
14	30.315	Dodecanoic acid	0.57
15	30.797	Tetradecanoic acid, 12-methyl-, methyl ester	0.69
16	31.456	Hexadecanoic acid	2.07
17	34.310	Cyclohexanol, 5-methyl-2-(1-methylethyl)	0.59
18	34.760	4-Pentenal, 2,2-dimethyl	0.30

that alters the chemical profile of both hosts and parasite. Differences in the number of phytochemical components, colour and health-promoting properties found altered in parasitic plants depend on the host on which it is parasitic and on the particular organs of the parasite (Renata et al 2020). Stem parasitic plants show different metabolic profiling and changes during parasitization and such differences are reflected in their life style and morphology (Takeshi et al. 2016)

In the present study the GC chromatograms and peaks obtained from the methanolic extract of *H. elasticus* accessions differed depending on the host. All of the eluted compounds were carefully examined and it was found that 13 different compounds could be considered as the products of *H. elasticus* and that their relative occurrence in different parasitic accessions was greatly influenced by the respective hosts (Table 8). Among these, two compounds were considered as marker compounds of the parasite, whereas some were recognized as assisted marker compounds that did not occur in all samples of *H. elasticus*, but were solely of parasitic origin. The presence of these assisted marker compounds was greatly influenced by the hosts species. 1,2,3-benzenetriol (pyrogallol) and methyl-3,4,5-tri-hydroxybenzoate (methylgallate) were the two major compounds found in all samples of *H. elasticus*, irrespective of their host and these two were the marker compounds of the methanolic extract of the parasite. The weight percentage ratio of these marker compounds found also varied among the host plants. The largest quantity of pyrogallol was obtained in HEN and least from HEC, whereas methyl gallate occurred in highest amount in the accession HEC and least in HEN. Other accessions

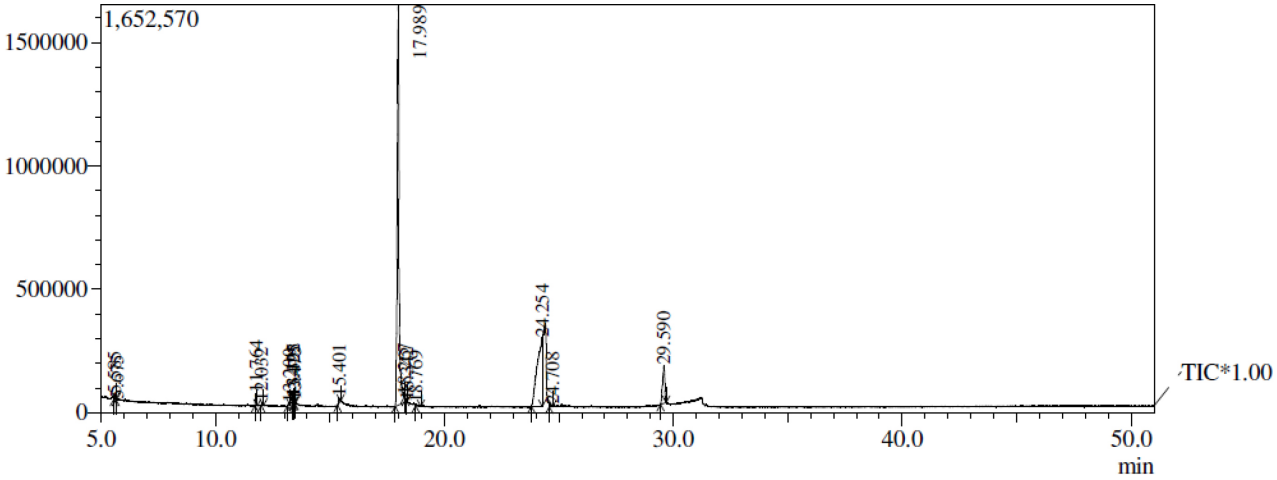

Fig. 5. GC chromatogram of *H. elasticus* growing on *Anacardium occidentale* (HEA).

Table 5. GC-MS peak report of methanolic extract of *H. elasticus* obtained from *Anacardium occidentale* (HEA) with compounds detected

Peak No.	RT	Compound	Area (%)
1	5.585	2(3H)-Furanone	0.34
2	5.675	Propanedioic acid	0.05
3	11.764	2,3-Dihydro-3,5-dihydroxy-6-methyl-4H-pyran-4-one	0.77
4	12.032	Delta(1,1')-biurea	0.24
5	13.200	Brenzkatechin	0.22
6	13.392	(CH3)3CD	0.47
7	13.425	2-Amino-succinamic acid	0.22
8	13.475	Trifluoro-ethene	0.06
9	15.401	2,5-Cyclohexadiene-1,4-dione compound with 1,4-benzenediol	0.60
10	17.989	1,2,3-Benzenetriol	63.36
11	18.267	Alpha-aminoisobutyronitrile	0.00
12	18.342	Thymine	0.01
13	18.769	2,5-Cyclohexadiene-1,4-dione compound with 1,4-benzenediol	0.19
14	24.254	1,3,4,5-Tetrahydroxy-cyclohexanecarboxylic acid	26.67
15	24.708	(CH3)3CD	0.34
16	29.590	Methyl 3,4,5-trihydroxybenzoate	6.45

also showed a large area percentage for these compounds. Both these compounds are phenolic derivatives that likely have a crucial role in parasitic adaptations. Converting surface phenolics to benzoquinons by parasitic derived oxidase enzymes acts as developmental signals for the transition from vegetative to parasitic growth (Kim et al. 1998). It has also been reported that a wide range of simple phenols can cause the establishment of haustoria in parasitic Scrophulariaceae members (Lynn, Chang 1990; Chang, Lynn 1986). The compound 1,3,4,5-tetrahydroxy cyclohexane carboxylic acid was also detected in all parasite sample except HEN. This compound was detected in its host *Nerium oleander*. The following compounds were found in all parasite accessions with the exception of those given in brackets: 1,2 benzenediol (except in HEC and HEA), hexadecanoic acid (except in HEN and HEA) and 2,3-dihydro-3,5-dihydroxy-6-methyl-4H-pyran-4-one (except in HEN and HES). Among these compounds hexadecenoic acid was detected in *Citrus maxima* (the host of HEC) and 2,3-dihydro-3,5-dihydroxy-6-methyl-4H-pyran-4-one in three host species: *Nerium oleander, Citrus maxima* and *Anacardium occidentale*. Absence of some of these compounds in hemi-parasitic plant samples collected from different hosts might be due to the hindrance in their production by the respective hosts. The marker compound 1,2,3-benzenetriol of the parasite found in the host plants *Hevea brasiliensis, Saraca asoca* and *Anacardium occidentale* could be derived from the attached parasite *H. elasticus*. Similarly, hexadecanoic acid and 2,3-dihydro-3,5-dihydroxy-6-methyl-4H-pyran-4-one are also transported from the parasite to the respective hosts. Absence of these compounds in some samples of

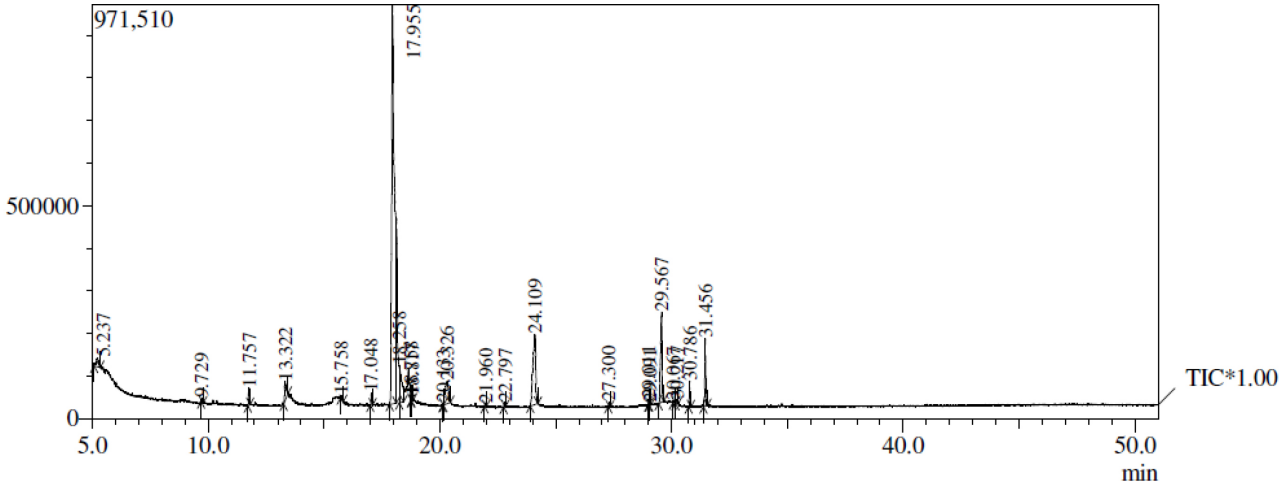

Fig. 6. GC chromatogram of *H. elasticus* growing on *Murraya koenigii* (HEM).

Table 6. GC-MS peak report of methanolic extract of *H. elasticus* obtained from *Murraya koenigii* (HEA) with compounds detected

Peak No.	RT	Compound	Area (%)
1	5.237	Propiolic acid	1.34
2	9.729	Ethyl 6-oxo-5-propylheptanoate	0.19
3	11.757	2,3-Dihydro-3,5-dihydroxy-6-methyl-4h-pyran-4-one	0.80
4	13.322	1,2-Benzenediol	1.95
5	15.758	Butyl 1-methyl-2-pyrrolidinecarboxylate	0.10
6	17.048	l-Proline, 1-methyl-5-oxo-, methyl ester	0.54
7	17.955	1,2,3-Benzenetriol	62.74
8	18.258	Methyl 5-oxo-2-pyrrolidinecarboxylate	4.53
9	18.758	3-Butyn-2-ol	0.11
10	18.817	2-Heptanamine	0.17
12	20.326	Pyrrolin-2-one-5-methanol, N-methyl-	4.08
13	21.960	Methyl 6-hydroxycaproate	0.14
14	22.797	Propane, 2-methoxy-2-methyl	0.21
15	24.109	1,3,4,5-Tetrahydroxy cyclohexanecarboxylic acid	10.92
16	27.300	Nitrous acid, 3-methyl butyl ester	0.22
17	29.011	1-Acetyl-1H-pyrazole	0.16
18	29.091	Butanoic acid	0.04
19	29.567	Methyl 3,4,5-trihydroxybenzoate	6.97
20	30.067	Acetic acid, cyano-	0.21
21	30.217	2-Methyl-5-hexen-3-ol	0.26
22	30.786	Heptadecanoic acid, methyl ester	1.03
23	31.456	Hexadecanoic acid	3.22

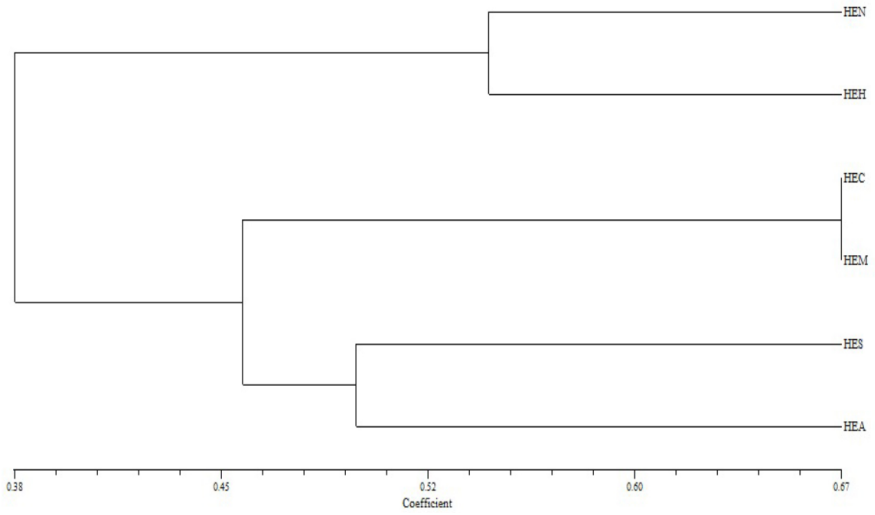

Fig. 6. Jaccard's UPGMA tree based on the occurrence of 13 compounds among six accessions of *Helicanthes elasticus*.

Table7. Jaccard's similarity matrix based on the occurrence of 13 compounds among six accessions of *H. elasticus*

	HEN	HEH	HEC	HES	HEA	HEM
HEN	1					
HEH	0.615	1				
HEC	0.385	0.62	1			
HES	0.385	0.62	0.54	1		
HEA	0.385	0.46	0.69	0.69	1	
HEM	0.462	0.54	0.77	0.62	0.62	1

H. elasticus might be due to the influence of hosts during the establishment of parasite. Such cases were previously reported in the holoparasitic plant *Cuscuta reflexa* in which GC-MS analysis the plant obtained from two hosts *Cassia fistula* and *Ficus benghalensis* differed in phytochemical constituents (Bais, Kakkar 2013; Bais, Kakakr 2014). Region dependent variation in phytoconstituents was also reported in ethanolic extract of *Cuscuta reflexa* assessed by GC-MS (Rai et al. 2016). Marked variation in secondary metabolites also occurred in the ethanolic bark extract of *Loranthus longiflorus* growing on *Casuarina equisetifolia* and *Ficus religiosa* (Chandrakasan, Neelamegham 2011a) and *Ficus religiosa* had greater tannin content in bark samples of *Loranthus longiflorus* than *Casuarina equisetifolia* (Chandrakasan, Neelamegham 2011b).

Transfer of specific compounds from parasite to host cells could be considered as a suppressing signal molecule that suppresses the so-called immune system of the host plant such that the parasite can establish within the hosts. Resistant host plants detect parasite molecules for immune system activation to eradicate the parasite, while the parasitic derived compounds have virulence functions such as host immunity suppression (Saucet, Shirasu 2016). Such a dynamic nature of adaptation often leads to co-evolution among the partners of the interaction and thereby leads to speciation. During such host-parasitic interactions, some chemical molecules might be transferred from parasite to hosts and hence such molecules would not be get detected in parasite samples. 1,3,4,5 tetrahydroxy cyclohexane carboxylic acid and 2,3-dihydro-3,5-dihydroxy-6-methyl-4H-pyran-4-one played such a role in *H. elasticus* growing on *Nerium oleander*, which can explain why these compounds were completely absent in the parasite but detected in the host plant. These compounds might get transported from the parasite to the host as soon as it was synthesized through the haustoria as a chemical signal that supported the parasite's survival on the particular host by reducing its fitness. The exchange of potential defense signalling molecules between host and parasite through a haustorial interface is well established in many parasitic plants (Christopher et al. 2019). Chemical signals in the form of cytokinin-like compounds were reported to be transported from the parasitic plant *Phtheirospermum japonicum* to its host *Arabidopsis thaliana* to reduce host fitness and thereby ensure well establishment of parasite within the host (Thomas et al. 2017). It was reported that presence of certain secondary metabolites that differ within a population of hemiparasites depend upon the host-parasitic association (Stermitz, Harris 1987). In *Nerium oleander*, the above mentioned chemical might have a suppressing role on the plants defense mechanism to eliminate the parasite, acting as an immunosuppressant in a human during organ transplantation, allowing the parasite to establish on *Nerium oleander*. Host susceptibility to parasite attack could result from the active suppression of the host defense system by parasite-derived molecules (Asai, Shirasu 2015)

When a parasite tries to establish within a new host, the host produces chemicals to suppress its growth. For example, sequestration of mangiferin from *Mangifera indica* to *Dendrophthoe falcata* was observed to occur in the initial stages of infection as an initial host defense mechanism in response to the biotic stress caused by parasite, and these host defense molecules were found to be further utilized by the parasite as host recognition cues (Jadhav et al. 2005). Deposition of phenolic compounds by host plants often leads to the arrest of invasion of parasite, leading to necrosis of the parasite's invading tissue (Swarbrick et al. 2008; Yohida, Shirasu, 2009). In such cases, the parasites must co-evolve to counteract their hosts by transferring their own secondary metabolites or similar compounds, which reduce the host fitness. Most of these compounds

Table 8. Compounds identified as parasitic in origin. Compound indicated by √ symbol obtained in the respective accession of *H. elasticus*. *Marker compounds ** Assisted marker compounds

No.	Compound	HEN	HEH	HEC	HES	HEA	HEM
1	1,2,3-Benzenetriol*	√	√	√	√	√	√
2	Methyl-3,4,5-trihydroxybenzoate*	√	√	√	√	√	√
3	1,3,4,5-Tetrahydroxy-cyclohexanecarboxylic acid**		√	√	√	√	√
4	1,2-Benzenediol**	√	√		√		√
5	Hexadecanoic acid**		√	√	√		√
6	2,3-Dihydro-3,5-dihydroxy-6-methyl-4h-pyran-4-one**		√	√		√	√
7	Hexadecanoic acid, methyl ester	√	√	√			
8	Tetradecanoic acid, 12-methyl-, methyl ester		√		√		
9	Nonanoic acid, methyl ester	√	√				
10	Butanoic acid	√					√
11	1-Butanol, 3-methyl-	√	√				
12	Methyl5-oxo-2-pyrrolidinecarboxylate			√			√
13	2,5-Cyclohexadiene-1,4-dione, compaund with 1,4-benzenediol				√	√	

have such a role in *H. elasticus* when infecting a host. The compounds 1,2-benezenediol, hexadecanoic acid and 2,3-dihydro-3,5-dihydroxy-6-methyl-4H-pyran-4-one can be considered as assisted markers of methanolic extract of *H. elasticus*, because the presence of these compounds was influenced by specific hosts only and their occurrence could not be confirmed in all the samples of parasite. The remaining seven compounds might be of parasitic origin alone, but their presence in the parasitic accessions depends on the host plant species. Most of the studied host trees might have suppressed the production of these compounds within the parasite. In *Cuscuta reflexa*, steroid properties and their amount were observed to differ during its establishment in *Momordica* (Takeshi et al. 2016). The life cycle of parasite weed is closely regulated by their hosts and the secondary metabolites produced by the hosts also playing an important role this interactions (Harro et al. 2003).

The parasite (*H. elasticus*) growing on different host plants produced different types of chemicals other than the major and assisted marker compounds and this clearly shows that the host had a significant influence on the phytochemical production of the parasite. Moreover, the UPGMA tree placed the hemi-parasitic accessions in various clusters, which clearly indicates the host effect on phytochemical production of the parasite. Except for the peak observed in marker compounds, the chromatograms and the number of compounds eluted differed among samples of *H. elasticus*, showing the effect of the host. This might occur during the preliminary infection stage or after the establishment of parasite within the host and the effect of the host on the parasite altered the metabolic pathways of the parasite, resulting in the production of variable chromatograms with a large number of significant chemicals within the parasite.

Conclusions

The work demonstrated that *H. elasticus* accessions collected from six different hosts that even though the parasite was of the same species, the production of chemical compounds could be altered by the influence of the host. Six accessions showed varied composition of compounds, in which 1,2,-benzenetriol and methyl-3,4,5-trihydroxybenzoate can be recognized as the marker compounds in the methanolic extract of *H. elasticus*. Along with these compounds, some are assisted marker compounds of this plant, whose occurrence and abundance are greatly affected by the host plant. The parasite growing in specific hosts can contain a greater number of therapeutically important chemicals. The UPGMA comparison of the studied accessions revealed host and *H. elasticus* covolution, which may lead to host-directed speciation in this mistletoe. A phytochemical mosaicism are apparently visible in this hemi-parasitic plant emerged as a result of mistletoe-host interactions. Therefore, when making preparations of a drug from the extracts, decoctions or powder of this parasitic plant, prime importance should be given to the host plant from which it was harvested or obtained. Comprehensive understanding of the chemical makeup and pro-health features of this species could lead to its use in a variety of medical disciplines as a spectacular product for treating a variety of human maladies.

Acknowledgements

We would like to express our sincere gratitude to all the staff of Department of Non timber products, Kerala Forest Research Institute, Thrissur, Kerala, India for providing the lab facilities for doing the analysis. This work did not receive any financial assistance from any of the funding agencies. All the authors declare that they have no interest conflict.

References

Ajith Kumar T.G., Mathew L. 2020. A short survey for new hosts of *Helicanthes elastica* (Desr.) Danser and its morphological diversity on selected hosts. *Indian For.* 146: 143–147.

Asai S., Shirasu K. 2015. Plant cells under siege: plant immune system versus pathogen effectors. *Curr. Opin. Plant Biol.* 28:1–8.

Bais N., Kakkar A. 2013. Comparative phytochemical analysis of *Cuscuta reflexa* parasite grown on *Cassia fistula* and *Ficus benghalensis* by GC-MS. *Int. J. Pharm. Pharm. Sci.* 5: 350–355.

Bais N., Kakkar A. 2014. Phytochemical analysis of methanolic extract of *Cuscuta reflexa* grown on *Cassia fistula* and *Ficus benghalensis* by GC-MS. *Int. J. Pharm. Sci. Rev. Res.* 25: 33–36.

Barlow B.A., Hawksworth F.G., Kuijt J., Polhill R.M., Wiens D. 1989. Genera of mistletoes. *The Golden Bough* 11: 1–4.

Betz J.M., Gay M.L., Mossoba M.M. Adams S., Portz B.S. 1997. Chiral gas chromatographic determination of ephedrine-type alkaloids in dietary supplements containing Ma Huang. *J. AOAC Int.* 80: 303–315.

Bouwmeester H.J., Matusova R., Sun Z., Beale M.H. 2003. Secondary metabolite signalling in host–parasitic plant interactions. *Curr. Opin. Plant Biol.* 6: 358–364.

Calder D.M., Lennox F.G., Bernhardt. 1982. Natural hybridazation between *Amyema pendulum* and *Amyema quandang*, Loranthaceae. *Austr. J. Bot.* 30: 625–633.

Cavar S., Zwanenburg B., Tarkow P. 2015. Strigolactones: occurrence, structure, and biological activity in the rhizosphere. *Phytochem. Rev.* 14: 691–711.

Chandrakasan L., Neelamegam R. 2011a. GC-MS analysis of *Loranthus longiflorus* Desr (a hemi-parasite) bark harvested from two host trees. *J. Pharm. Res.* 4: 3072–3074.

Chandrakasan L., Neelamegam R. 2011b. *In vitro* studies on antioxidants and free radical scavenging activities in the extracts of *Loranthus longiflorus* Desr bark samples obtained from two host trees. *J. Phytol.* 3: 22–30.

Chang M., Lynn D.G. 1986. The haustorium and the chemistry of host recognition in parasitic angiosperms. *J. Chem. Ecol.* 12:561–579

Clarke C.R., Timko M.P., Yoder J.I., Axtell M.J., Westwood J.H. 2019. Molecular dialog between parasitic plants and their hosts. *Annu. Rev. Phytopathol.* 57: 279–99.

Franklin U.O., Wintola O.A., Afolayan A.J. 2017.

Micromorphological studies of the Loranthaceae, *Phragmanthera capitata* (Sprengel) Balle. *J. Bot.* 2017: 5603140.

Furuhashi T., Nakamura T., Iwase K. 2016. Analysis of metabolites in stem parasitic plant interactions: interaction of *Cuscuta–Momordica* versus *Cassytha–Ipomoea*. *Plants* 5: 1–14.

Gamble J.S. 1967. *The Flora of the Presidency of Madras*. 2nd Ed. Botanical Survey of India, Culcutta, pp. 873–878.

Indrani N., Balasubhramanian K. 1985. Chemical examination of *Dendrophthoe falcata* growing on *Terminalia tomentosa*. *Leather Sci.* 32: 206

Jadhav R.B., Anarthe S.J., Surana S.J., Gokhale S.B. 2005. Host-hemiparasite transfer of the C-glucosyl xanthone mangiferin between *Mangifera indica* and *Dendrophthoe falcata*. *J. Plant Interact.* 1: 171–177.

Jain S K. 1965. Medicinal Plantlore of the tribals of Baster. *Econ. Bot.* 19: 236–250.

Jamison D.S., Yoder J.I. 2001. Heritable variation in quinine induced haustorium development in the parasitic plant *Triphysaria*. *Plant Physiol.* 125: 1870–1880.

Kim D., Kocz R., Boone L., W. Keyes J., Lynn D.G.1998. On becoming a parasite: evaluating the role of wall oxidases in parasitic plant development. *Chem. Biol.* 5: 103–117.

Lynn D.G., Chang M.1990. Phenolic signals in cohabitation: implications for plant development. *Annu. Rev. Plant Physiol. Plant Mol. Biol.* 41: 497–526.

Manickam D., Periyasamy L. 2014. GC-MS analysis of methanol extract of *Decalepis hamiltonii* root (Wight and Arn). *World J. Pharm. Pharm. Sci.* 3: 983–989.

Namboothiri K.R.R. 2011. *Albutha Oushadha Chedikal.* 5th Ed. H&C Pubishing House, Thrissur.

Nayar T.S., Rasiya Beegum A., Mohanan N., Rajkumar G., Sibi, M. 2006. *Flowering Plants of Kerala: A Handbook*. Tropical botanic garden and research institute, Palode, Thiruvanathapuram.

Okubamichael D.Y., Griffiths M.E., Ward D. 2017. Host specificity in parasitic plants – perspectives from mistletoes. *AoB Plants* 8: plw069.

Piwowarczyk R., Ochmian I., Lachowicz S., Kapusta I., Sotek Z., Blaszak B. 2020. Phytochemical parasite-host relations and interactions: A *Cistanche armena* case study. *Sci. Total Environ.* 716:1–11

Press M.C., Graves J. 1995. *Parasitic Plants*. Chapman and Hall, London, UK.

Rai D.K., Sharma V., Pal K., Gupta R. 2016. Comparative phytochemical analysis of *Cuscuta reflexa* Roxb parasite grown on North India by GC-MS. *Trop. Plant Res.* 3: 428–433.

Rajasekaran K. 2007. Studies in Indian Loranthaceae VIII-Inflorescence. *J. Econ. Taxon. Bot.* 31: 177–180.

Sasidharan N., Sivarajan V.V. 1996. Flowering plants of Thrissur forest (Western Ghats, Kerala, India). Scientific Publishers. Jodhpur, pp. 385.

Saucet S.B ., Shirasu K. 2016. Molecular parasitic plant-host interactions. *PLoS Pathol.* 12: 1–6.

Scot G.J. 1871. Loranthaceae – the mistletoe order germination and mode of attachment. *J. Agr. Hort. Soc. India* 2: 257

Shanavaskhan A.E., Sivadasan M., Ahmed H., Alfarhan, M.,Thomas, J. 2012. Ethnomedicinal aspects of angiospermic parasites and epiphytes of Kerala India. I*ndian J. Tradit. Knowl.* 11: 250–258.

Shanavaskhan A.E., Sivadasan M. 2009. *Epiphytes and Parasites of Kerala India*. 1st Ed. Bihen Singh Mahendrapal Singh, Dehradun, pp. 213–272.

Stermitz F.R., Harris G.H. 1987. Transfer of pyrrolizidine and quinolizidine alkaloids to *Castilleja* (Scrophulariaceae) hemiparasites from composite and legume host plants. *J. Chem. Ecol.* 13: 1917–1925.

Sunil Kumar K.N., Saraswathy A., Amerjothy S. 2015. Survey report on hosts and haustoria of *Helicanthes elastica* (Desr.) Danser in Udupi and Dakshina Kannada districts of Karnataka and Kasargod district of Kerala, India – A concise review plus some new additions. *Indian For.* 141: 448–451.

Swarbrick P.J., Huang K., Liu G., Slate J., Press M.C., Scholes J.D. 2008. Global patterns of gene expression in rice cultivars undergoing a susceptible or resistant interaction with the parasitic plant *Striga hermonthica*. *New Phytol.* 179:515–529

Thomas S., Melnyk C.W., Wakatake T., Zhang J. Sakamoto Y., Kiba T., Yoshida S., Matsunaga S., Sakakibara H., Shirasu K. 2017. Interspecies hormonal control of host root morphology by parasitic plants. *Proc. Natl. Acad. Sci. USA* 114: 5283–5288.

Thriveni M.C. 2013. Studies on Loranthaceae and Viscaceae of Karnataka. PhD Thesis. University of Mysore.

Tomilov A., Tomilova N., Shin D., Jamison D., Torres M., Reagan R., McGray H., Horning T., Truong R., Nava A., Yoder J. 2006. Chemical signalling between plants: mechanistic similarities between phytotoxic allelopathy and host recognition byparasitic plants. In: Dicke M., Takken W. (Eds.) *Chemical Ecology: from Gene to Ecosystem*. Springer, Dordrecht, pp. 55–69.

Warrier P.K., Nambiar V.P., Ramankutty C. 1996. *Indian Medicinal Plants*. Orient Longman, Madras.

Watson D.M. 2001. Mistletoe: a keystone resource in forests and woodlands worldwide. *Annu. Rev. Ecol. Syst.* 32: 219–249.

Wilson C.A., Calvin C.L. 2006. An origin of aerial branch parasitism in the mistletoe family, Loranthaceae. *Am. J. Bot.* 93: 787–796.

Xie X., Yoneyama K., Yoneyama K. 2010. The Strigolactone story. *Annu. Rev. Phytopathol.* 48: 93–117.

Yoshida S., Shirasu K. 2009. Multiple layers of incompatibility to the parasitic witchweed, *Striga hermonthica*. *New Phytol.* 183:180–189.

Received 27 June 2021; received in revised form 21 August 2021; accepted 10 September 2021

Facial Emotion Recognition

*Lakshmi Anand, Teena Thomas.

Assistant Professor, Carmel College, Mala, India
Email: lakshmi@carmelcollegemala.ac.in

Abstract

Facial Expression conveys non-verbal cues, which plays important roles in interpersonal relations. The Facial Expression Recognition system is the process of identifying the emotional state of a person. In this system captured image is compared with the trained dataset available in database and then emotional state of the image will be displayed.

This system is based on image processing and machine learning. For designing a robust facial feature descriptor, Gabor wavelet is applied which is well known for textural analysis and facial feature recognition

The recognition performance of the proposed method will be evaluated by using the trained database with the help of Support Vector Machine. K-Nearest Neighbor, Random Forest and Adaboost classifiers. Proposed method is evaluated on the COHN-KANADEdataset.

Keywords—Facial expression recognition (FER), Gabor wavelet, Support Vector Machine (SVM), k-Nearest Neighbor (kNN), Random Forest (RF), Adaboost classifier

Introduction

A Facial expression is the visible manifestation of the affective state, cognitive activity [1], intention, personality and psychopathology of a person and plays a communicative role in interpersonal relations. It has been studied for a long period of time and obtaining the progress recent decades. Though much progress has been made, recognizing facial expression with a high accuracy remains to be difficult due to the complexity and varieties of facial expressions [2].

Generally human beings can convey intentions and emotions through nonverbal ways such as gestures, facial expressions and involuntary languages. This system can be significantly useful, nonverbal way for people to communicate with each other. The important thing is how fluently the system detects or extracts the facial expression from image. The system is growing attention because this could be widely used in many fields like lie detection, medical assessment and human computer interface. The Facial Action Coding System (FACS), which was proposed in 1978 by Ekman and refined in 2002, is a very popular facial expression analysis tool [3].

On day to day basics humans commonly recognize emotions by characteristic features, displayed as a part of a facial expression. For instance happiness is undeniably associated with a smile or an upward movement of the corners

of the lips. Similarly other emotions are characterized by other deformations typical to a particular expression. Research into automatic recognition of facial expressions addresses the problems surrounding the representation and categorization of static or dynamic characteristics of these deformations of face pigmentation [8].

The system classifies facial expression of the same person into the basic emotions namely anger, disgust, fear, happiness, sadness and surprise. The main purpose of this system is efficient interaction between human beings and machines using eye gaze, facial expressions, cognitive modeling etc. Here, detection and classification of facial expressions can be used as a natural way for the interaction between man and machine. And the system intensity vary from person to person and also varies along with age, gender, size and shape of face, and further, even the expressions of the same person do not remain constant with time.

However, the inherent variability of facial images caused by different factors like variations in illumination, pose, alignment, occlusions makes expression recognition a challenging task. Some surveys on facial feature representations for face recognition and expression analysis addressed these challenges and possible solutions in detail [5].

Related Work

Research in the fields of face detection and tracking has been very active and there is exhaustive literature available on the same. The major challenge that the researchers face is the non-availability of spontaneous expression data [1]. Capturing spontaneous expressions on images and video is one of the biggest challenges ahead [2]. Many attempts have been made to recognize facial expressions. Zhang et al investigated two types of features, the geometry-based features and Gabor wavelets based features, for facial expression recognition.

Appearance based methods, feature invariant methods, knowledge based methods, Template based methods are the face detection strategies whereas Local Binary Pattern phase correlation, Haar classifier, AdaBoost, Gabor Wavelet are the expression detection strategies in related field [3]. Face reader is the premier for automatic analysis of facial expression recognition and Emotient, Affectiva, Kariosetc are some of the API's for expression recognition. Automatic facial expression recognition includes two vital aspects: facial feature representation and classifier problem [2].

Facial feature representation is to extract a set of appropriate features from original face images for describing faces. Histogram of Oriented Gradient (HOG), SIFT, Gabbor Fitters and Local Binary Pattern (LBP) are the algorithms used

for facial feature representation [3,4]. LBP is a simple yet very efficient texture operator which labels the pixels of an image by thresholding the neighborhood of each pixel and considers the result as a binary number. The operator labels the pixels of an image by thresholding the 3X3 neighborhood of each pixel with the center value and considering the result as a binary number [3]. HOG was first proposed by Dalal and Triggs in 2005. HOG numerates the appearance of gradient orientation in a local path of an image.

For classifier problem we use algorithms like Machine learning, Neural Network, Support Vector Machine, Deep learning, Naive Bayes. The formation of histogram by using any of facial feature representation will use Support Vector Machine (SVM) for expression recognition. SVM builds a hyperplane to separate the high dimensional space. An ideal separation is achieved when the distance between the hyper plane and the training data of any class is the largest [4].

The size of the block for the LBP feature extraction is chosen for higher recognition accuracy. The testing results indicate that by using LBP features facial expressions recognition accuracy is more than 97%. The block LBP histogram features extract local as well as global features of face image resulting higher accuracy. LBP is compatible with various classifiers, filters etc. [3].

Proposed method

he facial expression recognition system is trained using supervised learning approach in which it takes images of different facial expressions. The system includes the training and testing phase followed by image acquisition, face detection, image preprocessing, feature extraction and classification. Face detection and feature extraction are carried out from face images and then classified into six classes belonging to six basic expressions which are outlined below:

3.2.1. Image Acquisition

Images used for facial expression recognition are static images or image sequences. Images of face is captured.

3.2.2. Face detection

Face Detection is useful in detection of facial image. Face Detection is carried out in training dataset using Haar classifier called Voila-Jones face detector and implemented through Opencv. Haar like features encodes the difference in average intensity in different parts of the image and consists of black and white connected rectangles in which the value of the feature is the difference of sum of pixel values in black and white regions [6].

3.2.3. Image Pre-processing

Image pre-processing includes the removal of noise and normalization against the variation of pixel position or brightness.

a) Color Normalization

b) Histogram Normalization

3.2.4. Feature Extraction

Gabor wavelet method, which is well known for textural analysis and facial feature recognition, was chosen in our recognition system to represent the facial expressions. The signers' expression intensity and duration variations are not unique. Therefore, some common measuring criteria are required for modeling facial expression changes in an image sequence. Facial expressions were described with the help of Gabor wavelet parameters chosen from the partitioned facial areas. These feature parameters were incorporated with Euclidean distance measure to represent the facial expression changes in an image sequence.

3.2.4.1. Gabor Wavelet

Gabor features were calculated by convolution of input image with Gabor filter bank [12] [13]. Gabor filter works as a

band pass filter for the local spatial frequency distribution thereby achieving an optimal resolution in both the spatial and frequency domain. The 2D Gabor filter $\psi(x,y,f,\theta)$ can be represented as a complex sinusoidal signal, modulated by a Gaussian kernel function as in Eq (1).

$$\psi(x,y,f,\theta) = [1/2\pi\sigma^2]\,[\exp\{-(x_1^2+y_1^2)/2\sigma^2\}]\,[\exp\{2\pi f x_1\}]$$

where $x_1 = x\cos\theta + y\sin\theta$

$y_1 = -x\sin\theta + y\cos\theta$

σ is the standard deviation of Gaussian envelop along the x, y dimension, f is the central frequency of the sinusoidal plane wave, θ is the orientation of gabor filter.

Feature extraction procedure can then be written as the convolution of gray scale facial expression image $I(x,y)$, with the Gabor filter $\psi(x,y,f,\theta)$ as in Eq (2).

$$G_{x,y,f,\theta}(x,y) = I(x,y) * \psi(x,y,f,\theta)$$

In Eq (2) represent the complex convolution output which can decomposed into real and imaginary part as follows:

$$E_{x,y,f,\theta}(x,y) = Re[G_{x,y,f,\theta}(x,y)] \text{ and } O_{x,y,f,\theta}(x,y) = I_m[G_{x,y,f,\theta}(x,y)].$$

Based on these result, both the phase as well as the magnitude response of the filter can be computed. In this work

Gabor feature representation was based only on the magnitude response of the Gabor filter by neglecting the phase information. Small spatial displacement causes significant variation in phase value. Due to this variation, the two Gabor features could not be directly compared. Magnitude response of the filter can be computed as in Eq (3).

$$A_{(u,v)}(x,y) = \sqrt{(E^2 + O^2)}, \text{ where } E = E_{(u,v)}(x,y) \text{ and } O = O_{(u,}$$

A Gabor filter bank with 5 frequencies and 8 orientations was used to extract Gabor features in our work. Down sampling was done on all magnitude response, which were then normalized and concatenated into Gabor Feature Vector.

3.2.4.2. Distance Measure on Gabor Feature Vector

Gabor wavelet feature vector representing magnitude information in 2D real matrix form was converted to one dimensional matrix without any loss in information. For a facial expression corresponding to a frame, feature vectors were generated for upper and lower face regions which was partitioned horizontally alone the elliptical centre. In our work we concentrated only on first and last frames in the videos corresponding to isolated expression sentences. By this processing method, four feature vectors were extracted from a

video where two feature vectors were representing the upper part of the faces in the first and last frame and another two vectors representing the lower parts. Later, the Euclidean distance measure was applied between feature vectors corresponding to the upper parts and lower part feature vectors. In addition, the percentage change that occurs in the upper and lower face areas corresponding to the total change between the neutral and peak expression vectors were calculated. All these four measures later act as the feature descriptors for the facial expression changes.

3.2.5. Classification

The dimensionality of data obtained from the feature extraction method is very high so it is reduced using classification. Features should take different values for object belonging to different class so classification will be done using Support Vector Machine algorithm, k Nearest Neighbor, Random Forest Method and Adaboost Classifier.

3.2.5.1. Support Vector Machines

SVM is widely used in various pattern recognition tasks. SVM is a state-of-the-art machine learning approach based on the modern statistical learning theory. SVM can achieve a near optimum separation among classes. SVMs is trained to perform facial expression classification using the features proposed. In

general, SVM are the maximal hyperplane classification method that relies on results from statistical learning theory to guarantee high generalization performance.

Kernel functions are employed to efficiently map input data which may not be linearly separable to a high dimensional feature space where linear methods can then be applied. SVMs exhibit good classification accuracy even when only a modest amount of training data is available, making them particularly suitable to a dynamic, interactive approach to expression recognition [10].

An ideal separation is achieved when the hyper plane and the training data of any class is the largest. This separating hyper plane works as the decision surface. SVM has been successfully employed for a number of classification tasks such as text categorization, genetic analysis and face detection [11].

Given a training set of labeled samples:

$D=\{(xi,yi)|xi \in Rn,yi \in \{-1,1\}\}pi=1$ (1)

A SVM tries to find a hyperplane to distinguish the samples with the smallest errors.

$w.x-b=0$ (2)

For an input vector xi, the classification is achieved by

computing the distance from the input vector to the hyperplane. The original SVM is a binary classifier [4].

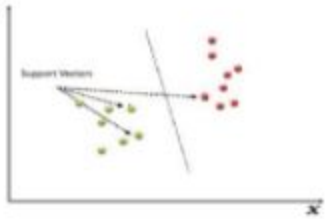

Figure 1: SVM classification

3.2.5.2. k Nearest Neighbor

k-nearest neighbors is a simple algorithm that can be used for solving both classification and regression problems. It has been used in statistical estimation and pattern recognition already in the beginning of 1970's. KNN is simple to understand and is one of the most widely used methods for its faster training phase. It is a nonparametric approach where it does not make any assumption on the underlying data distribution. This is convenient since most of the practical data does not get along with the theoretical assumptions (linearly separable, Gaussian mixture etc.). KNN is a lazy algorithm which means that it avoids using training data points for generalization. It also

means that KNN keeps all the training data which translates to a faster training phase. But the whole training data set or at least a subset of that is required to decide which makes the testing period longer.

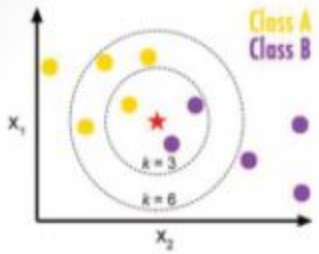

Figure 2: KNN classification

KNN classifier assigns a class label for unknown samples by estimating its k-nearest neighbors based on known samples. KNN assumes that the data is in a feature space. The data can be scalars or multidimensional vectors. Since the points are in feature space, they have a notion of distance. All the training examples are stored in the form of $(x_i, f(x_i))$, where x_i is the n- dimensional input feature vector $(x_{i1}, x_{i2}, x_3 \dots x_n)$ and $f(x)$ is the corresponding output. If there is a query point x_q

which is another vector with n-attributes $(x_{q1}, x_{q2}, x_{q3} \dots x_{qn})$. KNN finds the k training examples that are most similar to it using the standard Euclidean distance as a measure of similarity between each training example x_i and x_q :[14]

$$d(x_i, x_q) = \sqrt{(x_{i1} - x_{q1})^2 + (x_{i2} - x_{q2})^2 + \cdots + (x_{in} - x_{qn})^2}$$

If the target function is discrete-valued, KNN returns the most common target function value among the neighbors of the query point. A case is classified by majority vote of its neighbors. A case being assigned to the class most common amongst its k-nearest neighbors measured by a distance function. In case of $k = 1$, it is simply assigned to the class of its nearest neighbor. The value of k can be anywhere between 1 and the total number of instances in the training data set. Lower value of k might result in a noisier result. So, in general, a large value of k is more precise as it generally reduces the overall noise but there is no guarantee. Cross-validation is also an effective way to determine an optimal value of k by using an independent data set to validate the k value. Now, if k is equal to the total number of instances in the training data set, for any query instance, all the other instances in the training set becomes the nearest neighbor. If this happens, the predicted response for a new instance is just the frequent response variable in the training set. This is comparatively simpler compared to other

machine learning algorithm and produces predictions with high accuracy. With a large value of k when the number of the training instances becomes very big, it has been observed the asymptotic error rates gets aligned with the optimal Bayes error rate. For this reason, the KNN mechanism has a standard comparison method against which any new classifiers, such as neural networks, can be compared.

3.2.5.3. Random Forest Classifier

Random Forest is a flexible, easy to use machine learning algorithm that produces, even without hyper-parameter tuning, a great result most of the time. It is also one of the most used algorithms, because it's simplicity and the fact that it can be used for both classification and regression tasks.

Random Forest is a supervised learning algorithm. Like you can already see from it's name, it creates a forest and makes it somehow random. The "forest" it builds, is an ensemble of Decision Trees, most of the time trained with the "bagging" method. The general idea of the bagging method is that a combination of learning models increases the overall result.

One big advantage of random forest is, that it can be used for both classification and regression problems, which form the majority of current machine learning systems. I will talk

about random forest in classification, since classification is sometimes considered the building block of machine learning.

Random Forest has nearly the same hyper parameters as a decision tree or a bagging classifier. Fortunately, you don't have to combine a decision tree with a bagging classifier and can just easily use the classifier-class of Random Forest. Like I already said, with Random Forest, you can also deal with Regression tasks by using the Random Forest regressor.

Random Forest adds additional randomness to the model, while growing the trees. Instead of searching for the most important feature while splitting a node, it searches for the best feature among a random subset of features. This results in a wide diversity that generally results in a better model.

Therefore, in Random Forest, only a random subset of the features is taken into consideration by the algorithm for splitting a node. You can even make trees more random, by additionally using random thresholds for each feature rather than searching for the best possible thresholds (like a normal decision tree does).

Random forests is a supervised learning algorithm. It can be used both for classification and regression. It is also the most flexible and easy to use algorithm. A forest is comprised of trees. It is said that the more trees it has, the more robust a forest

is. Random forests creates decision trees on randomly selected data samples, gets prediction from each tree and selects the best solution by means of voting. It also provides a pretty good indicator of the feature importance.

Random forests has a variety of applications, such as recommendation engines, image classification and feature selection. It can be used to classify loyal loan applicants, identify fraudulent activity and predict diseases. It lies at the base of the Boruta algorithm, which selects important features in a dataset.

Figure 3: Random Forest Classification

3.2.5.4. Adaboost Classifier

Ada-boost or Adaptive Boosting is one of ensemble boosting classifier proposed by Yoav Freund and Robert Schapire in

1996. It combines multiple classifiers to increase the accuracy of classifiers. AdaBoost is an iterative ensemble method. AdaBoost classifier builds a strong classifier by combining multiple poorly performing classifiers so that you will get high accuracy strong classifier. The basic concept behind Adaboost is to set the weights of classifiers and training the data sample in each iteration such that it ensures the accurate predictions of unusual observations. Any machine learning algorithm can be used as base classifier if it accepts weights on the training set. Adaboost should meet two conditions:

1. The classifier should be trained interactively on various weighed training examples.
2. In each iteration, it tries to provide an excellent fit for these examples by minimizing training error.

It works in the following steps:

1. Initially, Adaboost selects a training subset randomly.
2. It iteratively trains the AdaBoost machine learning model by selecting the training set based on the accurate prediction of the last training.
3. It assigns the higher weight to wrong classified observations so that in the next iteration these

observations will get the high probability for classification.

4. Also, it assigns the weight to the trained classifier in each iteration according to the accuracy of the classifier. The more accurate classifier will get high weight.

5. This process iterate until the complete training data fits without any error or until reached to the specified maximum number of estimators.

6. To classify, perform a "vote" across all of the learning algorithms you built.

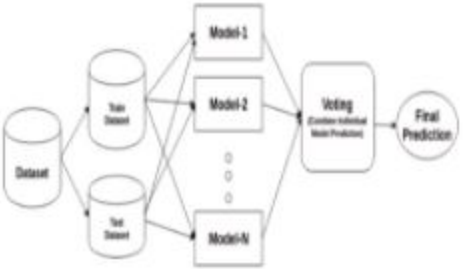

Figure 4: Adaboost classification

Results and analysis

Results

The aim of this project work is to develop a complete facial expression recognition system. COHN_KANADE dataset is used for the experimentations. First of all, system was trained using different random samples in each dataset by supervised learning. In each datasets the data were partitioned into two parts for training and testing in the ratio of 8:2 i.e.80% for train and 20% for test. Every dataset have completely different samples which are selected randomly in uniform manner from the pool of given dataset. The accuracy evaluation results of COHN-KANADE on SVM, k-NN,RF and Adaboost classifier are 93.76%, 89.80%, 90.71% and 91.22%

Figure 5: Preprocessed Neutral Face

This project proposes an approach for recognizing the category of facial expressions. Face Detection and Extraction of expressions from facial images is useful in many applications, such as robotics vision, video surveillance, digital cameras, security and human-computer interaction. This project's objective was to develop a facial expression recognition system implementing the computer visions and enhancing the advanced feature extraction and classification in face expression recognition.

In this project, six different facial expressions of different person's images from COHN-KANADE datasets have been analyzed. This project involves facial expression preprocessing of captured facial images followed by feature extraction using feature extraction using Gabor wavelet and classification of facial expressions based on training of datasets of facial images based on Support Vector Machines, k Nearest Neighbor, Random Forest and Adaboost classifier. This project recognizes more facial expressions based on COHN-KANADE face database. The same datasets were used for both training and testing by dividing the datasets into training samples and testing samples in the ratio of 8:2.

Facial expression recognition is a very challenging problem. More efforts should be made to improve the classification performance for important applications. Future

work will focus on improving the performance of the system and deriving more appropriate classifications which may be useful in many real world applications.

Evaluation Metric

The performance of the proposed system is evaluated qualitatively. The parameters considered for qualitative evaluation are defined below.

1) *Informativeness* represents to what extent the answers provided by the system is capable of providing useful information
2) *Relevance* evaluates to what extent the answers are appropriate to the question and how well it corresponds to the respective question category.
3) *Semantic score* is the measure of how well the meaning of the question is considered or related to interpret the answer.
4) *Correctness* is a measure used to determine the exactness of the object detected by the system.
5) *Overall score* is a value that determines the overall rating of the system based on ease of use and reliability.

Evaluation

For evaluation, 10 users were asked to score the system based on the above qualitative factors for each category of

questions. The users were asked to rate on a scale of 5 where 5 is the highest. The average value is considered for evaluation.

Fig.5 plots the evaluation results based on qualitative parameters for the various question categories. It can be observed that for dichotomous questions, the system exhibits high performance based on all the qualitative parameters. Whereas, a slight dip in informativeness can be observed in the performance of factual questions. This is because for factual questions, the expectation is to cover all the facts and objects related to the image which has not been completely attained. The results obtained for quantitative questions are also satisfactory. The dip in correctness owes to the same reason where all facts and objects are not completely covered by the system in certain scenarios. It can be seen that the semantic score and relevance factor achieved for all the three categories of questions are promising.

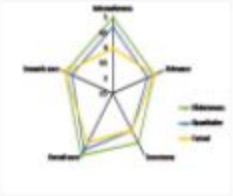

Fig 5. Evaluation on qualitative parameters for various question categories

Conclusion

This project proposes an approach for recognizing the category of facial expressions. Face Detection and Extraction of expressions from facial images is useful in many applications, such as robotics vision, video surveillance, digital cameras, security and human-computer interaction. This project's objective was to develop a facial expression recognition system implementing the computer visions and enhancing the advanced feature extraction and classification in face expression recognition.

In this project, six different facial expressions of different person's images from COHN-KANADE datasets have been analyzed. This project involves facial expression preprocessing of captured facial images followed by feature extraction using feature extraction using Gabor wavelet and classification of facial expressions based on training of datasets of facial images based on Support Vector Machines, k Nearest Neighbor, Random Forest and Adaboost classifier. This project recognizes more facial expressions based on COHN-KANADE face database. The same datasets were used for both training and testing by dividing the datasets into training samples and testing samples in the ratio of 8:2.

Facial expression recognition is a very challenging problem. More efforts should be made to improve the

classification performance for important applications. Future work will focus on improving the performance of the system and deriving more appropriate classifications which may be useful in many real world applications.

Face expression recognition systems have improved a lot over the past decade. The focus has definitely shifted from posed expression recognition to spontaneous expression recognition. Promising results can be obtained under face registration errors, fast processing time, and high correct recognition rate (CRR) and significant performance improvements can be obtained in this system. System is fully automatic and has the capability to work with images feed. It is able to recognize spontaneous expressions. This system can be used in Digital Cameras wherein the image can be captured only when the person smiles. In security systems which can identify a person, in any form of expression he presents himself. Rooms in homes can set the lights, television to a person's taste when they enter the room. Doctors can use the system to understand the intensity of pain or illness of a deaf patient. Our system can be used to detect and track a user's state of mind, and in mini-marts, shopping center to view the feedback of the customers to enhance the business etc.

References

1. The CMU multi-pie face database (2020) http://ww1.multipie.org/. Accessed 05 Jan 2020
2. Caltech Faces (2020) http://www.vision.caltech.edu/html-files/archive.html. Accessed 05 Jan 2020
3. Zafar B, Ashraf R, Ali N, Iqbal M, Sajid M, Dar S, Ratyal N (2018) A novel discriminating and relative global spatial image representation with applications in CBIR. Appl Sci 8(11):2242
4. Ali N, Zafar B, Riaz F, Dar SH, Ratyal NI, Bajwa KB, Iqbal MK, Sajid M (2018) A hybrid geometric spatial image representation for scene classification. PLoS ONE 13(9):e0203339
5. Ali N, Zafar B, Iqbal MK, Sajid M, Younis MY, Dar SH, Mahmood MT, Lee IH (2019) Modeling global geometric spatial information for rotation invariant classification of satellite images. PLoS ONE 14:7
6. Ali N, Bajwa KB, Sablatnig R, Chatzichristofis SA, Iqbal Z, Rashid M, Habib HA (2016) A novel image retrieval based on visual words integration of SIFT and SURF. PLoS ONE 11(6):e0157428

7. Sajid M, Iqbal Ratyal N, Ali N, Zafar B, Dar SH, Mahmood MT, Joo YB (2019) The impact of asymmetric left and asymmetric right face images on accurate age estimation. Math ProblEng 2019:1–10

8. NIST mugshot identification database(2020) https://www.nist.gov/itl/iad/image-group/resources/biometric-special-databases-and-software. Accessed 05 Jan 2020.

9. Zhao X, Liang X, Liu L, Li T, Han Y, Vasconcelos N, Yan S (2016) Peak-piloted deep network for facial expression recognition. In: European conference on computer vision. Springer, pp 425–442

10. [10] Jung H, Lee S, Yim J, Park S, Kim J (2015) Joint fine-tuning in deep neural networks for facial expression recognition. In: Proceedings of the IEEE international conference on computer vision. pp 2983–2991

11. Zhang K, Huang Y, Du Y, Wang L (2017) Facial expression recognition based on deep evolutional spatial-temporal networks. IEEE Trans Image Process 26(9):4193.

12. Wu YL, Tsai HY, Huang YC, Chen BH (2018) Accurate emotion recognition for driving risk prevention in driver

monitoring system. In: 2018 IEEE 7th global conference on consumer electronics (GCCE). IEEE, pp 796–797

13. Giannopoulos P, Perikos I, Hatzilygeroudis I (2018) Deep learning approaches for facial emotion recognition: a case study on FER-2013. In: Hatzilygeroudis I, Palade V (eds) Advances in hybridization of intelligent methods. Springer, Berlin, pp 1–16

14. Gajarla V, Gupta A (2015) Emotion detection and sentiment analysis of images. Georgia Institute of Technology, Atlanta

15. Ratyal N, Taj IA, Sajid M, Mahmood A, Razzaq S, Dar SH, Ali N, Usman M, Baig MJA, Mussadiq U (2019) Deeply learned pose invariant image analysis with applications in 3D face recognition. Math ProblEng 2019:1–21

16. Ratyal NI, Taj IA, Sajid M, Ali N, Mahmood A, Razzaq S (2019) Three-dimensional face recognition using variance-based registration and subject-specific descriptors. Int J Adv Robot Syst 16(3):1729881419851716